
Glacial-interglacial oceanic changes in the central Pacific sector of the Southern Ocean during the past 500 ka

Dissertation zur Erlangung des Doktorgrades der Naturwissenschaften
am Fachbereich Geowissenschaften der Universität Bremen

vorgelegt von

Johannes Ullermann

Bremen, Juli 2015

Gutachter:

Prof. Dr. Ralf Tiedemann

Prof. Dr. Gesine Mollenhauer

This PhD thesis was prepared between October 2010 and July 2015 at the marine geology department of the *Alfred-Wegener-Institut Helmholtz-Zentrum für Polar- und Meeresforschung, Bremerhaven*, within the ANT-XXVI/2 working group. It was integrated in the Helmholtz research project *PACES* (Programme Marine, Coastal and Polar Systems: Polar Regions and Coasts in a changing Earth System) Topic 3 WP 1, which aimed at identifying the role of processes at high latitudes on past, current and future changes of the Earth system.

Name: Johannes Ullermann

Datum: 07. 07. 2015

Anschrift: Stetten 3a, 83123 Amerang

Erklärung

Hiermit versichere ich, dass ich (1) die Arbeit ohne unerlaubte fremde Hilfe angefertigt habe, (2) keine anderen als die von mir angegebenen Quellen und Hilfsmittel benutzt habe und (3) die den benutzten Werken wörtlich oder inhaltlich entnommenen Stellen als solche kenntlich gemacht habe.

Bremen, den 07. 07. 2015

.....

Johannes Ullermann

Zusatzerklärung zum Eigenanteil an der Dissertation

Hiermit versichere ich, Johannes Ullermann, dass ich den Rahmentext der Dissertation “Glacial-interglacial oceanic changes in the central Pacific sector of the Southern Ocean during the past 500 ka” selbstständig angefertigt habe, in welchen die unter Kapitel 4, 5 und 6 aufgeführten Manuskripte eingebettet sind.

Die als Kapitel 4 und 5 beigefügten Manuskripte habe ich selbst geschrieben und bin verantwortlich für deren grundlegenden Inhalte und die Dateninterpretation. Sie beinhalten zudem inhaltliche Beiträge der Koautoren, deren Namen an den Kapitelanfängen aufgeführt sind. Das als Kapitel 6 beigefügte Manuskript habe ich ebenfalls selbst geschrieben und bin verantwortlich für dessen Inhalte, sowie für die dazugehörige Dateninterpretation. Die Namen der vorgesehenen Koautoren des noch in Vorbereitung befindlichen Manuskriptes sind zu Kapitelanfang aufgeführt.

Datensätze der untersuchten ANT-XXVI/2 Sedimentkerne, welche in der Dissertation oder auch in deren Appendix diskutiert werden, sind im Kapitel 3 in Tabelle 3.1 aufgeführt. Die Datensätze wurden zu großen Teilen von mir selbst generiert. Diejenigen Datensätze, die durch mein Mitwirken oder ohne mein Mitwirken generiert wurden, sind in Tabelle 3.1 mit den Fußnoten d und e gekennzeichnet. Zu letzteren zählen die in Manuskript 5 diskutierten Mg/Ca und $\delta^{18}\text{O}$ Datensätze des Kernes PS75/056-1. Diese stammen von Raul Tapia, welcher als Koautor an zweiter Stelle genannt ist. Außerdem zählen dazu die Karbonatgehalt Datensätze der Kerne PS75/076-2 und PS75/079-2, welche in Kapitel 6 diskutiert werden. Maßgeblich mitgewirkt habe ich bei der Generierung der XRF-Kernscan Datensätze der Kerne PS75/059-2, PS75/076-2 und PS75/079-2, ebenfalls diskutiert in Kapitel 6. Die XRF-Kernscans wie auch die Bestimmung des Karbonatgehaltes wurden an den eben erwähnten Kerne sowie an einer Vielzahl weiterer ANT-XXVI/2 Kerne routinemäßig unter Leitung von Gerhard Kuhn und Frank Lamy durchgeführt. Die Foraminiferengewichte des Kernes PS75/059-2, welche in Kapitel 5 diskutiert werden und welche im Zuge der Mg/Ca und $\delta^{18}\text{O}$ / $\delta^{13}\text{C}$ Datenerhebung von mir bestimmt wurden, sind nicht extra in Tabelle 3.1 aufgeführt.

Als Koautor bin ich vertraut mit dem Inhalt der in der Appendix beigefügten Veröffentlichung und habe diesbezüglich Beiträge geleistet. Die Datensätze, welche von mir stammen und mit denen ich zu der Veröffentlichung beigetragen habe, sind am zu Anfang der Appendix aufgeführt.

Abstract

Earth's climate has undergone repeated, dramatic changes between glacial and interglacial states throughout the past 500 ka years with dominant 100 ka cycles. Global mean temperatures during glacials were significantly lower than during interglacials, rising and falling in close correspondence with atmospheric CO₂ concentrations. To understand underlying climate mechanisms that operated throughout the past is an important topic of climate research, particularly as this provides information to better constrain predictions of future climate change. In this regard, changes in the Southern Ocean, both in physical ocean circulation and biological productivity, are commonly thought to have played a critical role in regulating the ocean-atmosphere CO₂ balance. However, paleoceanographic data from this oceanic region is sparse, thus rendering much of the understanding of the underlying processes incomplete, particularly for the central parts of the Pacific sector of the Southern Ocean.

This thesis reconstructs interglacial-glacial scale oceanographic changes in the high latitude (~55°S) central Pacific sector of the Southern Ocean with the aim to further improve the current understanding of climate dynamics. For this purpose, a number of proxy data were generated from marine sediment cores that were collected during R/V Polarstern cruise ANT-XXVI/2. The main outcome of this study is compiled in three manuscripts (*Capture 4, 5 and 6*) as follows:

1) Based on benthic foraminiferal $\delta^{13}\text{C}$ data, past Circumpolar Deep Water $\delta^{13}\text{C}$ compositional changes were reconstructed in the Southern Ocean Pacific sector, which displayed high glacial-interglacial amplitude fluctuations over the last 500 ka. When compared to reconstructions from the Atlantic sector, the results imply that a common Circumpolar Deep Water $\delta^{13}\text{C}$ composition was maintained throughout the last four glacial-interglacial cycles, thus evolving parallel in both basins. This finding modifies the current LGM picture on the deep water exchange between Atlantic and Pacific sector. In turn, new implications arise regarding the interpretation of past Antarctic Bottom Water lateral distribution and formation in the Atlantic Sector, and on past CO₂ storage in the deep Atlantic interior.

2) Based on planktonic foraminiferal Mg/Ca and $\delta^{18}\text{O}$, the surface water temperature and $\delta^{18}\text{O}$ evolution was reconstructed for the central Pacific sector over the past 500 ka. Sea surface temperatures in this open marine, high latitude (~55°S) setting closely co-evolved with Antarctic air temperatures, whereas the glacial-interglacial changes were characterized by moderate amplitudes. By contrast, the ice volume-corrected water $\delta^{18}\text{O}$ displayed no clear glacial-interglacial modulation. Overall, the results fit well into the current picture for the South Pacific, which supposes that surface oceanic changes in the eastern and western marginal areas were amplified by changes in South Pacific gyre circulation over glacial-interglacial cycles, thus underpinning a link of the gyre's boundary current circulation with Earth's climate change.

3) Using downcore carbonate contents in combination with planktonic foraminiferal $\delta^{13}\text{C}$, basic characteristics of carbonate sedimentation and surface carbonate productivity are outlined for the central Pacific sector with focus on the Marine Isotope Stage 11 interglacial. The sedimentation between the Subantarctic and Polar Front stands out during Marine Isotope Stage 11, when compared to other interglacials, by massive coccolith deposition as already documented for the Atlantic sector of the Southern Ocean. Contemporary changes in surface water $\delta^{13}\text{C}$ of approximately 1 ‰ occurred, pointing toward a turnover to a coccolithophorid dominated phytoplankton productivity, assumedly on cost of silica consuming diatoms. The beginning and end of this Marine Isotope Stage 11 changes can be within a few thousand years precisely determined in the central Pacific sector. Under presumption that the dominance of coccolithophorides has resulted in an excess of silica in central Pacific Sector surface waters, inferences were drawn on the validity of the Silica Leakage Hypotheses from an interglacial perspective – a hypotheses which links glacial diatom morphology and/or community structure changes in the Southern Ocean, which conceivably have caused a higher equatorward export of silica via Subantarctic Mode Water, to a potential strengthening of the ‘biological pump’ in the equator upwelling systems and which may constitute an important mechanism contributing to the recurring atmospheric CO_2 drawdown over glacial-interglacial cycles.

Zusammenfassung

Das Klima der Erde hat die letzten 500 000 Jahre hindurch wiederholte, dramatische Veränderungen zwischen glazialen und interglazialen Zeitabschnitten durchlaufen, die von starken 100 000 Jahr Zyklen geprägt waren. Während der Glaziale lagen die Temperaturen im globalen Mittel beträchtlich niedriger als während der Interglaziale, wobei die Temperaturwechsel im Zusammenspiel mit den CO₂ Konzentrationen der Atmosphäre erfolgten. Die zugrundeliegenden Klimamechanismen zu verstehen, welche in der Vergangenheit aktiv waren, ist ein wichtiges Thema der Klimaforschung, insbesondere weil dies Informationen liefert, um Prognosen zum zukünftigen Klimawandel besser einzugrenzen. In diesem Zusammenhang besteht die verbreitete Meinung, dass Veränderungen im Südlichen Ozean bezüglich der physikalisch kontrollierten Ozeanzirkulation wie auch der biologischen Produktion in der Regulation des Ozean-Atmosphären CO₂ Haushaltes eine wichtige Rolle gespielt haben. Allerdings ist die paläozeanographische Datenabdeckung in diesem Gebiet dürftig und folglich ist das derzeitige Verständnis über die genauen Vorgänge dort unvollständig. Dies trifft vor allem für die zentralen Pazifischen Sektor Bereiche des Südlichen Ozeans zu.

Die vorliegende Dissertation beschäftigt sich mit der Rekonstruktion der glazial-interglazialen ozeanographischen Veränderungen hoher, südlicher Breiten (~55°) im Bereich des zentralen Pazifischen Sektors des Südlichen Ozeans mit dem Ziel, das derzeitige Verständnis der Klimadynamik weiter zu verbessern. Zu diesem Zweck wurden eine Reihe von Proxy-Daten an marinen Sedimentkernen generiert, welche auf der R/V Polarstern Ausfahrt ANT-XXVI/2 gehoben wurden. Die wichtigsten Ergebnisse dieser Studie sind zusammengefasst in drei Manuskripten (*Kapitel 4, 5 und 6*) wie folgt:

- 1) Basierend auf den $\delta^{13}\text{C}$ -Werten, gemessen an benthischen Foraminiferen, wurden frühere Veränderungen der Zirkumpolaren-Tiefenwasser $\delta^{13}\text{C}$ Zusammensetzung im Pazifischen Sektor des Südlichen Ozeans rekonstruiert, welche demnach im Verlauf der letzten 500 000 Jahre hohe Amplitudenfluktuationen zeigte. Im Vergleich zu Rekonstruktionen aus dem Atlantischen Sektor lassen die Ergebnisse den Schluss zu, dass eine gemeinsame Zirkumpolare-Tiefenwasser $\delta^{13}\text{C}$ Zusammensetzung die letzten vier glazial-interglazialen Zyklen hindurch gewahrt blieb. Folglich entwickelte sich die $\delta^{13}\text{C}$ Zusammensetzung parallel in beiden Becken. Diese Erkenntnis modifiziert das gegenwärtige Bild, welches für den Zeitpunkt des letzten glazialen Maximums im Hinblick auf den Tiefenwasseraustausch zwischen dem Atlantischen und dem Pazifischen Sektor besteht. Im Weiteren ergeben sich daraus neue Implikationen zur Interpretation der früheren Verbreitung und Bildung von Antarktischem-Bodenwasser im Atlantischen Sektor sowie zur früheren CO₂ Speicherung im tiefen Atlantik.

2) Anhand planktonischer Foraminiferen Mg/Ca und $\delta^{18}\text{O}$ Werte wurde über den Zeitraum der letzten 500 000 Jahre die Oberflächenwassertemperatur und $\delta^{18}\text{O}$ Entwicklung für den zentralen Pazifischen Sektor rekonstruiert. Die Meeresoberflächentemperaturen in dieser offenen marinen, in hohen Breiten ($\sim 55^\circ\text{S}$) gelegenen Umgebung zeigten den gleichen Entwicklungsverlauf wie die antarktischen Lufttemperaturen, wobei sich die glazial-interglaziale Wechsel durch mäßige Amplitudenhöhen auszeichneten. Im Gegensatz dazu zeigte die Eisvolumen-korrigierte $\delta^{18}\text{O}$ Zusammensetzung des Oberflächenwassers keine offensichtlichen glazial-interglaziale Veränderungen. Insgesamt fügen sich die Ergebnisse gut in das derzeitige Bild zum Südpazifik, welches nahelegt, dass die ozeanischen Veränderungen an der Oberfläche in randnahen östlichen und westlichen Gebieten über glaziale-interglaziale Zyklen hinweg verstärkt wurden durch Zirkulationsänderungen der Südpazifischen Gyre. Somit untermauern die Ergebnisse einen Zusammenhang zwischen den Randstromsystemen der Gyre und Klimaveränderungen der Erde.

3) Unter Verwendung des kernparallel gemessenen Karbonatgehaltes und des $\delta^{13}\text{C}$ planktonischer Foraminiferen wurden, mit Augenmerk auf das Marine Isotopen Stadium 11 Interglazial, grundlegende Charakteristika der Karbonatsedimentation und Oberflächen Karbonatproduktion für den zentralen Pazifischen Sektor dargestellt. Zur Zeit des Marine Isotopen Stadiums 11 sticht die Sedimentation zwischen Subantarktischer und Polarer Front, verglichen mit der anderer Interglaziale, durch die massenhafte Ablagerung von Coccolithen heraus. Gleichzeitig haben Veränderungen in der Oberflächenwasser $\delta^{13}\text{C}$ Zusammensetzung von ungefähr 1‰ stattgefunden. Dies deutet auf einen Wandel zu einer Coccolithoporiden dominierten Phytoplanktonproduktion hin, vermutlich auf Kosten Silikat verbrauchender Diatomeen. Der Anfang und das Ende der Veränderungen im Marine Isotopen Stadium 11 können im zentralen Pazifischen Sektor im Rahmen weniger 1000 Jahre genau bestimmt werden. Unter der Annahme, dass diese Dominanz der Coccolithophoriden zu einem Silikat Überschuss im Oberflächenwasser des zentralen Pazifischen Sektors geführt hat, wurden aus einem interglazialen Blickwinkel heraus Rückschlüsse im Bezug auf die Gültigkeit der „Silica Leakage“ Hypothese gezogen – Diese verknüpft glaziale Veränderungen in der Diatomeen-Morphologie und/oder der Diatomeen-Vergesellschaftung, was möglicherweise einen erhöhten Silikattransport mittels Subantarktischen Zwischenwasser in Richtung Äquator bedingt hat, mit der potentiellen Stärkung der „biologischen Pumpe“ in den äquatorialen Auftriebsgebieten. Die Hypothese könnte einen wichtigen Mechanismus begründen, der beigetragen hat zu dem wiederkehrenden Abfall in den atmosphärischen CO_2 Konzentrationen über glazial-interglaziale Zyklen.

Acknowledgements

First, I would like to thank my supervisors Dr. Rainer Gersonde and Dr. Frank Lamy for providing me the opportunity to do my PhD at the Alfred Wegener Institute Bremerhaven and for introducing me in the interesting field of marine geology. Particularly, Dr. Frank Lamy is thanked for his scientific support over the last years as well as for his patience during the last months. Further, I would like to thank Prof Dr. Ralf Tiedemann for his helpful advices, his work as head of the marine geology department and for taking me along on the SO213/1-2 research cruises at R/V Sonne. Lastly, I thank him, but also Prof Dr. Gesine Mollenhauer from the University Bremen to act as reviewers of this thesis.

Furthermore, I appreciate the scientific and technical support of my colleges at Alfred Wegener Institute Bremerhaven and the University Bremen as well as the work-related and work-unrelated time we shared together. At this point I would like to mention Ute Bock, Dr. James Collins, Dr. Oliver Esper, Rita Fröhlking, Dr. Jens Hefter, Dr Andrea Jaeschke, Prof. Dr. Andreas Mackensen, Dr. Mariem Saavedra-Pellitero, Lisa Schönborn and Susane Wiebe to acknowledge some of them. Particularly, I thank Dr. Lester Lembke-Jene for supporting me during the last months, when I finally completed this thesis. Form the GEOMAR Kiel, I would like to thank Prof. Dr. Nürnberg for enabling me to use for two weeks the laboratory facilities at the GEOMAR Kiel and for the good cooperation from his side. Further, I thank Raul Tapia, PhD student at the GEOMAR Kiel, for the good cooperation and Nadine Gehre for the technical support in the laboratory.

I thank all my PhD colleagues, the previous and present ones, for the nice time at the institute as well as in Bremerhaven and Bremen – I really enjoined it with you. Thanks to my office mates Conni, Ines, David, Marc and particularly Thomas, with whom I was sitting side-by-side for almost 3.5 years, for all the fun we had, but also for the readily help, suggestions and scientific support. Thanks also to Verena, Hartmut and Sahra for motivating me over the years as well as for sharing good and bad moments during my PhD times.

Of course, I thank my friends I know from home and from Erlangen University days for hanging out with me at times, when I was not in Bremerhaven. Last but not least, I greatly thank my sister and my parents, who continuously supported me over all the years.

Table of Contents

Abstract	I
Zusammenfassung	III
Acknowledgements	V
1 Introduction and Objectives	2
2 Background	6
2.1 The present-day Southern Ocean oceanography	6
2.2 The present-day Pacific sector oceanography	8
2.3 The paleoceanography of the Southern Ocean and its Pacific sector	10
3 Material and Methods.....	15
3.1 Study material	15
3.2 Proxy methods and analyses	17
3.3 Age control	22
4 Pacific-Atlantic Circumpolar Deep Water coupling during the last 500 ka.....	23
4.1 Introduction	24
4.2 Modern deep water circulation and tracer distribution	25
4.3 Material and Methods	28
4.4 Results and Discussion	30
4.5 Conclusion	37
4.6 Supplemental Information	38
5 Evolution of the sea surface temperature and $\delta^{18}\text{O}$ in the central South Pacific during the past 500 ka: Implications on ocean circulation.....	39
5.1 Introduction	40
5.2 Material and Methods	40
5.3 Results	44
5.4 Discussion	45
5.5 Conclusion	60
5.6 Supplemental Information	61
6 Southern Ocean phytoplankton community changes during MIS 11: Implications for the silica leakage mechanism.....	63
6.1 Introduction	64
6.2 Material and Methods	65
6.3 Results and Discussion	68
6.4 Conclusion	76
6.5 Supplemental Information	77
7 Conclusions and Outlook	78
8 Data Handling.....	81
9 References	82
Appendix	98
A.1 Increased dust deposition in the Southern Ocean during glacial periods	98
A.2 Supplement: Increased dust deposition in the Southern Ocean during glacial periods	109

1 Introduction and Objectives

Earth's climate has continuously changed throughout the past, while it displayed dramatic variations between cold (glacial) and warm (interglacial) climatic states over the past 450 ka. Primary cause of climate variations, occurring at 100, 41 and 23 ka cycles, are external changes in Earth's orbital parameters, which regulate the temporal and spatial distribution, as well as the amount, of solar energy reaching Earth's atmosphere (Hays et al., 1976; Huybers and Denton, 2008; Milanković, 1941). Climate reconstructions reveal, however, that internal amplification mechanisms crucially contribute to these natural climatic changes. To identify and quantify these mechanisms, but also to understand their interactions, is an important topic in current climate research. In the light of modern, anthropogenic-influenced climate change, which has fundamental impact on human life, profound knowledge about the natural baseline of climatic variations is a basic prerequisite to make future climate predictions (IPCC, 2014).

Reconstructions from Antarctic ice cores showed that Earth's climate varied in step with atmospheric CO₂ concentrations, which fluctuated by approximately 90 p.p.m.v. within clear defined boundaries throughout the past 450 ka. Lower bounds of about 170 p.p.m.v. were reached during glacial stages, upper bounds of about 280 p.p.m.v. were reached during interglacial stages, including the late Holocene pre-industrial period (Lüthi et al., 2008 and references herein; Petit et al., 1999). These recurring minima and maxima in greenhouse gas concentrations imply that Earth's internal amplification mechanisms interact in a causal, clearly ordered way. A conclusive, likewise simple explanation for past atmospheric CO₂ fluctuations, which are tied to changes in the carbon cycle, appears thus as a major key to understand Earth's climate system. Connected with the carbon cycle, the ocean plays an important role due to its ability to capture and sequester atmospheric CO₂ at depths. Changes in the ocean's physical circulation and biological productivity are currently considered to have significantly contributed to the glacial 90 p.p.m.v. atmospheric CO₂ drawdown (Marinov et al., 2008; Sigman and Boyle, 2000).

The Southern Ocean, which encircles the ice-covered Antarctic continent, is in this regard central due to its global-scale importance related to the ocean physical circulation (Marshall and Speer, 2012). Alike, it plays an important role for biological productivity on global scale (Marinov et al., 2006; Sarmiento et al., 2004). In their impact, all the physical and biological processes act together there in such way that the Southern Ocean constitutes actually a valve for deeply sequestered CO₂ to escape from the ocean interior, which could have been closed during glacial times (Sigman et al., 2010). Thus, basic climate concepts take the Southern Ocean commonly into consideration when investigating mechanisms for pre-industrial atmospheric CO₂ and climate variability (Brzezinski et al., 2002; Francois et al., 1997; Martin, 1990; Matsumoto et al., 2002; Stephens and Keeling, 2000; Toggweiler, 1999). Currently, the Southern Ocean gains even increasing attention, as it becomes more and more apparent that it may have played not only a passive role as response to Northern

Hemisphere-dominated climate and North Atlantic overturning circulation changes, but that it was rather an active contributor to climate change. This is due to the fact that physical and also biological dynamics in the Southern Ocean are influenced by the Southern Hemisphere westerly wind circulation, which in turn may provide an important mechanism to amplify Southern Hemisphere atmospheric changes over glacial-interglacial cycles (Toggweiler et al., 2006). Although present proxy studies provide different results on the driving role of the Southern Hemisphere westerly winds (e.g., Kohfeld et al., 2013) and controversial opinions exist in this regard (e.g., Völker and Köhler, 2013).

Altogether, our current understanding of the Southern Ocean, even from a present-day perspective, is too limited. Despite its importance, the Southern Ocean represents a widely underexplored region in paleoceanography. This is particularly the case for the central part of the Pacific sector. Thus, detailed information from marine sediment cores there is of tremendous importance to further understand the Southern Ocean's role for Earth's climate system.

This thesis aims to reconstruct oceanographic changes in the high latitude (~55°S) central Pacific sector of the Southern Ocean throughout the past 500 ka to improve the current understanding of physical and biological dynamics in that area. For this purpose, downcore geochemical and sedimentological proxy data were generated from marine sediment cores, which were collected during R/V Polarstern cruise ANT-XXVI/2.

The structure of this thesis is as follows: *Chapter 2* provides an overview on the present-day physical and biological oceanography of the Southern Ocean and its central Pacific sector, including the role in Earth's climate system. Further, it is outlined how far current paleoceanographic findings modified the present-day oceanographic picture for the past. *Chapter 3* provides information on the sample material and the used proxy methods. *Chapters 4, 5, and 6* contain the scientific results of the thesis, sub-divided into three manuscripts, which have been prepared for submission to international, peer-reviewed scientific journals. They discuss the reconstruction results and their wider paleoceanographic implications on glacial-interglacial time scale. *Chapter 7* provides a short summary on the three manuscripts and proposes perspectives for future investigations. The *Appendix* contains a co-authorship article (Lamy et al., 2014), which discuss past changing dust inputs in the central Pacific sector as well as its implications on biological productivity and atmospheric CO₂ drawdown over the last climatic cycles. The topics and the respective research questions discussed in the three manuscripts of this thesis summarize as follows:

Manuscript 1 (*Chapter 4*) deals with the reconstruction of deep water $\delta^{13}\text{C}$ compositional changes in the Pacific sector, covering the last 500 ka. The results are discussed with a focus on the deep water $\delta^{13}\text{C}$ compositional evolution so far known from the Atlantic sector. The following questions are discussed:

- How was the Circumpolar Deep Water $\delta^{13}\text{C}$ evolution in the Pacific and was it different to those in the Atlantic?
- Was the development of a high $\delta^{13}\text{C}$ gradient between deep waters in the Pacific and Atlantic basins, as observed at the Last Glacial Maximum (Ninnemann and Charles, 2002), a typical feature of the other glacials as well?
- What implications arise from the new knowledge about past $\delta^{13}\text{C}$ evolution of Pacific Circumpolar Deep Water, which enters through Drake Passage into the Atlantic, on the past lateral extent and formation of Antarctic Bottom Water?
- What are the implications for the atmospheric CO_2 sequestration in the deep Atlantic, which is related to the oceanic physical circulation?

Manuscript 2 (*Chapter 5*) deals with the reconstruction of orbital-scale surface water temperature and $\delta^{18}\text{O}$ changes in the central Pacific sector over the last 500 ka, thereby tackling the following questions:

- How has the surface water temperature and $\delta^{18}\text{O}$ evolved at high southern latitudes over the past five glacial interglacial cycles?
- How do the open ocean, central Pacific sector changes compare to the Antarctic air temperature record? How do they compare to those documented by marine records from the Pacific basin's western and eastern marginal areas?
- Do the results from central Pacific sector confirm the current paleoceanographic picture on the Pacific Ocean surface circulation, which suggest systematic changes in the South Pacific gyre's western and eastern boundary current strength?

Manuscript 3 (*Chapter 6*) outlines changes in carbonate deposition and surface water $\delta^{13}\text{C}$ for the central Pacific sector with a focus on the Marine Isotope Stage (MIS) 11, an interglacial with a carbonate facies distinguished from later interglacials by dramatically higher coccolith concentrations. The arising inferences on biological productivity changes at that time are used to discuss particular aspects of the Silica Leakage Hypothesis, which states a potential glacial-interglacial mechanism on atmospheric CO_2 drawdown. The following questions are addressed:

- Does the exceptional MIS carbonate depositional facies in the central Pacific sector reflect an increased coccolithophorid algae productivity in the surface layer?
- How abruptly occurred the MIS 11 changes in the central Pacific sector?
- Which inferences from the exceptional interglacial MIS 11 changes can be drawn on the Silica Leakage Hypothesis mechanism, in particular on its functioning during glacial time?

2 Background

2.1 The present-day Southern Ocean oceanography

The Southern Ocean, which covers large areas of the world ocean's surface, encircles the ice-capped Antarctic continent and connects the major ocean basins, namely the Indian, Pacific and Atlantic (Figure 2.1). Due to its capacity in distributing heat, salinity and nutrients, the Southern Ocean is central to Earth's climate system and the carbon cycle (e.g., Gruber et al., 2009; Rintoul et al., 2001). Its surface circulation is largely zonal, dominated by the eastward flowing Antarctic Circumpolar Current (ACC), the largest current system in the world. The ACC is structured into a series of seafloor reaching circumpolar fronts, identifiably by increased physical and chemical gradients at the surface – traditionally pooled together as the Subantarctic Front, Polar Front and Southern-ACC Front. The Subantarctic Front defines the northern boundary of the ACC system (Orsi et al., 1995; Sokolov and Rintoul, 2009a, b). North of the ACC follows the non circumpolar Subtropical Front, which represents on the eastern side of each Southern Ocean sector a sharp surface water mass boundary, separating cold and fresh ACC waters from more warm and salty subtropical waters circulating in the Southern Hemisphere gyre systems (Graham and De Boer, 2013; Orsi et al., 1995).

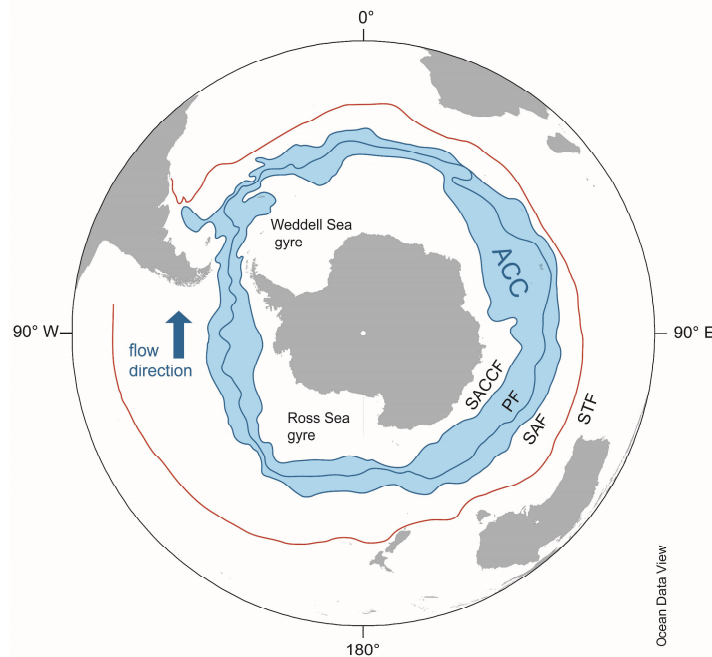


Figure 2.1. The Southern Ocean and its ACC frontal system; displayed are the Subtropical (STF), Subantarctic (SAF), Polar (PF) and Southern-ACC (SACCF) Front, as defined by Orsi et al. (1995); The figure was constructed using Ocean Data View (Schlitzer, 2012).

The Southern Ocean's role is unique in respect the world ocean's meridional overturning circulation, as it represents the only region where deep waters can return from the ocean interior back to the surface (Figure 2.2). This process occurs all along the circumpolar path of the Polar Front by wind-driven upwelling of Circumpolar Deep Water (Marshall and Speer, 2012; Speer et al., 2000). Circumpolar Deep Water is volumetrically the most important Southern Ocean water mass and which

continuously forms by mixing of northern- and southern-derived water masses from all world ocean basins (Orsi et al., 1999; Pardo et al., 2012). Additionally, the Southern Ocean is an important region of deep water formation, which takes place near the Antarctic coast, particularly in the Ross and Weddell seas (Figure 2.2). In these areas, Antarctic shelf water gains increasing density due to interactions occurring in the sea ice zone or below the ice shelf, before it finally sinks down the continental slope to form Antarctic Bottom Water (Orsi et al., 1999; Pardo et al., 2012). Likewise, the Southern Ocean has a fundamental role in the renewal of waters masses of the shallow to mid-depth ocean (Figure 2.2). This occurs by Subantarctic Mode Water and Antarctic Intermediate Water formation around the Subtropical Front and their subduction below the permanent thermocline of the Southern Hemisphere gyre systems (McCartney, 1977; Sallée et al., 2010b).

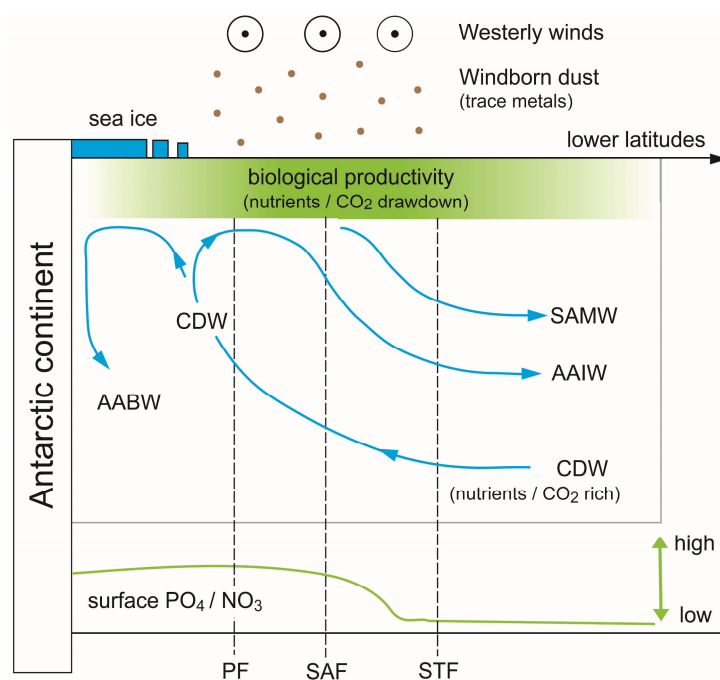


Figure 2.2. Schematic latitudinal section displaying physical ocean circulation and biological productivity related processes in the Southern Ocean, which considerably control the CO₂ transfer between the atmosphere and the deep ocean interior; The figure was constructed based on graphics of Sarmiento et al. (2004) and of Ayers and Strutton (2013).

The upwelling of aged, CO₂-rich Circumpolar Deep Water at the Polar Front brings large amounts of nutrients, e.g. phosphate and nitrogen, from ocean depths to the surface, thus stimulates phytoplankton growth (Figure 2.2). The availability of these nutrients, but also of light, reflects today in the spatial distribution in phytoplankton productivity and seasonality, which is mainly zonal. Coherent to the ACC frontal system, over the year most productivity take place in a band from 30° to 50° latitude, accounting to about 80 % of the total annual Southern Ocean productivity (Comiso et al., 1993; Moore and Abbott, 2000; Thomalla et al., 2011). Although high on a worldwide view, the Southern Ocean biological productivity appears low with regard to its total nutrient inventory. This is most probably due to the limitation of particular trace elements, like iron, which are required for phytoplankton

growth (Boyd et al., 2000; Martin, 1990). Only around land masses higher surface water trace metal concentration occur and originate mainly from sediment resuspension or continental drainage. Open ocean trace metal concentrations are throughout low, while their primary source is wind born dust (Figure 2.2). The nutrients, which remain unutilized by phytoplankton growth, leak from the Southern Ocean's surface trough Antarctic Bottom Water formation or Subantarctic Mode Water and Antarctic Intermediate Water export. Parts thereof, when carried by Subantarctic Mode Water, may later become available for phytoplankton growth at lower latitudes, facilitated, for instance, by coastal upwelling at the equator (Brzezinski et al., 2002; Matsumoto et al., 2002; Sarmiento et al., 2004). Southern Ocean phytoplankton growth promotes the fixation of atmospheric CO₂ within organic matter and its subsequent transfer back to ocean interior by particle sinking, a mechanism commonly known as the 'biological pump' (Hain et al., 2014; Volk and Hoffert, 1985). Consequently, the Southern Ocean 'biological pump' counteracts the effect of CO₂ outgassing caused by the upwelling of CO₂-rich Circumpolar Deep Water.

Intense Southern Hemisphere westerly winds, which circulate with maximum strengths between 40° to 60° latitude zonal around Antarctica, cause the eastward directed flow of the ACC and are an important contributor to the physical circulation of the Southern Ocean. Westerly wind-induced Ekman pumping is further the reason for the upwelling of Circumpolar Deep Water to the surface, which is fundamental for ocean's conveyor circulation (Marshall and Speer, 2012; Speer et al., 2000). Besides, local changes in the wind field, for instance linked to ENSO or SAM anomalies, can influence air-sea heat fluxes, surface mixed-layer depths or surface circulation patterns (Sallée et al., 2008; Sallée et al., 2010a). This, in turn, impacts numerous physical and biological processes, for instance the export of Subantarctic Mode Water, the extent of Antarctic sea ice with consequences for the formation of Antarctic Bottom Water, and the phytoplankton growth in the surface mixed-layer (Ayers and Strutton, 2013; Jullion et al., 2010; Sallée et al., 2010a; Stammerjohn et al., 2011). Surface temperature, another decisively parameter in oceanography, is also affected in this respect (Dong et al., 2007; Gupta and England, 2006).

2.2 The present-day Pacific sector oceanography

The basic oceanic conditions, as outline in *Section 2.1* above, also apply to the in this thesis studied central part of the Pacific sector of the Southern Ocean (Figure 2.3). Continents and islands, namely South America, Antarctica and New Zealand with their broad shelf areas are far distant, thus do not compromise the major Southern Ocean circulation pattern. Though, the topography of the Pacific Antarctic Ridge and the East Pacific Rise at depths has some local influence on the surface positions the ACC frontal system (Orsi et al., 1995; Sokolov and Rintoul, 2009a, b). The study area, at the position of the Subantarctic and Polar Front, is dominated by the eastward ACC flow, while further downstream parts of it are deflected at the tip of South America and feed into the equatorward flowing eastern boundary current of the South Pacific gyre system, thereby transferring subantarctic surface waters to the equator. Vice versa, subtropical surface waters are transported poleward within the South

Pacific gyre's western boundary current, carrying heat and salinity poleward. Although these surface waters interact at the Subtropical Front around New Zealand and Tasmania with the ACC, the downstream located study area is unaffected due to its high latitudinal position, thus due to its high distance to the Subtropical Front (Chaigneau and Pizarro, 2005; Ridgway and Dunn, 2003; Stramma et al., 1995).

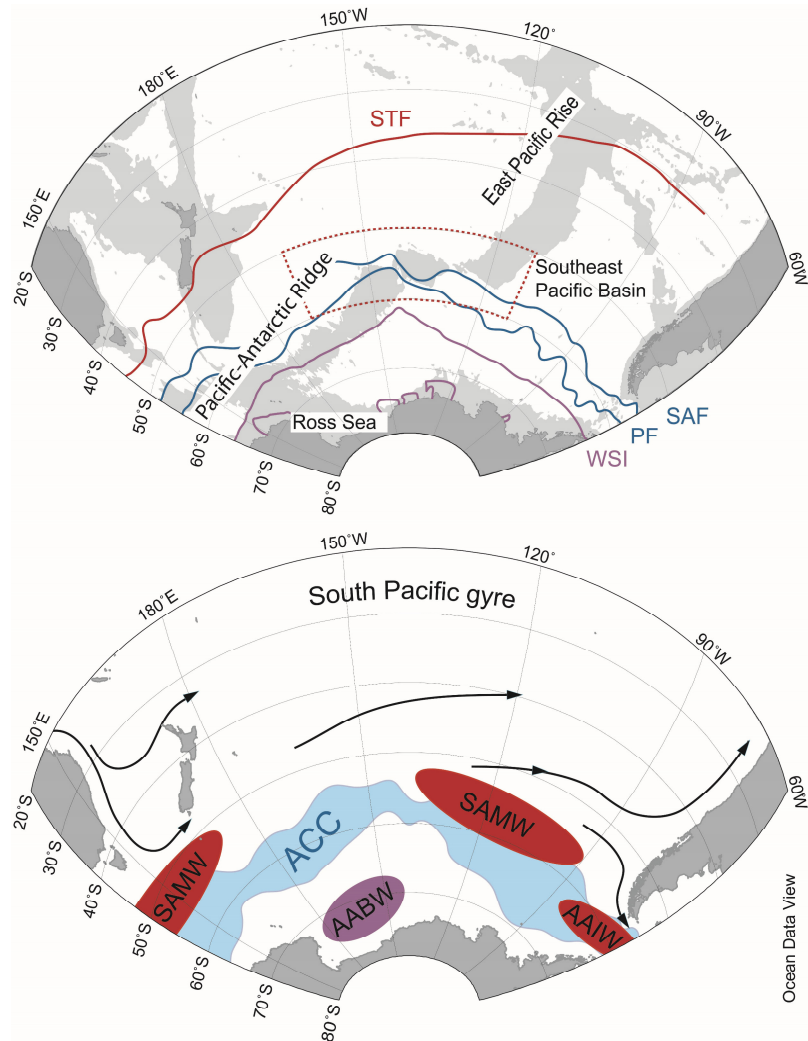


Figure 2.3. Overview maps the Southern Ocean's Pacific sector and adjoining southern Pacific Ocean areas; (upper panel) Oceanic bathymetry above 3500 m water depth is shaded in gray; The study area is outlined by the red dashed frame; The positions of the Subtropical (STF), the Subantarctic (SAF) and the Polar Front (PF) are displayed by red and blue lines; The winter (WSI) and summer sea ice extent is displayed by purple lines; (lower panel) The formation areas of Antarctic Bottom Water (AABW), Subantarctic Mode Water (SAMW) and Antarctic Intermediate Water (AAIW) are schematic displayed by purple or red ellipsoids; The surface circulation is indicated by black arrows; The figure compiles contents from oceanographic publications (Orsi et al., 1999; Orsi et al., 1995; Rintoul et al., 2001; Sallée et al., 2010b; Schlitzer, 2012) and was constructed using Ocean Data View (Schlitzer, 2012).

Regarding the ocean's conveyor circulation, Pacific CDW is the oldest, nutrient-rich CDW of the three Southern Ocean sectors. At the end of the circumpolar path, Pacific CDW enters through the Drake Passage into the Atlantic, where it is restored again by nutrient-poor NADW (Kroopnick, 1985; Orsi et al., 1999). Toward Antarctica, in the Ross Sea embayment Antarctic Bottom Water is formed, which today accounts to about 20 % of the total Antarctic Bottom Water volume (Pardo et al., 2012). Controlled by local mid-oceanic ridge topography, it spreads to largest parts into the East Pacific Basin (Orsi et al., 1999; Pardo et al., 2012). Downstream of the study area, close to the Drake Passage, lies one of the most important formation regions of Antarctic Intermediate Water worldwide. In contrast, Subantarctic Mode Water forms less localized all along the circumpolar path of the Subtropical Front, as also in central oceanic area of the Pacific sector. Both water masses play an important part in replenishing the shallow to mid-depth water masses circulating in the subsurface of the South Pacific gyre (McCartney, 1977; Sallée et al., 2010b).

The Pacific sector is the largest of the Southern Ocean and its central part is far from landmasses, so that wind born dust inputs are negligible. The resultant lack of trace metals in the upper surface layer, where phytoplankton productivity occurs, makes the central Pacific sector despite high nutrient levels a rather unproductive Southern Ocean area (Comiso et al., 1993; Moore and Abbott, 2000; Thomalla et al., 2011). Unused, large quantities of the nutrients are equatorward transported towards the eastern Pacific and Peruvian coastal upwelling systems. This occurs either on surface or shallow subsurface paths, with latter being tied to Subantarctic Mode Water circulation (Goodman et al., 2005; Sarmiento et al., 2004; Toggweiler et al., 1991).

2.3 The paleoceanography of the Southern Ocean and its Pacific sector

Ice core reconstructions from Antarctica reveal several glacial-interglacial Southern Hemisphere climate cycles (Figure 2.4), characterized by coupled changes in air temperatures and atmospheric CO₂ concentrations (Jouzel et al., 2007; Lüthi et al., 2008 and references herein; Petit et al., 1999). In connection therewith, the sea ice distribution around the Antarctic continent changed (Figure 2.4), while it expanded much further northward during glacials (Gersonde et al., 2005; Wolff et al., 2006). Likewise, several glacial ice shelf advances are documented from a glaciomarine sediment sequence drilled in the Ross Sea embayment (Naish et al., 2009). Changes around Antarctica occurred together with Southern Ocean wide changes in physical and biological dynamics, which are overall less quantified, but already implemented in common concepts on Earth's climate change and the carbon cycle (e.g., Francois et al., 1997; Keeling and Stephens, 2001; Martin, 1990; Stephens and Keeling, 2000; Toggweiler, 1999). This arises from the wide consent that the Southern Ocean acts basically as a valve, controlling the CO₂ exchange between the ocean interior and Earth's atmosphere.

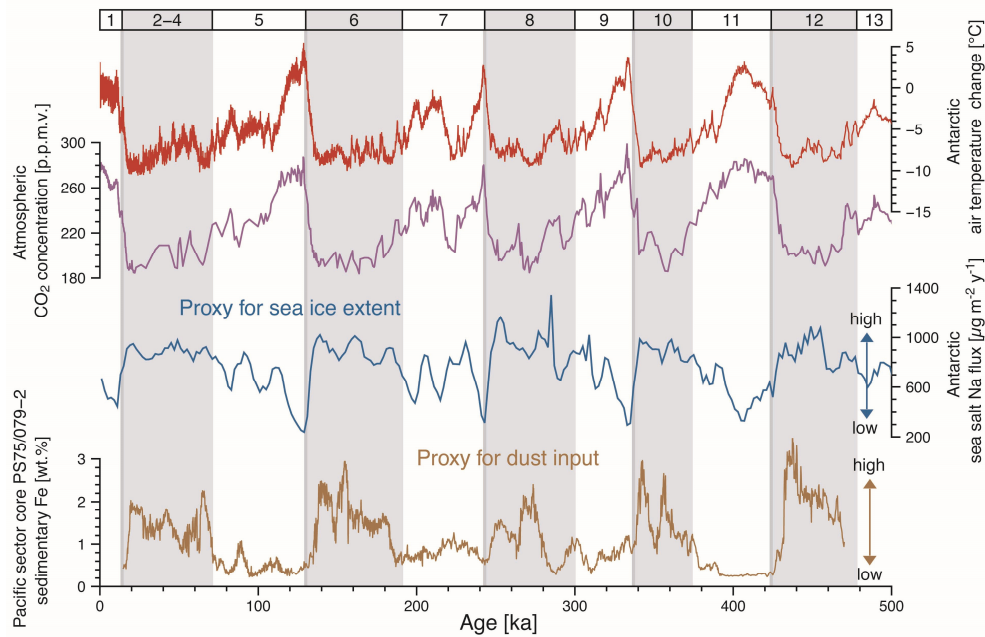


Figure 2.4. Overview on Antarctic and Southern Ocean proxy reconstructions; Antarctic air temperature change (red), atmospheric CO₂ concentration (purple) and Southern Ocean sea ice extent (blue) from Antarctic ice core data (Jouzel et al., 2007; Lüthi et al., 2008; Wolff et al., 2006); Sedimentary iron contents (brown) from a sediment core collected in the central Pacific sector, reflecting the dust flux in this region (Lamy et al., 2014).

A recent review by Sigman et al. (2010) referred to number of mechanisms to reduce the CO₂ leakage, which may have contributed to the glacial 90 p.p.m.v. decline in the atmospheric CO₂ concentrations, as documented in the Antarctic ice cores (Figure 2.4). They include (1) the decreased upward transport of CO₂-rich Circumpolar Deep Water, (2) the increased formation of Antarctic Bottom Water on expense of NADW, which increases the deep oceans CO₂ storage capacity, (3) the expanded sea ice coverage preventing CO₂ outgassing at the surface and (4) the more efficient transfer of atmospheric CO₂ to the ocean interior by phytoplankton productivity. However the cited mechanisms have not necessary worked in same direction. For instance, a decrease upwelling of Circumpolar Deep Water may provide less nutrients to the surface ocean, which, in turn, reduce the strength of the biological pump. Thus, the upwelling related decrease in CO₂ outgassing may in its effect, at least to parts, be countered by a decreasing biological CO₂ drawdown (e.g., Marinov et al., 2006). As such mechanisms may have differed in their impact among the Southern Ocean sectors, an in broadly improved paleoceanographic understanding is also important for the central Pacific sector. Current understanding is mostly based on marine sediment cores obtained during R/V *Eltanin* or R/V *Robert Conrad* cruises and deduce from a number of proxy parameters, as listed in Table 1. Their records either have less stratigraphic coverage, often spanning not more than the last climate cycle, or they have only low temporal resolution. Besides, first higher resolved long-term proxy records were obtained from the sediment core material of Polarstern cruise ANTXXVI/2.

Table 1.1. Published downcore proxy data obtained from marine sediment cores of the central Pacific sector listed together with the respective references.

Proxy method	References
Temperature; Mg/Ca-based,	(Mashiotta et al., 1999)
Temperature; diatom assemblage-based	(Gersonde et al., 2005)
Temperature; foraminiferal assemblage-based	(Luz, 1977)
Sea ice extent; diatom assemblage-based	(Gersonde et al., 2005)
Planktonic foraminiferal $\delta^{18}\text{O}$, $\delta^{13}\text{C}$	(Loubere and Bennett, 2008; Ninnemann and Charles, 1997)
Benthic foraminiferal $\delta^{18}\text{O}$, $\delta^{13}\text{C}$	(Hodell et al., 2000; Matsumoto and Lynch-Stieglitz, 1999; Ninnemann and Charles, 2002)
Carbonate, opal, lithic contents/ fluxes	(Bradtmiller et al., 2009; Catubig et al., 1998; Chase et al., 2003; Lamy et al., 2014; Luz, 1977)
Diatom C_{org} -bound $\delta^{13}\text{C}$, $\delta^{15}\text{N}$, $\Delta^{14}\text{C}$	(Ingalls et al., 2004; Robinson et al., 2005; Rosenthal et al., 2000a)
Planktonic foraminiferal Cd/Ca	(Rickaby and Elderfield, 1999; Robinson et al., 2005)
Spong spiculae $\delta^{30}\text{Si}$	(Ellwood et al., 2008)

The currently available proxy data altogether indicate that in central parts of the Southern Ocean Pacific sector a lot of changes have occurred throughout the past, albite during glacial the conditions in central Pacific sector regarding the structure of the ACC frontal system were supposedly not, or not much, distinct from today. Benthic and planktonic $\delta^{18}\text{O}$ based observations indicate for the Last Glacial Maximum (LGM) that the Polar Front, when physical defined, stayed within $\pm 2^\circ$ latitude at its modern surface position (Matsumoto et al., 2001). Although the rather small number of data from the central Pacific sector allows only preliminary conclusions, it appears that Circumpolar Deep Water continuously upwelled at the Polar Front over glacial-interglacial cycles (Matsumoto et al., 2001).

For the central Pacific sector, current reconstructions indicate modest glacial cooling, with surface temperatures at $\sim 55^\circ$ latitude, where the sediment cores used for this thesis were obtained, being 2°C to 4°C lower at the LGM (Benz et al., in prereration; Luz, 1977; Mashiotta et al., 1999). Together with the glacial cooling, the winter sea ice realm around Antarctica expanded as far north as 57° latitude, accounting to a $7\text{-}10^\circ$ latitudinal displacement from its modern position (Gersonde et al., 2005). By contrast, reconstructed surface temperature changes in the western Pacific sector were more pronounced over glacial-interglacial cycles. Near the Chilean coast, the glacial cooling accounted to 8°C at the LGM, thus it was at least twice as high as in the central Pacific sector (Ho et al., 2012). This indicates a changed surface circulation in the western Pacific sector. Consistent with interpretations on latest LGM sea surface temperature map, which comprehensively compiles data from the Pacific and from the other world oceans (MARGO Project Members, 2009), the cooling in the western Pacific sector imply a glacially increased northward advection of cold, polar-derived surface waters, linked to an intensification of the South Pacific gyre's eastern boundary current (Ho et al., 2012). The reconstructed surface temperature changes in the western Pacific sector, off Chile, were already high during previous glacial-interglacial cycles. This point toward an important, the distribution of heat, salinity and nutrients impacting, climate mechanism behind, perhaps forced by glacial-interglacial changing Southern Hemisphere westerly winds (Ho et al., 2012). To date, temperature changes for central Pacific sector were constructed only over the last glacial-interglacial cycle (Benz et al., in

preparation; Luz, 1977; Mashiotta et al., 1999). To further constrain this concept, there is a need for long term reconstructions on past temperature evolution there. Changes in the surface circulation are also indicated for the eastern Pacific sector around New Zealand, conceivably tied to changes in the South Pacific gyre's western boundary current circulation (Barrows and Juggins, 2005; Barrows et al., 2007; Bostock et al., 2006; Cortese et al., 2013; Crundwell et al., 2008; Hayward et al., 2012; Hayward et al., 2008; Neil et al., 2004; Pahnke et al., 2003; Pelejero et al., 2006; Schaefer et al., 2005). The extension of current central Pacific sector temperature record is in this regard likewise important.

Downcore benthic $\delta^{13}\text{C}$ data from sediment cores provided valuable information on past changes in the $\delta^{13}\text{C}$ composition of Circumpolar Deep Water occupying the central Pacific sector (Hodell et al., 2000; Matsumoto and Lynch-Stieglitz, 1999; Ninnemann and Charles, 2002). The most comprehensive information on past water $\delta^{13}\text{C}$ evolution comes from one single record (E11-2), which spans however only the last glacial-interglacial cycle (Ninnemann and Charles, 2002). Another record (E22-11) spans the last four glacial-interglacial cycles, but has low resolution, complicating its interpretation (Hodell et al., 2000). A comparison to downcore benthic $\delta^{13}\text{C}$ data from the Atlantic indicates a diverging evolution for the Pacific and Atlantic sectors, ultimately indicating that the glacial deep water exchange between both basins differed significantly in respect to today. The LGM observations have fundamental impact on the interpretation on the glacial ocean's conveyor circulation, with particular implications on glacial Antarctic Bottom Water formation in the Atlantic sector, which occurs today in the Weddell Sea area (Ninnemann and Charles, 2002). After all, they give direction to oceans physical circulation related climate concepts dealing with the atmospheric CO_2 sequestration in the ocean interior (e.g., Adkins, 2013; Curry and Oppo, 2005). However, conclusions regarding the reconstructed central Pacific sector $\delta^{13}\text{C}$ changes are still not constrained for previous glacial stages due to the lack of higher resolved records.

Beside changes in oceans physical circulation and its impact on atmospheric CO_2 sequestration, the central Pacific sector attracted attention regarding the atmospheric CO_2 drawdown by the biological pump. As stated by the Iron Hypothesis (Martin, 1990), increased dust accumulation, thus increased inputs of iron and other trace elements, may have strengthened the biological pump during glacial times, finally contributing to an important portion of the glacial 90 p.p.m.v. decline in the atmospheric CO_2 concentrations (Figure 2.4). Correspondingly, downcore changes in terrigenous fluxes reveal an increased dust accumulation in the subantarctic central Pacific sector during glacial times, when compared to today (Chase et al., 2003; Lamy et al., 2014). Dry glacial conditions in Australia and New Zealand as well as changes in Southern Hemisphere westerly wind field may have promoted dust deflation, prompting a higher dust inputs in the central Pacific sector. Contemporary higher sedimentary opal fluxes point toward higher phytoplankton productivity (Lamy et al., 2014). Taken together, this proposes the subantarctic central Pacific as potential candidate contributing to the glacial atmospheric CO_2 drawdown by a strengthened biological pump, although a decline in phytoplankton

productivity polewards, for instance caused by an extended sea ice coverage, may have countered the net effect (Lamy et al., 2014). Nevertheless, in consistence to the Iron Hypothesis, downcore changes in diatom bound $\delta^{13}\text{C}$, $\delta^{15}\text{N}$ and planktonic foraminiferal $\delta^{13}\text{C}$ indicate lower LGM surface ocean nutrient levels in conjunction with an increased nutrient consumption by phytoplankton for the central Pacific sector, at subantarctic $\sim 55^\circ$ latitude (Loubere and Bennett, 2008; Robinson et al., 2005; Rosenthal et al., 2000a), although on base of planktonic foraminiferal Cd/Ca downcore changes contrasting conclusions were drawn in this regard (Rickaby and Elderfield, 1999).

Another important, biological pump related mechanism for atmospheric CO_2 drawdown, which involves Southern Ocean surface water changes, is proposed by the Silica Leakage Hypothesis. In this regard, maps of the areal distribution in the sedimentary opal fluxes, which yield hints on diatom productivity, indicates for LGM times that the Pacific sector, by comparison to the other Southern Ocean sectors, best fulfill the primary requirements of the Silica Leakage Hypothesis (Bradtmiller et al., 2009). According to the Silica Leakage Hypothesis, changes in diatom community or diatom morphology in adaption to glacial increased dust inputs would result in increased Pacific Sector's surface water silica concentrations. After subduction and equatorward export by Subantarctic Mode Water, this excess silica may have favored phytoplankton productivity in the equatorial Pacific and Chilean costal upwelling zone, in that way intensifying the biological pump there (Brzezinski et al., 2002; Matsumoto et al., 2002; Sarmiento et al., 2004). However, so far reconstructions from the equatorial Pacific upwelling zone either support or weaken the validity of this mechanism (Hendry and Brzezinski, 2014 and references herein). In this regard, inferences based on diatom-bound $\delta^{13}\text{C}$ and $\delta^{15}\text{N}$ from the central Pacific sector indicate that at least a subsurface connection persisted during the LGM, which allow an efficient communication of the central Pacific sector with the equatorial Pacific upwelling zone on Subantarctic Mode Water paths (Robinson et al., 2007). By contrast, inferences on diatom $\delta^{30}\text{Si}$ downcore changes in western Pacific sector supposed the opposite (Crosta et al., 2007). All in all more research is needed on this topic, in particularly as the Silica Leakage Hypothesis mechanism may account with a large, not negligible portion to the 90 p.p.m.v. drop in the atmospheric CO_2 concentrations during glacial times (Matsumoto et al., 2014).

3 Material and Methods

3.1 Study material

This study is based on sediment core samples obtained from the central Pacific sector of the Southern Ocean during R/V Polarstern cruise ANT-XXVI/2 in 2009-2010 austral summer (Figure 3.1). After starting in Chile, cruise ANT-XXVI/2 ended in New Zealand, whereby it explored wide areas of the Pacific ACC domain (Gersonde, 2011, cruise report). With the objective to reconstruct past hydrographic conditions in the subantarctic Pacific sector, on total four sediment cores from the central area were investigated, namely PS75/059-2, PS75/056-1, PS75/079-2 and PS75/076-2. They are from $\sim 55^\circ$ latitude and ~ 3600 m water depth. Their precise coordinates are given in Table 3.1.

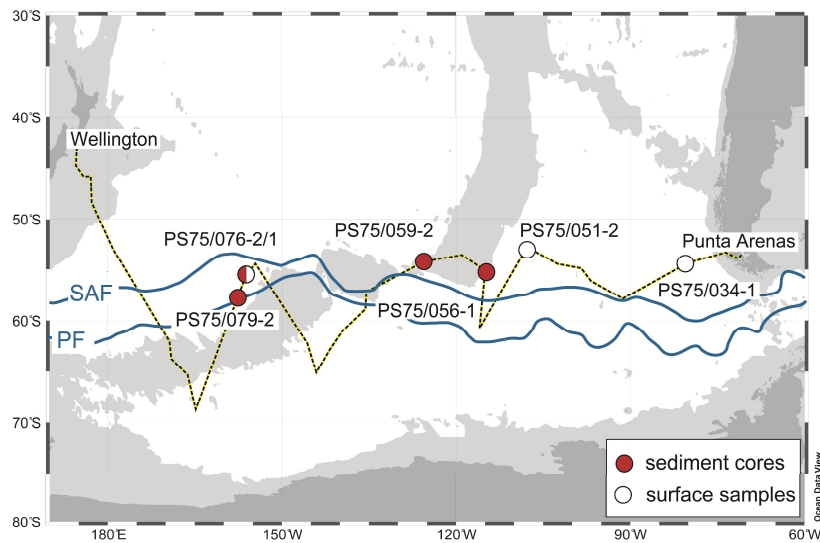


Figure 3.1. Position of the investigated Pacific sector sediment cores (red) and surface samples (white), collected during the ANT-XXVI/2 cruise; Dashed black line indicate the ANT-XXVI/2 cruise track; Blue lines indicate the positions of the Subantarctic (SAF) and Polar (PF) Front; Ocean bathymetry above 3500 m water depth is shaded in gray; The figure was constructed using Ocean Data View (Schlitzer, 2012).

The focus of the investigations was on cores PS75/059-2 and PS75/056-1, which were obtained from opposing sides of the East Pacific Rise, near to the Eltanin Fracture Zone, and display continuously high sedimentary carbonate contents. Their surface positions are immediately north to the Subantarctic Front (Figure 3.1). Cores PS75/079-2 and PS75/076-2 were raised from the Antarctic-Pacific Ridge, close to the Polar Front and south of the Subantarctic Front, respectively. They have high opal content downcore, while their sedimentary carbonate content records are discontinuously, with carbonate occurring only in interglacial sections. According their age models (*Section 3.3*), cores PS75/059-2, PS75/079-2 cover approximately the last 500 ka. Core PS75/076-2 dates back to about 1000 ka, but was closer investigated only for the past 500 ka. Their corresponding core lengths are given in Table 3.1. Characterized by moderate sedimentation rates of ~ 3 cm/ka in average, their sediment records provide on orbital timescales valuable information on the most recent climate cycles. Core PS75/056-1 dates back to only about 260 ka, while its average sedimentation rate is ~ 6.0 cm/ka in the upper part

(6-110 ka) and ~3.0 cm/ka further downcore (110-260 ka). Additionally to the sediment cores, few surface samples from multi-cores were investigated in this study (Table 3.1).

Table 3.1. Coordinates of the investigated Pacific sector sediment cores and surface samples, listed together with the used proxy methods. Proxy data collections, which were not completely or not self-performed, are denoted as superscripts d and e.

Core ID	Latitude [°]	Longitude [°]	Depth [m]	Length [m]	
SL PS75/056-1	-55,16	-114,79	3581	10,21	benthic $\delta^{18}\text{O}$, $\delta^{13}\text{C}$; planktonic $\delta^{18}\text{O}^e$, $\delta^{13}\text{C}^e$, Mg/Ca ^e
KOL PS75/059-2	-54,22	-125,43	3613	13,98	benthic $\delta^{18}\text{O}$, $\delta^{13}\text{C}$; planktonic $\delta^{18}\text{O}$, $\delta^{13}\text{C}$, Mg/Ca; XRF-scan ^d ; carbonate ^c ; opal ^c
KOL PS75/076-2 ^{a,b}	-55,53	-156,14	3742	20,59	benthic $\delta^{18}\text{O}$, $\delta^{13}\text{C}$; planktonic $\delta^{18}\text{O}$, $\delta^{13}\text{C}$, Mg/Ca; XRF-scan ^d ; carbonate ^{c,e}
KOL PS75/079-2 ^a	-57,50	-157,23	3770	18,51	benthic $\delta^{18}\text{O}$, $\delta^{13}\text{C}$; planktonic $\delta^{18}\text{O}$, $\delta^{13}\text{C}$, Mg/Ca; XRF-scan ^d ; carbonate ^{c,e}
MUC PS75/034-1	-54,37	-80,08	4450	-	planktonic $\delta^{18}\text{O}$, $\delta^{13}\text{C}$, Mg/Ca
MUC PS75/051-2	-52,82	-107,80	3977	-	planktonic $\delta^{18}\text{O}$, $\delta^{13}\text{C}$, Mg/Ca
MUC PS75/076-1	-55,53	-156,13	3745	-	planktonic $\delta^{18}\text{O}$, $\delta^{13}\text{C}$, Mg/Ca; benthic $\delta^{18}\text{O}$, $\delta^{13}\text{C}$

^a sampled only in intervals, where enough carbonate was present ^b sampled down to 11.88 m ^c contents in weight percent of dry bulk sediment ^d involvement in data collection ^e no involvement in data collection

During Polarstern cruise ANT-XXVI/2 the studied sediment cores were recovered either by gravity or piston corer devices. The sediment cores were subdivided into 1 m long segments on board such that sequences of core sections, each sealed in a plastic liner, were obtained. After analyses of the physical properties (GRA-density, magnetic susceptibility) with a GEOTEK Multi-Sensor Core Logger (MSCL), the core sections were split into archive and working halves. From the working halves small amounts of sample material (~10 cm³ sample volume) were taken in 10 cm resolution for later bulk parameter analysis. Further, a visual core description was performed on the archive halves. As an exception, the core sections of core PS75/056-1 were split ashore at the Alfred Wegener Institute, Bremerhaven. The surface sediments were recovered by a multi-core device. If sediment filled, the multi-core tubes were cooled down to -20 °C. Afterwards the tubes were removed from the frozen sediment material, which was then vacuum-packed for transport. A more detail description of the full work flow on the ANT-XXVI/2 cruise is given in the cruise report (Gersonde, 2011).

The sampling was carried out at the laboratories of the Alfred Wegener Institute, Bremerhaven, between the years 2010 and 2013. In case of cores PS75/059-2 (13.98 m core length) and PS75/056-1 (10.21 m core length), the working halves were sampled in 1 cm thick slices (~25 cm³ sample volume) with continuous 5 cm resolution. Cores PS75/079-2 (18.51 m core length) and PS75/076-2 (20.59 m core length, sampled down to 11.88 m) were sampled only in intervals, where enough carbonate was present. There, samples of 1 cm thick slices were taken in 10 cm or 5 cm resolution. Both, planktonic and benthic foraminifera occurred in almost all samples. This allowed the primary use of carbonate-based proxies to reconstruct past oceanic changes at the surface and at depth. An overview of the different proxies, which were applied to the sediment cores, is provided in Table 3.1, while a basic background to each proxy method is given in *Section 3.2* below.

3.2 Proxy methods and analyses

In *Chapters 3, 4, 5* and in the *Appendix* paleoceanographic data are discussed, which were obtained by a number of proxy methods, primary based on the isotopic and chemical analysis of foraminiferal shell calcite. Prior to the data generation, the sample material was freeze dried, wet sieved at mesh size 63 μm , rinsed with deionized water and dried at temperatures lower than 40 $^{\circ}\text{C}$. Afterwards the planktonic and benthic foraminiferal species used for the analyses were manually removed from the 250-315 μm and 315-355 μm sand size fractions, respectively.

3.2.1 Stable isotope analysis

The stable oxygen ($\delta^{18}\text{O}$) and carbon ($\delta^{13}\text{C}$) isotopic composition of benthic and planktonic foraminiferal shell calcite is routinely used in paleoceanography, as it records ancient sea water characteristics during shell calcification. The foraminiferal $\delta^{18}\text{O}$ signature is controlled by two components, namely the sea water $\delta^{18}\text{O}$ composition and the sea water temperature. Dating back to early observations (Emiliani, 1955; Shackleton, 1967), it is today clear that first order downcore variations in $\delta^{18}\text{O}$, which occur globally, display primary whole-ocean changes in the sea water $\delta^{18}\text{O}$ composition caused by the glacial storage of $\delta^{18}\text{O}$ -depleted water in continental ice sheets. As these changes occur within ~ 4 ka almost contemporaneously in all major ocean basins (Lisiecki and Raymo, 2009; Skinner and Shackleton, 2005), foraminiferal $\delta^{18}\text{O}$ provides an important stratigraphic tool on orbital timescales. Apart from the whole-ocean changes, the foraminiferal $\delta^{18}\text{O}$ signature yields insights on local changes in the sea water $\delta^{18}\text{O}$ composition and temperature. This offers further paleoceanographic applications, such as the tracing of water masses by their individual $\delta^{18}\text{O}$ -temperature characteristics (e.g., Lynch-Stieglitz, 2003; Ravelo and Hillaire-Marcel, 2007).

The foraminiferal $\delta^{13}\text{C}$ signature reflects primary the $\delta^{13}\text{C}$ signature of sea water dissolved inorganic carbon (DIC), while its present day distribution in the ocean is closely related to nutrient cycling, thus to the biological production and decay of organic matter. At depth, it is therefore linearly, inversely related to the distribution of labile nutrients, like phosphate (Kroopnick, 1985). Physical carbon isotope fractionation during air–sea exchange represents another important factor, which influence the sea water $\delta^{13}\text{C}$ composition. At the surface, air–sea exchange can cause $\delta^{13}\text{C}$ values, which are much different to the $\delta^{13}\text{C}$ values expectable from the nutrient concentrations only (Broecker and Maier-Reimer, 1992; Lynch-Stieglitz et al., 1995). Its present-day impact on the deep ocean $\delta^{13}\text{C}$ distribution pattern is comparably minor (Broecker and Maier-Reimer, 1992; Lynch-Stieglitz et al., 1995), while it was probably major in the past (Marchitto and Broecker, 2006). Foraminiferal $\delta^{13}\text{C}$ is an important paleoceanographic proxy for reconstructing the distribution of water masses and their changing characteristics. Mainly it is used to infer changes in deep water circulation. Further it provides valuable information on surface biological processes, for instance on the nutrient consumption by phytoplankton. Downcore variations of foraminiferal $\delta^{13}\text{C}$ display besides local, also whole-ocean changes in the sea water $\delta^{13}\text{C}$ composition. In turn, this allows inferences on the carbon transfer

between Earth's major carbon reservoirs (atmosphere, biosphere, ocean and ocean sediments) and, thus, provides clues to past carbon cycling (e.g., Lynch-Stieglitz, 2003; Ravelo and Hillaire-Marcel, 2007).

Benthic foraminiferal species, which are commonly used in paleoceanographic studies, incorporate the sea water $\delta^{13}\text{C}$ signal in linear, one to one relationship into their shell calcite, while in dependency of the used species type, constant, clearly defined offsets to the sea water $\delta^{13}\text{C}$ signature are documented (Curry et al., 1988; Duplessy et al., 1984; Duplessy et al., 1988). Yet, there are observations from a few areas, which indicate that the $\delta^{13}\text{C}$ incorporation can be locally impaired by biological and environmental factors (Hodell et al., 2003; Mackensen et al., 1993). Thus, the benthic foraminiferal $\delta^{13}\text{C}$ signal may not always mirror the water mass $\delta^{13}\text{C}$ composition properly, what needs to be considered in its paleoceanographic interpretation. In contrast to benthic foraminifera, the $\delta^{13}\text{C}$ incorporation of planktonic foraminifera occurs in less predictable manner, as besides the sea water $\delta^{13}\text{C}$ signal other factors play a role. For instance, in case of species *Globigerina bulloides*, used in this study, the $\delta^{13}\text{C}$ incorporation is considerably co-determined by ambient sea water temperature and carbonate ion concentration (Bemis et al., 2000; Spero et al., 1997). Further, limited information on planktonic foraminifera live today and particularly for the past, for instance with regard to calcification depth or shell flux seasonality, complicates the paleoceanographic use of the planktonic foraminiferal $\delta^{13}\text{C}$ signal. Altogether, caution is required in interpreting the planktonic, but also the benthic foraminiferal $\delta^{13}\text{C}$ signature. Even so, it is a widely applied, very important proxy parameter in paleoceanography (e.g., Lynch-Stieglitz, 2003; Ravelo and Hillaire-Marcel, 2007).

The foraminiferal $\delta^{18}\text{O}$ the $\delta^{13}\text{C}$ composition of, if possible, 3-4 tests of the benthic foraminiferal species *Cibicidoides wuellerstorfi* and *Cibicidoides kullenbergi* was analyzed on Finnigan MAT 251 and Finnigan MAT 253 mass spectrometers, each coupled with a Kiel Carbo (II, IV) carbonate preparation device at the Alfred Wegener Institute, Bremerhaven. Besides, subsamples of initially about 35 tests of the planktonic foraminiferal species *Globigerina bulloides* were analyzed on Finnigan MAT 253 mass spectrometers coupled to Kiel Carbo (IV) carbonate preparation devices at the GEOMAR, Kiel, and the Alfred Wegener Institute, Bremerhaven. The subsamples form pairs with those used for the Mg/Ca analyses and were likewise treated with the cleaning method outlined in Section 3.2.2. All mass spectrometers were calibrated via the NIST19 international standard to the PDB scale, with the isotope ratios of $\text{O}^{18}/\text{O}^{16}$ and $\text{C}^{13}/\text{C}^{12}$ being expressed in δ -notation versus Vienna Peedee Belemnite (VPDB). The reproducibility of the results (68% confidence level) based on the repeated analyses of internal-laboratory carbonate standards was on all machines better than $\pm 0.08\text{‰}$ and $\pm 0.06\text{‰}$ for $\delta^{18}\text{O}$ and $\delta^{13}\text{C}$, respectively.

3.2.2 Mg/Ca analysis - paleotemperature reconstructions

The Mg/Ca ratio of foraminiferal shell calcite is a widely used paleothermometer, which is applicable for benthic and planktonic foraminiferal species. Though, in this study, Mg/Ca ratios were determined only on the planktonic foraminiferal species *Globigerina bulloides*. The method bases on the fact that trace amounts of Mg are incorporated during shell formation, substituting for Ca lattice positions in the shell calcite. As the incorporation of Mg into calcite depends on the ambient sea water temperature, the respective Mg/Ca ratios allow reconstructing sea water temperatures at depths where the shell formation has occurred. A principle which was early reported by Chave (1954), before it was continuously refined for wide paleoceanographic use (e.g., Cronblad and Malmgren, 1981; Lea et al., 1999; Mashiotta et al., 1999; Nürnberg, 1995; Rosenthal et al., 2000b). The sea water Mg/Ca ratio remained in practice constant on glacial-interglacial timescales, owing to the high ocean residence times for Mg and Ca. Thus, downcore Mg/Ca ratios can be directly converted to sea water temperatures without any whole-ocean corrections (e.g., Barker et al., 2005; Lea, 2003).

The incorporation of Mg into shell calcite follows according thermodynamic considerations an exponential function, with higher Mg/Ca ratios corresponding to higher temperatures. However, the way of Mg incorporation is further controlled by different, very complex biological and environmental factors, while their individual impacts are still insufficient assessed. Thus, current calibrations of the Mg/Ca ratios to temperatures were obtained empirically based on the information from core-top, culture and sediment trap observations. This led to the development of a number of calibration equations for different foraminiferal species, which are exponential, but differ in their specific parameterization (e.g., Barker et al., 2005; Lea, 2003). In this study the Mg/Ca ratios were converted in temperatures by the *Globigerina bulloides* specific equation (1) below, which base on Southern Ocean core-top and laboratory culturing data (Mashiotta et al., 1999).

$$(1) \text{ Mg/Ca} = 0.474 \exp(0.107 T) \quad (\text{Mashiotta et al., 1999})$$

The equation yields mean-annual surface temperatures, while it has a calibration range from 10 °C to 26 °C. Its standard error is 0.8 °C (Mashiotta et al., 1999). As discussed in *Chapter 4*, at the study location the equation overestimates modern surface temperatures at depths where *Globigerina bulloides* calcifies, even when taking seasonality into account. Despite consistently ~3 °C too high absolute values, it produces however adequate amplitudes, thus it provides valuably information on the paleotemperature evolution there.

Prior to analyses of the Mg/Ca ratio of the foraminiferal shell calcite, the shells were cleaned with the aim to remove diagenetic contaminates as 1) clay minerals, 2) organic matter, 3) Fe/Mn coatings and 4) barite (Barker et al., 2003). Sample cleaning was performed at the laboratories of the GEOMAR, Kiel. Following the cleaning protocol of Barker et al. (2003) with modifications of Nürnberg and Groeneveld (2006), ~35 shells of the planktonic foraminiferal species *Globigerina bulloides* were gently crushed between glass plates to open their chambers. After homogenization, the sample

material was split into two subsamples aliquots, which were then transferred in plastic vials. To remove the diagenetic contaminants, the sample material was stepwise treated with 1) ultrapure methanol, 2) ultrapure (1%) NaOH/H₂O₂ and 3) ultrapure (10%) HNO₃. Ruinously intercalated were rinsing steps with deionized water together with ultrasonification to promote the removal of contaminant particles and reagents from the sample material. The rinsing solution, overlying the sample material in the plastic vials, was respectively removed by pipette. After completion of the sample cleaning, one half of the subsamples was used for stable isotope analyses, as described in *Section 3.2.1*, the other half was used for chemical analyses to determine the Mg/Ca ratio of the foraminiferal shell calcite.

The chemical composition or precisely the Mg/Ca of the first half of the subsamples was analyzed on a Varian 720-ES inductively coupled plasma – optical emission spectrometer (ICP-OES) at the GEOMAR Kiel. The reproducibility for Mg/Ca based on the ECRM752-1 standard was better than ± 0.1 mmol/mol. The cleaning efficiency was ensured by parallel analyzed of the Fe/Ca and Mn/Ca ratios, which are indicative for contaminants such as clay minerals.

3.2.3 Mg/Ca and $\delta^{18}\text{O}$ pairs - sea water $\delta^{18}\text{O}$ reconstructions

Paired Mg/Ca and $\delta^{18}\text{O}$ data determined on the same spited sample material find increasing use in paleoceanography, as this ensures that the respective sea water signals were simultaneously incorporated during times of foraminiferal shell calcification. As also applied in this study on planktonic foraminiferal species *G. bulloides*, their combination allows removing the temperature part from the $\delta^{18}\text{O}$ signal to infer the sea water $\delta^{18}\text{O}$ composition (e.g., Lea et al., 2000; Mashiotta et al., 1999). The sea water $\delta^{18}\text{O}$ composition was derived by calibration equation (2) (Shackleton, 1974). The respective temperatures were derived from the Mg/Ca ratios as described in *Section 3.2.2*. The standard error of sea water $\delta^{18}\text{O}$ calculations is commonly high and has typical values of $\pm 0.2\%$ (68% confidence level) and $\pm 0.4\%$ (95% confidence level) (Rohling, 2007)

$$(2) \delta^{18}\text{O}_w = \delta^{18}\text{O}_c + 0.27 - (4.38 - \sqrt{(4.38^2 - 0.4(16.9 - T))}) / 0.2 \quad (\text{Shackleton, 1974})$$

Past whole-ocean changes in the sea water $\delta^{18}\text{O}$ composition caused by continental ice volume changes were removed downcore by subtracting the mean-ocean sea water $\delta^{18}\text{O}$ curve constructed by Waelbroeck et al. (2002). As the surface water $\delta^{18}\text{O}$ composition is controlled by evaporation and precipitation, the ice volume-corrected sea water $\delta^{18}\text{O}$ provides valuable insights on local changes in the freshwater fluxes. Today, the surface water $\delta^{18}\text{O}$ composition is linearly related to sea surface salinity, while the $\delta^{18}\text{O}$ -salinity slopes and intercepts differ regionally (LeGrande and Schmidt, 2006; LeGrande and Schmidt, 2011). The sea water $\delta^{18}\text{O}$ composition inferred from planktonic foraminifera such as *G. bulloides*, which dwell in the ocean's surface layer, is thus linked to the surface salinity. As modern $\delta^{18}\text{O}$ -salinity slopes and intercepts presumably changed throughout the past, it is though critical to convert downcore sea water $\delta^{18}\text{O}$ values quantitatively into paleosalinity (LeGrande and Schmidt, 2011; Rohling, 2007). Nevertheless, sea water $\delta^{18}\text{O}$ reconstructions yield semi-quantitative

salinity estimates and are widely applied in paleoceanography. Not least, this is due to the fact that beside temperature, salinity is a fundamental parameter to characterize the climate state in particular, if it is reconstructed for the sea surface, where ocean and atmosphere interact.

3.2.4 Biogenic opal analysis

The biogenic opal (biogenic silica) content determined on bulk sediments is often used to infer changes in productivity by surface dwelling diatom algae and other silica secreting organisms, although factors such as dilution by non-opal material or opal dissolution after deposition can complicate its downcore interpretation. According the automatic leaching method of Müller and Schneider (1993), the biogenic opal content was determined at the Alfred Wegener Institute, Bremerhaven, using a small amount of the sample material initially taken for bulk parameter analyses. The biogenic opal was brought in solution by treating the sample material with (1M) NaOH at 85 °C for 4-5 minutes, carried out in a cylindrical steel container within a water bath. The silica concentration increase during the dissolution process was continuously detected with a simple autoanalyser for continuous flow analyses by molybdate-blue spectrometry. From so obtained concentration-time curve the opal content was then graphically determined, based on a procedure initially described by de DeMaster (1981).

3.2.5 Biogenic carbonate analysis

The biogenic carbonate content of bulk sediments is controlled by a number of factors such as dilution by non-carbonate material, carbonate dissolution at the seafloor or surface carbonate productivity. Depending on the specific oceanic setting, downcore carbonate content patterns can provide paleoceanographic hints on past surface carbonate productivity or bottom water corrosively changes. The biogenic carbonate content was inferred from the total carbon (TC) and organic carbon (C_{org}) contents, all expressed in weight percent of dry bulk sediment. The TC and C_{org} contents were, respectively, determined on CNS analyzer (Elementar Vario EL III) and CS analyzer (CS-2000 Eltra) at the Alfred Wegener Institute, Bremerhaven, on small amounts of the freeze dried and homogenized sediment material taken for bulk parameter analyses. The $CaCO_3$ content was calculate from the equation: $CaCO_3 [wt. \%] = 8.33(TC [wt. \%] - TOC[wt. \%])$

3.2.6 X-ray florescence core scans

X-ray florescence core scanning provide high resolution records on the downcore, semi-quantitative elemental changes in sediment cores, detected as intensities in counts per second [cps]. When calibrated against data from bulk sediment analyses, these intensities can be directly converted into elemental concentrations or mineralogical contents, such as carbonate contents. Using an AvaatechTM X-ray florescence core scanner, the intensities for a number of elements were obtained from the studied sediment cores at the Alfred Wegener Institute, Bremerhaven. This includes the intensities for the elements Fe, Ti, Si, Al, Ca, Sr and Ba, which find, besides stratigraphic purpose, wide paleoceanographic application. For instance, changes in the downcore Ca intensities can provide

information on the downcore changes in sedimentary carbonate content and, thus, on past variations in carbonate preservation or carbonate surface production.

The Avaatech™ X-ray fluorescence core scanner is a nondestructive analytical system, which conducts fast elemental analyses along the plane surfaces of sediment core halves, with downcore resolution of up to 1 mm. Its functioning uses the principle that atoms, when stimulated by an external X-ray source, emit an element characteristic X-ray wavelength spectrum, which is then detected. In this way the elements can be identified and also quantified. For analyses, the studied core halves were covered with a thin SPEXCerti Prep Ultralene foil to avoid contamination of the measurement unit and desiccation of the sediment during the XRF scanning operation. The scans were performed in 5 to 10 mm resolution, with energy settings of 10, 30 and 50 kV for the X-ray generation to gain intensities for each required element. A more detailed description of the method is given by Richter et al. (2006) and on the Avaatech™ homepage (<http://www.avaatech.com>).

3.3 Age control

In *Chapter 4*, the age models for cores PS75/059-2 and PS75/056-1 were constructed by correlating their benthic foraminiferal $\delta^{18}\text{O}$ records to the LR04 benthic $\delta^{18}\text{O}$ stack on its own LR04 age scale (Lisiecki and Raymo, 2005). In *Capture 6*, in case of core PS75/059-2, again the LR04 benthic $\delta^{18}\text{O}$ stack based age model was used. Past benthic $\delta^{18}\text{O}$ changes occurred diachronous in the Atlantic and the Pacific around glacial terminations, with the Atlantic changes leading ~ 4 ka on average (Lisiecki and Raymo, 2009). Thus, although the age models of cores PS75/059-2 and PS75/056-1 are robust on orbital timescale, at terminations they are afflicted with higher uncertainty. In *Capture 5*, the age models of core PS75/059-2 and PS75/056-1 base on the correlation of their Mg/Ca temperature records to the Antarctic EPICA Dome C deuterium (δD) temperature record on the EDC3 timescale (Jouzel et al., 2007; Parrenin et al., 2007). Downcore glacial-interglacial changes in iron concentrations and intensities in the central Pacific sector reflect varying dust inputs (Lamy et al., 2014). As discussed in the *Appendix* (Lamy et al., 2014), this allows a direct correlation with the Antarctic EPICA Dome C dust record (Lambert et al., 2008) and provides a chronostratigraphic framework for the different Pacific sector sediment cores. In *Chapter 5*, the age model of core PS75/079-2 bases on the correlation of its iron content record to the Antarctic EPICA Dome C dust record (Lamy et al., 2014), but was further modified by aligning the in interglacial intervals obtained benthic $\delta^{18}\text{O}$, planktonic $\delta^{18}\text{O}$ and Mg/Ca temperature data of core PS75/079-2 to the respective records of cores PS75/059-2 on the EDC3 timescale.

Chapter 4 – Pacific-Atlantic Circumpolar Deep Water coupling during the last 500 ka

Johannes Ullermann (1), Frank Lamy (1), Ulysses Ninnemann (2), Lester Lembke-Jene (1), Rainer Gersonde (1), Gerhard Kuhn (1), Ralf Tiedemann (1)

Prepared to be submitted to Paleocyanography

1. Alfred-Wegener-Institut Helmholtz-Zentrum für Polar- und Meeresforschung, Am Alten Hafen 26, 27568 Bremerhaven, Germany

2. Department of Earth Science and Bjerknes Centre of Climate Research, University of Bergen, Allegaten 55, Bergen, N-5007, Norway

Abstract

Investigating the inter-basinal deep water communication between the Pacific and Atlantic basins over glacial-interglacial climate cycles is important for understanding circum-Antarctic Southern Ocean circulation changes and their impact on oceanic CO₂ storage. We use benthic foraminiferal $\delta^{13}\text{C}$ records from the southern East Pacific Rise to characterize the $\delta^{13}\text{C}$ composition of Circumpolar Deep Water in the South Pacific, prior to its transit through the Drake Passage into the deep South Atlantic. A comparison with published South Atlantic deep water records from the northern Cape Basin suggests a continuous water mass exchange throughout the past 500 ka. Almost identical glacial-interglacial $\delta^{13}\text{C}$ variations imply a common deep water evolution in both basins through persistent Circumpolar Deep Water exchange. By contrast, deep waters occupying the abyssal southern Cape Basin and the southernmost South Atlantic likely evolved independently as benthic $\delta^{13}\text{C}$ indicate an irregular, but recurring northward expansion of Antarctic Bottom Water, associated with dynamic changes in its $\delta^{13}\text{C}$ endmember signature. Overall, the delimitation of Circumpolar Deep Water yields new insights on past changes in Antarctic Bottom Water lateral extent in the South Atlantic. It appears that the current Last Glacial Maximum picture, with the occurrence of extremely depleted $\delta^{13}\text{C}$ values in the southernmost South Atlantic, was unusual in the context of previous glaciations. This must be taken into account when drawing inferences about the ocean's role on atmospheric CO₂ storage in the Atlantic interior.

4.1 Introduction

For decades, benthic foraminiferal $\delta^{13}\text{C}$ -based studies in the Southern Ocean have focused largely on the South Atlantic, as the region is an important intersection point of major deep water masses and thus crucial for understanding the role of ocean's physical circulation over glacial-interglacial climate change, particularly with regard to the carbon cycle. At this critical junction, North Atlantic Deep Water (NADW) and Weddell Sea-derived Antarctic Bottom Water (AABW) mix with Circumpolar Deep Water (CDW), which is inflowing from the South Pacific.

So far, past $\delta^{13}\text{C}$ compositional changes of Pacific CDW, prior to its transition through Drake Passage into the Atlantic, have been less well constrained and remain largely uncertain. Only a few benthic foraminiferal $\delta^{13}\text{C}$ -based studies have attempted to define its $\delta^{13}\text{C}$ composition from the Southeast Pacific (SE Pacific) and discussed the inter-basin coupling to the Southeast Atlantic (SE Atlantic) (Hodell et al., 2000; Matsumoto and Lynch-Stieglitz, 1999; Ninnemann and Charles, 2002). Of these studies, the detailed work by Ninnemann and Charles (2002) revealed that an interbasin $\delta^{13}\text{C}$ gradient of $\sim 0.6\text{‰}$ developed between the East Pacific Rise and the deep southern Cape Basin for the Last Glacial Maximum (LGM). In contrast, today the eastward advection of CDW continuously homogenizes the deep water properties between both areas (Orsi et al., 1999; Orsi et al., 2002; Reid, 1986; Reid, 1989). At present, nearly no interbasin $\delta^{13}\text{C}$ gradient exists (Kroopnick, 1985). Its glacial development apparently originates from a much higher $\delta^{13}\text{C}$ decrease of the deep waters occupying the southern Cape Basin and adjoining southernmost South Atlantic areas (Curry and Oppo, 2005; Mackensen et al., 2001; Martínez-Méndez et al., 2009; Ninnemann and Charles, 2002) than those occupying the East Pacific Rise (Ninnemann and Charles, 2002). Accordingly, past $\delta^{13}\text{C}$ compositional evolution of CDW was diverging in the Pacific and Atlantic, indicating a fundamentally altered deep water exchange between both basins at the LGM. This reconfiguration was accompanied by changes in the formation mode of Atlantic-generated AABW or its glacial equivalent (Ninnemann and Charles, 2002), which apparently had a highly depleted endmember $\delta^{13}\text{C}$ signature, probably due to changes in its formation mechanisms (e.g., Marchitto and Broecker, 2006). However, this knowledge about the deep water exchange between the Pacific and Atlantic basins is mainly restricted to the last glacial-interglacial cycle and based on the benthic $\delta^{13}\text{C}$ record of only a single core (E11-2) (Ninnemann and Charles, 2002) to define the Pacific CDW changes. That record was retrieved from $\sim 3000\text{ m}$ water depth, close to the core layer of poleward-flowing Pacific Deep Water (PDW). Potential changes in the influence of this deep water mass may therefore have compromised the Pacific CDW record (Ninnemann and Charles, 2002).

Changes in physical ocean circulation likely accounted to a large portion for the $\sim 90\text{ p.p.m.v}$ declines in atmospheric CO_2 concentrations, which occurred during each of the last five glaciations (Lüthi et al., 2008; Petit et al., 1999). Concepts, that invoke atmospheric CO_2 storage in the deep ocean (Adkins, 2013 and references herein; Toggweiler, 1999), particularly in the Atlantic interior, commonly assume that the LGM distribution of $\delta^{13}\text{C}$ in the Atlantic displayed a higher vertical

gradient than today at mid-depth, thus indicating a much stronger intermediate to deep ocean stratification (Curry et al., 1988; Curry and Oppo, 2005; Duplessy et al., 1988; Hoffman and Lund, 2012; Ninnemann and Charles, 2002). Accordingly, the LGM distribution of $\delta^{13}\text{C}$ may imply less vertical mixing of glacial-AABW (low- $\delta^{13}\text{C}$) and glacial-NADW (high- $\delta^{13}\text{C}$), which in essence would increase the deep oceans ability to sequester atmospheric CO_2 . In this regard, a quantified understanding of the LGM $\delta^{13}\text{C}$ distribution in the Atlantic is important. Particularly, the occurrence of the extremely low $\delta^{13}\text{C}$ values in the southernmost South Atlantic is critical, as they provide indications on the LGM endmember $\delta^{13}\text{C}$ signature of AABW (Curry and Oppo, 2005; Marchitto and Broecker, 2006), which is a basic parameter for ocean modeling and numerical calculations (e.g., Gebbie, 2014; Hoffman and Lund, 2012). In terms of understanding the cycling in atmospheric CO_2 concentrations it is therefore also a decisive question, whether the extreme glacial depletion of southernmost South Atlantic $\delta^{13}\text{C}$ values, compared to those of the South Pacific, occurred systematically during previous glaciations, in particular, since stronger ocean stratification in the Atlantic was an obviously recurring pattern (Hodell et al., 2003b). An improved characterization of the Pacific CDW changes over previous climate cycles is a prerequisite in this regard.

In this study, we extend and improve the temporal and spatial coverage of the currently sparse Pacific CDW record by presenting two new, well-resolved benthic foraminiferal $\delta^{13}\text{C}$ records (PS75/059-2, PS75/056-1) from the SE Pacific, southern East Pacific Rise that were recovered from the core Pacific CDW layer (about 500 m deeper than existing reference record E11-2 (Ninnemann and Charles, 2002)). We discuss the inter-basin link to the SE Atlantic and its implications on atmospheric CO_2 storage over the past 500 ka, by comparing our results to published records RC13-229 (~4200 m water depth) and ODP Site 1089 (~4600 m water depth) from sites in the abyssal northern and southern Cape Basin, respectively. The Cape Basin sites are both today bathed in CDW, but are well located to detect Atlantic-internal changes of past AABW export (*Section 4.2*).

4.2 Modern deep water circulation and tracer distribution

All core sites in this study are presently bathed in CDW (Figures 4.1 and 4.2), which continuously forms through mixing with northern- and southern-sourced deep water masses as it flows eastward within the Antarctic Circumpolar Current (ACC) (Broecker et al., 1998; Johnson, 2008). In the SE Pacific, Ross Sea-generated AABW spreads into the SE Pacific Basin at abyssal depths, without directly influencing the shallower core sites at the East Pacific Rise (Orsi et al., 1999; Pardo et al., 2012). Unlike in the SE Pacific, the core sites in the SE Atlantic are directly influenced by the SW Atlantic inflow of two major water masses, namely NADW and AABW generated in the Weddell Sea. Their incorporation into CDW is facilitated by turbulent vertical mixing over rough topography in the Scotia Sea, immediately after CDW has entered the South Atlantic through the Drake Passage (Naveira Garabato et al., 2002; Naveira Garabato et al., 2007; Orsi et al., 1999). Thus, the South Atlantic CDW composition gradually becomes modified. Even so, the source of the deep water that

fills the Cape Basin today is Pacific CDW, which enters the South Atlantic basin through the Drake Passage (Orsi et al., 1999; Reid, 1989).

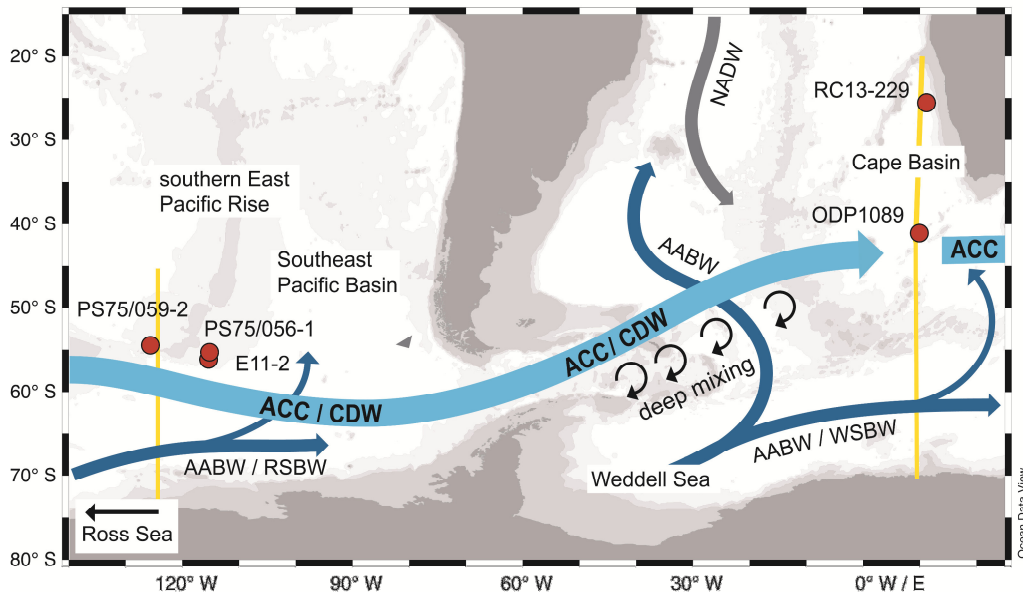


Figure 4.1. Map showing positions of discussed cores in the context of the modern deep water hydrography; Circles indicate position of cores discussed in this study; Arrows shows schematic flow path of major deep water masses (CDW, Circumpolar Deep Water; AABW, Antarctic Bottom Water; NADW, North Atlantic Deep Water); Two subtypes of AABW are indicated (RSBW, Ross Sea Bottom Water; WSBW, Weddell Sea Bottom Water); Positions of the hydrographic sections displayed in Figure 4.2 are indicated as yellow lines.

Sea water $\delta^{13}\text{C}$ is a non-conservative tracer, thus its modern distribution in the deep sea depends, besides water mass mixing, mainly on biological cycling. Further, isotopic fractionation during air-sea gas exchange has a contributing influence on sea water $\delta^{13}\text{C}$ (e.g., Lynch-Stieglitz, 2003). Altogether, it is today linearly related to sea water nutrient concentrations at depths, for instance to the phosphate concentrations (Kroopnick, 1985). Figure 4.2 (a, b) shows the sea water $\delta^{13}\text{C}$ distribution obtained from phosphate in two north-south sections at longitudes of the SE Pacific and SE Atlantic core sites. Accordingly, they are overlain by CDW with similar $\delta^{13}\text{C}$ signature, which accounts to ~ 0.25 ‰ (Table 4.1). In the SE Pacific, CDW at the core sites is rather uniform distributed. Only at water depths above ~ 1200 m, comparably closely to core site E11-2, a higher influence of poleward flowing, aged PDW (low- $\delta^{13}\text{C}$) is indicated. This contrasts to the SE Atlantic, where the sea water $\delta^{13}\text{C}$ distribution is much differentiated. The high values at mid-depth (2000 m to 3500 m) are due to the intrusion of NADW (high- $\delta^{13}\text{C}$), intersecting CDW into an upper and lower layer. After passing through Drake Passage, CDW interacts also with Weddell Sea AABW (low- $\delta^{13}\text{C}$) at its base (Orsi et al., 1999). In connection therewith, a notable north-south gradient exists across the entire SE Atlantic at depths, due to continuously increasing contributions of AABW toward Antarctica (Broecker et al., 1998; Johnson, 2008). Considering the Cape Basin, the regional north-south gradient is small, accounting for less than 0.1 ‰ higher bottom water $\delta^{13}\text{C}$ values at northern Cape Basin core site RC13-229 than at southern Cape Basin core site ODP 1089 (Table 4.1). The apparent oxygen

utilization (AOU) distribution further illustrates water masses interaction in both basins (Figure 4.2 c, d). For the SE Pacific section, the AOU shows that nearly homogenous CDW occupies wide areas, whereas AABW from the Ross Sea is isolated to the deep southeast Pacific basin. For the SE Atlantic section the AOU clearly outlines CDW as a separate water mass, together with NADW and AABW from the Weddell Sea. The high AOU signature at the East Pacific Rise is traceable to the northern and southern Cape Basin.

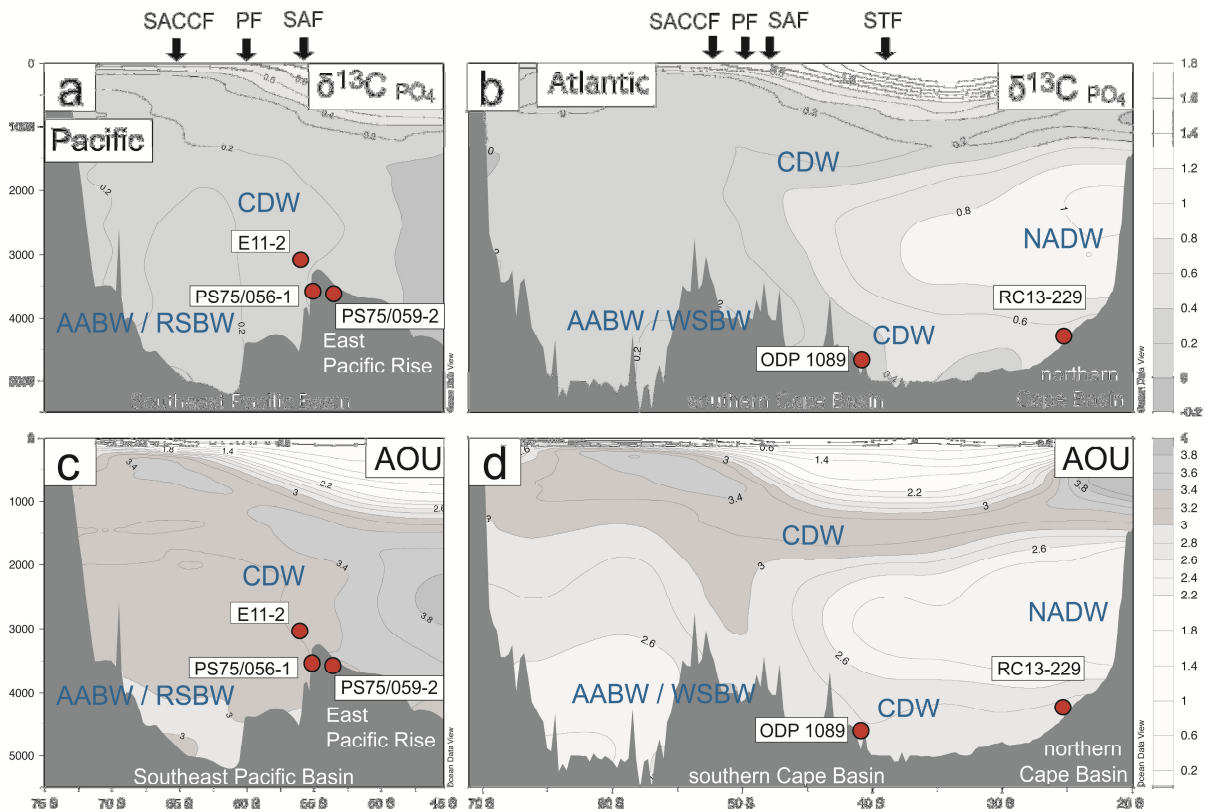


Figure 4.2. Modern $\delta^{13}\text{C}$ (PO_4^{3-} derived) and AOU distribution for the Southeast Pacific (left panels; a, c) and the Southwest Atlantic (right panels; b, d); The position of sections are indicated in Figure 4.1 as yellow lines; $\delta^{13}\text{C}$ is derived from $[\text{PO}_4^{3-}]$ without considering the air-sea exchange term ($\delta^{13}\text{C}_{\text{air-sea}}$) (see Table 4.1 for calculation); The $[\text{PO}_4^{2-}]$ are from the WOA09 (gridded) data compilation; Circles indicate positions of cores discussed in this study; Surface positions of Southern Ocean fronts are marked by arrows (STF, Subtropical Front; SAF, Subantarctic Front; PF, Polar Front; SACCF, Southern ACC Front), according to Orsi et al. (1995); Southern Ocean deep water masses are indicated (CDW, Circumpolar Deep Water; AABW, Antarctic Bottom Water; NADW, North Atlantic Deep Water); Two subtypes of AABW are distinguished (RSBW, Ross Sea Bottom Water; WSBW, Weddell Sea Bottom Water)

In summary, the SE Atlantic core sites appear ideally positioned to detect regional changes in AABW distribution, as they are located below the tongue, thus out of the direct reach of poleward-flowing NADW. By contrast, the SE Pacific core sites are located in well-mixed CDW and their records presumably reflect mean compositional changes of CDW there.

Table 4.1. Locations of the cores discussed in this study, together with estimates of the modern near-bottom water $\delta^{13}\text{C}^{\text{b}}$ (PO_4^{3-} derived) composition at the core locations.

Core ID	Latitude	Longitude	Water depth	$[\text{PO}_4^{3-}]^{\text{a}}$	$\delta^{13}\text{C}^{\text{b}}$
	[°]	[°]	[m]	[$\mu\text{mol/kg}$]	[‰]
PS75/059-2	-54.22	-125.43	3613	2.24	0.24
PS75/056-1	-55.16	-114.79	3581	2.23	0.25
E11-2	-56.07	-115.08	3094	2.24	0.24
RC13-229	-25.49	11.31	4191	2.14	0.35
ODP 1089	-40.94	9.89	4621	2.21	0.27

^a Estimates based on the GLODAP (bottle) data compilation ^b $\delta^{13}\text{C}$ is derived from $[\text{PO}_4^{3-}]$ after the equation $\delta^{13}\text{C} = 2.7 - 1.1 \text{ PO}_4$, according to Broecker and Maier-Reimer (1992) without considering the air-gas exchange term.

4.2. Material and Methods

4.2.1. Sample material

Piston core PS75/059-2 (54°12.90'S 125°25.53'W; 3613 m water depth; 13.98 m core length) and gravity core PS75/056-1 (55°09.74'S; 114°47.31'W; 3581 m water depth; 10.21 m core length) were recovered during R/V Polarstern cruise ANT-XXVI/2 in 2009-2010 austral summer (Gersonde, 2011). The sites are located on the western (PS75/059-2) and eastern (PS75/056-1) flank of the southern EPR, immediately north of the Eltanin Fracture Zone (Figure 4.1).

4.2.2. Stable isotopes

For oxygen and carbon isotope analyses the working halves of both cores were sampled in 1 cm thick slices at 5 cm intervals. After freeze drying, the samples were wet sieved at mesh size 63 μm , rinsed with deionized water and dried at a temperatures under 40°C. Benthic foraminiferal species *Cibicidoides wuellerstorfi* and *Cibicidoides kullenbergi* were picked from the 250-400 μm size fraction. The stable isotope composition of one to six foraminiferal tests (three to four on average) was analyzed on a Finnigan MAT 251 or Finnigan MAT 253 mass spectrometer, each coupled with a Kiel Carbo (II, IV) carbonate preparation device at the Alfred Wegener Institute, Bremerhaven. Isotope ratios of $\text{O}^{18}/\text{O}^{16}$ and $\text{C}^{13}/\text{C}^{12}$ are expressed in the δ -notation versus Vienna Peedee Belemnite (VPDB). The isotope measurements were calibrated to the VPDB scale using the international NIST 19 standard. The precision of the measurements based on the repeated analyses an internal laboratory carbonate standard (Solnhofen limestone) was better than ± 0.08 ‰ for $\delta^{18}\text{O}$ and ± 0.06 ‰ for $\delta^{13}\text{C}$ throughout the measurement period. The samples of core PS75/059-2 were measured primarily on the Finnigan MAT 251 mass spectrometer, while PS75/056-1 samples were measured entirely on the Finnigan MAT 253 mass spectrometer. The benthic $\delta^{18}\text{O}$ data of core PS75/059-2 and core PS75/056-1 have been published previously (Lamy et al., 2014). For core PS75/059-2, isotope measurements were primarily carried out on monospecific samples of *Cibicidoides kullenbergi*. Only in few cases, monospecific samples of *Cibicidoides wuellerstorfi* and mixed specific samples were measured

(supplemental information, Figure S4.1). These samples mainly come from the interval between 390 and 430 ka (MIS 11). For core PS75/056-1, all measurements were done on monospecific samples of *Cibicidoides kullenbergi*.

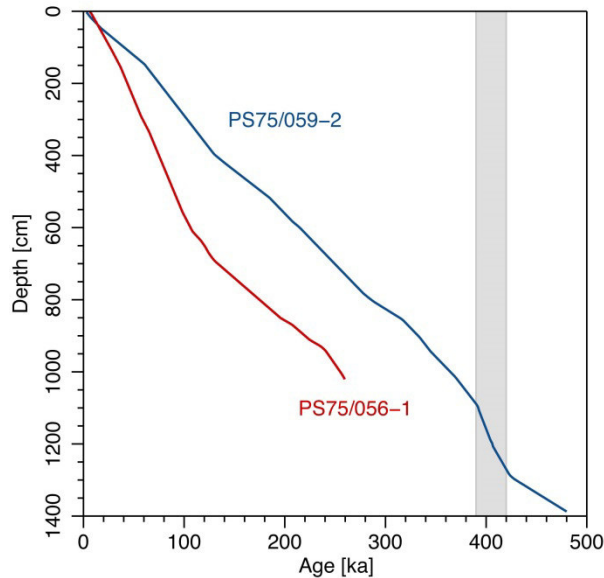


Figure 4.3. Age-depth plot for sediment cores PS75/059-2 and PS75/056-1 according to the age models used in this study; Gray shaded area highlight an interval in core PS75/059-2, characterized by very high coccolith contents; Note that the sedimentation rates are contemporarily high in that interval.

4.2.3 Age model and sedimentation rates

The age models of cores PS75/059-2 and PS75/056-1 are based on correlation of the benthic $\delta^{18}\text{O}$ records to the LR04 benthic $\delta^{18}\text{O}$ stack (Lisiecki and Raymo, 2005), using the Match software (Lisiecki and Lisiecki, 2002). For consistency, we likewise tuned the published records of E11-2, RC13-229 and ODP Site 1089 (see Table 4.2 for reference) to the LR04 benthic $\delta^{18}\text{O}$ stack. The tuned $\delta^{18}\text{O}$ records are shown in the supplemental information, Figure S4.2. According to the used age models, for core PS75/059-2 the average sedimentation rate is ~ 3 cm/ka, but for the interval between 390 ka and 420 ka (MIS 11) the sedimentation rate reaches ~ 6.2 cm/ka (Figure 4.3). The depositional facies of this interval is exceptional, as it contrasts to those from the rest of the core by significantly higher coccolith contents and carbonate components constituting virtually 100 wt. % (Gersonde, 2011). For core PS75/056-1, the average sedimentation rate is ~ 6.0 cm/ka in the upper part (6-110 ka) and ~ 3.0 cm/ka further downcore (110-260 ka) (Figure 4.3).

Table 4.2. Downcore data used in this study, together with references

Core ID	References	
	benthic $\delta^{18}\text{O}$	benthic $\delta^{13}\text{C}$
PS75/059-2	(Lamy et al., 2014)	this study
PS75/056-1	(Lamy et al., 2014)	this study
E11-2	(Ninnemann and Charles, 2002)	(Ninnemann and Charles, 2002)
RC13-229	(Oppo and Fairbanks, 1987; Oppo et al., 1990)	(Oppo and Fairbanks, 1987; Oppo et al., 1990)
ODP 1089	(Hodell et al., 2003c; Hodell et al., 2001)	(Hodell et al., 2003c; Hodell et al., 2001)

4.3.4 Data source and software

Beside our new data, we use previously published benthic $\delta^{13}\text{C}$ and $\delta^{18}\text{O}$ data, measured on the foraminiferal species *Cibicoides wuellerstorfi*, *Cibicoides kullenbergi* (or *Cibicoides mundulus*). All data along with the corresponding references are listed in Table 4.2. The modern oceanographic data displayed in the hydrographic sections in Figure 4.2 are from the WOA09 (gridded) data compilation (Garcia et al., 2010a; Garcia et al., 2010b). The oceanographic data listed in Table 4.1 are from the GLODAP (bottle) data compilation (Key et al., 2004). For data processing and graphical visualization we used the freely available software, AnalySeries (Paillard et al., 1996), Match (Lisiecki and Lisiecki, 2002) Ocean Data View (ODV) (Schlitzer, 2012) and diverse R CRAN packages (<http://cran.r-project.org/>).

4.3 Results and Discussion

4.3.1 East Pacific Rise – Pacific CDW reference locations

The $\delta^{13}\text{C}$ signature measured on tests of the benthic foraminiferal *Cibicoides wuellerstorfi* record the bottom water $\delta^{13}\text{C}$ composition in an one to one relationship (Curry et al., 1988; Duplessy et al., 1984; Duplessy et al., 1988). Parallel measurements of the benthic foraminifera *Cibicoides wuellerstorfi* and *Cibicoides kullenbergi* (or *Cibicoides mundulus*) on a mid-latitude SE Pacific (off Chile) core reveal constant downcore deviations of $\sim 0.16\text{‰}$ between both species (Martínez-Méndez et al., 2013). Given that records PS75/059-2 and PS75/056-1 almost completely consist of monospecific samples of *Cibicoides kullenbergi* (Section 4.2.2; supplemental information, Figure S4.1), we assume that their amplitude changes reflect bottom water $\delta^{13}\text{C}$ compositional changes at the East Pacific Rise adequately. Yet, their absolute values could be about $\sim 0.16\text{‰}$ offset.

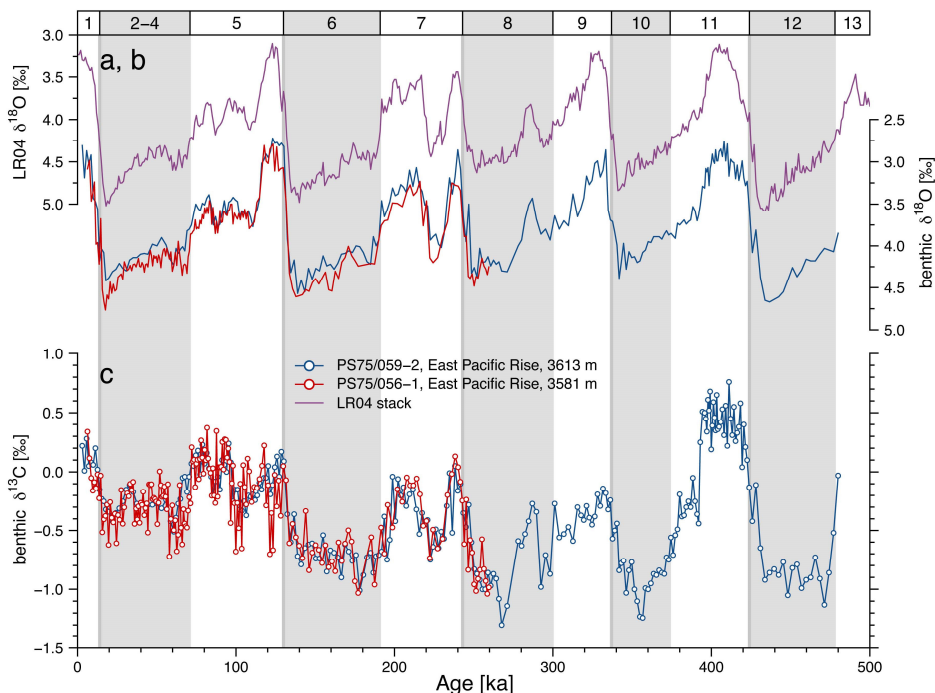


Figure 4.4. (continued on the next page)

Figure 4.4. East Pacific Rise records from opposite ridge flanks; a) LR04 benthic $\delta^{18}\text{O}$ stack for stratigraphic reference; b) Benthic $\delta^{18}\text{C}$ records of cores PS75/059-2 and PS75/056-1; c) Benthic $\delta^{13}\text{C}$ records of cores PS75/059-2 and PS75/056-1; Areas shaded in grey highlight glacial intervals.

Record PS75/059-2 (3613 m water depth), recording past bottom water $\delta^{13}\text{C}$ composition at the western East Pacific Rise side, displays large glacial-interglacial variations over the last 480 ka (Figure 4.4), with amplitudes ranging between $\sim 0.3\text{‰}$ and $\sim 1.5\text{‰}$ at glacial terminations. Underlying is a decreasing trend, with lowest values of $\sim -1.3\text{‰}$ and $\sim -1.2\text{‰}$ occurring at 270 ka and 360 ka, respectively. Record PS75/056-1 (3581 m water depth), which comes from the other, eastern side of the East Pacific Rise shows an almost perfect match on orbital timescales (Figure 4.4). This suggests that the topography of the intervening ridge crest had no significant influence on the local sea water $\delta^{13}\text{C}$ distribution.

Notably is the constant offset of $\sim 0.1\text{‰}$ between the benthic foraminiferal $\delta^{18}\text{O}$ records PS75/059-2 and PS75/056-1 (Figure 4.4). As the $\delta^{18}\text{O}$ signature of benthic foraminiferal tests vary as a function of ambient bottom water temperature and sea water $\delta^{18}\text{O}$ distribution (e.g., Lynch-Stieglitz, 2003) slight contrasts in these two water mass parameters may have been present across the East Pacific Rise. Today, cold Ross Sea-derived AABW flows down the Antarctic continental slope before it fills the Eastern Pacific Basin at abyssal depth (Figure 4.1 and 4.2), approaching the East Pacific Rise from north and east, the side there core site PS75/056-1 lies (Orsi et al., 1999; Orsi et al., 2002). Based on inferences from benthic foraminiferal $\delta^{18}\text{O}$ based studies from the Atlantic (Hoffman and Lund, 2012), the $\sim 0.1\text{‰}$ enriched benthic $\delta^{18}\text{O}$ values at core site PS75/056-1 may thus originate from a slightly higher influence of AABW there throughout the past, which is not reflected in the respective benthic $\delta^{13}\text{C}$ records. However, such a small offset may alternatively explain by a constant machine offset, as most analyses for core PS75/059-2 were carried out on a different mass spectrometer than the analyses for core PS75/056-1

Today, the $\delta^{13}\text{C}$ distribution at the East Pacific Rise, as derived from phosphate (Figure 4.2), is almost homogeneous in the water column below 1200 m. The match between the benthic $\delta^{13}\text{C}$ records of PS75/059-2, PS75/056-1 and of E11-2 (3094 m water depth) located ~ 500 m shallower confirms that an almost homogeneous distribution persisted across a substantial depth range, at least over the last glacial-interglacial cycle (Figure 4.5). This relates, however, only to orbital timescales, as on suborbital timescales transient differences of up to $\sim 0.4\text{‰}$ occur among the three records. Partly, these differences result from their different temporal resolutions. Record PS75/056-1, for instance, shows stronger suborbital variability between 6 ka to 120 ka, precisely when the sedimentation rate is highest (Figures 4.3 and 4.4), yet some differences remain even after smoothing (Figure 4.5). Thus, some temporary heterogeneity in the local sea water $\delta^{13}\text{C}$ distribution is indicated by records PS75/059-2, PS75/056-1 and E11-2 throughout the past, if ignoring that other factors, e.g. age-model uncertainties, may also have influenced the observed patterns.

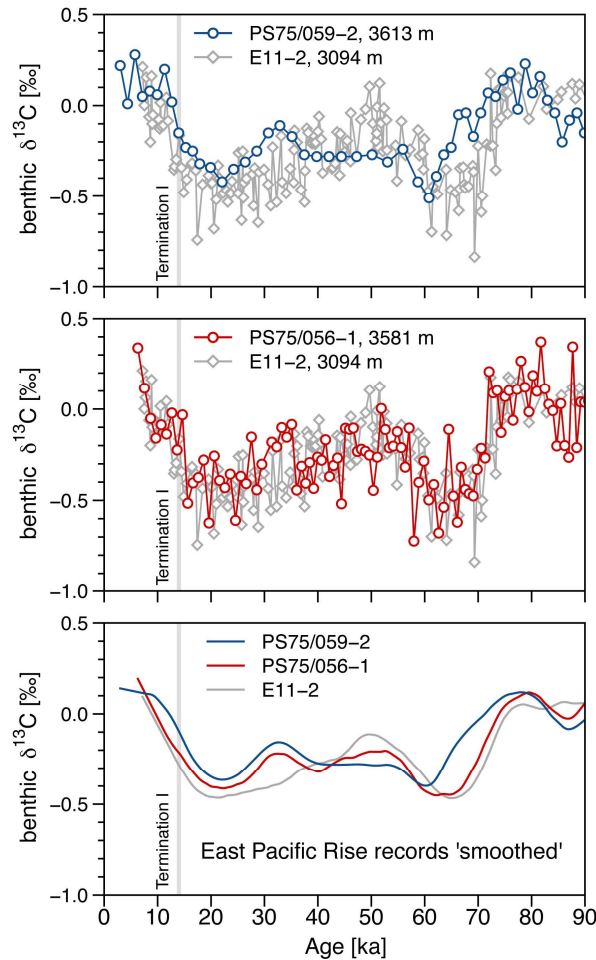


Figure 4.5. Comparison between benthic $\delta^{13}\text{C}$ records from the East Pacific Rise; a) Records PS75/059-2 and E11-2; b) Records PS75/056-1 and E11-2; c) Smoothed time series of records PS75/059-2, PS75/056-1 and E11-2, calculated by kernel method; Gray vertical line marks the last glacial termination.

Overall, our results imply that all three benthic $\delta^{13}\text{C}$ records are representative for an, almost homogeneous water mass on glacial-interglacial timescales, which occupies the East Pacific Rise area over a larger depth range, thus has volumetric importance. We therefore denote the water mass documented at the respective core locations as CDW, being aware that its $\delta^{13}\text{C}$ composition represents actually the lower portion of CDW (lower CDW). Referring to the previous study by Ninnemann and Charles (2002), our reconstructions from deeper cores, thus the increased vertical core coverage, validate previous CDW reference record E11-2, which rests most closely to the core of poleward-flowing PDW.

4.3.2 Pacific-Atlantic interbasin link

Below, we discuss past interbasin deep water exchange between the SE Pacific, southern East Pacific Rise area, and the SE Atlantic. Therefore, we compare our results to the published benthic $\delta^{13}\text{C}$ reference records RC13-229 and ODP Site 1089, from core locations in the abyssal northern and southern Cape Basin, respectively, and are presently bathed in CDW (Figure 4.2).

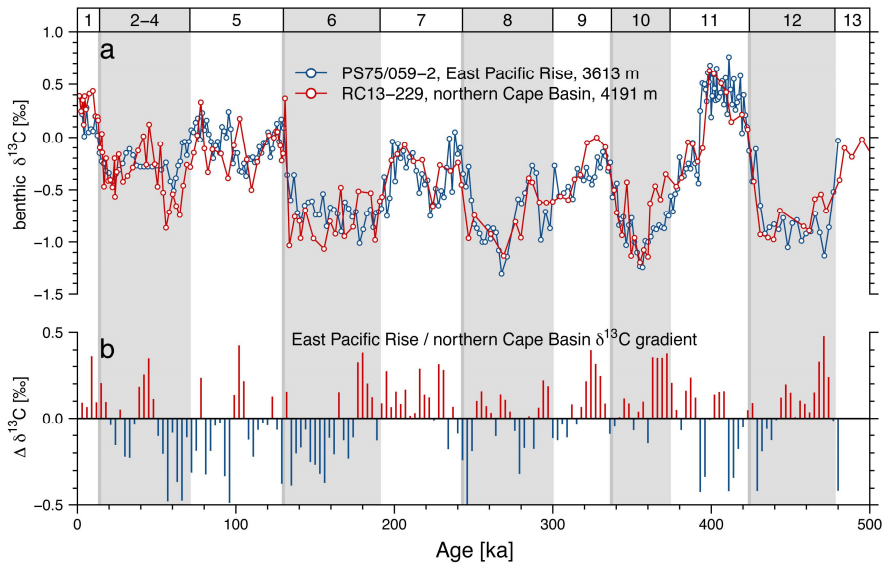


Figure 4.6. Comparison between East Pacific Rise and northern Cape Basin; a) Benthic $\delta^{13}\text{C}$ records PS75/059-2 and RC13-229; b) Difference between benthic $\delta^{13}\text{C}$ records PS75/059-2 and RC13-229 ($\Delta \delta^{13}\text{C} = \delta^{13}\text{C}_{\text{RC13-229}} - \delta^{13}\text{C}_{\text{PS75/059-2}}$); Note that it shows any long-term trend; Before subtraction the original time series were resampled in 3 ka spacing with linear interpolation between data points; Areas shaded in grey highlight glacial intervals.

On orbital timescales, the benthic $\delta^{13}\text{C}$ records PS75/059-2 and RC13-229, which is based on benthic foraminiferal *Cibicidoides wuellerstorfi* measurements, are visually identical (Figure 4.6 a), showing similar absolute values and downcore variability. The consistency of the records is displayed by the absence of a long-term trend in the difference between both records (Figure 4.6 b). It amounts to ~ 0.0 ‰, similar to the phosphate-derived modern sea water $\delta^{13}\text{C}$ difference of ~ 0.1 ‰ of the water masses overlying both core sites (Table 4.1). It is notable that the actual fit with modern conditions would be even improved if record PS75/059-2 yielded indeed slightly too low absolute values as discussed previously in Section 4.3.1. On suborbital timescales, the difference between both records shows significant variability, attributable to a number of factors, e.g. differences in the temporal resolution of both records or age model uncertainties. Partly, this variability may also indicate true changes in ocean circulation, induced by a varying influence of local, northern and southern-sourced water masses in the SE Atlantic (Piotrowski et al., 2004; Piotrowski et al., 2008). Nonetheless, if the benthic $\delta^{13}\text{C}$ record PS75/059-2 reliably reflects the evolution of past CDW composition at the East Pacific Rise, the comparison implies for orbital timescales that a common CDW composition was maintained for the Pacific and the Atlantic basin over the past 480 ka. In turn, this suggests a continuous coupling between CDW at the East Pacific Rise and in the northern Cape Basin, consistent with the notion that benthic $\delta^{13}\text{C}$ values of northern Cape Basin core RC13-229 reflect the $\delta^{13}\text{C}$ composition of well mixed CDW (Oppo et al., 1990).

It is important to note that, in contrast to our results, former benthic $\delta^{13}\text{C}$ -based observations by Ninnemann and Charles (2002) implied a diverging $\delta^{13}\text{C}$ evolution for the SE Pacific and SE Atlantic area, associated with the development of a high inter-basin $\delta^{13}\text{C}$ gradient (~ 0.6 ‰) at the LGM. This discrepancy apparently arises from the fact that the authors used only records from further poleward,

thus they considered records from the deep southern, but not from the deep northern Cape Basin. Consequently, differences are visible, when comparing the East Pacific Rise record PS75/059-2 with the southern Cape Basin reference record ODP Site 1089 (Hodell et al., 2001). The record from ODP Site 1089 shows considerably heavier $\delta^{13}\text{C}$ values over much of its length, particularly during the LGM (Figure 4.7). The difference between the records, thus the East Pacific Rise – southern Cape Basin interbasin $\delta^{13}\text{C}$ gradient, was with ~ 0.8 ‰ highest at the LGM, but it re-occurred with significant amplitude several times in the past. Approximately similarly high values occurred during the glacial MIS 6, 10 and 12. On the whole, the gradient displays an irregular rather than clearly visible glacial-interglacial modulation, as visible, for instance, in its absence during glacial MIS 8. The fact that our LGM interbasin $\delta^{13}\text{C}$ gradient (~ 0.8 ‰) is ~ 0.2 ‰ higher than the originally observed one (~ 0.6 ‰) stems from relatively high glacial values of core PS75/059-2, when compared to E11-2, which was used in the previous study (Ninnemann and Charles, 2002). We conclude that the strength of the interbasin $\delta^{13}\text{C}$ gradient is actually not indicative for the degree of deep water decoupling between the SE Pacific and SE Atlantic. It rather describes the independent evolution of the deep waters that bathed the southern Cape Basin and adjoining southernmost South Atlantic areas, with regard to a common SE Pacific and SE Atlantic CDW evolution.

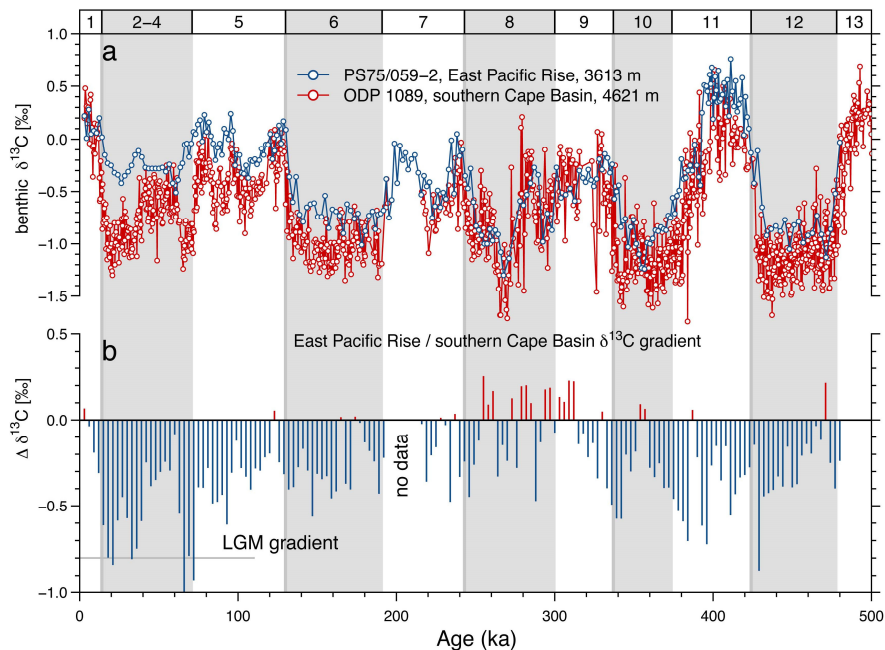


Figure 4.7. Comparison between East Pacific Rise and southern Cape Basin; a) Benthic $\delta^{13}\text{C}$ records PS75/059-2 and ODP Site 1089; b) Difference between benthic $\delta^{13}\text{C}$ records PS75/059-2 and ODP Site 1089 ($\Delta \delta^{13}\text{C} = \delta^{13}\text{C}_{\text{ODP Site 1089}} - \delta^{13}\text{C}_{\text{PS75/059-2}}$); The original time series ODP Site 1089 was smoothed using a 5-point moving average. Before subtraction the smoothed time series ODP Site 1089 and the original time series PS75/059-2 were resampled in 3 ka spacing with linear interpolation between data points; The LGM gradient (~ -0.6 ‰) is an average of the values between 18 ka and 24 ka; Areas shaded in grey highlight glacial intervals.

4.3.3 Past Atlantic AABW distribution and its implication on CO₂ storage

LGM studies often link the occurrence of the extremely depleted benthic $\delta^{13}\text{C}$ values in the southern Cape Basin to changes in the expansion and formation mechanisms of Weddell Sea AABW, resulting in a drastic lowering of its endmember $\delta^{13}\text{C}$ signature. This is evident in the negative LGM difference between the CDW record PS75/059-2 and record ODP Site 1089 (Figure 4.7). The major cause for much of the LGM $\delta^{13}\text{C}$ depletion was apparently an altered air-sea exchange during AABW formation, assumedly related to changes in the sea ice coverage around Antarctica (e.g., Curry and Oppo, 2005; Marchitto and Broecker, 2006), as locally, less distinctly observable also today (Mackensen, 2012). Likewise for pre-LGM times, more negative $\delta^{13}\text{C}$ values for the southern Cape Basin record ODP Site 1089 may therefore point towards an increased influence of very $\delta^{13}\text{C}$ depleted AABW there. If true, the difference between both records indicate very complex CDW and AABW interactions further back in time, associated with vigorous changes in past AABW endmember $\delta^{13}\text{C}$ composition (Figure 4.7). For instance, during the LGM an invasion of very low $\delta^{13}\text{C}$ AABW at the expense of current CDW is indicated, while the missing difference during the MIS 8 glaciation implies either that no AABW invasion occurred at that time or that the AABW endmember $\delta^{13}\text{C}$ composition was undistinguishable from CDW. Even some combination of both is conceivable, thus, the difference between both records can be interpreted in a number of ways. Without going further into detail, it is nonetheless indicated that the conditions related to AABW extant and endmember $\delta^{13}\text{C}$ composition differed in the southern Cape Basin abyss among individual glacial and even among interglacial stages. The current LGM picture with the exceptional, low benthic $\delta^{13}\text{C}$ values in the southernmost South Atlantic appears to be not simply transferable to other glacial stages.

Further implications on past AABW extant from its modern position come from our inferences regarding the deep northern Cape Basin. As proposed in *Section 3.2*, the permanent presence of CDW in the northern Cape Basin would constitute a boundary for undiluted AABW to extend northward. Actually, this is a very simplistic picture. As southern Cape Basin ODP Site 1089 is located 450 m deeper than northern Cape Basin core site RC13-229, there is some space for AABW once occurring in the south Cape Basin to flow further north. Even so, there would be significant restrictions for its maximal extent. As total AABW production was in all likelihood higher during glacial times (e.g., Adkins, 2013), Weddell Sea AABW or, more precisely, its glacial equivalent may have found its way into the Atlantic interior by continues admixing into common CDW, which itself represents ultimately a mix between the endmember water masses NADW and total AABW (Broecker et al., 1998). Yet, it appears according our results unlikely that AABW invaded in undiluted form via the Cape Basin directly further north towards in equatorial Atlantic direction. Of cause, its direct invasion into the Atlantic interior via the basin's deep western boundary current, where today the major inflow occurs (Figure 4.1), is in spite of our inferences not precluded. Indeed, Atlantic-wide highest published LGM $\delta^{18}\text{O}$ values, obtained from the Brazil margin, indicate that during the LGM almost undiluted AABW,

close to its endmember composition, penetrated along the western boundary far northward into the Atlantic interior (Hoffman and Lund, 2012).

A quantified understanding of past tracer distributions in the Atlantic basin is immanently important to infer potential changes in physical ocean circulation, which may have influenced the oceans capacity in sequestering atmospheric CO₂ at depth (e.g., Curry and Oppo, 2005; Gebbie, 2014; Hesse et al., 2011; Hoffman and Lund, 2012; Lund et al., 2011; Wunsch, 2003). Amongst others, so far a key unknown in this regard is past AABW endmember $\delta^{13}\text{C}$ composition (e.g., Gebbie, 2014; Hoffman and Lund, 2012), caused by a current lack of data in the water formation regions around Antarctica. Thus, many LGM studies use South Atlantic-wide published $\delta^{13}\text{C}$ minimum values ($\sim 0.9\text{‰}$) as fix points, which occur further northward in the abyssal SE Atlantic, and are restricted to the southern Cape Basin and parts of its adjacent areas (Curry and Oppo, 2005; Mackensen et al., 2001; Martínez-Méndez et al., 2009; Ninnemann and Charles, 2002). These SE Atlantic $\delta^{13}\text{C}$ values were at the LGM by far lower than the SE Pacific $\delta^{13}\text{C}$ values from the East Pacific Rise area (Ninnemann and Charles, 2002). However, our comparison of the SE Atlantic and SE Pacific records suppose that the former's unique minima, outweighing those in other oceanic areas, were particularly pronounced during the LGM, as indicated by the changes of the interbasin $\delta^{13}\text{C}$ gradient (Figure 4.7). They obviously occurred in weaker form during most of the other glaciations, but were absent during the MIS 8 glaciation. In future, such differentiations should be taken into account when discussing past AABW endmember $\delta^{13}\text{C}$ characteristics and its implications on glacial atmospheric CO₂ drawdown, which occurred on regular glacial-interglacial scales, in contrast to the more irregular East Pacific Rise – southern Cape Basin interbasinal $\delta^{13}\text{C}$ gradient development. Moreover, the proposed persistent Pacific-derived CDW presence in the northern Cape Basin prevents a direct propagation of low- $\delta^{13}\text{C}$ deep Antarctic-sourced waters into the lower latitude Atlantic, which has consequences for the volumetric importance of deep waters bathing the SE Atlantic southern Cape Basin. If true, this should further impact the deep oceanic CO₂ storage capacity. In that regard it is notable that due to its characteristic $\delta^{18}\text{O}$ and $\delta^{13}\text{C}$ composition, deep southern Cape Basin waters may represent an individual glacial-AABW variety at the LGM, distinct to a much lesser $\delta^{13}\text{C}$ depleted glacial-AABW, which flowed into the Atlantic interior along its western boundary (Hoffman and Lund, 2012). We speculate that after production in the periphery of Antarctica, the former AABW variety turned directly northward and firstly interacted with CDW on its downstream flow along the ACC path.

For the above interpretations we assumed that lower $\delta^{13}\text{C}$ values in southern Cape Basin (ODP Site 1089) than at the East Pacific Rise (PS75/059-2) and, as a consequence, in the northern Cape Basin (RC13-229), reflect an increased AABW influence there. One should, however, bear in mind that it is still under discussion whether the very depleted $\delta^{13}\text{C}$ values measured on benthic foraminifera *Cibicidoides wuellerstorfi* and *Cibicidoides kullenbergi* from the southern Cape Basin reflect a true water mass signal downcore, or whether they are considerably compromised by local, biological or environmental factors (Hodell et al., 2003b; Mackensen et al., 1993), as outlined also from a

neodymium isotope based perspective (Piotrowski et al., 2004). In any case, our results show that the benthic foraminiferal $\delta^{13}\text{C}$ records from the abyssal southern Cape Basin core locations (e.g. ODP Site 1089) likely not fully represent circumpolar deeper water conditions, and thus the past $\delta^{13}\text{C}$ compositional evolution of a common CDW in the Southern Ocean. Besides, their usability to infer basin-wide glacial-AABW characteristics should be considered with care.

4.4 Conclusion

In this study we examined the deep water exchange between the Pacific and Atlantic basins over the past 500 ka. Using benthic foraminiferal $\delta^{13}\text{C}$ downcore data from the East Pacific Rise we characterized the $\delta^{13}\text{C}$ composition of SE Pacific CDW, prior to its transition through the Drake Passage and showed that it closely co-evolved with the CDW composition in the deep SE Atlantic, northern Cape Basin. Our results imply a continuous deep water exchange between the SE Pacific and SE Atlantic throughout the past 500 ka. We conclude that a common CDW was maintained. This is not in complete contrast to the current, prevailing scenarios focusing on the LGM, as our results confirm that deep waters in the southernmost areas of the SE Atlantic, including the southern Cape Basin, evolved divergent to the SE Pacific, thus from the common CDW. As proposed in a previous study by Ninnemann and Charles (2002), this may explain by repeated northward expansion of AABW into that area, combined with changes in its endmember $\delta^{13}\text{C}$ signature. However, past interactions of CDW and AABW in the southern Cape Basin appear complex, not strictly following known glacial- interglacial patterns and indicating distinct differences in AABW areal extent and its endmember composition. Altogether, defining CDW as an individual deep water mass in the Atlantic manifests a more differentiated picture on past AABW areal extent. In that regard, the current LGM picture associated with the extremely low LGM benthic $\delta^{13}\text{C}$ values in the southernmost SE Atlantic seems too simplistic. This should be taken into account when quantifying the role of oceans physical circulation on glacial-interglacial atmospheric CO_2 cycling.

Acknowledgments

The data reported in this manuscript will be made available online in PANGAEA. We thank the captain, crew, and scientific party of R/V Polarstern for their support during the ANT-XXVI/2 cruise. U. Bock, G. Meier and L. Schönborn provided technical support at the Alfred Wegener Institute. In particular, we thank A. Mackensen for discussions and S. Steph for providing unpublished isotope data and for supporting the isotope measurements. J. Collins, C. Lange and S. Romahn provided valuable comments and suggestions that helped to improve the manuscript. M. Menzel assisted in software questions. We finally thank G. Martínez-Méndez and one anonymous reviewer for their critical and constructive comments that greatly improved this manuscript. This work was financially supported by the Alfred Wegener Institute, Helmholtz Centre for Polar und Marine Research.

4.5 Supplemental Information

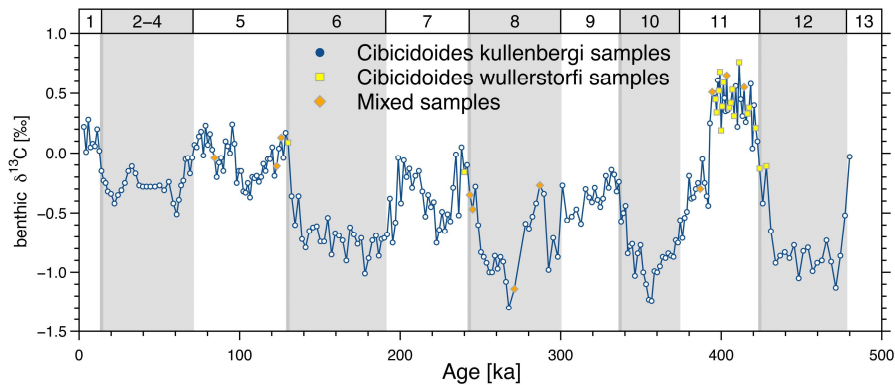


Figure S4.1. Supplement information on the type of foraminiferal samples used for the stable isotope measurements on core PS75/059-2; The downcore benthic $\delta^{13}\text{C}$ data obtained from monospecific *C. wuellerstorfi*, monospecific *C. kullenbergi* and mixed-species samples are illustrated individually for core PS75/059-2; Note that for the mixed-species measurements only the foraminiferal species *C. wuellerstorfi* and *C. kullenbergi* were used.

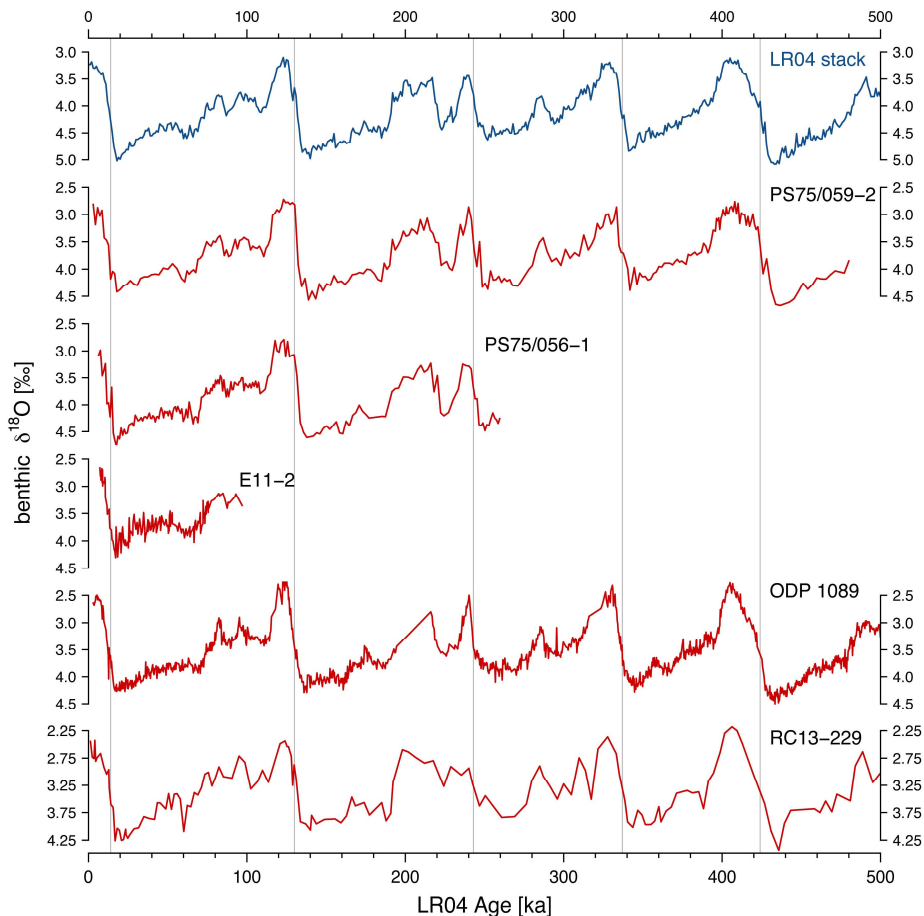


Figure S4.2. Supplementary information on age-model development; Comparison of the benthic $\delta^{18}\text{O}$ records PS75/059-2, PS75/056-1, E11-2, ODP 1089 and RC13-229 to the LR04 benthic $\delta^{18}\text{O}$ stack; For references see Table 4.2 in the main text.

Chapter 5 – Evolution of the sea surface temperature and $\delta^{18}\text{O}$ in the central South Pacific during the past 500 ka: Implications on ocean circulation

Johannes Ullermann (1), Raul Tapia (2), Frank Lamy (1), Dirk Nürnberg (2) Rainer Gersonde (1), Ralf Tiedemann (1)

Prepared to be submitted to Quaternary Science Reviews

1. Alfred-Wegener-Institut Helmholtz-Zentrum für Polar- und Meeresforschung, Am Alten Hafen 26, 27568 Bremerhaven, Germany

2. GEOMAR Helmholtz-Zentrum für Ozeanforschung Kiel, Wischhofstraße 1-3, 24148 Kiel, Germany

Abstract

Despite the Southern Ocean is central to understand past climate change, the long term paleoceanographic evolution of its Pacific sector remains largely unknown. Here, we present orbital scale surface water temperature (Mg/Ca-based) and $\delta^{18}\text{O}$ records of planktonic foraminiferal species *G. bulloides*. The records from sediment cores collected in the Subantarctic and Polar Frontal Zone, central South Pacific (~55°S), at both sides of the East Pacific Rise and at the Pacific Antarctic Ridge, reach back to ~500 ka. Our results indicate that commonly used Mg/Ca calibration equations systematically overestimate temperatures by ~3 °C for the central South Pacific study area, whereas the amplitude ranges are correctly reflected. Further our results reveal that sea surface temperatures covaried with Antarctic air temperatures showing similar relative strengths of glacials and interglacials, with amplitude changes ranging from 2.5 °C to 6.5 °C. The surface water $\delta^{18}\text{O}$ values show no glacial-interglacial modulation after ice volume correction, implying rather stable sea surface salinity. In consistence to previous studies, larger glacial-interglacial surface water temperature and $\delta^{18}\text{O}$ variations off New Zealand and Chile may imply surface circulation changes linked to the Antarctic Circumpolar Current and subtropical South Pacific gyre systems – an inference, which is partly supported by Earth System model simulations

5.1 Introduction

The Southern Ocean is central to Earth's climate due to its intrinsic role in distributing heat, salinity and nutrients, thereby impacting the carbon cycle (e.g., Marshall and Speer, 2012; Sigman et al., 2010). To understand paleoceanographic mechanisms acting there over climatic cycles, sea surface temperature (SST) and salinity (SSS) represent fundamental parameters. First, ocean surface temperature reflects atmospheric influences (air-sea heat flux) and thus provides insight about Southern Ocean responses with respect to Antarctic climate evolution, as best resolved in East Antarctic ice core records. Second, ocean surface temperature and salinity allows drawing inferences on ocean surface circulation changes (advective heat and salt flux).

The Southern Ocean encircles Antarctic continent and connects the South Atlantic, South Indian and South Pacific. Despite its large extent, the South Pacific exhibits only few marine paleoclimate records covering larger timescales. So far, there are observations on past South Pacific temperature and salinity evolution for the central oceanic area, which span only about 200 ka (Luz, 1977; Mashiotta et al., 1999; Tapia et al., 2015). Observations further back in time are limited to its western and eastern continental margins around New Zealand (Crundwell et al., 2008; Hayward et al., 2012; Hayward et al., 2008; Pahnke et al., 2003; Pelejero et al., 2006; Schaefer et al., 2005) and the tip of South America (Ho et al., 2012). However, these areas represent environments, which may have different hydrographical dynamics and may thus not be representative for the wider Pacific Southern Ocean. Changes there are strongly modulated by the interplay of subantarctic (cold/fresh) with subtropical (warm/salty) surface waters around the Subtropical Front, respectively circulating within the Antarctic Circumpolar Current (ACC) and the subtropical South Pacific gyre.

Here we report orbital scale changes in central South Pacific surface temperature and salinity using paired Mg/Ca-derived SST and $\delta^{18}\text{O}$ downcore data of the planktonic foraminiferal species *G. bulloides* covering the past ~500 ka. By documenting past temperature and salinity evolution for the central Pacific Southern Ocean, we complete the picture of South Pacific wide surface oceanic circulation changes. The following text is structured in three main parts dealing with (1) an assessment of our temperature and salinity estimates for the central South Pacific (2) a comparison to East Antarctic air temperature record (3) a discussion of the changes in the central South Pacific with respect to surface oceanic changes reported from its western and southern coastal areas. Finally, the inferences thereof are briefly considered by use of Earth System model simulations (LOVECLIM/TR400) (Timmermann et al., 2014).

5.2 Material and Methods

5.2.1 Sample material

The hydrographic evolution of the central South Pacific oceanic area is discussed based on the planktonic Mg/Ca and $\delta^{18}\text{O}$ records of gravity core PS75/056-1 (55°09.74'S; 114°47.31'W; 3581 m water depth, 10.21 m core length) and piston core PS75/059-2 (54°12.90'S; 125°25.53'W; 3613 m

water depth; 13.98 m core length), which were recovered from the eastern (PS75/056-1) and western (PS75/059-2) flank of the southernmost East Pacific Rise on R/V Polarstern cruise ANT-XXVI/2 (Figure 5.1). The records span the past 260 ka and 480 ka, respectively. According the used age models (Section 2.4), for core PS/75-056-1 the sedimentation rate is ~ 6.0 cm/ka in the upper part (0-125 ka) and ~ 3.0 cm/ka further downcore (125-260 ka). For core PS/75-059-2 the average sedimentation rate is ~ 3 cm/ka. Besides, planktonic Mg/Ca data are presented from piston core PS75/079-2 and its respective pilot core ($57^{\circ}30.16'S$; $157^{\circ}14.25'W$; 3770 m water depth, 18.51 m core length), which was retrieved from the northwestern Pacific Antarctic Ridge (Figure 5.1). The Mg/Ca SST record of core PS75/079-2 dates back to about 500 ka, but is discontinuous due to low or absent carbonate during glacial intervals. In order to confirm a late Holocene core top age, few benthic $\delta^{18}O$ data measured on foraminiferal species *Cibicidoides* spp. were obtained from pilot core PS75/079-2. Along with the downcore data, we present surface sediment Mg/Ca data, which were collected with a multi corer device on R/V Polarstern cruise ANT-XXVI/2 (Figure 5.1). The surface sediment samples come from areas around the modern position of the Subantarctic Front. Their exact locations and recovery depths are given in Table 5.1. The quality of the Mg/Ca in the foraminiferal calcite with respect to carbonate dissolution was confirmed by use of *G. bulloides* shell weights obtained from cores PS75/059-2 and PS75/079-2.

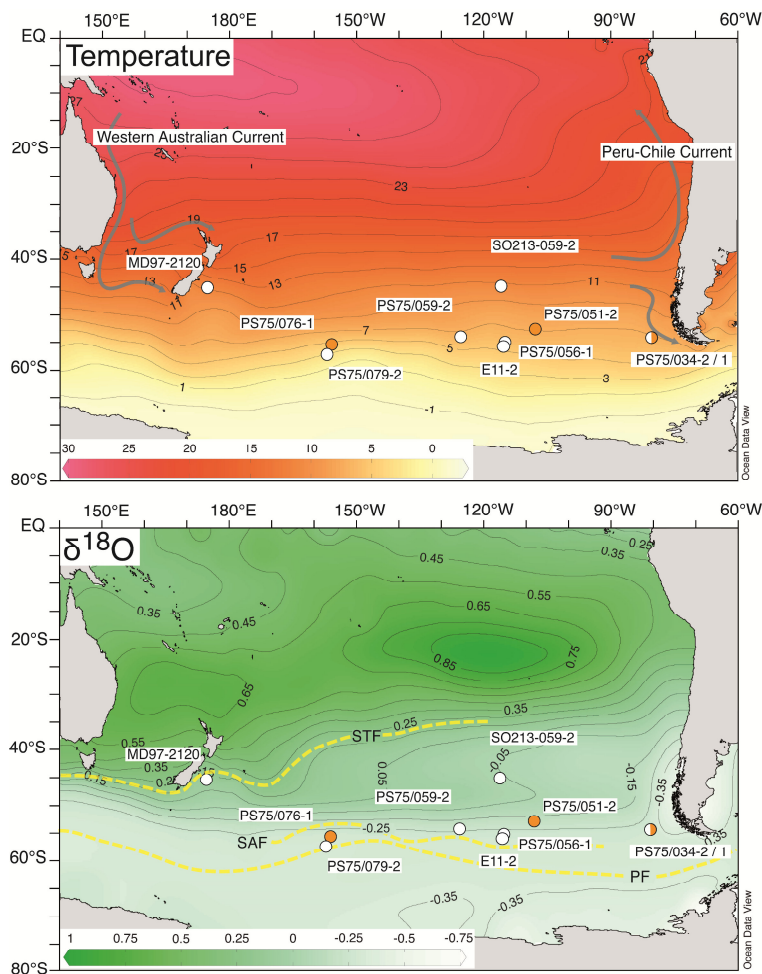


Figure 5.1. Modern mean annual temperature and $\delta^{18}O$ distribution at 50 m water depth of the Southern Hemisphere Pacific Ocean, displayed with ODV software (Schlitzer 2012), using the gridded data sets of Locarnini et al. (2010) (WOA09) and LeGrande and Schmidt (2006); Positions of discussed cores and surface samples are indicated by white circles and orange circles, respectively; Gray arrows (upper panel) indicate the schematic flow paths of the western and eastern boundary currents of the subtropical South Pacific gyre, which transport warm/salty (high- $\delta^{18}O$) and cold/fresh (low- $\delta^{18}O$), respectively; Yellow lines (upper panel) indicate the positions of major ACC fronts as defined by Orsi et al. (1995)

Table 5.1. Geographic position and sampling depth of the surface and core top samples listed together with their respective Mg/Ca and benthic $\delta^{18}\text{O}$ values.

Core ID	Depth [cm]	Latitude [°]	Longitude [°]	Mg/Ca [mmol/mol] [mmol/mol]	benthic $\delta^{18}\text{O}$ [‰]
MUC PS75/034-1	0-1	-54.37	-80.08	1.44	NA
MUC PS75/051-2	0-1	-52.82	-107.80	1.31	NA
MUC PS75/076-1	0-1	-55.53	-156.13	1.19	3.42
KOL PS75/056-1	0-1	-55.16	-114.79	1.08	3.08
KOL PS75/059-2	2-3	-54.22	-125.43	1.17	2.81
KOL PS75/079-2 (pilot core)	2-3	-57.50	-157.23	0.85	3.06

5.2.2 Oceanographic setting

Today, the core positions of cores PS75/056-1 and PS75/059-2 rest closely north of the Subantarctic Front within the Subantarctic Zone, while core PS75/079-2 is located in the Polar Frontal Zone close to the Polar Front (Figure 5.1). Across the core locations the sea surface temperature decreases in poleward direction uniformly by about 0.5 °C per degree latitude (Figure 5.2). By contrast, the surface water salinity remains almost unchanged around the core locations. Substantially enhanced latitudinal temperature and salinity gradients, as characteristic for the further equatorward positioned Subtropical Front, are absent. Accordingly, a potential displacement in the positions of the Subantarctic Front may have comparably less impact on the local temperature and salinity distribution. As previous LGM inferences from the area indicate largely unchanged conditions regarding the ACC frontal system (Matsumoto et al., 2001), the core sites are well situated to detect past background temperature and salinity changes of the surface waters circulating eastward within the ACC.

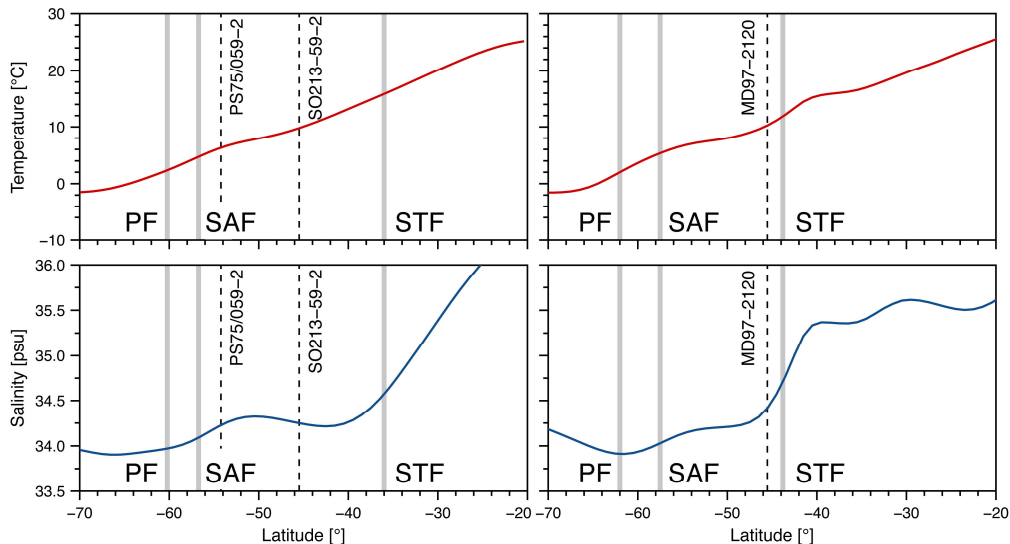


Figure 5.2. Modern mean annual temperature and salinity distribution at 50 m water depth displayed for two N-S profiles across core positions PS75/059-2 (right panels) and MD97-2120 (left panels); The data were extracted from WOA09 gridded data sets of Locarnini et al. (2010) and Antonov et al. (2010); Cores positions PS75/059-2 and MD97-2120 are indicated by black, dashed lines; Core position SO213-059-2 is longitudinally projected into the profiles (right panels) and is indicated by black, dashed lines; Gray vertical lines indicate the surface position of major ACC fronts as defined by Orsi et al. (1995).

5.2.3 Foraminiferal Mg/Ca and $\delta^{18}\text{O}$ analyses

For chemical (Mg/Ca) and oxygen isotope ($\delta^{18}\text{O}$) analyses the working halves of core PS75/056-1 and core PS75/059-2 were sampled every 5 cm over their full length of 10.21 m and 13.98 m respectively. Core PS75/079-2 together with its pilot was sampled every 5 cm down to 18 m for intervals where carbonate was present. The surface sediment samples were taken from the uppermost 1 cm of the undisturbed multi-cores (Table 5.1).

After freeze drying the samples were wet sieved at mesh size 63 μm , rinsed with deionized water and dried at a temperature lower 40 °C. In most cases about 35 tests of planktonic foraminiferal species *G. bulloides* were picked from the 315-355 μm size fraction, gently crushed, homogenized and split into subsamples. Before chemical and oxygen isotope analyses, the subsamples were cleaned at the laboratory facility of the GEOMAR, Kiel, following the protocol of Barker et al. (2003), as modified by Nürnberg and Groeneveld (2006). For cores PS75/059-2 and PS75/079-2 average shell weights of *G. bulloides* were determined in an additional step before crushing and cleaning. For this purpose a Sartorius 4503 MP6E micro balance was used.

The chemical composition, thus the Mg/Ca of the first half of the subsamples was analyzed on a Varian 720-ES inductively coupled plasma – optical emission spectrometer (ICP-OES) at the GEOMAR, Kiel. The reproducibility for Mg/Ca based on the ECRM752-1 standard was better than ± 0.1 mmol/mol. The cleaning efficiency for the subsamples was ensured by parallel analyzed Fe/Ca and Mn/Ca.

The oxygen isotope composition of the second half of the subsamples was analyzed on Finnigan MAT 253 mass spectrometers coupled to a Kiel Carbo IV carbonate preparation devices at the GEOMAR, Kiel, (PS75/056-1, PS75/059-2) and at the AWI, Bremerhaven (PS75/079-2, surface samples). The mass spectrometers were calibrated via the NBS19 international standard to the PDB scale, respectively. Isotope ratios of $\text{O}^{18}/\text{O}^{16}$ are expressed in δ -notation versus Vienna Pee Dee Belemnite (VPDB). The reproducibility based on internal laboratory standards was better than ± 0.8 ‰ for both machines.

5.2.4 Sea water temperature and $\delta^{18}\text{O}$ estimates

For the calculation of past Mg/Ca temperatures and sea water $\delta^{18}\text{O}$ composition, same equations were used as already applied in other southern high-latitude studies (Nürnberg and Groeneveld, 2006; Pahnke et al., 2003). The Mg/Ca data were translated into temperature using the *G. bulloides* specific calibration equation of Mashiotta et al. (1999), $\text{Mg/Ca} = 0.474 \exp(0.107 T)$. The sea water $\delta^{18}\text{O}$ ($\delta^{18}\text{O}_w$) composition was calculated from the foraminiferal calcite $\delta^{18}\text{O}$ ($\delta^{18}\text{O}_c$) data and the derived Mg/Ca temperatures according the equation of Shackleton (1974), $\delta^{18}\text{O}_w = \delta^{18}\text{O}_c + 0.27 - (4.38 - \sqrt{4.38^2 - 0.4(16.9 - T)}) / 0.2$. The equation includes the conversion from the Pee Dee Belemnite (PDB) scale to the Standard Mean Ocean Water (SMOW) scale with constant offset of 0.27 ‰ (Hut, 1987). Afterwards, the global ice volume effect was removed to obtain a corrected sea water $\delta^{18}\text{O}$

($\delta^{18}\text{O}_{\text{ivc-w}}$) composition. For this purpose the mean ocean $\delta^{18}\text{O}_{\text{w (mean ocean)}}$ curve, given by Waelbroeck et al. (2002), was subtracted from previously derived sea water $\delta^{18}\text{O}_{\text{w}}$ composition, $\delta^{18}\text{O}_{\text{ivc-w}} = \delta^{18}\text{O}_{\text{w}} - \delta^{18}\text{O}_{\text{w (mean ocean)}}$

5.2.5 Chronology

The age models of cores PS75/056-1 and PS75/059-2, which were obtained in this study, are based on the correlation of their SST records to the Antarctic EPICA Dome C deuterium (δD) temperature record on the EDC 3 timescale (Jouzel et al., 2007; Parrenin et al., 2007). The correlations for cores PS75/056-1 and PS75/059-2 were performed visually with the AnalySeries software (Paillard et al., 1996). This allows a consistent comparison to records of cores PS75/034-1 and MD97-2120, whose age scales are likewise based on a synchronisation of their SST records to Antarctic ice-core records (EPICA δD temperatures, Vostok δD) (Ho et al., 2012; Pahnke et al., 2003). The age model of core PS75/079-2 is based originally on correlation of its iron content record to the Antarctic EPICA Dome C dust record on the AICC12 timescale (Lamy et al., 2014), which was further modified by aligning in sections available benthic $\delta^{18}\text{O}$, planktonic $\delta^{18}\text{O}$ and Mg/Ca temperature data for core PS75/079-2 to the respective records of cores PS75/059-2.

5.3 Results

Downcore the Mg/Ca values of core PS75/059-2 display glacial-interglacial cycles with the Mg/Ca values varying between $2.05 \text{ mmol mol}^{-1}$ and $0.89 \text{ mmol mol}^{-1}$. Low values occur during glacial times, high values occur during interglacial times. The Mg/Ca values of core PS75/056-1 vary from $1.57 \text{ mmol mol}^{-1}$ to $0.75 \text{ mmol mol}^{-1}$ over the full core length and fit the Mg/Ca values of PS75/059-2, but differences occur in detail. For core PS75/079-2 downcore Mg/Ca values were obtained only for interglacial intervals with values ranging from $1.43 \text{ mmol mol}^{-1}$ to $0.71 \text{ mmol mol}^{-1}$ (Figure 5.6). The core top Mg/Ca values are 1.08, 1.17 and $0.85 \text{ mmol mol}^{-1}$ for cores PS75/056-1, PS75/059-2 and pilot core PS75/079-2, respectively. According the used calibration equation (Mashiotta et al., 1999), the corresponding temperatures are 7.7, 8.5 and $5.5 \text{ }^\circ\text{C}$. Modern summer temperatures at the core locations are 5.6, 6.7 and $3.3 \text{ }^\circ\text{C}$ at 50 m water depth (Locarnini et al., 2010, WOA09) and are thus considerably lower. The Mg/Ca values of the surface samples PS75/034-1, PS75/051-2 and PS75/076-1 are 1.44, 1.31 and $1.31 \text{ mmol mol}^{-1}$, which corresponds to temperatures of 10.4, 9.5 and $8.6 \text{ }^\circ\text{C}$. Again modern summer temperatures at 50 m water depth are lower at each site, amounting to 7.2, 7.2 and $5.1 \text{ }^\circ\text{C}$ (Locarnini et al., 2010, WOA09). A Holocene age for the uppermost Mg/Ca values coming from the PS75/056-1, PS75/059-2, PS75/079-2 and PS75/076-1 samples is indicated by low benthic $\delta^{18}\text{O}_{\text{c}}$ value of 3.08, 2.81, 3.06 and $3.42 \text{ }^\circ\text{‰}$, respectively.

Downcore the $\delta^{18}\text{O}_{\text{c}}$ values of core PS75/059-2 vary between $4.23 \text{ }^\circ\text{‰}$ and $2.12 \text{ }^\circ\text{‰}$ and display typical glacial-interglacial cycles (Figure 5.3). The glacial-interglacial changes are about 1.6, 1.9, 1.1, 1.2 and $1.9 \text{ }^\circ\text{‰}$ for terminations I, II, II, IV and V, respectively. The $\delta^{18}\text{O}_{\text{c}}$ values of core PS75/056-1 are almost identical to those of core PS75/059-2 and vary between $4.34 \text{ }^\circ\text{‰}$ and $2.18 \text{ }^\circ\text{‰}$, with glacial-

interglacial changes accounting to 1.8 ‰ at termination I (Figure 5.4). For core PS75/059-2, the calculated $\delta^{18}\text{O}_{\text{ivc-w}}$ values are rather constant, thus no glacial-interglacial cyclicity is apparent. Yet, high frequent downcore variability is present. The core top $\delta^{18}\text{O}_{\text{ivc-w}}$ (0.82 ‰) is much lower than modern surface ocean $\delta^{18}\text{O}_w$ (-0.25 ‰) at the location (LeGrande and Smith, 2006). Due to the similarity of the Mg/Ca and $\delta^{18}\text{O}_c$ pairs with core PS75/059-2, the core PS75/056-1 $\delta^{18}\text{O}_{\text{ivc-w}}$ values fit those of core PS75/059-2 (supplemental information S5.1)

The foraminiferal shell weight values of core PS75/059-2 vary between 31.7 μg to 18.0 μg , whereas no glacial-interglacial cyclicity is visible downcore. In the upper part of the record (0-185 ka), the shell weights stay rather constant at a level of $26.5 \pm 1.7 \mu\text{g}$, which coincides with Holocene shell weights of 27 μg . At 185 ka, the shell weights drop to a level of $23.8 \pm 2.4 \mu\text{g}$ and remain low for the older part of the record. In this part, the shell weights display more pronounced fluctuations with short term maxima around 346 and 401 ka. The foraminiferal shell weight values of core PS75/079-2, obtained for sections where carbonate is present, vary around 22.0 μg (supplemental information S5.2). Highest values of up to 27.0 μg occur generally around peak interglacial conditions.

5.4 Discussion

5.4.1 Dissolution-Evaluation of the Mg/Ca signal

Cores PS75/056-1, PS75/059-2 and PS75/079-2 were collected from water depths, approximately 600-800 m below the modern calcite saturation horizon (Takahashi et al., 1981). In the past the depth of the calcite saturation horizon and, thus, the lysocline depth varied in the Southern Ocean. During glacial times the calcite saturation horizon may have located up to 900 m shallower in the Atlantic and Indian sector, as it is the case today (Howard and Prell, 1994). Carbonate dissolution has the potential to lower the initial Mg/Ca signature derived at the surface during foraminiferal shell calcification, but also to affect the initial $\delta^{18}\text{O}_c$ signature recorded in foraminiferal shell calcite (Brown and Elderfield, 1996; Lohmann, 1995). Therefore, we have first to evaluate the validity of the here reported Mg/Ca and the $\delta^{18}\text{O}_c$ data.

Carbonate dissolution at the sediment surface also lowers the initial shell weights of foraminifera after deposition. Dissolution unaffected shell weights of *G. bulloides* were reported from the subantarctic western South Pacific, off New Zealand (Moy et al., 2009). These shell weights were obtained from the size fraction 300–355 μm , somewhat wider than the 315–355 μm used in our study for core PS75/059-2. Yet, according to additional measurements on the 300–355 μm size fraction of core PS75/059-2, the associated weight deviation amount to only ~5 %. The Holocene shell weights of core PS75/059-2 are ~27.0 μg in the 315–355 μm size fraction (Figure 5.3), consequently corresponding to ~25.7 μg in the 300–355 μm size fraction. Thus, the western South Pacific shell weights, which have values of ~24.5 μg for the Holocene, are about the same than those of core PS75/059-2. If assuming comparable surface ecological conditions to the subantarctic central South Pacific, we infer that during

the Holocene dissolution had only a minor effect on *G. bulloides* shells at core side PS75/059-2. However the overall shift to lower shell weight values downcore indicates enhanced shell test corrosion further back in time (Figure 5.3). In contrast, the Mg/Ca data do not reflect the overall decreasing trend in shell weights. As dissolution of foraminiferal carbonate shells in general lowers the initial Mg/Ca values (Brown and Elderfield, 1996), we regard the Mg/Ca values of core PS75/059-2 therefore largely as unaltered on orbital timescales. The same should also apply to the $\delta^{18}\text{O}_c$ signature, which tend to be interrelated to the Mg/Ca signature (Elderfield et al., 2002; Friedrich et al., 2012). Core PS75/056-1 comes from almost same water depth as neighboring core PS75/059-2, thus its downcore data are likewise regarded as unaffected. This is also assumed for core PS75/079-2, at least during interglacial optima, as its shell weights have there the same order of magnitude than the shell weights in the lower parts of core PS75/059-2 (supplemental information S5.2). Finally, we note that the Mg/Ca signature of *G. bulloides* derived during shell calcification was proposed to be in general resistant to post depositional alteration caused by carbonate dissolution (Mekik et al., 2007).

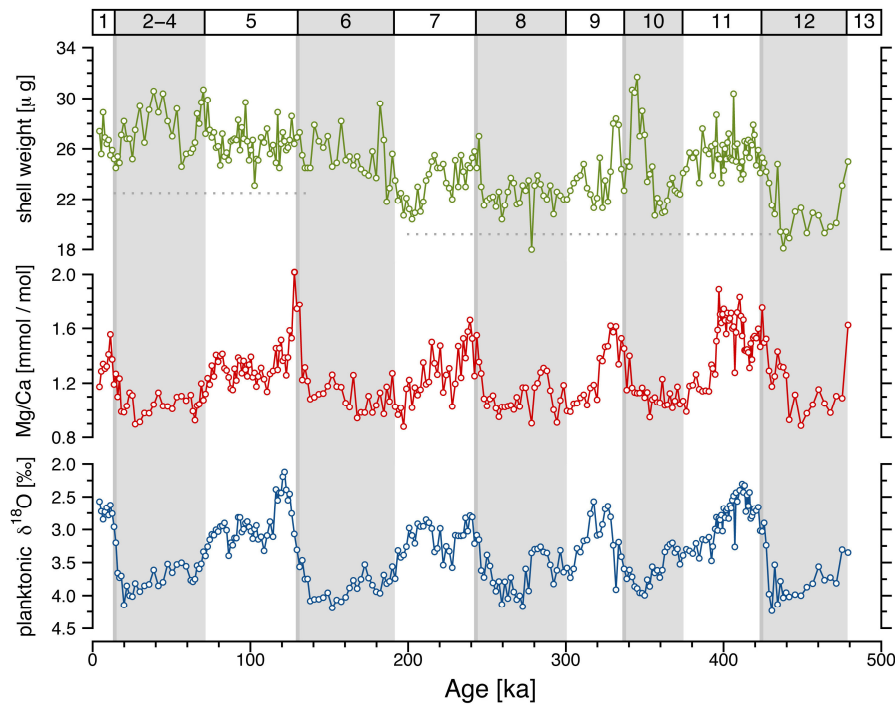


Figure 5.3. Records of core PS75/059-2 from the central South Pacific; a) *G. bulloides* shell weights, 315-355 μm size fraction; b) Mg/Ca measured on *G. bulloides*; c) Calcite $\delta^{18}\text{O}_c$ measured on *G. bulloides*; Note that the trend toward decreased *G. bulloides* shell weights is not reflected in the Mg/Ca data.

5.4.2 Interpretation of SST and $\delta^{18}\text{O}_{\text{ivc-w}}$ estimates

Today the surface hydrography at the central South Pacific is strongly affected by changes in the mixed layer depth, which vary on a seasonal cycle. Mixed layer depths range from 300 m during winter (August) to 50 m during summer (January) at core sites PS75/056-1 and PS75/059-2 (Monterey and Levitus, 1997). Associated are seasonal changes in mixed layer temperature driven by ocean-atmosphere heat exchange or heat advection (e.g., Sallée et al., 2010a), resulting in year around surface temperatur variations of $\sim 1^\circ\text{C}$ at the core positions (Locarnini et al., 2010, WOA09). Changes

in the mixed layer depths also affect phytoplankton productivity due to associated changes in vertical nutrient supply and light availability. In particular, light limitation during intensive winter mixing restricts the phytoplankton growth to the period from spring to autumn (Sallée et al., 2010a; Thomalla et al., 2011). As a consequence, the food-dependent planktonic foraminifera *G. bulloides* should also experience seasonality with highest shell fluxes out of the surface layer occurring during the summer months. In turn, the reported downcore SST signal should have a strong seasonal imprint. In this regard, the Mg/Ca-derived SST records PS75/059-2 and PS75/056-1 are assumed to reflect mixed layer temperature changes at about 50 m water depth weighted toward summer temperatures. This corresponds to the depth habitat and the seasonality in shell fluxes of the planktonic foraminiferal species *G. bulloides* according to sediment trap results from the western South Pacific (King and Howard, 2005). The same is assumed to apply also for core PS75/079-2. Modelling studies suppose for high latitudes that the growth season of *G. bulloides* shifts towards the warmer summer months during glacials in direct adaption to the lower water temperatures (Fraile et al., 2009a; Fraile et al., 2009b). However, as phytoplankton productivity at our core positions occurs today almost entirely during the summer months (Thomalla et al., 2011), we consider the seasonal bias in case of SST records PS75/056-1 and PS75/059-2 as comparatively minor.

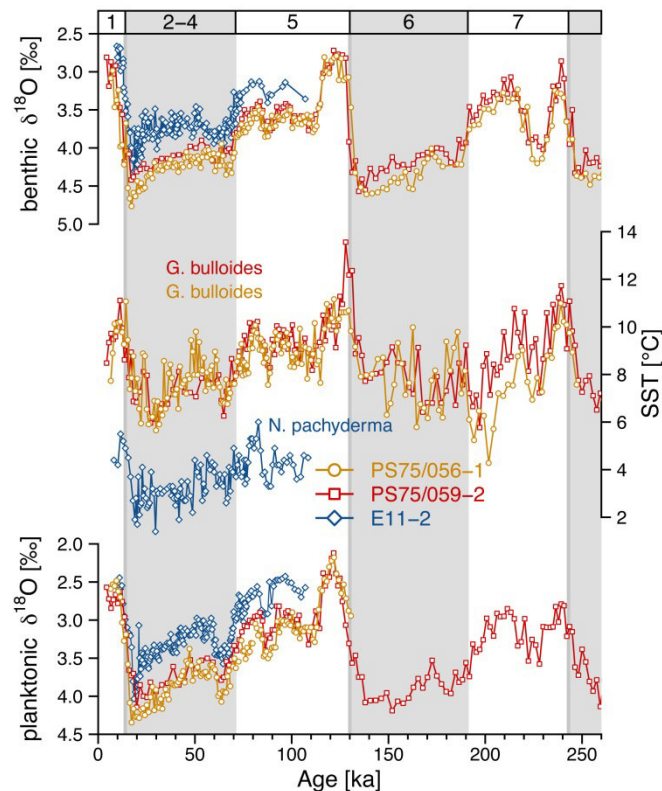


Figure 5.4. Past surface water hydrographic changes reconstructed on central South Pacific cores PS75/056-1, PS75/059-2 and E11-2 (Mashiotta et al. 1999), each recovered from the southernmost East Pacific Rise area; a) Benthic $\delta^{18}\text{O}_C$ records; b) Planktonic Mg/Ca SST records based on *G. bulloides* and *N. pachyderma* (E11-2); c) Planktonic $\delta^{18}\text{O}_C$ records based on *G. bulloides* and *N. pachyderma* (E11-2); The age model of core E11-2 is from Ninnemann and Charles (1997).

4.3 Evaluation of the SST and SSS estimate

The here used temperature equation has a calibrated range from 10 °C to 25 °C (Mashiotta et al., 1999). We thus extrapolate across its lower temperature end, which may induce a systematic bias in the SST estimate from cores PS75/056-1 and PS75/059-2 (Figure 5.4). However, applying another *G. bulloides* specific calibration equation on our Mg/Ca data would result in almost identical large downcore SST variations apart from a constant offset in its absolute values (Elderfield and Ganssen, 2000). Moreover, our obtained temperature decrease of 2.5 °C across the last termination is consistent with the Mg/Ca-derived SST reconstruction on directly northward situated core E11-2 measured on the more cold-water adapted planktonic foraminiferal species *N. pachyderma* (Mashiotta et al., 1999) (Figure 5.4). At site E11-2, the Mg/Ca-derived SSTs were independently estimated by a *N. pachyderma* specific calibration equation with a constrained calibration range down to 0 °C (Nürnberg et al., 1996). Further, a 2.5 °C temperature decrease is in line with close by diatom-based and foraminifera-based SST constructions (Benz et al., in preparation; Luz, 1977). Therefore we conclude that the SST amplitudes and thus the orbital scale changes are correctly reconstructed in our Mg/Ca records from cores PS75/056-1 and PS75/059-2.

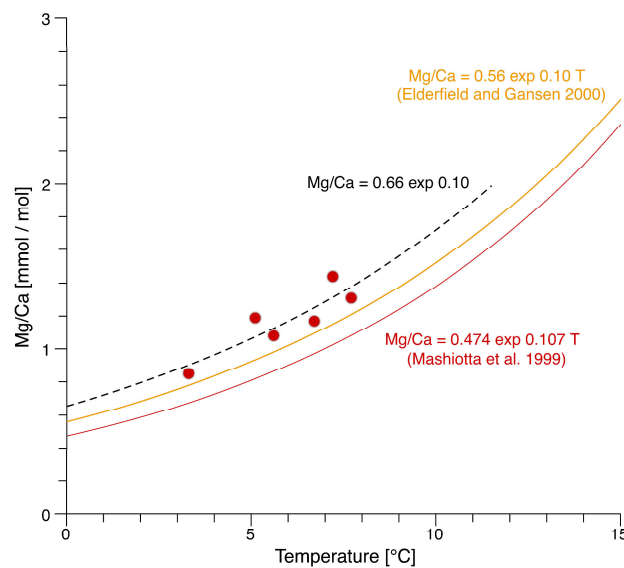


Figure 5.5. Cross plot of the *G. bulloides* Mg/Ca data from studied surface and core top samples versus the modern summer (August) temperature at 50 m water depth, respectively estimated from the WOA09 data compilation; Details to the used Mg/Ca data are given in Table 5.1; The dashed black curve represents the regression line of Mg/Ca on temperature, constructed under assumption of an exponential relationship; Further the curves (red, orange) of two published temperature equations are also displayed

The Mg/Ca–T cross plot (Figure 5.5) of the central South Pacific surface sediment and core top data, whilst latter are interpreted to represent late Holocene age due to their correspondingly low benthic $\delta^{18}\text{O}_c$ values (Table 5.1), leads us to following conclusions: First, it confirms our above inference that the amplitudes are correctly reflected at low temperatures as the data points follow the slope of commonly used *G. bulloides* specific calibration curves. Second that the absolute values are not adequately described as the current calibrations curves have much too low interception points. Even if

the Mg/Ca-derived SSTs reflect full summer conditions, they systematically overestimate modern summer temperatures at 50 m water depth. Whereas in case of our used calibration of Mashiotta et al. (1999) the discrepancies account to as much as 3 °C. Thus, a theoretical upward shift of the intersect point by 1 Mg/Ca [mmol/mol] would yield more appropriate Mg/Ca-derived SST estimates for the study area. This would result in generally 3 °C lower temperatures for cores PS75/056-1 and PS75/059-2 with glacial values of 4 °C still remaining within the optimal temperature range for the *G. bulloides* growth, which has its lower end at 4 °C (Žaric et al., 2005). Consequently, also the constant temperature contrast of ~4 °C to more northern located core E11-2 would reduce to ~1 °C (Figure 5.4), what is consistent with today's situation (Locarnini et al., 2010, WOA09).

The records were either reconstructed on planktonic foraminiferal species *G. bulloides* (PS75/056-1, PS75/059-2) or *N. pachyderma* (E11-2), both dwelling in the same depth habitat at high southern latitudes, thus also in the Subantarctic Zone (King and Howard, 2005). Partly, the remaining ~1 °C contrast may thus stem from a difference in shell flux seasonality of both species (King and Howard, 2005). However, as temperatures at their depth habitat (~50 m) vary far less than 1 °C over the growing season (spring to autumn) around the core locations (Locarnini et al., 2010, WOA09), this factor can only have a minor impact. Particularly, as a strong vertical stratification is year around absent (Figure 5.10), so that uncertainties regarding their depth habitat carry little weight. The fact that the temperature contrast of records PS75/056-1 and PS75/059-2 to record E11-2 remained rather stable throughout the past (Figure 5.4), further indicates that potential changes in foraminiferal depth habitat and shell flux seasonality in adaptation to glacially changing hydrographic conditions played no larger role.

The uncertainties in the absolute temperature estimate has a strong impact on sea water $\delta^{18}\text{O}_w$ ($\delta^{18}\text{O}_{\text{ivc-w}}$) estimates, that are unrealistically high compared to modern values. For instance core PS75/059-2 has a core top value of 0.82 ‰ (Figure 5.6), about one per mil higher than the modern value of -0.25 ‰ (LeGrande and Schmidt, 2006). According to the here chosen temperature- $\delta^{18}\text{O}$ equation, a temperature decrease of 1 °C leads to a $\delta^{18}\text{O}_w$ decrease of about 0.25 ‰ (Shackleton, 1974). Thus, a 3 °C lower temperatures estimate (corr. ~0.75 ‰) for the core would bring the sea water $\delta^{18}\text{O}_w$ estimates much close to the modern value with a remaining deviation of about 0.3 ‰. Taken into account the large uncertainties in the absolute values of commonly used temperature- $\delta^{18}\text{O}$ equations (Bemis et al., 1998), we regard the 0.3 ‰ deviation as realistic, thus the sea water $\delta^{18}\text{O}_w$ estimate by itself as reliable. Due to the virtual linearity of the used equation (Shackleton, 1974), an overestimation in SST has no impact on downcore sea water $\delta^{18}\text{O}_w$ ($\delta^{18}\text{O}_{\text{ivc-w}}$) amplitude ranges. Taken together, we conclude that the Mg/Ca-based SST and $\delta^{18}\text{O}_c$ amplitudes and thus the orbital scale changes are correctly reconstructed. Though, the absolute SST and $\delta^{18}\text{O}_c$ values are consistently too high by ~3 °C and ~0.75 ‰. Given that the downcore variations for core PS75/056-1 closely fits those for core PS75/059-2 (Figure 5.4, supplemental information S5.1), in the following we will focus on the records of core PS75/059-2.

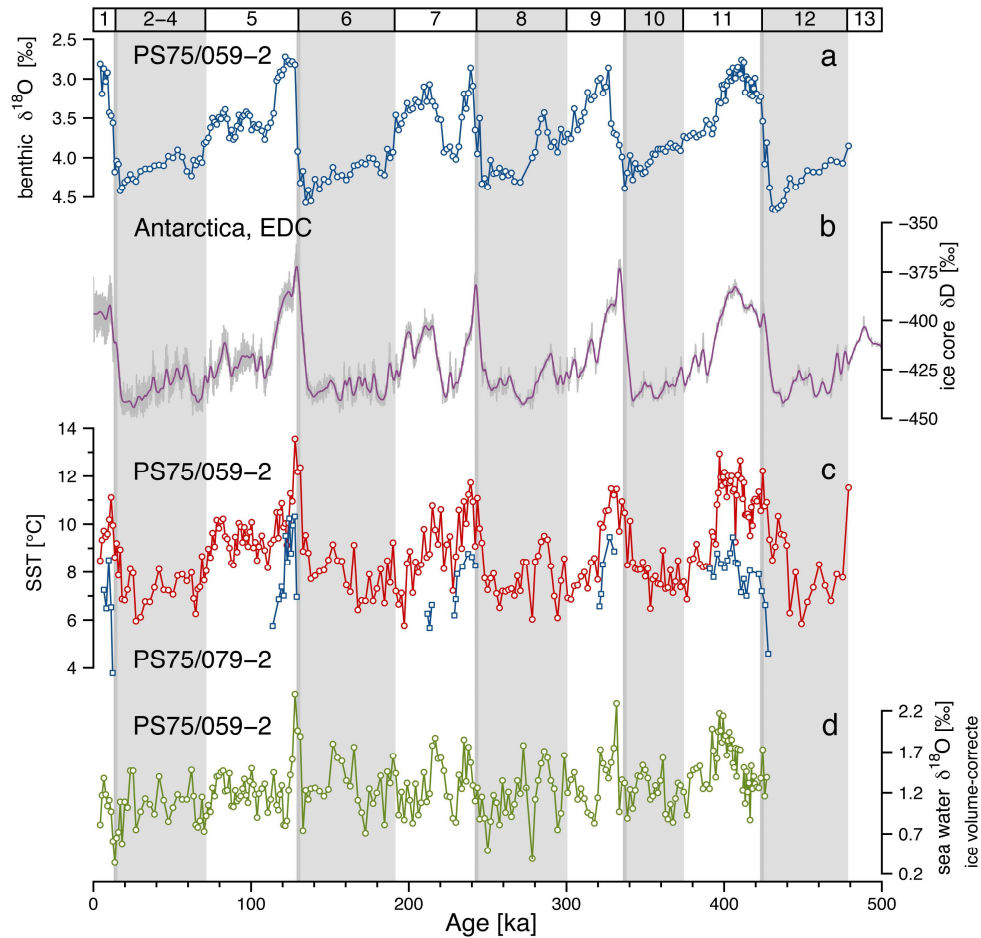


Figure 5.6. Records of central South Pacific cores PS75/059-2 and PS75/079-2 in comparison to the EPICA Dome C ice core deuterium (δD) record (Jouzel et al. 2007), which reflects air temperature changes over East Antarctica (Antarctic Plateau); a) Benthic $\delta^{18}O_c$ record of core PS75/059-2; b) EPICA δD record; c) *G. bulloides* Mg/Ca-SST records of cores PS75/059-2 and PS75/079-2, the record of core PS75/079-2 is discontinuous due to temporarily low or absent carbonate content; d) Global ice volume-corrected *G. bulloides* $\delta^{18}O_{ivc-w}$ record of core PS75/059-2.

5.4.4 Surface hydrographic evolution in the central South Pacific

First, we compare our reconstructed SST variations for the central Pacific Ocean to past continental East Antarctica plateau air temperature variations (Figure 5.6). On the whole, changes in our SST records from cores PS75/059-2 and PS75/079-2 vary along with Antarctic air temperature variations as recorded in the EPICA Dome C ice core δD record (EPICA Community Members, 2004; Jouzel et al., 2007). Our SST records show about the same low temperature during each of the past five glacial periods, a pattern that is also evident in Antarctica. Likewise, the interglacial peak warming was relatively the same. Indeed, the SST record from core PS75/059-2 indicates that the MIS 9 interglacial was less pronounced in the central South Pacific area. However, complementary SST values from more poleward situated core PS75/079-2 display comparatively high SSTs for MIS 9 (Figure 5.6). This implies that SSTs during MIS 9 peak warm are not correctly reflected for core PS75/059-2, which may, for instance, stem from bioturbational sediment homogenization. Thus, temperatures in the central South Pacific area have reached a level during MIS 9, which was almost the same as during

MIS 5. Compared to the other interglacials, the MIS 11 interglacial is not characterized by outstanding warm temperatures as observed for example from Mg/Ca-derived SST reconstructions from the tropical Pacific (Lea et al., 2003; Lea et al., 2000). This is remarkable as the depositional facies of the central South Pacific cores PS75/059-2 and PS75/079-2 is characterized by extremely high coccolith contents (Gersonde, 2011) at that time which may imply much warmer conditions. For core PS75/059-2 the glacial-interglacial amplitudes are about 2.5, 6.5, 5.0, 5.0 and 5.0 °C for terminations I, II, II, IV and V, respectively. Taken together, our comparison implies that East Antarctic and central South Pacific temperatures in general closely co-varied regarding the strength of individual glacial-interglacial cycles. However, the central South Pacific records display moderate temperature changes over the last transition. This is consistent to previous observations by Mashiotta et al. (1999).

Highly resolved SST records throughout the South Pacific are overall linked to East Antarctic air temperature changes (Barrows and Juggins, 2005; Barrows et al., 2007; Calvo et al., 2007; Lamy et al., 2004; Mashiotta et al., 1999; Pahnke et al., 2003). Although, at its western oceanic areas, close to New Zealand, climatic decoupling from Antarctica was observed, with glacial stages displaying higher short term SST variability than interglacial stages (Pahnke et al., 2003). In case of the Mg/Ca-derived SST record PS75/059-2 the early Holocene climatic optimum is present in the record, as it is typical for the circum-Antarctic ocean (e.g., Bianchi and Gersonde, 2004). Despite its high downcore variance of the Mg/Ca-derived SST, and the low resolution, some other short term features may represent ‘true’ climatic signals. For instance, the pronounced temperature rise at termination V (424 ka), in transition from MIS 12 to MIS 11, which occur contemporary to a short warming phase visible in the Antarctic air temperature record. Such an MIS 11 climate optimum was previously observed from the South Atlantic (Vázquez Riveiros et al., 2010).

In contrast to SST, the downcore $\delta^{18}\text{O}_{\text{ivc-w}}$ variations do not display a detectable glacial-interglacial modulation at core location PS75/059-2 (Figure 5.6). Therefore, our records suggest that in the higher latitude ($\sim 55^\circ\text{S}$) oceanic areas of the central South Pacific past surface $\delta^{18}\text{O}_{\text{ivc-w}}$ remained largely unchanged. Besides evaporation-precipitation changes, varying surface freshwater flux due to iceberg melting would have the potential to impact surface ocean $\delta^{18}\text{O}_{\text{ivc-w}}$ and salinity at the core location. Thus, our results do not indicate a much higher, glacially increased melt water influence through iceberg discharges in the more distal subantarctic South Pacific. However, according to modern $\delta^{18}\text{O}_w$ -salinity observations (Srivastava et al., 2007), sea ice melting and freezing near Antarctica influence the surface freshwater flux and the surface ocean salinity, but it has less effect on surface oceans $\delta^{18}\text{O}_w$ signature. As sea ice expand northwards during glacial times (Benz et al., in preparation; Gersonde et al., 2005), the $\delta^{18}\text{O}_{\text{ivc-w}}$ record does therefore not necessarily reflect salinity. This has been discussed on local to ocean-wide scale (LeGrande and Schmidt, 2011; Rohling and Bigg, 1998).

5.4.5 The timing across climate transitions

Changes in central South Pacific SSTs lead those of benthic $\delta^{18}\text{O}_c$ during climate transitions. With regard to core PS75/059-2, this is most evident at termination IV, in transition from MIS 10 to MIS 9 (Figures 5.4 and 5.6). Whereby, the SST leads amount to about 1.0, 3.5, 4, 7.5 and 3.5 ka for terminations I, II, III, IV and V, when taking the respective mid-transition values of its two records. Such SST leads have been reported from several marine Southern Ocean records (e.g., Becquey and Gersonde, 2003; Chase et al., 2003; Labeyrie et al., 1996; Mashiotta et al., 1999; Pichon et al., 1992) and indicate that local surface temperature changes predated changes in the continental ice volume, thus in the ocean's total $\delta^{18}\text{O}_w$ composition. Further, delayed changes in local deep water temperature may have contributed to the SST leads, as the benthic foraminiferal $\delta^{18}\text{O}_c$ reflects besides the $\delta^{18}\text{O}_w$ composition also ambient seawater temperatures during shell calcification (Lisiecki and Raymo, 2009; Skinner and Shackleton, 2005; Waelbroeck et al., 2011).

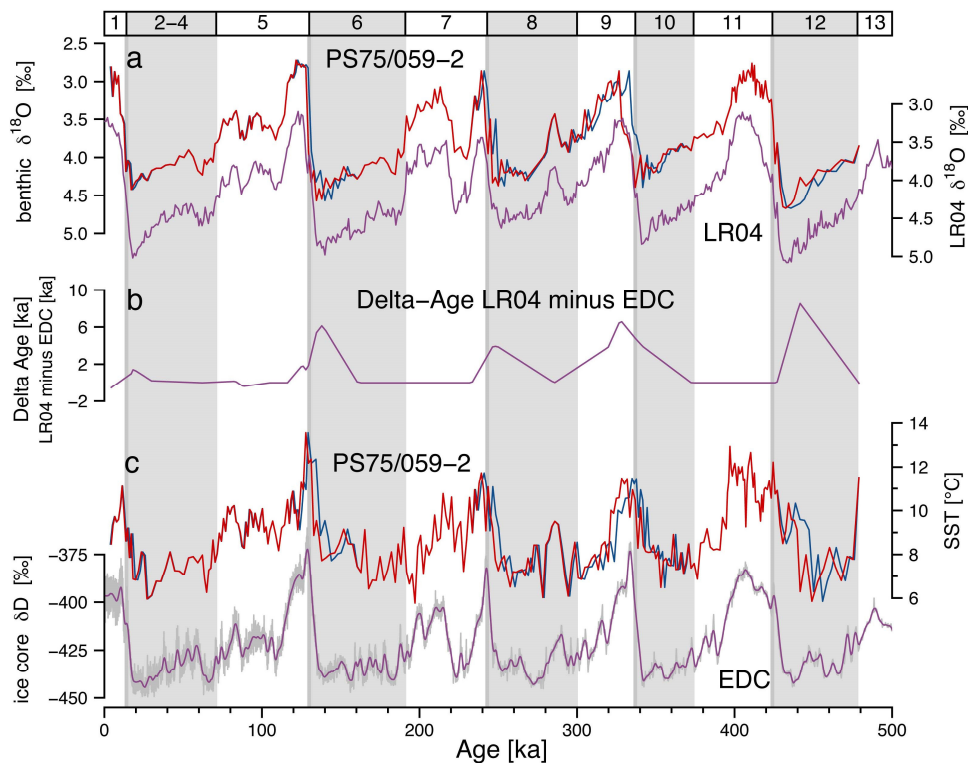


Figure 5.7. Comparison of core PS75/059-2 records on different chronologies; the chronology of the red curves, used in this study, was obtained from correlation of its Mg/Ca-SST record to the EPICA δD record on the EDC3 timescale; The chronology of the blue curves was obtained from correlation of its benthic $\delta^{18}\text{O}$ record to the benthic $\delta^{18}\text{O}$ stack on the LR04 timescale. The allinmant was done visually, while retaining, if possible, the initial pointers used for corralation to the EDC3 timescale; a) Benthic $\delta^{18}\text{O}_c$ records displayed next to the LR04 benthic $\delta^{18}\text{O}$ stack (purple curve); b) Age difference between LR04 and EDC3; c) *G. bulloides* Mg/Ca-SST records displayed next to the EPICA δD record.

Our chronology of core PS75/059-2 is based on visual correlation of its SST record to the records to the EPICA Dome C ice core δD deuterium record on the EDC 3 timescale. We modified this chronology around climate transitions by aligning the benthic $\delta^{18}\text{O}_c$ record in a further step to the

LR04 benthic $\delta^{18}\text{O}$ -stack. Comparing the benthic $\delta^{18}\text{O}_c$ record of core PS75/059-2 on its two chronologies displays deviations in timing around climate transitions (Figure 5.7). They amount to 1.0 ka for the last and 6.0, 4.0, 6.0, 8.0 ka for the preceding transitions, whilst the benthic $\delta^{18}\text{O}_c$ changes occur earlier on the EDC chronology. Of course, deviations may first not be unexpected, as the timescales of both chronologies were constructed on independent ways (Parrenin et al., 2007). Focusing only on climate transitions, in our case the deviations are however much higher. A comparison of numerous benthic $\delta^{18}\text{O}_c$ records on the LR04 chronology yield a significant Atlantic lead over Central Pacific $\delta^{18}\text{O}_c$ changes. This is likewise displayed by deviations in timing, which are confined in their occurrence to terminations and amount to 1.6 ka on average. Temporarily, these deviations are up to 4 ka high (Lisiecki and Raymo, 2009). As above, the diachronous $\delta^{18}\text{O}_c$ changes relate to ocean circulation, whereby they reflect the time delay of Atlantic initiated $\delta^{18}\text{O}_w$ and temperature signals, which originate over the course of deglaciations, to convey into the Central Pacific basin (Lisiecki and Raymo, 2009; Skinner and Shackleton, 2005). We may speculate that our central South Pacific observations are closely linked to this issue. If true, they may indicate that it took considerable time for climate signals researching the central South Pacific at depths, even though the area lies, in simple terms, only on halfway position with respect to ocean's conveyor circulation. With regard the findings of Stern and Lisiecki (2014), a much differentiated timing of past $\delta^{18}\text{O}_w$ changes across climate transitions is conceivably for the South Pacific at depths. This may be important to archive for future studies dealing with the sequencing of oceanic mechanisms involved in the global shift from glacial to interglacial climate conditions.

5.4.6 Linkage to the western South Pacific – New Zealand

Compiled surface temperature estimates covering the last glacial time interval illustrate much higher glacial-interglacial surface temperature variations for the western and eastern coastal areas of the South Pacific basin than for its central oceanic areas (MARGO Project Members, 2009). Below, we examine the long term evolution among these basin domains by addressing first the western South Pacific coastal areas, around New Zealand. Today, the surface hydrography there is decisively determined by the interaction of subtropical waters, which flow poleward along the western boundary of the tropical South Pacific gyre (Figure 5.1), and subantarctic waters flowing within the Antarctic Circumpolar Current system (e.g., De Boer et al., 2013; Graham and De Boer, 2013; Hill et al., 2008; Ridgway and Dunn, 2003). Overall the available paleoceanographic studies indicate a changing supply of subtropical waters during glacial times, which in turn lead to an increased presence of subantarctic waters in the New Zealand area (e.g., Crundwell et al., 2008; Hayward et al., 2012; Hayward et al., 2008; Neil et al., 2004; Pelejero et al., 2006; Schaefer et al., 2005). In accordance, a noticeable strong cooling in the region is documented on foraminiferal assemblage-based temperature maps produced for modern and last glacial times (Barrows and Juggins, 2005; Barrows et al., 2007). In order to place our results from the central South Pacific in existing picture, we focus on the comparison to records of east New Zealand core MD97-2120 (Pahnke et al., 2003). Core site MD97-2120 rest close to the

Subtropical Front (Figures 5.1 and 5.2), which defines the poleward limit of the South Pacific gyre, and seems appropriate positioned to detect wider surface hydrographic changes amongst the tropical and subtropical domains in the western South Pacific oceanic area.

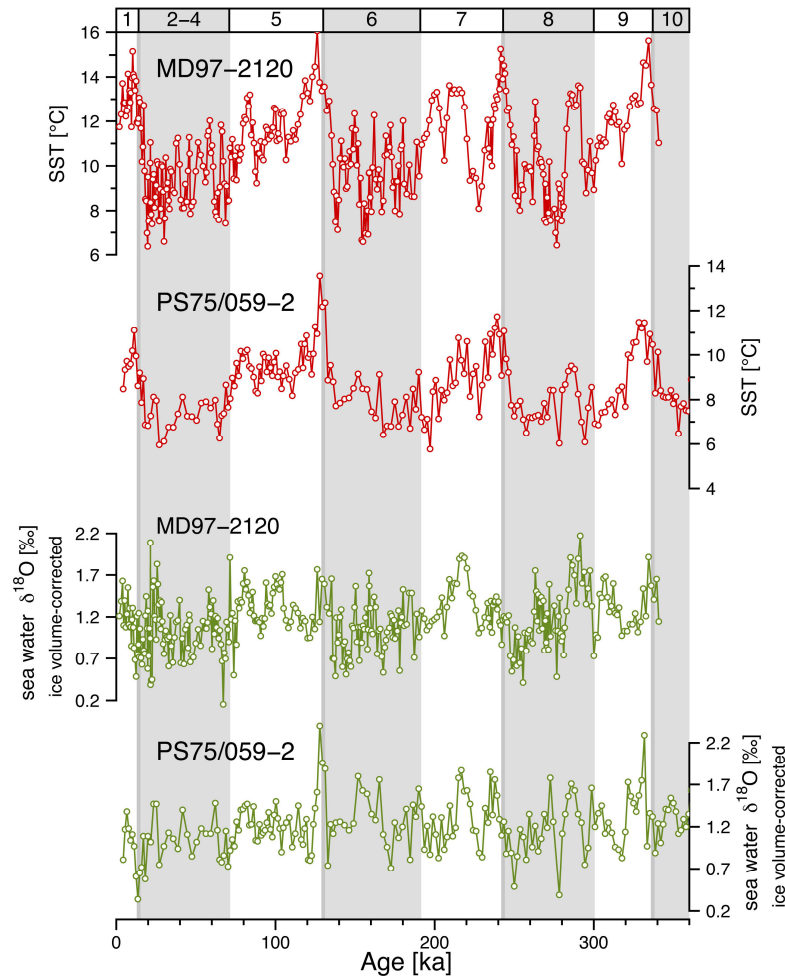


Figure 5.8. Comparison between records of the central South Pacific core PS75/059-2 and west New Zealand core MD97-2120 (Pahnke et al. 2003); a, b) *G. bulloides* Mg/Ca-SST records; c, d) Global ice volume-corrected $\delta^{18}\text{O}_{\text{ivc-w}}$ records

Figure 5.8 shows the Mg/Ca-based SST and $\delta^{18}\text{O}_{\text{ivc-w}}$ records of cores PS75/059-2 and MD97-2120 (~45°S latitude) obtained from *G. bulloides*, respectively. On orbital timescales, past surface water temperature and salinity variations were accordingly stronger close to New Zealand, where glacial-interglacial amplitudes amounted to 6 °C or more. This is even more apparent considering the reconstructed SST and $\delta^{18}\text{O}_w$ gradients between New Zealand and the central South Pacific core positions (Figure 5.9). Hence, the oceanic area around New Zealand experienced recurrently an overproportional cooling and freshening during glacial times. This indicates an increased equatorward advection of cold and fresh subantarctic waters, or vice versa, a reduced poleward advection of warm and salt subtropical waters. Our comparison results are consistent to the findings of earlier studies (e.g., Crundwell et al., 2008; Hayward et al., 2012; Hayward et al., 2008; Neil et al., 2004; Pelejero et al., 2006; Schaefer et al., 2005), which focus on the examination of past temperature changes in

vicinity to the STF – what contrasts to our approach. Importantly, *G. bulloides* obtained downcore Mg/Ca-based SST and $\delta^{18}\text{O}_{\text{ivc-w}}$ changes were recently reconstructed for central South Pacific core SO213-59-2 (~45°S latitude) (Figures 5.1 and 5.2) (Tapia et al., 2015), thus document open ocean conditions from the same latitudes as New Zealand core MD97-2120. Covering two climate cycles, its SST record displays glacial-interglacial changes of 2 °C (Termination I) and 4 °C (Termination II), which is in the same order as observed 10° latitude further southward at our core location PS75/059-2. The corresponding $\delta^{18}\text{O}_{\text{ivc-w}}$ record also indicates comparable conditions (supplemental information S5.3). Thus, the considerably stronger hydrographic changes near New Zealand were not caused by basin scale changes in the latitudinal SST and $\delta^{18}\text{O}_w$ gradients, but invoke again an amplification mechanism linked to the interplay between subantarctic and subtropical surface water.

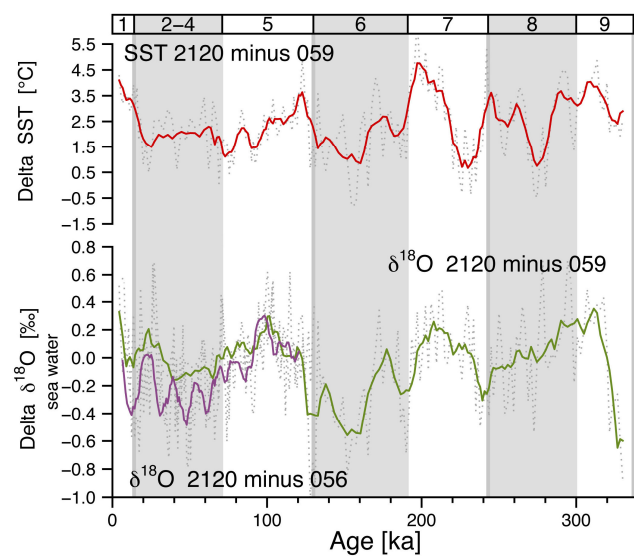


Figure 5.9. Evolution of the SST and $\delta^{18}\text{O}_w$ gradients between the subantarctic cores PS75/059-2 and MD97-2120 (Pahnke et al., 2003); Gradients were calculated by subtracting the original values (SST, $\delta^{18}\text{O}_w$) of core PS75/059-2 from the resampled values (SST, $\delta^{18}\text{O}_w$) of core MD97-2120, before resampling record MD97-2120 was smoothed by a 3-point moving average; Note that the ice volume effect cancels out in the calculation of the $\delta^{18}\text{O}_w$ gradient; a) Mg/Ca-SST gradient (gray dotted) together with its 7-point moving average (red curve); b) $\delta^{18}\text{O}_w$ gradient (gray dotted) together with its 7-point moving average (green curve), further the $\delta^{18}\text{O}_w$ gradient and its 7-point moving average (purple curve) is displayed for core PS75/056-1.

The interpretation of the temperature gradient can be affected by changes in the ecology of the foraminiferal species *G. bulloides* as adaption to changing surface hydrographic conditions in the past. This includes changes in foraminiferal seasonality or depth habitat (Fraile et al., 2009a; Fraile et al., 2009b). Moreover the SST gradient may reflect local, core site specific changes in the ocean atmosphere heat exchange, what may influence past surface water temperature variations on orbital, but also on seasonal timescales. Unlike temperature, salinity and thus $\delta^{18}\text{O}_w$ varies year around only minimal and stays almost constant over a wide depth range (Figure 5.10). Year around surface salinity changes are less than 0.1 psu at both core positions (Antonov et al., 2010; Locarnini et al., 2010) (WOA09), which corresponds to changing $\delta^{18}\text{O}_w$ values of only ~0.03 ‰ according the modern $\delta^{18}\text{O}_w$

salinity slope for the Southern Ocean (LeGrande and Schmidt, 2006). Thus, it is conceivably that the $\delta^{18}\text{O}_w$ gradient gives more robust results than the SST gradient. The $\delta^{18}\text{O}_w$ gradient displays more irregular variations than the temperature gradient (Figure 5.9). Accordingly, the individual glacial stages differ among each other, whereas the influence of fresh, subantarctic waters east of New Zealand was highest during MIS 6.

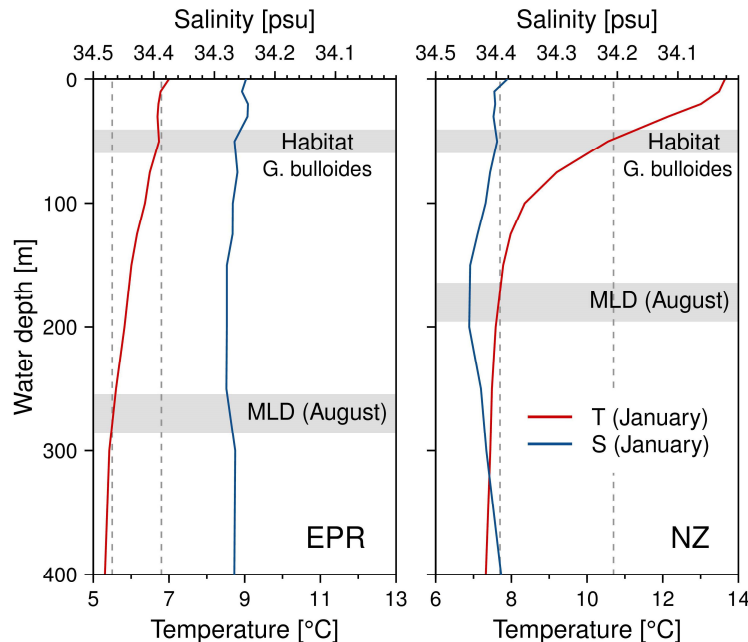


Figure 5.10. Summer temperature (red) and salinity (blue) profiles from the East Pacific Rise (left panel) and the western margin of New Zealand (right panel), obtained from the (January) WOA09 gridded data compilation (Antonov et al., 2010; Locarnini et al., 2010) at core locations PS75/059-2 and MD97-2120; Winter mixed layer depths (winter-MLD, August) are indicated by gray horizontal bars and were obtained from the monthly global MLD data compilation (Monterey and Levitus, 1997); Note that summer temperature and salinity at winter-MLD depths approximate winter near-surface temperature and salinity.

5.4.7 Western South Pacific STF displacement – New Zealand

Our current understanding of glacial-interglacial changes in the western South Pacific is strongly constrained by poleward limited core coverage. In particular with respect to longer time intervals, there is a lack of information regarding past surface water temperature and salinity variations in distance to the STF. Referring to this, we may use our central South Pacific record PS75/059-2 as a reference to estimate, in which extent the STF changed its position in the western South Pacific over glacial-interglacial cycles. By comparison to core site PS75/059-2, at the last glacial surface waters at core site MD97-2120, which lies on New Zealand east coast, displayed stronger freshening, associated with a relative depleted by about 0.4–0.5‰ in their $\delta^{18}\text{O}_w$ composition (Figure 5.9). Taken modern $\delta^{18}\text{O}_w$ gradients as a base (Figure 5.2), this corresponds to an equatorward displacement of the STF by more than 11° latitude. In case of temperature, a somewhat lower estimate of approximately 9° latitude is yielded. For the previous MIS 6 glacial intervals the frontal displacement was accordingly higher, whilst during MIS 8 the STF may have rested in similar position as it was the case during last

glaciation. Our estimates regarding a glacial STF displacement are comparable but somewhat higher than those inferred by (Nürnberg and Groeneveld, 2006). Assuming a modern SST-salinity relationship, the authors yield a substantial STF displacement of 6° to 8° latitude for core position MD97-2120. By contrast, local reconstructions around New Zealand prompt a much lesser STF displacements. For the west New Zealand area an about 3° latitudinal glacial migration was supposed (Hayward et al., 2012). For east New Zealand, where core MD97-2120 was collected, it was even suggested that the STF remained near to its modern position due to topographic constrains (Sikes et al., 2002; Weaver et al., 1998), with an inferred frontal displacement of not more than 2° latitude during the LGM (Sikes et al., 2002). In order to reconcile the observations, we propose that the regional, STF connected changes around New Zealand were underlain by much larger, trans-regional oceanic changes. During glacial intervals the equatorward expansion of ACC influence was probably higher as inferred from a STF position only. In turn, this implies a considerable contraction of the South Pacific gyre in the western South Pacific during glacial times. Taken the modern situation as a base (Hill et al., 2008; Ridgway and Dunn, 2003), such changes may further comprise changes the South Pacific gyres western boundary current circulation (East Australian current). Not at least, as profound changes in the western boundary current circulation paths were observed further north along the Australian west coast (Bostock et al., 2006). Today, the temperature gradient across the STF increases only moderately, whilst the salinity gradient increases much more distinctly (Figure 5.2). For future, salinity records on a larger number of sediment cores from either STF sides would thus be useful to constrain, whether the STF position near New Zealand varied partly independently or not.

5.4.8 Linkage to the eastern South Pacific – Chile

As for the western South Pacific, considerable surface hydrographic changes were also supposed for the eastern South Pacific. Near Chile, core PS75/034-2 (~54°S latitude) reveals glacial-interglacial alkenone-based SST changes of 7 °C to 11 °C (Ho et al., 2012). Thus, they are about two times higher than those constructed from the central South Pacific core PS75/059-2 (Figure 5.11). The same is also displayed by the marked modulations of the corresponding SST gradient (Figure 5.11). Both cores are positioned at comparable high, subantarctic latitudes (Figure 5.1). The substantially larger amplitudes at downstream situated core site PS75/034-2 indicate therefore an active amplification mechanism. To explain different amplitudes between the eastern and central South Pacific, we follow previous interpretation of Ho et al. (2012), as inferred from a number of alkenone-based SST records, each documenting the long term SST evolution from along the Chilean coastline. Accordingly, a repeated, glacially increased advection of very cold, polar originating surface waters has induced an additional temperature drawdown in the eastern South Pacific oceanic area near Chile, on top of the general glacial SST decrease. In turn, this imply a glacial expansion in the ACC influence or more precisely, an enhanced equatorward flow of cold ACC waters within the South Pacific gyre's eastern boundary current (Ho et al., 2012). Reason therefore might be a reduced water volume trough-flow through Drake Passage during glacial times, consequently causing an intensified deflection of ACC waters

northwards (Lamy et al., under review). Consistent to current LGM observations (Benz et al., in preparation), our results confirm for the past 500 ka that the eastern South Pacific changes in the surface circulation pattern were regionally restricted. The main equatorward deflection of colder surface waters apart from the ACC main flow obviously occurred downstream to the central South Pacific core positions. Thus, the observed glacial changes from western South Pacific are not result of a broad, South Pacific basin wide expansion of the ACC system, but reflect the narrow surface water export along the eastern margin of the subtropical South Pacific gyre. On a larger view, our results are in line with the proposed changes in the eastern boundary current (Peru-Chile Current) transport at lower latitudes (Feldberg and Mix, 2002, 2003; Kaiser et al., 2005; Rincón-Martínez et al., 2010) and the observed LGM increase in the zonal SST gradient across the equatorial Pacific (MARGO Project Members), altogether indicating vigorous western boundary dynamics of the giant subtropical Southern Pacific gyre systems over glacial-interglacial cycles.

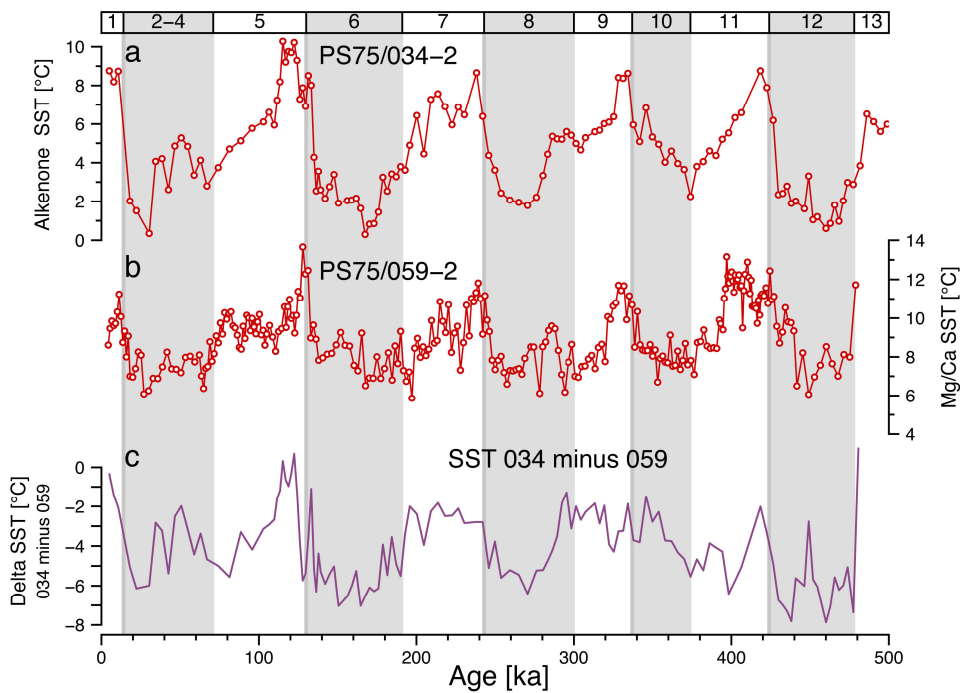


Figure 5.11. Comparison between temperature records of the central South Pacific core PS75/059-2 and Chilean core PS75/034-2 (Ho et al., 2012); a) Alkenone-based SST record of core PS75/034-2; b) *G. bulloides* Mg/Ca-based SST record of core PS75/059-2; c) Evolution of the SST gradient between the subantarctic cores PS75/059-2 and PS75/034-2; The gradient was calculated by subtracting the resampled SST values of core PS75/059-2 from the original SST values of core PS75/034-2.

It must be noted, however, that depending on the used SST reconstruction method, for instance Mg/Ca-based (PS75/059-2) or alkenon-based (PS75/034-2), differences can occur in the resultant amplitude changes (e.g., MARGO Project Members, 2009; Sikes et al., 2002). We therefore consider climate model simulation (TR400) results for core position PS75/059-2 and PS75/034-2 produced with an up to date Earth System model of intermediate complexity (LOVECLIM) (Timmermann et al., 2014) (Figure 5.12). The climate model simulation (TR400) reproduce diverse Southern Hemisphere

proxy records such as Antarctic air temperature in a realistic way and allowed among others to draw inferences on past Southern Oceans sea ice, oceanic and atmospheric circulation dynamics (Timmermann et al., 2014).

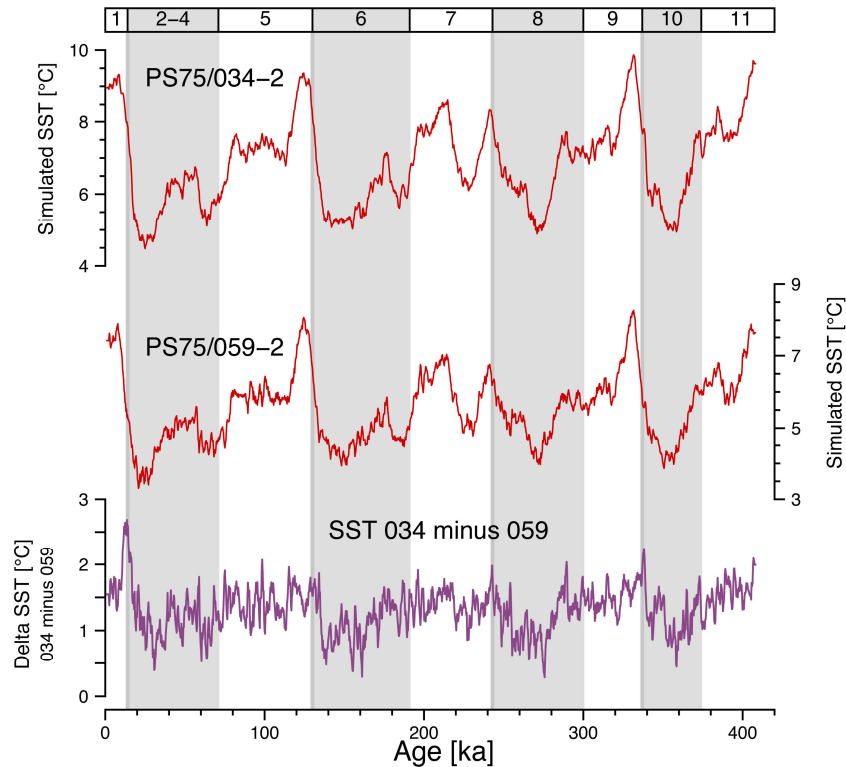


Figure 12. Simulated mean annual SST records by Earth System model (LOVERCIM) obtained from model run TR400 (Timmermann et al., 2014); a) Simulated SST evolution at core location PS75/034-2; b) Simulated SST evolution at core location PS75/059-2; c) Evolution of the simulated SST gradient between both locations; the gradient were calculated by subtracting the simulated SST values of core PS75/059-2 from those of core PS75/034-2.

For the central Southern Pacific the simulated glacial-interglacial SST changes reasonably fit our observations for core PS75/059-2, likewise displaying moderate glacial-interglacial amplitude change. Though they yields a somewhat higher amplitude change for the last glacial-interglacial transition due to comparable lower LGM SSTs (Figures 5.11 and 5.12). The simulated SSTs are throughout lower by $\sim 3\text{-}4$ °C, what supports our conclusion in *Section 5.3* that our reconstructed Mg/Ca-based SSTs display consistently ~ 3 °C too high absolute values. The simulated glacial-interglacial SST changes for the western South Pacific are far smaller as there alkenone-based SST changes constructed for core PS75/034-2 (Figures 4.11 and 5.12). Simulated amplitudes reach up to 5 °C only, whereas the constructed amplitudes are 7 °C or higher (Ho et al., 2012). Nonetheless, for glacial times the climate model simulation (TR400) results indicate a small, but recurring build-up of a SST gradient among both oceanic areas. In principle, the model results support that surface circulation changed locally in the western South Pacific, towards Chile, during glacial times. However, above outlined discrepancies to the constructed SST changes imply insufficient model sensitivity, incompatibility of the SST

reconstruction methods or both. Thus, a further constrained, more quantitative description of past western South Pacific SST variations remains an issue for further investigations.

5.5 Conclusion

We reconstructed past 480 ka SST and $\delta^{18}\text{O}_{\text{ivc-w}}$ changes for the central South Pacific oceanic area using paired Mg/Ca and $\delta^{18}\text{O}_c$ data from sediment cores. At first, the reliability of the reconstructions was assessed, considering also paired Mg/Ca and $\delta^{18}\text{O}_c$ data from surface sediment samples. The reconstructions reproduce correctly the amplitudes ranges of the downcore variations, but generate consistently $\sim 3^\circ\text{C}$ and $\sim 1\text{‰}$ too high absolute values. Independently thereof, our results show that the SSTs closely covaried with Antarctic air temperatures. The glacial-interglacial amplitudes were moderate, whereas they accounted to 2.5°C at the last glacial transition and ranged from 5°C to 6.5°C at the previous ones. The surface ocean $\delta^{18}\text{O}_w$ shows no conspicuous glacial-interglacial modulation after ice volume correction. Taken into account the oceanic setting of the study location, when related to past Antarctic sea ice advances, it is however questionable if the $\delta^{18}\text{O}_w$ also indicates that salinity remained unchanged. Further our results indicate that deep water temperature and $\delta^{18}\text{O}_w$ changes occurred at glacial terminations by $\sim 1\text{--}7$ ka delayed to the SST change in the study location and, apparently, also by $\sim 1\text{--}8$ ka delayed to deep water temperature and $\delta^{18}\text{O}_w$ changes in the Atlantic. By comparison, past glacial-interglacial SST changes were less pronounced in the central South Pacific than at its western and eastern coastal area. Consistent to previous proposes this point toward systematic amplification, linked to glacial-interglacial changes in the western and eastern boundary current dynamics of the subtropical South Pacific gyre. For the western South Pacific area this is further confirmed by Earth System model simulations. We tempted to quantify past hydrographic changes for the western South Pacific area around New Zealand, where both SST and $\delta^{18}\text{O}_w$ downcore reconstructions exist. Accordingly, we yield a hypothetical STF displacement of $\sim 10^\circ$ latitude during glacial times, which is much higher than often quoted.

Acknowledgements

We thank the captain, crew, and scientific party of R/V Polarstern for their support during the ANT-XXVI/2 cruise. Further we thank for the support from N Gehre with the Mg/Ca analyses (GEOMAR, Kiel) and from A. Mackensen, G. Meier, L. Haxhijaj and L. Schönborn with the stable isotope analyses (GEOMAR, Kiel; Alfred Wegener Institute, Bremerhaven). Particularly, we thank A. Timmermann, who kindly provided the simulated temperature data from Earth System model (LOVECLIM). The data presented in this study will be made available online in PANGAEA.

5.6 Supplemental Information

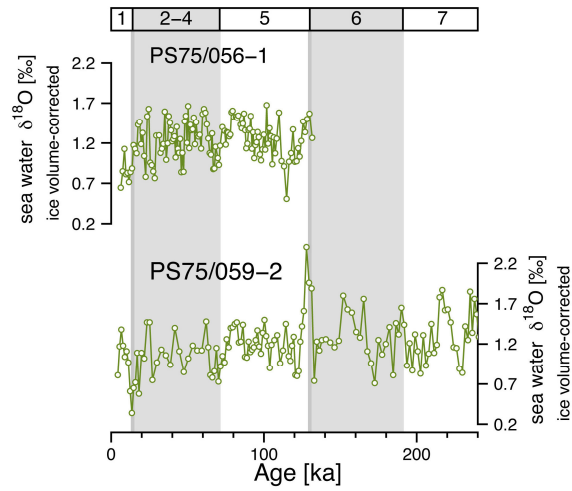


Figure S5.1. Comparison between the global ice volume-corrected $\delta^{18}\text{O}_{\text{ice-w}}$ records of nearby located central South Pacific cores PS75/056-1 (a) and PS75/059 (b).

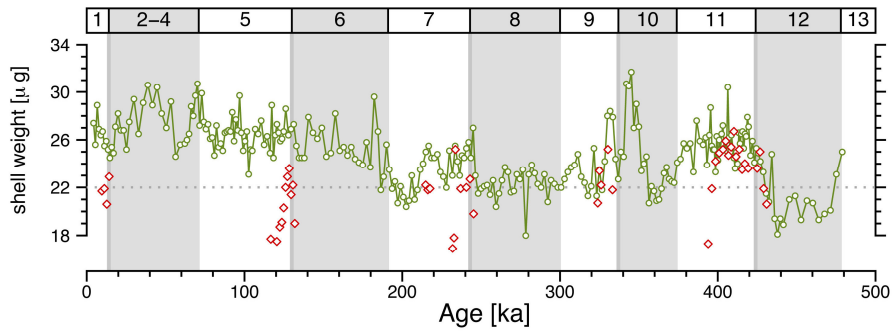


Figure S5.2. Comparison of the *G. bulloides* shell weight record (green) of core PS75/059-2 to the *G. bulloides* shell weight values (red) of core PS75/079-2

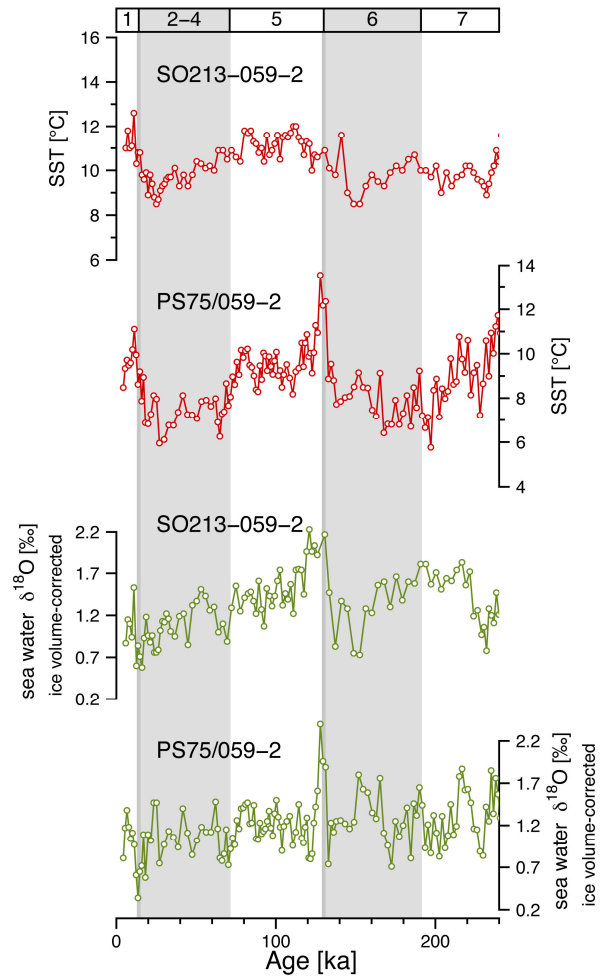


Figure S5.3. Comparison between records of the central South Pacific core PS75/059-2 (~55°S) and central South Pacific core SO213-059-2 (~45° S) (Tapia et al., 2015); a, b) *G. bulloides* Mg/Ca-SST records; c, d) Global ice volume-corrected $\delta^{18}O_{\text{ivc-w}}$ records; The age model of core SO213-059-2 is from Tapia et al. (2015).

Chapter 6 – Southern Ocean phytoplankton community changes during MIS 11: Implications for the silica leakage mechanism

Johannes Ullermann (1), Frank Lamy (1), Gerhard Kuhn (1), Mariem Saavedra-Pellitero (2), Rainer Gersonde (1), Dirk Nürnberg (3), Ralf Tiedemann (1)

In preparation, considered to be submitted to Palaeoceanography Palaeoclimatology Palaeoecology

1. Alfred-Wegener-Institut Helmholtz-Zentrum für Polar- und Meeresforschung, Am Alten Hafen 26, 27568 Bremerhaven, Germany

2. Universität Bremen, Fachbereich Geowissenschaften, Postfach 330440, 28334 Bremen, Germany

3. GEOMAR Helmholtz-Zentrum für Ozeanforschung Kiel, Wischhofstraße 1-3, 24148 Kiel, Germany

Abstract

The Silica Leakage Hypothesis is proposed as an important climate mechanism, which may have considerably contributed to the changing atmospheric CO₂ concentrations over glacial-interglacial cycles. It invokes an increased silica escape from the Southern Ocean on shallow subsurface water mass flow paths for glacial times. After reappearing in the equatorial upwelling regions, this silica may fuel diatom primary productivity, thereby strengthening the biological pump. However changing glacial boundary conditions regarding both oceanic and atmospheric aspects challenge to validate the Silica Leakage Hypothesis, thus it is subject to ongoing investigations. We present new carbonate content and planktonic foraminiferal $\delta^{13}\text{C}$ records from the central Pacific sector. Consistent to former observations, the records document ecological disturbances for the MIS 11 interglacial, characterized by an immense coccolithophorid growth together with $\sim 1\text{‰}$ higher surface water $\delta^{13}\text{C}$ values. Combining the $\delta^{13}\text{C}$ with a corresponding sea surface temperature record permits us to define precisely the on- and offset of these ecological disturbances, which started abruptly, but somewhat delayed after Termination V. Under assumption that the coccolithophorid dominance occurred on the expense of silica consuming diatoms and thus caused an enhanced silica escape, we compare to central equatorial Pacific productivity records. Accordingly, the ecological changes in the Southern Ocean had no impact on diatom productivity in the equatorial upwelling areas. If the MIS 11 boundary conditions were comparable to today, our results imply that the Silica Leakage Hypothesis mechanism can only have worked, when the shallow subsurface oceanic circulation changed during glacial times, so that the high to low latitudinal connection was improved.

6.1 Introduction

The Silica Leakage Hypothesis follows the prerequisite that an increased iron availability due to higher atmospheric dust inputs influenced Southern Ocean's diatom algae physiology during glacial times, while the resultant changes in diatom species composition or morphology lower the total Si:N uptake ratio by diatoms (Takeda, 1998). The Silica Leakage Hypothesis states that as a consequence Southern Ocean's surface water becomes more silica rich compared to today. After subduction, this silica rich water is exported equatorward via Subantarctic Mode Water (SAMW), there it ultimately fuels diatom primary production in the equatorial upwelling areas (Brzezinski et al., 2002; Matsumoto et al., 2002; Sarmiento et al., 2004). There, the shift to a more diatom dominated primary production on cost of coccolithophorides, thus in the $\text{CaCO}_3:\text{C}_{\text{org}}$ rain ratio, leads to an enhanced drawdown of atmospheric CO_2 into the ocean (Dymond and Lyle, 1985; Keir and Berger, 1983). Beside iron fertilization induced changes in Southern Ocean primary production (Harrison, 2000), silica leakage is thought to constitute another important, biological pump related, mechanisms to explain the lower atmospheric CO_2 concentrations during glacial times (Brzezinski et al., 2002; Matsumoto et al., 2002; Sarmiento et al., 2004).

Observations on opal burial in Southern Ocean sediments showed that the Pacific sector has a high potential regarding the glacial export of silica rich waters on SAMW paths (Bradtmitter et al., 2009). Further, a subsurface oceanic connection may have existed during the last glacial, as changes in oxygen and nutrient inventory of SAMW, which was formed in the central Pacific sector, supposedly have influenced the degree of denitrification in the equatorial Pacific upwelling area (Robinson et al., 2007). Nonetheless, the opal burial in the equatorial Pacific upwelling area was lower throughout glacial times, when the supply of silica rich water from the Southern Ocean was supposedly high (Bradtmitter et al., 2006; Dubois et al., 2010; Higginson and Altabet, 2004; Kienast et al., 2006; Pichon et al., 1992). Only for the northern marginal areas higher opal burial rates were observed (Arellano-Torres et al., 2011). Overall, this indicates a glacial decrease in diatom productivity, what in turn challenges the Silica Leakage Hypothesis.

However interpreting the net opal burial rates for the equatorial Pacific in terms of the Silica Leakage Hypothesis is critical, as potential changes in the basal conditions entail high uncertainty. With respect to modern conditions, higher equatorial dust inputs may have impacted diatom morphology, thereby lowering the opal export and burial despite high diatom productivity (e.g., Pichon et al., 1992). Likewise, changes in opal preservation have potential to lower the opal burial (e.g., Warnock et al., 2007). Even, changes in the supply of subsurface waters, linked to changes in upwelling activity, may have impacted diatom productivity in a way that opal export and burial lowered at glacial times (e.g., Bradtmiller et al., 2006). Notably, changes in subsurface water supply may also compromise interpretations based on other proxies as $\delta^{15}\text{N}$ or $\delta^{30}\text{Si}$, which allow inferences on diatom productivity and on the Silica Leakage Hypothesis independently from the net opal burial rates.

In this study we discuss the Silica Leakage Hypothesis mechanism with regard to the MIS 11 interglacial, when basal conditions at the equator were potentially comparable to today. We present new carbonate content, sand size fraction and planktonic $\delta^{13}\text{C}$ records, which document at that time a considerably dominance of coccolithophorid algae in Southern Ocean's Pacific sector surface productivity. As already observed for the Atlantic sector, this occurs together with massive carbonate deposition, accompanied by a surface water $\delta^{13}\text{C}$ increase (Hodell et al., 2000). In our discussion, we presume commitment changes in diatom productivity, thereby causing a pulsed silica escape from the Pacific sector. On this base, we discuss, if this turnover had detectable impact in the equatorial Pacific upwelling area, or not. The study is structured as follows: 1) The main features of carbonate sedimentation in the Pacific sector of the Southern Ocean are outlined for the past 480 ka. 2) The exact timing and extent of the MIS 11 changes are defined, amongst others, by exploiting in our study documented interrelationships of the planktonic $\delta^{13}\text{C}$ data with paired, unpublished Mg/Ca-based sea surface temperature (SST) data. 3) The MIS 11 changes are discussed in the light of published productivity records (opal, biogenic barium) from the equatorial Pacific to gain insights on the Silica Leakage Hypothesis mechanism.

6. 2 Material and Methods

6.2.1 Core material and setting

To provide an overview of the carbonate sedimentation for the Pacific sector of the Southern Ocean data of piston cores PS75/059-2, PS75/076-2 and PS75/079-2 are displayed, which were retrieved on R/V Polarstern cruise ANT-XXVI/2. Their respective surface locations range from the Subantarctic Front to the Polar Front (Figure 6.1), thus cover an oceanic area where surface waters are subducted today, before flowing as SAMW equatorward (McCartney, 1977). For cores PS75/059-2, PS75/076-2 and PS75/079-2 downcore carbonate contents are presented. Downcore carbonate fine fraction contents were obtained for core PS75/059-2 by combining its carbonate contents with its sand fraction (>63 μm sieve size) contents (For details see *Section 6.2.5*). For cores PS75/076-2 and PS75/079-2 carbonate fine fraction contents were obtained only for the MIS 11 interval. Further, X-ray Fluorescence (XRF) core scanning data for the element strontium (Sr) were obtained for all three cores to increase the resolution of their carbonates content records by calibrating the XRF Sr data to the measured carbonate contents, respectively. Calibration was done for each core individually. For core PS75/059-2 new $\delta^{13}\text{C}$ data of the planktonic foraminiferal species *G. bulloides* are presented, which constitute pairs to unpublished Mg/Ca temperature data (Ullermann et al., in preparation b, *Chapter 5*).

To discuss the link to the equator Pacific upwelling area, records of core PS75/059-2 are compared to published opal flux records of central Pacific core TT013-PC72 (Hayes et al., 2011; Murray et al., 2012), which is positioned in the western, marginal area of the equatorial Pacific upwelling tongue

(Figure 6.1). The published opal flux records of core TT013-PC72 were combined in this study to increase the downcore resolution across the MIS 11 interval. Furthermore, the published sedimentary barium (Ba/Ti) record of core TT013-PC72 is displayed (Murray et al., 2000).

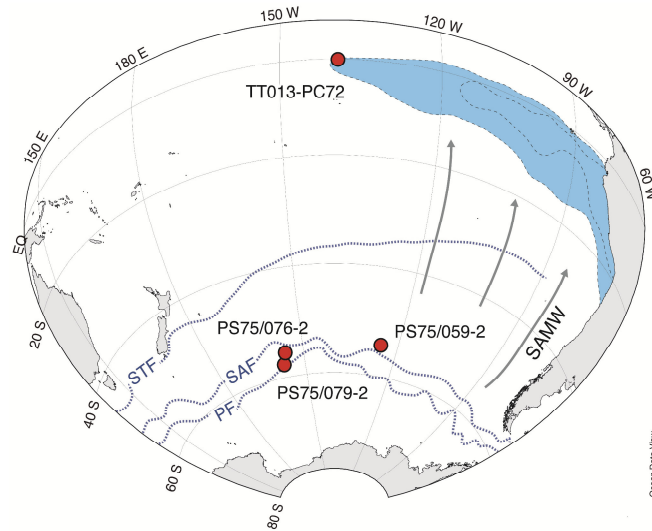


Figure 6.1. Overview map of the Southern Hemisphere Pacific Ocean, displayed with ODV software (Schlitzer, 2012); Red circles indicate cores discussed in this study; Blue shaded area outlines the equatorial Pacific upwelling area; Blue dotted lines display the modern surface positions of the STF, SAF and PF, as defined by Orsi et al. (1995); Dark gray arrows display schematically the subsurface flow paths of SAMW, which forms today all along the SAF (McCartney, 1977).

6.2.2 Carbon isotope data

For the carbon isotope ($\delta^{13}\text{C}$) measurements the working halves of core PS75/059-2 (13.98 m core length) was sampled at 5 cm downcore resolution. After freeze drying the samples were wet sieved at mesh size 63 μm , rinsed with deionized water and dried at a temperature lower 40 $^{\circ}\text{C}$. About 35 tests of the planktonic foraminiferal species *G. bulloides* were picked from the 315-355 μm size fraction, gently crushed, homogenized and split into subsamples, while one subsample portion was used for separate chemical (Mg/Ca) analyses (Ullermann et al., in preparation b, Chapter 5).

The subsamples reserved for the isotope measurements were cleaned at the laboratory facility of the GEOMAR Kiel, following the protocol of Barker et al. (2003) with modifications of Nürnberg and Groeneveld (2006). Afterwards, their carbon isotopic composition was determined on a Finnigan 253 mass spectrometer coupled to a Kiel Carbo IV carbonate preparation device at the GEOMAR Kiel. The mass spectrometers were calibrated via the NBS international standard to the PDB scale, respectively. Isotope ratios of $\text{C}^{12}/\text{C}^{13}$ are expressed in δ -notation versus Vienna Pee Dee Belemnite (VPDB). The reproducibility based on internal laboratory standards was better than ± 0.06 ‰.

6.2.3 Carbonate content

The carbonate contents of sediment cores PS75/059-2, PS75/076-2 and PS75/079-2 derive from their total carbon (TC) and total organic carbon (TOC) contents, respectively, expressed in weight percent of dry bulk sediment. Therefore a volume of ~ 10 cm^3 sample material was taken in 10 cm resolution

from the working halves of both cores. After freeze drying and homogenization, the TC and TOC content was determined on Elementar Vario ELIII and Eltra 2000 analyzers, respectively, at the Alfred Wegener Institute, Bremerhaven. The carbonate (CaCO_3) content was calculated according the equation: $\text{CaCO}_3 = (\text{TC} - \text{TOC}) * 8.333$

The elemental abundance of strontium (Sr) was determined at the Alfred Wegener Institute, Bremerhaven, using an AvaatechTM X-ray fluorescence (XRF) core scanner (For details see Richter et al., 2006). The measurements were performed at 0.5 downcore resolution on the archive halves of cores PS75/059-2, PS75/076-2 and PS75/079-2 at a tube voltage of 30 kV. The results are expressed as intensity in counts per second [cps]. The counting rates of the detector were set different for respective cores. High resolution downcore carbonate content records for cores PS75/059-2, PS75/076-2 and PS75/079-2 were obtained from polynomial regression of the measured bulk sediment carbonate (CaCO_3) content data on the XRF Sr data (Figure 6.2). For this propose the XRF Sr records were resampled at depths there carbonate content measurements exist. Before resampling a 9-point moving average was applied to the XRF Sr records.

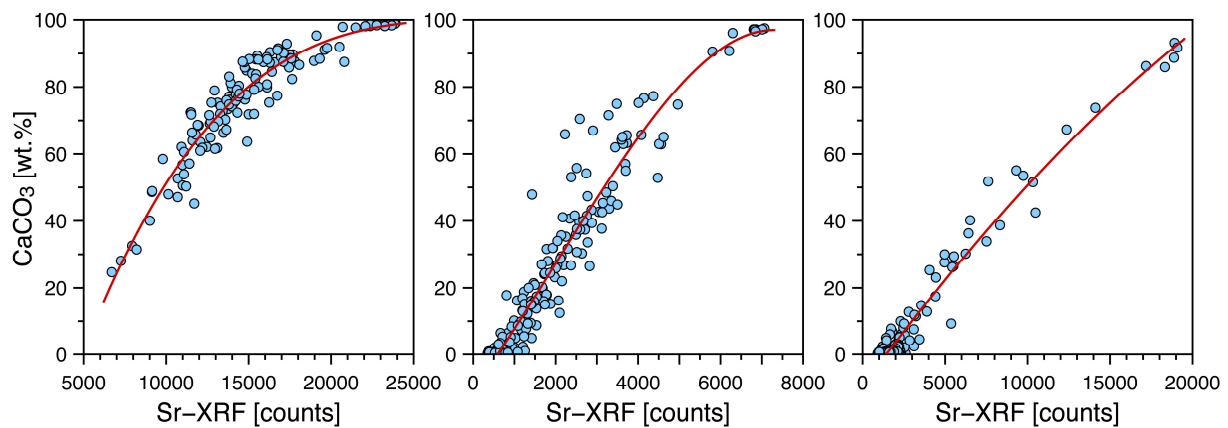


Figure 6.2. Calibration of the resampled Sr-XRF data to the bulk sediment carbonate (CaCO_3) content data using polynomial regression models; Red lines are the regression curves calculated for core PS75/059-2 (left panel), PS75/076-2 (middle panel) and PS75/079-2 (right panel), respectively.

6.2.4 Carbonate fine fraction contents – Coccolith contents

Sedimentary carbonate fine fraction contents are specified by defining a semi-quantitative index, named hereafter as CFF-index. It is simply calculated by dividing the carbonate content by the sand fraction (>63 μm sieve size) content, each expressed in weight percent of dry bulk sediment. The CFF-index varies in this study between values of 0 and 14, with increasing numbers indicating higher carbonate fine fraction contents. According to visual observations this is the case (Gersonde, 2010), as the sand fractions of core PS75/059-2 and of the displayed carbonates rich intervals of cores PS75/076-2 and PS75/079-2 predominantly consist of carbonate components composed of foraminiferal shells. The carbonate particles of the silt and clay fraction consist primarily of coccoliths with only some juvenile foraminifera and foraminiferal fragments. As a consequence, the CFF-index provides also an indication on bulk coccolith contents. At the core locations the sedimentation is

characterized by changing contributions of three main components over glacial-interglacial cycles, namely carbonate, opal and terrigenous components (Gersonde, 2011). While terrigenous components are throughout rare in the sand fraction, opal components, which consist largely of radiolarian shells, are more abundant there during glacial times. As its specific weight is comparably low, the resultant bias of the carbonates fine fraction estimates is nevertheless acceptable for the purposes of this study.

6.2.5. Sedimentary opal fluxes

Sedimentary opal fluxes are shown for core TT013-PC72, which derive from merging its opal data from two published data sets (Hayes et al., 2011; Murray et al., 2012). To obtain consistent opal flux estimates for core TT013-PC72, the opal contents of Hayes et al. (2011) were multiplied with reconstructed ^{230}Th -based and $\delta^{18}\text{O}$ -based accumulation rates given by Murray et al. (2012). Therefore, the ^{230}Th -based and $\delta^{18}\text{O}$ -based accumulation-rate records were resampled at depths where opal content measurements exist. After multiplication, the thereby obtained opal flux values were complemented to the opal fluxes record of core TT013-PC72 reported by Murray et al. (2000). The used ^{230}Th -based and $\delta^{18}\text{O}$ -based accumulation rates were initially obtained from the ^{230}Th data set of Winckler et al. (2008) and the $\delta^{18}\text{O}$ stratigraphy of Murray et al. (2000).

6.2.6 Chronology

The chronologies used in this study for cores PS757059-2 and TT013-PC72 are from Murray et al. (2000) and Ullermann et al. (in preparation a, *Chapter 4*). In case of core PS75/059-2 the age scale was obtained by correlating its downcore benthic $\delta^{18}\text{O}$ data to the LR04 $\delta^{18}\text{O}$ stack (Lisiecki and Raymo, 2005). In case of core TT013-PC72 the age scale is based on the correlation of its downcore benthic $\delta^{18}\text{O}$ data to the SPECMAP $\delta^{18}\text{O}$ stack (Imbrie et al., 1984).

6.3. Results and Discussion

6.3.1 Carbonate production during MIS 11

In the Pacific sector the sedimentation during the MIS 11 interglacial differs notably from the sedimentation during other interglacials. The downcore carbonate contents from cores PS75/059-2, PS75/076-2 and PS75/079-2, which are commonly higher during interglacials, are particularly high during MIS 11 (Figure 6.3). The same was also observed from the Atlantic sector (Hodell et al., 2000). Besides changes in primary carbonate productivity, the downcore variations in the carbonate contents may have originated from dilution by non-carbonate material or from carbonate dissolution at the sea floor. However, the carbonate fine fraction content is also notably increased during MIS 11 (Figure 6.3). According to visual observations (Gersonde, 2011), this is due to differences in its depositional facies, which is characterized by much higher coccolith contents and, concurrent therewith, by lower foraminiferal contents. Thus, independent from any dilution or carbonate dissolution bias, a much higher importance of coccolithophorid algae as primary producers is exemplified for that time. At the

base of core PS75/059-2, the carbonate fine fraction starts to increase once more, which coincides again with increasing coccolith content (Figure 6.3). This indicates comparable conditions to MIS 11 at the very end of MIS 13. Today diatoms constitute a large fraction of the total primary production in the surface waters above the core sites, while their importance increases toward the Polar Front (Honjo et al., 2000). Thus, the much higher carbonate fine fraction contents during MIS 11 than during the Holocene, which was nearly completely recovered in core PS75/059-2, reveal an entirely different situation to today. The fact that high carbonate fine fraction contents are also found even at southernmost core position PS75/079-2 implies that coccolithophorides flourished over a wide latitudinal range during MIS 11.

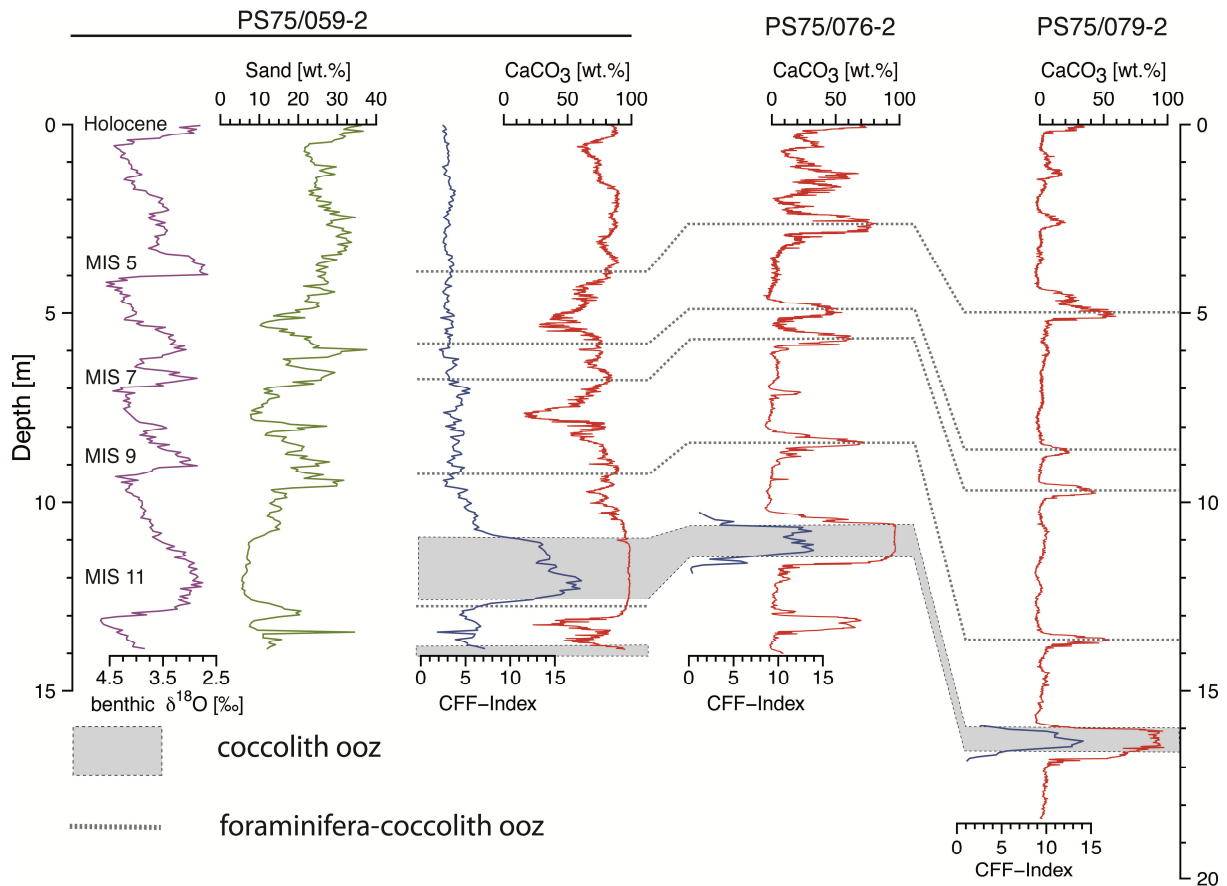


Figure 6.3. Overview on carbonate sedimentation in the central Pacific sector; Cores PS75/059-2 (~54°S), PS75/076-2 (~55°S) and PS75/079-2 (~57°S) are arranged according to latitude, with their locations being north of the SAF, south of the SAF and north of the PF, respectively; Purple curve displays the benthic $\delta^{18}\text{O}$ data of core PS75/059-2; Green curve displays the sand fraction ($> 63 \mu\text{m}$) content of core PS75/059-2; Blue and red curves displays, respectively, the carbonate fine fraction (CFF) index and carbonate (CaCO_3) content of cores PS75/059-2, PS75/076-2 and PS75/079-2; High CFF values indicate high weight portions of clay and silt-size carbonate particles ($< 63 \mu\text{m}$) on the total carbonate content; Gray shaded areas displays intervals of massive coccolith oozes deposition; Gray dotted lines indicate intervals (MIS 5, MIS 7 and MIS 9) of foraminifera-coccolith oozes deposition in cores PS75/076-2 and PS75/079-2 and their stratigraphic correlation to PS75/059-2; Due to throughout high carbonate content, foraminifera-coccolith oozes prevail in core PS75/059-2 over much of its core length including the short interval at the very beginning of MIS 11 (gray dotted line); A detailed description of the three cores is provided in the ANT-XXVI/2 cruise report (Gersonde, 2011).

Referring to the study of Hodell et al. (2000), the MIS 11 disturbances in carbonate deposition outlined above co-occurred with notably high planktonic $\delta^{13}\text{C}$ values, if compared to the interglacial stages thereafter. In view of the *G. bulloides* based planktonic $\delta^{13}\text{C}$ record PS75/059-2 this is also true (Figure 6.4), as evident when considering the SST record PS75/059-2. The planktonic $\delta^{13}\text{C}$ values vary inversely to the SST values, with most depleted $\delta^{13}\text{C}$ values occurring during peak warm, interglacial conditions (Figure 6.4). Only during MIS 11 and at the end of MIS 13 this relationship interrupts. The corresponding cross-plot displays for that times ~ 1 ‰ increased planktonic $\delta^{13}\text{C}$ values, which coincide with increased carbonate fine fraction content and thus coccolith content (Figure 6.5).

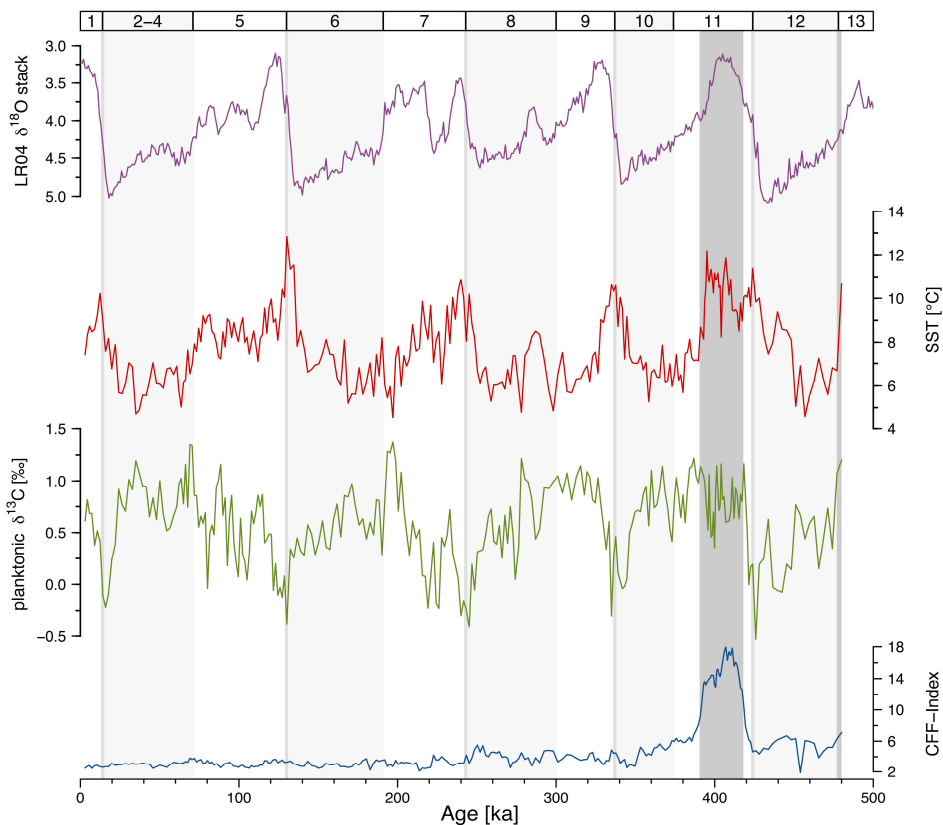


Fig 6.4. Mg/Ca-SST (red) (Ullermann et al., in prepreparation b, *Chapter 5*), planktonic foraminiferal $\delta^{13}\text{C}$ (green) and carbonate fine fraction (CFF) index (blue) records of core PS75/059-2 displayed together with the LR04 benthic $\delta^{18}\text{O}$ stack (purple) (Lisiecki and Raymo, 2005); Note that the planktonic foraminiferal $\delta^{13}\text{C}$ values vary inversely to the SST values, except for the dark gray shaded intervals (MIS 11, end of MIS 13), where the CFF index is high due to massive coccolith oozes deposition; Vertical lines indicate glacial terminations.

Today the surface waters $\delta^{13}\text{C}$ signature at high southern latitudes is much determined by biological cycling, thus it is linked to surface water nutrient concentrations. Besides, air-sea interactions influence considerably the $\delta^{13}\text{C}$ signature, while their impact is among others temperature dependent. Considering the temperature-related part only, surface water $\delta^{13}\text{C}$ lowers as temperature increases (0.1 ‰ per 1 °C) (Lynch-Stieglitz et al., 1995). This sea water $\delta^{13}\text{C}$ signal is then incorporated into the shell calcite of planktonic foraminifera, which dwell in the surface layer. In case of planktonic

foraminiferal species *G. bulloides* this occurs however not in simply one-to-one manner. Culturing studies showed that the incorporation of the sea water $\delta^{13}\text{C}$ signal into the calcite of *G. bulloides* is strongly temperature dependent, as revealed by a linear $\delta^{13}\text{C}$ lowering with increasing temperatures of the ambient sea water (0.1 ‰ per 1 °C) (Bemis et al., 2000). More recently, a sediment trap study from the Southern Ocean confirmed these results under non-laboratory conditions (King and Howard, 2004). Taken together, we explain the inverse $\delta^{13}\text{C}$ -SST correlation observed for core PS75/059-2 by the temperature dependency linked to air-sea interactions, linked to the *G. bulloides* specific signal incorporation or both. Either way, the temperature effects would act in the same direction.

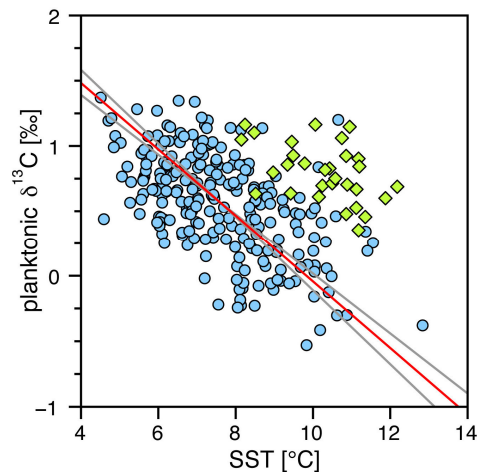


Figure 6.5. Cross plot of the planktonic foraminiferal $\delta^{13}\text{C}$ and Mg/Ca-SST data pairs from core PS75/059-2; Blue circles indicate data pairs, where the corresponding CFF-index is lower than 10; Green diamonds indicate data pairs, where the corresponding CFF-index is higher than 10; Red line is the linear regression on the blue labeled values only, obtained by standard major axis method; Gray lines display the 95% confidence interval of the regression; Note that the green labeled values offset from the regression line by ~ 1 ‰ in y-axis direction.

There are indications that the sea water $\delta^{13}\text{C}$ signal incorporation into foraminiferal calcite depends not only on temperature, but also on ambient sea water $[\text{CO}_3^{2-}]$. Thus, in case of *G. bulloides*, changing surface water $[\text{CO}_3^{2-}]$ on glacial interglacial cycle has potentially countered the temperature impact to some part (Bemis et al., 2000; Spero et al., 1997). Today and throughout the past, the surface water pH and thus $[\text{CO}_3^{2-}]$ paralleled the atmospheric CO_2 concentrations (Foster, 2008; Hönisch and Hemming, 2005; Yu et al., 2007). As the atmospheric CO_2 concentrations during MIS 11 did not notably differ from the other interglacial stages (Lüthi et al., 2008 and references herein; Petit et al., 1999), atmospheric-driven changes in $[\text{CO}_3^{2-}]$ cannot have induced the ~ 1 ‰ $\delta^{13}\text{C}$ increase during MIS 11.

The rise of coccolithophorid algae as primary producers together with the high $\delta^{13}\text{C}$ values during MIS 11 points toward a lowering of Southern Ocean surface water nutrient contents. Hodell et al. (2000) supposed amongst others a lowering in nutrient supply as cause for the MIS 11 changes, which is facilitated by Circumpolar Deep Water upwelling at the Polar Front. This is in fact compatible with contemporarily high carbonate fine fraction content, given that coccolithophorides flourish today under nutrient poor conditions, as it is the case north of core location PS75/059-2 in the subtropical

South Pacific gyre region. However, for core PS75/059-2 the sedimentation rate was considerably increased during MIS 11 (~6 cm/ka), reaching value twice as high as for the rest of the core (~3 cm/ka) (Ullermann et al., in preparation a, *Chapter 4*). This excludes a nutrient-starved scenario, proposing an uninterrupted nutrient supply instead. We therefore argue that higher coccolithophorid production rates during MIS 11 time favored the nutrient drawdown by organic matter fixation, in turn causing a $\delta^{13}\text{C}$ increase in the surface ocean. We note that the higher coccolith calcite production itself can have influenced surface ocean $[\text{CO}_3^{2-}]$ (Hodell et al., 2000). This could have impacted the foraminiferal $\delta^{13}\text{C}$ of *G. bulloides*, aside from the surface water $\delta^{13}\text{C}$ signature (Bemis et al., 2000; Spero et al., 1997).

One can argue that contemporarily with the surface ocean changes, the much higher sedimentation rates during MIS 11 were caused by a decrease in deep water carbonate corrosivity, thus by an increase in deep water $[\text{CO}_3^{2-}]$, and that a wherewith tied upward displacement of the calcite saturation depth ($\Omega = 1$) from its modern position finally resulted in higher MIS 11 carbonate accumulation rates. Though, Atlantic sector (or South Atlantic) cores, which are currently bathed in the same water mass (Circumpolar Deep Water) and are similarly positioned with regard to the calcite saturation depth as our Pacific cores (Key et al., 2004, GLODAP; Orsi et al., 1999; Orsi et al., 2002), display co-variations in downcore CaCO_3 content and foraminiferal fragmentation ratio, whereas the latter is a widely-used proxy for deep water carbonate corrosivity (Hodell et al., 2001; Howard and Prell, 1994). Whereby, the foraminiferal fragmentation ratio indicates that the carbonate corrosivity was never lower during MIS 11 than during the other interglacials, for its second half even the opposite was the case. (Figure 6 in Hodell et al., 2001). Previous inferences for the Atlantic and Indian sector, based on different carbonate dissolution proxies, further confirm that the carbonate corrosivity was not enhanced during MIS 11, despite Southern Ocean wide increased carbonate accumulation rates (Howard and Prell, 1994). Our carbonate record from the Pacific sector closely fits its counterparts in the Atlantic sector (supplemental information S5.1), displaying same ‘Atlantic type’ (glacial low- CaCO_3 [wt. %], interglacial high- CaCO_3 [wt. %]) downcore changes. If it is true, that the Southern Ocean carbonate sedimentation was much controlled by carbonate corrosivity at depths (Hodell et al., 2001; Howard and Prell, 1994; Rickaby et al., 2007), this suggests parallel deep water chemical changes in both sectors or, more precisely, at the Pacific and Atlantic core locations throughout the past. Actually, this is strongly supported by benthic $\delta^{13}\text{C}$ base observations (Ullermann et al., in preparation a, *Chapter 4*). In view of the findings in the Atlantic sector, we propose therefore that the high MIS 11 sedimentation rates at our Pacific core site are not the product of decreased deep water carbonate corrosivity, but of an enhanced surface productivity. The continues decline in the sand fraction contents core PS75/059-2, which likely indicates an increasing foraminiferal shells disaggregation due to dissolution, underpins this conclusion (supplemental information S5.1). It implies that carbonate corrosivity intensified toward MIS 11, probably caused by, globally observed,

long term changes in ocean's carbonate corrosivity and carbon system with ~400 ka cyclicity (e.g., Bassinot et al., 1994; Hodell et al., 2003b; Russon et al., 2010).

Around 250 to 550 ka, coccolithophorides, primary constituted by bloom species *Gephyrocapsa oceanica*, had a higher importance worldwide as primary producers than today, what appears related to cyclic changes in orbital forcing on ~400 ka frequency (Rickaby et al., 2007). The mechanism behind is not understood in detail, but may on theoretical base, for instance, linked to an inverse relation of growing season length and isolation, which increase with eccentricity. This in turn may have analog to modern observations (Beaufort et al., 1997) control on coccolithophorid algae production (Rickaby et al., 2007). Although our MIS 11 and end of MIS 13 observations may be associated to such concept, it is not the objective of this study to further discuss the ultimate causes of the massive MIS 11 coccolithophorid growth in the Pacific sector.

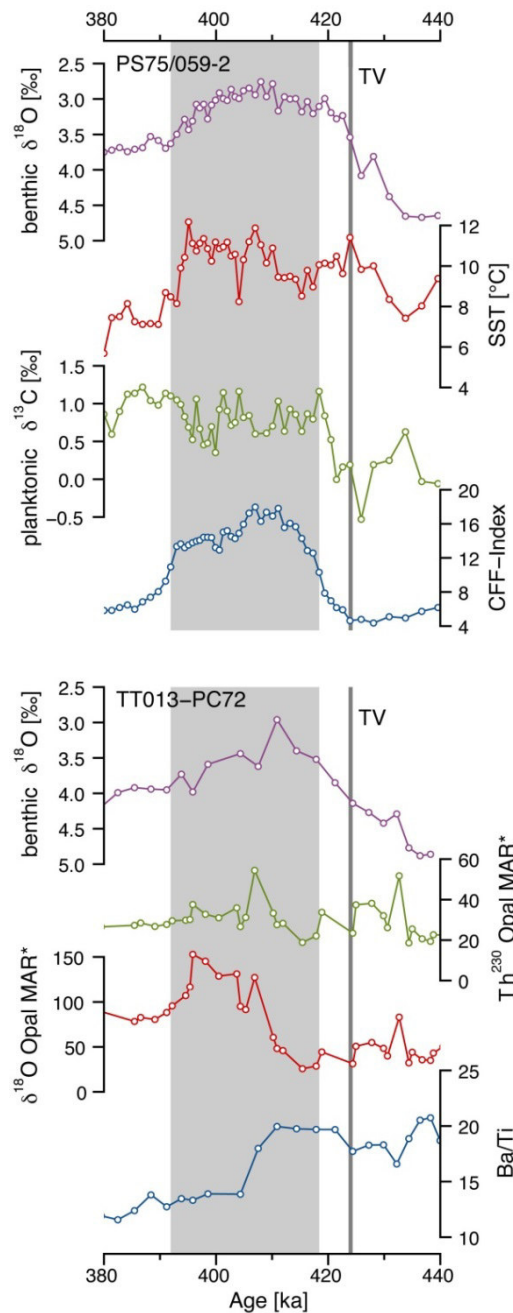


Figure 6.6. Records of cores PS75/059-2 and TT013-PC72 from the Pacific sector of the Southern Ocean and the central equatorial Pacific Ocean, respectively; They cover the complete MIS 11 as well as the MIS 10/11 and MIS 11/12 transitions; Upper panel displays the benthic foraminiferal $\delta^{18}\text{O}$ (purple), Mg/Ca-SST (red), planktonic foraminiferal $\delta^{13}\text{C}$ (green) and carbonate fine fraction (CFF) index (blue) records of core PS75/059-2; Lower panel displays the benthic foraminiferal $\delta^{18}\text{O}$ (purple), ^{230}Th -based opal accumulation, $\delta^{18}\text{O}$ -based opal accumulation and Ba/Ti (biogenic barium) records of core TT013-PC72; * all mass accumulation rates (MAR) are expressed in $\text{mg/cm}^2/\text{ka}$; Figure 6.6 contains data from other studies (Hayes et al., 2011; Murray et al., 2000; Murray et al., 2012; Ullermann et al., in preparation a b, *Chapters 4 and 5*); Details on the calculation of the opal accumulation rates are given in *Section 6.2.5*; Gray shaded area highlights the interval of massive coccolith oozes deposition (CFF-Index > 10).

6.3.2 Timing during MIS 11

In closer detail, the main increase in the carbonate fine fraction (CFF index of ~ 10) and in the $\delta^{13}\text{C}$ values occurred at ~ 418 ka (Figure 6.6). Thus, the onset of the massive coccolith ooze deposition lagged the glacial termination by 6 ka, using the MIS 11 boundary age defined by Lisiecki and Raymo (2005). The increase in the carbonate contents started already earlier at ~ 435 ka, with foraminifera constituting a large portion thereof (Figure 6.2). Thus, to the very begin of MIS 11 the surface oceanic conditions were apparently the same as during the later interglacial stages. It appears that the typical deglacial change was already completed, before the coccolith productivity increased. The massive coccolith deposition ended as abruptly as it started at ~ 392 ka, which is displayed by the declining carbonate fine fraction contents (CFF index of ~ 10) (Figure 6.6). By contrast, the carbonate contents remained continuously high. Taken together the changes during MIS 11 occurred within a precisely defined time interval. As apparent from foraminiferal $\delta^{13}\text{C}$, the MIS 11 changes caused an easily identifiable, pulsed biochemical signal in the surface waters of the Pacific sector of the Southern Ocean.

6.3.3 Implications on the Silica Leakage Hypothesis

According to our inferences in *Section 6.3.1*, nutrients were continuously brought to the surface ocean by Circumpolar Deep Water upwelling during MIS 11 times, providing steadily phosphate, nitrate as well as silica to fuel primary productivity. We presume that the higher nutrient consumption by coccolithophorid algae during MIS 11 deprived these nutrients for diatom growth. As a consequence the silica consumption by diatom algae should also have much reduced, making the surface waters of the Pacific sector of the Southern Ocean much more silica-rich at that time. Similar to the glacial scenario predicted by the Silica Leakage Hypothesis, this excess silica should then escape via SAMW to lower latitudes, where it then reoccur in the equatorial Pacific upwelling areas - even if the cause of the silica enrichment in the Silica Leakage Hypothesis was another one.

In view of the Silica Leakage Hypothesis an also abrupt change in phytoplankton ecology with a rising dominance of diatoms, contemporarily to the Pacific sector phytoplankton community changes, can theoretically be expected for the equatorial Pacific upwelling area. However when considering published productivity records for the central equatorial Pacific core TT013-PC72 (Figure 6.1), this was apparently not the case. At the core site the ^{230}Th -normalized sedimentary opal fluxes were not increased at times of the Pacific sector ecological turnover, which occurred from 392 ka to 418 ka (Figure 6.6). Downcore reconstructions from core TT013-PC72 showed that sedimentary ^{230}Th -based fluxes for the central equatorial Pacific area deviate significantly from respective $\delta^{18}\text{O}$ -based fluxes (Murray et al., 2012). Considering the $\delta^{18}\text{O}$ -based constructions instead, opal accumulation at core position TT013-PC72 displays a temporarily increase by contrast, which falls together with the Pacific sector ecological turnover. However, its onset occurs ~ 8 ka delayed at ~ 410 ka. Moreover, these opal accumulation rates ($\sim 140 \text{ mg cm}^{-2} \text{ ka}^{-1}$) are lower than the Holocene accumulation rates ($\sim 180 \text{ mg cm}^{-2} \text{ ka}^{-1}$) reported for core position TT013-PC72 (Murray et al., 2012). On this base, we see no indication

for a high latitudinal control on equatorial Pacific opal accumulation. If the opal accumulation reflects in appropriate way surface productivity conditions (e.g., Hayes et al., 2011), then past equatorial Pacific diatom productivity was not systematically enhanced in response to the higher Pacific sector coccolith production, thus to our presumed export of excess silica – an inference, which holds true either if using the ^{230}Th -based or the $\delta^{18}\text{O}$ -based method.

The barium to titanium ratio (Ba/Ti) constitutes an estimate for biogenic barium ($\text{Ba}_{\text{excess}}$), which allows reconstructing changes in the integrated flux of organic matter to the sediment (Dymond et al., 1992). Although the Ba/Ti ratio does not strictly reflect diatom productivity, we assume that an addition of silica in the otherwise silica-starved area (Garcia et al., 2010, WOA09) would lead to an increase organic matter flux. The Ba/Ti record of core TT013-PC72 gives therefore additional evidence that diatom productivity was not increased during times of the supposedly high silica escape in Southern Ocean (Figure 6.6). A previous study by Murray et al. (2000) assessed productivity changes throughout MIS 11 on several cores covering a latitudinal transect across the central equatorial Pacific. Consistent to our inferences, the authors concluded on base of Ba/Ti and other elemental ratios that the export production during MIS 11 was not higher than today. Notably, core TT013-PC72 was among the investigated cores. Thus, our comparison to its records should be representative for the central equatorial Pacific upwelling area.

As inferred in *Section 6.4.1*, the high surface ocean $\delta^{13}\text{C}$ signature in the Pacific Sector of the Southern Oceans reflects low nutrient concentrations during MIS 11, with the restriction that coccolith production itself with its impact on surface ocean $[\text{CO}_3^{2-}]$ may partly have compromised the $\delta^{13}\text{C}$ signal. Based on similar assumptions Mohtadi et al. (2006) investigated a number of long term $\delta^{13}\text{C}$ records of sediment cores, covering the Pacific Sector of the Southern Ocean, the oceanic area along South American coast and the entire equatorial Pacific. They showed that the high $\delta^{13}\text{C}$ signal, which occurred during MIS 11, but also during MIS 13, is traceable only as far equatorward as to the Chilean coastal upwelling zone. In the central equatorial Pacific instead it is lacking. Thus, from our perspective, the Pacific sector high $\delta^{13}\text{C}$ signal failed to reach the equatorial Pacific upwelling areas during MIS 11 on shallow subsurface SAMW circulation paths. Consequently, the missing increase in the equatorial Pacific opal flux as response to our presumed escape of excess silica from the Pacific sector might explain by an inefficient oceanic connectivity.

Taken together, we come to the first order conclusion that under interglacial, thus under comparable to modern circulation conditions an enhanced silica leakage from the Southern Ocean would have no impact on equatorial Pacific diatom productivity. Aside all biological aspects, the Silica Leakage Hypothesis may only have worked if oceanic circulation changed during glacial times, so that the subsurface connectivity between both oceanic areas was improved. This is an important finding, as an atmospheric CO_2 drawdown by the Silica Leakage Hypothesis mechanism could then first occur when ocean circulation already rearranges, thus when change toward a glacial climate is already on its way. Our conclusions are confirmed by previous inferences on the Silica Linkage Hypothesis, which base

on downcore observations on diatom $\delta^{30}\text{Si}$ and opal accumulation rates from the westernmost Pacific sector, near New Zealand (Crosta et al., 2007). Accordingly, it was proposed that physical factors that impact the SAMW transport dominated over biological factors that impact surface water silica concentrations over glacial-interglacial cycles, as they ultimately control the magnitude of silica escape from the Southern Ocean (Crosta et al., 2007). Further, our conclusions are consistent with a recent review of Hendry and Brzezinski (2014), which supposes a fundamental role of ocean circulation with respect to the Silica Leakage Hypothesis.

We documented for the first time that Southern Ocean changes in phytoplankton ecology through MIS 11 occurred rapidly, with a precisely defined beginning and end of the turnover. This was not without effect on surface water biochemistry, as apparent from foraminiferal $\delta^{13}\text{C}$. Thus, MIS 11 may constitute an ideal target for future investigations to infer the sensitivity of various paleo-biochemical tracers, such as diatom $\delta^{30}\text{Si}$ or $\delta^{15}\text{N}$, under close to modern conditions.

6.4 Conclusion

In this study we tested the Southern Ocean's Pacific sector connection to lower latitudes with respect to the Silica Leakage Hypothesis. For this purpose we focused on the MIS 11 time interval, when the conditions at the eastern equatorial Pacific upwelling area were potentially comparable to today. With reference to previous study of Hodell et al. (2000), our results show that during MIS 11 times a turnover in Southern Ocean plankton ecology occurred, as documented by an immense coccolithophorides production. The widespread dominance of coccolithophorides was linked to a ~ 1 ‰ surface water $\delta^{13}\text{C}$ increase. Further, the beginning of this turnover in plankton ecology was abruptly, whereby it occurred at ~ 418 ka, ~ 6 ka delayed after Termination V. The ending, which occurred at ~ 392 ka, was likewise abruptly. We assume that the enormous coccolithophorides growth displaced silica utilizing diatoms as primary producers, in turn, causing a clearly defined silica excess signal in the Pacific sector surface waters. Productivity records from the central equatorial Pacific area reveal meanwhile any response to our proposed Southern Ocean changes, which in turn does not validate the Silica Leakage Hypothesis. According a previous study, the high MIS 11 surface water $\delta^{13}\text{C}$ values are not traceable from the Pacific sector to the central equatorial Pacific (Mohtadi et al., 2006). On this base, we conclude that the Silica Leakage Hypothesis mechanism can only have played a role in atmospheric CO_2 drawdown during glacial times, if subsurface oceanic circulation was changed, so that the equatorward export of Pacific sector surface waters on shallow subsurface paths was improved.

Acknowledgements

We thank the captain, crew, and scientific party of R/V Polarstern for their support during the ANT-XXVI/2 cruise. Further we thank R. Fröhlking, N. Gehre, L. Haxhijaj and S. Wiebe for their technical support at the GEOMAR Kiel and at the Alfred Wegener Institute, Bremerhaven. The data reported in this manuscript will be made available online in PANGAEA.

6.5 Supplemental Information

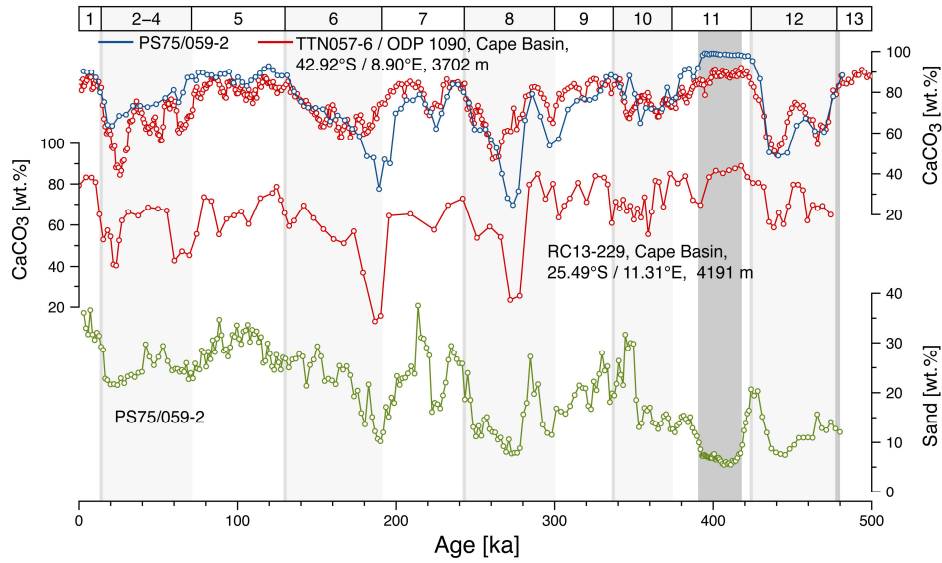


Figure S6.1. Downcore carbonate and sand (> 63 μm) contents of Pacific sector core PS75/059-2 (blue, green) and Atlantic sector (or South Atlantic) cores TTN057-6/ ODP Site 1090 (red, upper graph) and RC13-229 (red, lower graph); Today, the Pacific and Atlantic cores locations are bathed in Circumpolar Deep Water (Orsi et al., 1999; Orsi et al., 2002) and rest in water depths, which are with, respectively, 600, 200 and 200 m close to the positions of the calcite saturation depth ($\Omega = 1$) (Key et al., 2004, GLODAP); Carbonate contents of cores TTN057-6/ ODP Site 1090 and RC13-229 are published (Embley and Morley, 1980; Hodell et al., 2000; Hodell et al., 2001) and their chronologies are from Hodell et al. (2003c) and Oppo et al. (1990); Dark gray shaded intervals (MIS 11, end of MIS 13) indicate where the CFF-index is high due to massive coccolith oozes deposition; Vertical lines indicate glacial terminations.

7 Conclusions and Outlook

The overall aim of this thesis was to reconstruct oceanic changes in the high latitude central Pacific sector of the Southern Ocean throughout the past 500 ka to contribute to an improved understanding of the climate-related, physical and biological processes acting in that area. For this purpose, a number of geochemical and sedimentological proxies were used to infer orbital scale changes, for instance in deep water $\delta^{18}\text{O}$ and $\delta^{13}\text{C}$ composition, surface water temperature and $\delta^{18}\text{O}$ composition or carbonate deposition. The respective results are detailed discussed in the implemented manuscripts of *Chapters 4, 5 and 6*. They can briefly be summarized as follows:

Chapter 4 dealt with the reconstruction of deep water $\delta^{13}\text{C}$ compositional changes in the central Pacific sector based on benthic foraminiferal $\delta^{13}\text{C}$. The results reveal a common deep water $\delta^{13}\text{C}$ compositional evolution to the Atlantic sector, with Circumpolar Deep Water in both sectors displaying the same pronounced $\delta^{13}\text{C}$ variations trough the past 500ka. This is contrasting previous inferences (Ninnemann and Charles, 2002), which based only on sediment records covering the last glacial-interglacial cycle. In turn, this impacts the interpretation on past Antarctic Bottom Water expansion in the Atlantic sector and its interaction with the North Atlantic interior. Overall the results imply that the current LGM paleoceanographic picture on the Atlantic sector deep water hydrography is too simplistic, what needs to be taken into account when discussing mechanisms on atmospheric CO_2 drawdown and storage in the deep North Atlantic.

Chapter 5 dealt with the sea water temperatures and $\delta^{18}\text{O}$ evolution central Pacific sectors, which was reconstructed from the Mg/Ca and $\delta^{18}\text{O}$ signature of planktonic foraminiferal calcite. Accordingly, the surface water temperature evolution in that high latitude ($\sim 55^\circ\text{S}$) area was characterized by glacial-interglacial changes of 2.5 °C to 6.5 °C over the last 500 ka, that parallel the East Antarctic air temperature evolution as reconstructed from ice-cores. The surface water $\delta^{18}\text{O}$ evolution displays no glacial-interglacial modulation after correction for the ice volume effect indicating only minor paleosalinity changes. By comparison, the sea surface temperature changes documented from the western and eastern Pacific sector margins were more pronounced over glacial-interglacial cycles. This can be interpreted consistently to the overall paleoceanographic picture, that surface water changes at the South Pacific Ocean basin sides were amplified, most likely through changes of the subtropical South Pacific gyre's boundary current circulation. What, in turn, underpins that surface, high-low latitude heat and salinity fluxes between the tropical, subtropical and subantarctic oceanic domains changed in a systematic way over glacial-interglacial cycles and thus may constitute an important amplification mechanism for the Earth's climate system.

Chapter 6 outlines carbonate depositional changes for the central Pacific sector over the last 500 ka. Further, it provides insights on past surface water $\delta^{13}\text{C}$ changes inferred from planktonic foraminiferal $\delta^{13}\text{C}$. As previously observed from the Atlantic sector (Hodell et al., 2000), it is also characteristic for the Pacific that carbonate production by coccolithophorides algae was strongly enhanced during MIS

11 compared to the later interglacials up to the Holocene. During MIS 11 also changes in surface water biochemistry occurred, as indicated by ~ 1 ‰ higher than expected planktonic foraminiferal $\delta^{13}\text{C}$ values. The results from the Pacific sector reveal for the first time that the MIS 11 increased coccolithophorid productivity began and ended rather abruptly. Conceivably, the dominance of coccolithophorides constrains the silica consumption by diatom algae, thus prompting an enhanced silica escape from the Pacific sectors. Building on this assumption, particular aspects of the Silica Linkage Hypotheses mechanism were examined for MIS 11 interglacial conditions, a mechanism which may explain a large fraction of the glacial decline in atmospheric CO_2 concentrations (Brzezinski et al., 2002; Matsumoto et al., 2002; Sarmiento et al., 2004). Consistent to previous inferences (Crosta et al., 2007), it appears that the Silica Leakage Hypothesis mechanism can only have worked during glacial times, if the subsurface Subantarctic Mode Water transport to the equatorial Pacific upwelling areas was more efficient than today.

With reference to *Chapters 4* and *5*, the central Pacific sector core sites appear well-located for defining undisturbed deep and surface water compositional changes comparatively close to Antarctica on base of their records, which means that local changes in ocean circulation had less interfering influence. In terms of deep water circulation, it was possible to reconstruct undistorted lower Circumpolar Deep Water compositional changes over the past 500 ka, as the used cores PS75/059 and PS75/056-2 were recovered out of the direct reach of poleward flowing Pacific Deep Water. In terms of surface water circulation, the reconstructions reflect open marine conditions far distant from any continental influences. Disturbing influences from advection of heat, salinity and nutrients by local surface currents, as proposed for costal realms of the Pacific sector, are excluded. Future investigations should further build up on such location specific advantages of the study area, when discussing surface and deep water changes in wider, superregional context. For instance, Circumpolar Deep Water records from there may provide a future basis for monitoring glacial-interglacial changes in the Antarctic Bottom Water to North Atlantic Deep Water mixing portion within circumpolar Deep Water on worldwide scale – an important prerequisite when quantifying the role of ocean's physical circulation on the atmospheric CO_2 changes over glacial-interglacial cycles. It is notably, that not only with regard to surface and deep water circulation the study area is well located. As addressed in *Chapter 6*, today Subantarctic Mode Water formation occurs at those latitudes, so that surface records from there provide also a fix point with regard to the Pacific Oceans shallow subsurface circulation.

South of the central Pacific sector core sites, at the Polar Front, today nutrient and CO_2 laden deep water upwells, allowing the escape of CO_2 from the deep ocean to the atmosphere. Apart from that, the supply of upwelled nutrients favor phytoplankton production in the surface layer, what in turn promote atmospheric CO_2 fixation by organic matter and its subsequent transfer back to the deep ocean interior. Thus around the study area fundamental physical and biological mechanism tightly interact today, with have crucial impact on atmospheric CO_2 concentrations (see *Chapter 2*). Future investigations should thus establish a much more differentiated picture on surface and deep water dynamics, as it was

feasible in the framework of this thesis, so that changes in upwelling intensity and phytoplankton productivity, but also their impact on atmospheric CO₂ concentrations, can be quantified one day. Further evaluated by climate modelling, this would constitute an important step toward understanding the Southern Ocean's role in glacial-interglacial climate change.

To make full use of the location-specific advantages of the central Pacific sector study area, of course many other proxy methods needs to be applied. So far, quite few proxies were successfully used in this area (*Capture 2*, Table 1.1), but their records cover mainly the last climate cycle. Fortunately, in this thesis investigated cores PS75/056-1 and PS75/059-2 allow the use of carbonate proxies over their full length. Both cores have robust age models, according those reconstructions throughout the past 480 ka and 260 ka are producible. By contrast, the cores PS75/076-2 and PS75/079-2 have a discontinuous carbonate record throughout the past ~500 ka and ~1000 ka, respectively, with sufficient high carbonate contents occurring only during interglacial intervals. Yet, they have throughout higher opal contents. Lamy et al. (2014) (*Appendix*) provided a robust chronostratigraphic framework for numerous cores from the central Pacific sector by correlating their sedimentary iron downcore changes. This offers an excellent opportunity to use, with high age control, besides carbonate-based proxies also opal-based proxies in the central Pacific sector area.

With regard to the deep water circulation, besides in this thesis used foraminiferal $\delta^{13}\text{C}$, other proxy methods were recently applied to the sediment cores, so that the paleoceanography information in that area is increasing now. Current investigations deal with past deep water compositional characterization by fish teeth Nd isotopes (ϵ_{Nd}) (Marine Isotope Chemistry group, University Oldenburg) and the reconstruction of its ^{14}C ventilation ages (Marine Geology Department, Alfred-Wegener-Institute), which indicates the presence of glacially, very old deep waters at core site PS75/059-2 (Ronge et al., under review). Thus, in future it would be consequent to infer, how the corresponding results tie to the here presented benthic foraminiferal $\delta^{13}\text{C}$ results. In particular, as proxy methods commonly have their own limitations, so that a combined interpretation may yield the most valid inferences on the central Pacific sector's deep water history and, lastly, on the Southern Ocean's role in interglacial-glacial carbon cycling.

Finally, it is worth noting that a more detailed investigation of the MIS 11 interglacial should be a future issue. As outlined in *Chapter 6*, at that time the carbonate productivity in central Pacific sectors surface waters was much higher, when compared to the following interglacials, including the Holocene. Contemporarily, the surface water chemical characteristics changed as displayed by foraminiferal $\delta^{13}\text{C}$. All these changes occurred abruptly, with clearly defined beginning and end, and thus provide a very precise paleoceanographic signal. In view of the inferences by Barker et al. (2006), a closer inspection of this time interval for the central Pacific sector, but also world-wide, can aid at identifying basic mechanisms of the carbon cycle and ,in turn, can much improve our understanding on natural climate change, which is still far from complete.

8 Data Handling

All data presented in this thesis are stored electronically and will be available online on the Pangaea database (<http://www.pangaea.de>).

9 References

- Adkins, J. F. (2013), The role of deep ocean circulation in setting glacial climates, *Paleoceanography*, 28(3), 539-561.
- Antonov, J. I., D. Seidov, T. P. Boyer, R. A. Locarnini, A. V. Mishonov, and H. E. Garcia (2010), World Ocean Atlas 2009 Volume 2: Salinity, in *NOAA Atlas NESDIS 69*, edited by S. Levitus, p. 184, U.S. Government Printing Office, Washington, D.C.
- Arellano-Torres, E., L. E. Pichevin, and R. S. Ganeshram (2011), High-resolution opal records from the eastern tropical Pacific provide evidence for silicic acid leakage from HNLC regions during glacial periods, *Quaternary Science Reviews*, 30(9-10), 1112-1121.
- Ayers, J. M., and P. G. Strutton (2013), Nutrient variability in Subantarctic Mode Waters forced by the Southern Annular Mode and ENSO, *Geophysical Research Letters*, 40(13), 3419-3423.
- Barker, S., M. Greaves, and H. Elderfield (2003), A study of cleaning procedures used for foraminiferal Mg/Ca paleothermometry, *Geochemistry Geophysics Geosystems*, 4(9), 8407.
- Barker, S., I. Cacho, H. Benway, and K. Tachikawa (2005), Planktonic foraminiferal Mg/Ca as a proxy for past oceanic temperatures: A methodological overview and data compilation for the Last Glacial Maximum, *Quaternary Science Reviews*, 24(7-9), 821-834.
- Barker, S., D. Archer, L. Boot, H. Elderfield, J. Henderiks, and R. E. M. Rickaby (2006) Globally increased pelagic carbonate production during the Mid-Brunhes dissolution interval and the CO₂ paradox of MIS 11, *Quaternary Science Reviews* 25, 3278-3293.
- Barrows, T. T., and S. Juggins (2005), Sea-surface temperatures around the Australian margin and Indian Ocean during the Last Glacial Maximum, *Quaternary Science Reviews*, 24(7-9), 1017-1047.
- Barrows, T. T., S. Juggins, P. De Deckker, E. Calvo, and C. Pelejero (2007), Long-term sea surface temperature and climate change in the Australian-New Zealand region, *Paleoceanography*, 22(2), PA2215.
- Bassinot, F. C., L. Beaufort, E. Vincent, L. D. Labeyrie, F. Rostek, P. J. Muller, X. Quidelleur, and Y. Lancelot (1994), Coarse fraction fluctuations in pelagic carbonate sediments from the tropical Indian Ocean: A 1500 kyr record of carbonate dissolution, *Paleoceanography*, 9(4), 579-600.
- Beaufort, L., Y. Lancelot, P. Camberlin, O. Cayre, E. Vincent, F. C. Bassinot, and L. Labeyrie (1997), Insolation cycles as a major control on equatorial Indian Ocean primary production, *Science*, 278, 1451-1454.
- Becquey, S., and R. Gersonde (2003), A 0.55 Ma paleotemperature record from the Subantarctic Zone: Implications for Antarctic Circumpolar Current development, *Paleoceanography*, 18(1), 1014.
- Bemis, B. E., H. J. Spero, J. Bijma, and D. W. Lea (1998), Reevaluation of the oxygen isotopic composition of planktonic foraminifera: Experimental results and revised paleotemperature equations, *Paleoceanography*, 13(2), 150-160.
- Bemis, B. E., H. J. Spero, D. W. Lea, and J. Bijma (2000), Temperature influence on the carbon isotopic composition of *Globigerina bulloides* and *Orbulina universa* (planktonic foraminifera), *Marine Micropaleontology*, 38(3-4), 213-228.
- Benz, V., O. Esper, R. Gersonde, F. Lamy, and R. Tiedemann (in preparation), Last Glacial Maximum sea surface temperature and sea ice extent in the Pacific sector of the Southern Ocean.

- Bianchi, C., and R. Gersonde (2004), Climate evolution at the last deglaciation: The role of the Southern Ocean, *Earth and Planetary Science Letters*, 228(3-4), 407-424.
- Bostock, H. C., B. N. Opdyke, M. K. Gagan, A. E. Kiss, and L. K. Fifield (2006), Glacial/interglacial changes in the East Australian Current, *Climate Dynamics*, 26(6), 645-659.
- Boyd, P. W., A. J. Watson, C. S. Law, E. R. Abraham, T. Trull, R. Murdoch, D. C. E. Bakker, A. R. Bowie, K. O. Buesseler, H. Chang, M. Charette, P. Croot, K. Downing, R. Frew, M. Gall, M. Hadfield, J. Hall, M. Harvey, G. Jameson, J. LaRoche, M. Liddicoat, R. Ling, M. T. Maldonado, R. M. McKay, S. Nodder, S. Pickmere, R. Pridmore, S. Rintoul, K. Safi, P. Sutton, R. Strzepak, K. Tanneberger, S. Turner, A. Waite, and J. Zeldis (2000), A mesoscale phytoplankton bloom in the polar Southern Ocean stimulated by iron fertilization, *Nature*, 407(6805), 695-702.
- Bradtmilller, L. I., R. F. Anderson, M. Q. Fleisher, and L. H. Burckle (2006), Diatom productivity in the equatorial Pacific Ocean from the last glacial period to the present: A test of the silicic acid leakage hypothesis, *Paleoceanography*, 21(4), PA4201.
- Bradtmilller, L. I., R. F. Anderson, M. Q. Fleisher, and L. H. Burckle (2009), Comparing glacial and Holocene opal fluxes in the Pacific sector of the Southern Ocean, *Paleoceanography*, 24, PA2214.
- Broecker, W. S., and E. Maier-Reimer (1992), The influence of air and sea exchange on the carbon isotope distribution in the sea, *Global Biogeochemical Cycles*, 6(3), 315-320.
- Broecker, W. S., S. L. Peacock, S. Walker, R. Weiss, E. Fahrbach, M. Schroeder, U. Mikolajewicz, C. Heinze, R. Key, T. H. Peng, and S. Rubin (1998), How much deep water is formed in the Southern Ocean?, *Journal of Geophysical Research-Oceans*, 103(C8), 15833-15843.
- Brown, S. J., and H. Elderfield (1996), Variations in Mg/Ca and Sr/Ca ratios of planktonic foraminifera caused by postdepositional dissolution: Evidence of shallow Mg-dependent dissolution, *Paleoceanography*, 11(5), 543-551.
- Brzezinski, M. A., C. J. Pride, V. M. Franck, D. M. Sigman, J. L. Sarmiento, K. Matsumoto, N. Gruber, G. H. Rau, and K. H. Coale (2002), A switch from Si(OH)_4 to NO_3^- depletion in the glacial Southern Ocean, *Geophysical Research Letters*, 29(12), 1564.
- Calvo, E., C. Pelejero, P. De Deckker, and G. A. Logan (2007), Antarctic deglacial pattern in a 30 kyr record of sea surface temperature offshore South Australia, *Geophysical Research Letters*, 34(13), L13707.
- Catubig, N. R., D. E. Archer, R. Francois, P. deMenocla, W. Howard, and E. F. Yu (1998), Global deep sea burial rate of calcium carbonate during the Last Glacial Maximum, *Paleoceanography* 13(3), 298-310.
- Chaigneau, A., and O. Pizarro (2005), Surface circulation and fronts of the South Pacific Ocean, east of 120°W, *Geophysical Research Letters*, 32(8), L08605.
- Chase, Z., R. F. Anderson, M. Q. Fleisher, and P. W. Kubik (2003), Accumulation of biogenic and lithogenic material in the Pacific sector of the Southern Ocean during the past 40,000 years, *Deep-Sea Research Part II-Topical Studies in Oceanography*, 50(3-4), 799-832.
- Chave, A. R. (1954), Aspects of the biogeochemistry of magnesium 1. Calcareous marine organisms, *Journal of Geology*, 62, 266-283.
- Comiso, J. C., C. R. McClain, C. W. Sullivan, J. P. Ryan, and C. L. Leonard (1993), Coastal zone color scanner pigment concentrations in the Southern Ocean and relationships to geophysical surface features, *Journal of Geophysical Research-Oceans*, 98(C2), 2419-2451.

- Cortese, G., G. B. Dunbar, L. Carter, G. Scott, H. Bostock, M. Bowen, M. Crundwell, B. W. Hayward, Howard, W., J. I. Martínez, A. Moy, H. Neil, A. Sabaa, and A. Sturm (2013), Southwest Pacific Ocean response to a warmer world: Insights from Marine Isotope Stage 5e, *Paleoceanography*, 28(3), 585-598.
- Cronblad, H. G., and B. A. Malmgren (1981), Climatically controlled variation of Sr and Mg in Quaternary planktonic foraminifera, *Nature*, 291(5810), 61-64.
- Crosta, X., C. Beucher, K. Pahnke, and M. A. Brzezinski (2007), Silicic acid leakage from the Southern Ocean: Opposing effects of nutrient uptake and oceanic circulation, *Geophysical Research Letters*, 34(13), L13601.
- Crundwell, M., G. Scott, T. Naish, and L. Carter (2008), Glacial-interglacial ocean climate variability from planktonic foraminifera during the mid-Pleistocene transition in the temperate Southwest Pacific, ODP Site 1123, *Palaeogeography Palaeoclimatology Palaeoecology*, 260(1-2), 202-229.
- Curry, W. B., and D. W. Oppo (2005), Glacial water mass geometry and the distribution of $\delta^{13}\text{C}$ of ΣCO_2 in the western Atlantic Ocean, *Paleoceanography*, 20(1), PA1017.
- Curry, W. B., J. C. Duplessy, L. D. Labeyrie, and N. J. Shackleton (1988), Changes in the distribution of $\delta^{13}\text{C}$ of deep water ΣCO_2 between the last glaciation and the Holocene, *Paleoceanography*, 3(3), 317-341.
- De Boer, A. M., R. M. Graham, M. D. Thomas, and K. E. Kohfeld (2013), The control of the Southern Hemisphere Westerlies on the position of the Subtropical Front, *Journal of Geophysical Research-Oceans*, 118(10), 5669-5675.
- Dong, S., S. T. Gille, and J. Sprintall (2007), An assessment of the Southern Ocean mixed layer heat budget, *Journal of Climate*, 20(17), 4425-4442.
- Dubois, N., M. Kienast, S. Kienast, S. E. Calvert, R. Francois, and R. F. Anderson (2010), Sedimentary opal records in the eastern equatorial Pacific: It is not all about leakage, *Global Biogeochemical Cycles*, 24, GB4020.
- Duplessy, J.-C., N. J. Shackleton, R. K. Matthews, W. Prell, W. F. Ruddiman, M. Caralp, and C. H. Hendy (1984), ^{13}C Record of benthic foraminifera in the last interglacial ocean: Implications for the carbon cycle and the global deep water circulation, *Quaternary Research*, 21(2), 225-243.
- Duplessy, J. C., N. J. Shackleton, R. G. Fairbanks, L. Labeyrie, D. Oppo, and N. Kallel (1988), Deepwater source variations during the last climatic cycle and their impact on the global deepwater circulation, *Paleoceanography*, 3(3), 343-360.
- Dymond, J., and M. Lyle (1985), Flux comparisons between sediments and sediment traps in the eastern tropical Pacific: Implications for atmospheric CO_2 variations during the Pleistocene, *Limnology and Oceanography*, 30(4), 699-712.
- Dymond, J., E. Suess, and M. Lyle (1992), Barium in deep sea sediment: A geochemical proxy for paleoproductivity, *Paleoceanography*, 7(2), 163-181.
- Elderfield, H., and G. Ganssen (2000), Past temperature and $\delta^{18}\text{O}$ of surface ocean waters inferred from foraminiferal Mg/Ca ratios, *Nature*, 405(6785), 442-445.
- Elderfield, H., M. Vautravers, and M. Cooper (2002), The relationship between shell size and Mg/Ca, Sr/Ca, $\delta^{18}\text{O}$, and $\delta^{13}\text{C}$ of species of planktonic foraminifera, *Geochemistry Geophysics Geosystems*, 3, 1052.

Ellwood, M. J., M. Wille, and W. Maher (2008), Glacial silicic acid concentrations in the Southern Ocean, *Science*, 330, 1088-1091.

Embley, R. W., and J. J. Morley (1980), Quarternary sedimentation and paleoenvironmental studies off Namibia (South-West Africa), *Marine Geology* 36, 183-204.

Emiliani, C., (1955), Pleistocene temperatures, *Journal of Geology* 63, 538-578

EPICA Community Members – Augustin, L., C. Barbante, P. R. F. Barnes, J. M. Barnola, M. Bigler, E. Castellano, O. Cattani, J. Chappellaz, D. DahlJensen, B. Delmonte, G. Dreyfus, G. Durand, S. Falourd, H. Fischer, J. Fluckiger, M. E. Hansson, P. Huybrechts, R. Jugie, S. J. Johnsen, J. Jouzel, P. Kaufmann, J. Kipfstuhl, F. Lambert, V. Y. Lipenkov, G. V. C. Littot, A. Longinelli, R. Lorrain, V. Maggi, V. Masson-Delmotte, H. Miller, R. Mulvaney, J. Oerlemans, H. Oerter, G. Orombelli, F. Parrenin, D. A. Peel, J. R. Petit, D. Raynaud, C. Ritz, U. Ruth, J. Schwander, U. Siegenthaler, R. Souchez, B. Stauffer, J. P. Steffensen, B. Stenni, T. F. Stocker, I. E. Tabacco, R. Udisti, R. S. W. van de Wal, M. van den Broeke, J. Weiss, F. Wilhelms, J. G. Winther, E. W. Wolff, and M. Zucchelli (2004), Eight glacial cycles from an Antarctic ice core, *Nature*, 429(6992), 623-628.

Feldberg, M. J., and A. C. Mix (2002), Sea surface temperature estimates in the Southeast Pacific based on planktonic foraminiferal species; modern calibration and Last Glacial Maximum, *Marine Micropaleontology*, 44(1-2), 1-29.

Feldberg, M. J., and A. C. Mix (2003), Planktonic foraminifera, sea surface temperatures, and mechanisms of oceanic change in the Peru and South Equatorial Currents, 0-150 ka BP, *Paleoceanography*, 18(1), 1016.

Foster, G. L. (2008), Seawater pH, $p\text{CO}_2$ and $[\text{CO}_3^{2-}]$ variations in the Caribbean Sea over the last 130 kyr: A boron isotope and B/Ca study of planktic foraminifera, *Earth and Planetary Science Letters*, 271(1-4), 254-266.

Fraile, I., S. Mulitza, and M. Schulz (2009a), Modeling planktonic foraminiferal seasonality: Implications for sea surface temperature reconstructions, *Marine Micropaleontology*, 72(1-2), 1-9.

Fraile, I., M. Schulz, S. Mulitza, U. Merkel, M. Prange, and A. Paul (2009b), Modeling the seasonal distribution of planktonic foraminifera during the Last Glacial Maximum, *Paleoceanography*, 24, PA2216.

Francois, R., M. A. Altabet, E. F. Yu, D. M. Sigman, M. P. Bacon, M. Frank, G. Bohrmann, G. Bareille, and L. D. Labeyrie (1997), Contribution of Southern Ocean surface water stratification to low atmospheric CO_2 concentrations during the last glacial period, *Nature*, 389(6654), 929-935.

Friedrich, O., R. Schiebel, P. A. Wilson, S. Weldeab, C. J. Beer, M. J. Cooper, and J. Fiebig (2012), Influence of test size, water depth, and ecology on Mg/Ca, Sr/Ca, $\delta^{18}\text{O}$ and $\delta^{13}\text{C}$ in nine modern species of planktic foraminifera, *Earth and Planetary Science Letters*, 319-320, 133-145.

Garcia, H. E., R. A. Locarnini, T. P. Boyer, J. I. Antonov, M. M. Zweng, and O. K. Baranova (2010a), World Ocean Atlas 2009, Volume 4: Nutrients (phosphate, nitrate, silicate), in *NOAA Atlas NESDIS 71*, edited by S. Levitus, p. 398, U.S. Government Printing Office, Washington, D.C.

Garcia, H. E., R. A. Locarnini, T. P. Boyer, J. I. Antonov, O. K. Baranova, M. M. Zweng, and D. R. Johnson (2010b), World Ocean Atlas 2009, Volume 3: Dissolved Oxygen, Apparent Oxygen Utilization, and Oxygen Saturation, in *NOAA Atlas NESDIS 70*, edited by S. Levitus, p. 344, U.S. Government Printing Office, Washington, D.C.

Gebbie, G. (2014), How much did Glacial North Atlantic Water shoal?, *Paleoceanography*, 29(3), 190-209.

- Gersonde, R. (2011), The expedition of the research vessel "Polarstern" to the polar South Pacific in 2009/2010 (ANT-XXVI/2 – BIPOMAC) *Berichte zur Polar- und Meeresforschung (Reports on Polar and Marine Research)*, 632, 326 pp.
- Gersonde, R., X. Crosta, A. Abelmann, and L. Armand (2005), Sea surface temperature and sea ice distribution of the Southern Ocean at the EPILOG Last Glacial Maximum – A circum-Antarctic view based on siliceous microfossil records, *Quaternary Science Reviews*, 24(7-9), 869-896.
- Goodman, P. J., W. Hazeleger, P. De Vries, and M. Cane (2005), Pathways into the Pacific Equatorial Undercurrent: A trajectory analysis, *Journal of Physical Oceanography*, 35(11), 2134-2151.
- Graham, R. M., and A. M. De Boer (2013), The Dynamical Subtropical Front, *Journal of Geophysical Research-Oceans*, 118(10), 5676-5685.
- Gruber, N., M. Gloor, S. E. M. Fletcher, S. C. Doney, S. Dutkiewicz, M. J. Follows, M. Gerber, A. R. Jacobson, F. Joos, K. Lindsay, D. Menemenlis, A. Mouchet, S. A. Mueller, J. L. Sarmiento, and T. Takahashi (2009), Oceanic sources, sinks, and transport of atmospheric CO₂, *Global Biogeochemical Cycles*, 23, GB1005.
- Gupta, A. S., and M. H. England, (2006), Coupled ocean-atmosphere-ice response to variations in the Southern Annular Mode, *Journal of Climate*, 19, 4457-4486.
- Hain, M. P., D. M. Sigman, and G. H. Haug (2014), The biological pump in the past, in *Treatise on Geochemistry*, edited by H. Holland and K. Turekian, pp. 485-517, Elsevier, Oxford.
- Harrison, K. G. (2000), Role of increased marine silica input on paleo-pCO₂ levels, *Paleoceanography*, 15(3), 292-298.
- Hayes, C. T., R. F. Anderson, and M. Q. Fleisher (2011), Opal accumulation rates in the equatorial Pacific and mechanisms of deglaciation, *Paleoceanography*, 26, PA1207.
- Hays, J. D., J. Imbrie, and N. J. Shackleton (1976), Variations in Earth's orbit: Pacemaker of the ice ages, *Science*, 194(4270), 1121-1132.
- Hayward, B. W., A. T. Sabaa, A. Kolodziej, M. P. Crundwell, S. Steph, G. H. Scott, H. L. Neil, H. C. Bostock, L. Carter, and H. R. Grenfell (2012), Planktic foraminifera-based sea surface temperature record in the Tasman Sea and history of the Subtropical Front around New Zealand, over the last one million years, *Marine Micropaleontology*, 82-83, 13-27.
- Hayward, B. W., G. H. Scott, M. P. Crundwell, J. P. Kennett, L. Carter, H. L. Neil, A. T. Sabaa, K. Wilson, J. S. Rodger, G. Schaefer, H. R. Grenfell, and Q. Li (2008), The effect of submerged plateaux on Pleistocene gyral circulation and sea surface temperatures in the Southwest Pacific, *Global and Planetary Change*, 63(4), 309-316.
- Hendry, K. R., and M. A. Brzezinski (2014), Using silicon isotopes to understand the role of the Southern Ocean in modern and ancient biogeochemistry and climate, *Quaternary Science Reviews*, 89, 13-26.
- Hesse, T., M. Butzin, T. Bickert, and G. Lohmann (2011), A model-data comparison of $\delta^{13}\text{C}$ in the glacial Atlantic Ocean, *Paleoceanography*, 26, PA3220.
- Higginson, M. J., and M. A. Altabet (2004), Initial test of the silicic acid leakage hypothesis using sedimentary biomarkers, *Geophysical Research Letters*, 31(18), L18303.
- Hill, K. L., S. R. Rintoul, R. Coleman, and K. R. Ridgway (2008), Wind forced low frequency variability of the East Australia Current, *Geophysical Research Letters*, 35(8), L08602.

- Ho, S. L., G. Mollenhauer, F. Lamy, A. Martínez-García, M. Mohtadi, R. Gersonde, D. Hebbeln, S. Nunez-Ricardo, A. Rosell-Melé, and R. Tiedemann (2012), Sea surface temperature variability in the Pacific sector of the Southern Ocean over the past 700 kyr, *Paleoceanography*, 27, PA4202.
- Hodell, D. A., C. D. Charles, and U. S. Ninnemann (2000), Comparison of interglacial stages in the South Atlantic sector of the Southern Ocean for the past 450 kyr: Implications for Marine Isotope Stage (MIS) 11, *Global and Planetary Change*, 24(1), 7-26.
- Hodell, D. A., C. D. Charles, and F. J. Sierro (2001), Late Pleistocene evolution of the ocean's carbonate system, *Earth and Planetary Science Letters*, 192(2), 109-124.
- Hodell, D. A., K. A. Venz, C. D. Charles, and U. S. Ninnemann (2003a), Pleistocene vertical carbon isotope and carbonate gradients in the South Atlantic sector of the Southern Ocean, *Geochemistry Geophysics Geosystems*, 4, 1004.
- Hodell, D. A., S. L. Kanfoush, K. A. Venz, C. D. Charles, and F. J. Sierro (2003b), The Mid-Brunhes transition in ODP Sites 1089 and 1090 (subantarctic South Atlantic), in *Earth's climate and orbital eccentricity: The Marine Isotope Stage 11 question*, edited by A. W. Droxler, R. Z. Poore and L. H. Burckle, pp. 113-129, American Geophysical Union, Washington, D.C.
- Hodell, D. A., C. D. Charles, J. H. Curtis, P. G. Mortyn, U. S. Ninnemann, and K. A. Venz (2003c), Data report: Oxygen isotope stratigraphy of ODP Leg 177 Sites 1088, 1089, 1090, 1093, and 1094, 177, 26 pp.
- Hoffman, J. L., and D. C. Lund (2012), Refining the stable isotope budget for Antarctic Bottom Water: New foraminiferal data from the abyssal southwest Atlantic, *Paleoceanography*, 27, PA1213.
- Hönisch, B., and N. G. Hemming (2005), Surface ocean pH response to variations in $p\text{CO}_2$ through two full glacial cycles, *Earth and Planetary Science Letters*, 236(1-2), 305-314.
- Honjo, S., R. Francois, S. Manganini, J. Dymond, and R. Collier (2000), Particle fluxes to the interior of the Southern Ocean in the western Pacific sector along 170°W, *Deep-Sea Research Part II-Topical Studies in Oceanography*, 47(15-16), 3521-3548.
- Howard, W. R., and W. L. Prell (1994), Late Quaternary CaCO_3 production and preservation in the Southern Ocean: Implications for oceanic and atmospheric carbon cycling, *Paleoceanography*, 9(3), 453-482.
- Hut, G. (1987), Stable isotope reference samples for geochemical and hydrological investigations, 42 pp, International Atomic Energy Agency, Vienna.
- Huybers, P., and G. Denton (2008), Antarctic temperature at orbital timescales controlled by local summer duration, *Nature Geoscience*, 1(11), 787-792.
- Imbrie, J., J. D. Hays, D. G. Martinson, A. McIntyre, A. C. Mix, J. J. Morley, N. G. Pisias, W. L. Prell, and N. J. Shackleton (1984), The orbital theory of Pleistocene climate: Support from a revised chronology of the marine $\delta^{18}\text{O}$ record, in *Milankovitch and Climate, Part 1*, edited by A. Berger, pp. 269-305, Springer New York.
- Ingalls, A. E., R. F. Anderson, and A. Pearson (2004), Radiocarbon dating of diatom-bound organic compounds, *Marine Chemistry*, 92, 91-105.
- IPCC (2014), Climate Change 2014: Synthesis report. Contribution of working groups I, II and III to the fifth assessment report of the Intergovernmental Panel on Climate Change, 151 pp, IPCC, Geneva, Switzerland.

- Johnson, G. C. (2008), Quantifying Antarctic Bottom Water and North Atlantic Deep Water volumes, *Journal of Geophysical Research-Oceans*, 113(C5), C05027.
- Jouzel, J., V. Masson-Delmotte, O. Cattani, G. Dreyfus, S. Falourd, G. Hoffmann, B. Minster, J. Nouet, J. M. Barnola, J. Chappellaz, H. Fischer, J. C. Gallet, S. Johnsen, M. Leuenberger, L. Loulergue, D. Luethi, H. Oerter, F. Parrenin, G. Raisbeck, D. Raynaud, A. Schilt, J. Schwander, E. Selmo, R. Souchez, R. Spahni, B. Stauffer, J. P. Steffensen, B. Stenni, T. F. Stocker, J. L. Tison, M. Werner, and E. W. Wolff (2007), Orbital and millennial Antarctic climate variability over the past 800,000 years, *Science*, 317(5839), 793-796.
- Jullion, L., S. C. Jones, A. C. Naveira Garabato, and M. P. Meredith (2010), Wind-controlled export of Antarctic Bottom Water from the Weddell Sea, *Geophysical Research Letters*, 37, L09609.
- Kaiser, J., F. Lamy, and D. Hebbeln (2005), A 70 kyr sea surface temperature record off southern Chile (Ocean Drilling Program Site 1233), *Paleoceanography*, 20(4), PA4009.
- Keeling, R. F., and B. B. Stephens (2001), Antarctic sea ice and the control of Pleistocene climate instability, *Paleoceanography*, 16(1), 112-131.
- Keir, R. S., and W. H. Berger (1983), Atmospheric CO₂ content in the last 120,000 years: The phosphate extraction model, *Journal of Geophysical Research-Oceans and Atmospheres*, 88(NC10), 6027-6038.
- Key, R. M., A. Kozyr, C. L. Sabine, K. Lee, R. Wanninkhof, J. L. Bullister, R. A. Feely, F. J. Millero, C. Mordy, and T. H. Peng (2004), A global ocean carbon climatology: Results from Global Data Analysis Project (GLODAP), *Global Biogeochemical Cycles*, 18(4), 23, GB4031.
- Kienast, S. S., M. Kienast, S. Jaccard, S. E. Calvert, and R. Francois (2006), Testing the silica leakage hypothesis with sedimentary opal records from the eastern equatorial Pacific over the last 150 kyrs, *Geophysical Research Letters*, 33(15), L15607.
- King, A. L., and W. R. Howard (2004), Planktonic foraminiferal $\delta^{13}\text{C}$ records from Southern Ocean sediment traps: New estimates of the oceanic Suess effect, *Global Biogeochemical Cycles*, 18, GB2007.
- King, A. L., and W. R. Howard (2005), $\delta^{18}\text{O}$ seasonality of planktonic foraminifera from Southern Ocean sediment traps: Latitudinal gradients and implications for paleoclimate reconstructions, *Marine Micropaleontology*, 56(1-2), 1-24.
- Kohfeld, K. E., R. M. Graham, A. M. De Boer, L. C. Sime, E. W. Wolff, C. Le Quéré, and L. Bopp (2013), Southern Hemisphere westerly wind changes during the Last Glacial Maximum: Paleo-data synthesis, *Quaternary Science Reviews*, 68, 76-95.
- Kroopnick, P. M. (1985), The distribution of ^{13}C of ΣCO_2 in the world oceans, *Deep-Sea Research Part I-Oceanographic Research Papers*, 32(1), 57-84.
- Labeyrie, L., M. Labracherie, N. Gorfti, J. J. Pichon, M. Vautravers, M. Arnold, J. C. Duplessy, M. Paterné, E. Michel, J. Duprat, M. Caralp, and J. L. Turon (1996), Hydrographic changes of the Southern Ocean (Southeast Indian sector) over the last 230 kyr, *Paleoceanography*, 11(1), 57-76.
- Lambert, F. B. Delmonte, J. R. Petit, M. Bigler, P. R. Kaufmann, M. A. Hutterli, T. F. Stocker, U. Ruth, J. P. Steffensen, and V. Maggi (2008), Dust-climate couplings over the past 800,000 years from the EPICA Dome C ice core, *Nature*, 452(7187), 616-619.
- Lamy, F., H. W. Arz, R. Kilian, C. B. Lange, L. Lembke-Jene, M. Wengler, J. Kaiser, O. Baeza Urrea, I. R. Hall, N. Harada, and R. Tiedemann (under review), Glacial reduction and millennial-scale variations in Drake Passage throughflow, *PNAS*.

- Lamy, F., J. Kaiser, U. Ninnemann, D. Hebbeln, H. W. Arz, and J. Stoner (2004), Antarctic timing of surface water changes off Chile and Patagonian ice sheet response, *Science*, 304(5679), 1959-1962.
- Lamy, F., R. Gersonde, G. Winckler, O. Esper, A. Jaeschke, G. Kuhn, J. Ullermann, A. Martinez-Garcia, F. Lambert, and R. Kilian (2014), Increased dust deposition in the Pacific Southern Ocean during glacial periods, *Science*, 343(6169), 403-407.
- Lea, D. W. (2003), Elemental and isotopic proxies of past ocean temperatures, in *Treatise on Geochemistry*, edited by H. D. Holland and K. K. Turekian, pp. 365-390, Elsevier-Pergamon, Oxford.
- Lea, D. W., T. A. Mashiotta, and H. J. Spero (1999), Controls on magnesium and strontium uptake in planktonic foraminifera determined by live culturing, *Geochimica et Cosmochimica Acta*, 63(16), 2369-2379.
- Lea, D. W., D. K. Pak, and H. J. Spero (2000), Climate impact of Late Quaternary equatorial Pacific sea surface temperature variations, *Science*, 289(5485), 1719-1724.
- Lea, D. W., D. K. Pak, and H. Spero (2003), Sea Surface Temperatures in the Western Equatorial Pacific During Marine Isotope Stage 11, in *Earth's climate and orbital eccentricity: The Marine Isotope Stage 11 question*, edited by A. W. Droxler, R. Z. Poore and L. H. Burckle, pp. 147-156, American Geophysical Union, Washington, D.C.
- LeGrande, A. N., and G. A. Schmidt (2006), Global gridded data set of the oxygen isotopic composition in seawater, *Geophysical Research Letters*, 33(12), L12604.
- LeGrande, A. N., and G. A. Schmidt (2011), Water isotopologues as a quantitative paleosalinity proxy, *Paleoceanography*, 26, PA3225.
- Lisiecki, L. E., and P. A. Lisiecki (2002), Application of dynamic programming to the correlation of paleoclimate records, *Paleoceanography*, 17(4), 12, 1049.
- Lisiecki, L. E., and M. E. Raymo (2005), A Pliocene-Pleistocene stack of 57 globally distributed benthic $\delta^{18}\text{O}$ records, *Paleoceanography*, 20(1), PA1003.
- Lisiecki, L. E., and M. E. Raymo (2009), Diachronous benthic $\delta^{18}\text{O}$ responses during late Pleistocene terminations, *Paleoceanography*, 24, PA3210.
- Locarnini, R. A., A. V. Mishonov, J. I. Antonov, T. P. Boyer, and H. E. Garcia (2010), World Ocean Atlas 2009, Volume 1: Temperature, in *NOAA Atlas NESDIS 68*, edited by S. Levitus, p. 184, U.S. Government Printing Office, Washington, D.C.
- Lohmann, G. P. (1995), A model for variation in the chemistry of planktonic foraminifera due to secondary calcification and selective dissolution, *Paleoceanography*, 10(3), 445-457.
- Loubere, P., and S. Bennett (2008), Southern Ocean biogeochemical impact on the tropical ocean: Stable isotope records from the Pacific for the past 25,000 years, *Global and Planetary Change*, 63(4), 333-340.
- Lund, D. C., J. F. Adkins, and R. Ferrari (2011), Abyssal Atlantic circulation during the Last Glacial Maximum: Constraining the ratio between transport and vertical mixing, *Paleoceanography*, 26, PA1213.
- Lüthi, D., M. Le Floch, B. Bereiter, T. Blunier, J. -M. Barnola, U. Siegenthaler, D. Raynaud, J. Jouzel, H. Fischer, K. Kawamura, and, T. F. Stocker. (2008), High resolution carbon dioxide concentration record 650,000-800,000 years before present, *Nature*, 453(7193), 379-382.

- Luz, B. (1977), Late Pleistocene paleoclimates of the South Pacific based on statistical analysis of planktonic foraminifers, *Palaeogeography Palaeoclimatology Palaeoecology* 22(1), 61–78.
- Lynch-Stieglitz, J. (2003), Tracers of past ocean circulation, in *Treatise on Geochemistry* edited by H. C. Holland and K. K. Turekian, pp. 433-451, Elsevier-Pergamon, Oxford.
- Lynch-Stieglitz, J., T. F. Stocker, W. S. Broecker, and R. G. Fairbanks (1995), The influence of air-sea exchange on the isotopic composition of oceanic carbon: Observations and modeling, *Global Biogeochemical Cycles*, 9(4), 653-665.
- Mackensen, A. (2012), Strong thermodynamic imprint on recent bottom water and epibenthic $\delta^{13}\text{C}$ in the Weddell Sea revealed: Implications for glacial Southern Ocean ventilation, *Earth and Planetary Science Letters*, 317-318 20–26.
- Mackensen, A., M. Rudolph, and G. Kuhn (2001), Late Pleistocene deep water circulation in the subantarctic eastern Atlantic, *Global and Planetary Change*, 30(3-4), 197-229.
- Mackensen, A., H. W. Hubberten, T. Bickert, G. Fischer, and D. K. Fütterer (1993), The $\delta^{13}\text{C}$ in benthic foraminiferal tests of *Fontbotia Wuellerstorfi* (Schwager) relative to the $\delta^{13}\text{C}$ of dissolved inorganic carbon in Southern Ocean deep water: Implications for glacial ocean circulation models, *Paleoceanography*, 8(5), 587-610.
- Marchitto, T. M., and W. S. Broecker (2006), Deep water mass geometry in the glacial Atlantic Ocean: A review of constraints from the paleonutrient proxy Cd/Ca, *Geochemistry Geophysics Geosystems*, 7, Q12003.
- MARGO Project Members – Waelbroeck, C., A. Paul, M. Kucera, A. Rosell-Mele, M. Weinelt, R. Schneider, A. C. Mix, A. Abelmann, L. Armand, E. Bard, S. Barker, T. T. Barrows, H. Benway, I. Cacho, M. T. Chen, E. Cortijo, X. Crosta, A. de Vernal, T. Dokken, J. Duprat, H. Elderfield, F. Eynaud, R. Gersonde, A. Hayes, M. Henry, C. Hillaire-Marcel, C. C. Huang, E. Jansen, S. Juggins, N. Kallel, T. Kiefer, M. Kienast, L. Labeyrie, H. Leclaire, L. Londeix, S. Mangin, J. Matthiessen, F. Marret, M. Meland, A. E. Morey, S. Mulitza, U. Pflaumann, N. G. Pisias, T. Radi, A. Rochon, E. J. Rohling, L. Saffi, C. Schaefer-Neth, S. Solignac, H. Spero, K. Tachikawa, and J. L. Turon (2009), Constraints on the magnitude and patterns of ocean cooling at the Last Glacial Maximum, *Nature Geoscience*, 2(2), 127-132.
- Marinov, I., A. Gnanadesikan, J. R. Toggweiler, and J. L. Sarmiento (2006), The Southern Ocean biogeochemical divide, *Nature*, 441(7096), 964-967.
- Marinov, I., A. Gnanadesikan, J. L. Sarmiento, J. R. Toggweiler, M. Follows, and B. K. Mignone (2008), Impact of oceanic circulation on biological carbon storage in the ocean and atmospheric $p\text{CO}_2$, *Global Biogeochemical Cycles*, 22(3).
- Marshall, J., and K. Speer (2012), Closure of the meridional overturning circulation through Southern Ocean upwelling, *Nature Geoscience*, 5(3), 171-180.
- Martin, J. H. (1990), Glacial-interglacial CO_2 change: The Iron Hypothesis, *Paleoceanography*, 5(1), 1-13.
- Martínez-Méndez, G., E. G. Molyneux, I. R. Hall, and R. Zahn (2009), Variable water column structure of the South Atlantic on glacial-interglacial time scales, *Quaternary Science Reviews*, 28(27-28), 3379-3387.
- Martínez-Méndez, G., D. Hebbeln, M. Mohtadi, F. Lamy, R. De Pol-Holz, D. Reyes-Macaya, and T. Freudenthal (2013), Changes in the advection of Antarctic Intermediate Water to the northern Chilean coast during the last 970 kyr, *Paleoceanography*, 28(4), 607-618.

- Mashiotta, T. A., D. W. Lea, and H. J. Spero (1999), Glacial-interglacial changes in subantarctic sea surface temperature and $\delta^{18}\text{O}$ -water using foraminiferal Mg, *Earth and Planetary Science Letters*, 170(4), 417-432.
- Matsumoto, K., and J. Lynch-Stieglitz (1999), Similar glacial and Holocene deep water circulation inferred from southeast Pacific benthic foraminiferal carbon isotope composition, *Paleoceanography*, 14(2), 149-163.
- Matsumoto, K., J. Lynch-Stieglitz, and R. F. Anderson (2001), Similar glacial and Holocene Southern Ocean hydrography, *Paleoceanography*, 16(5), 445-454.
- Matsumoto, K., J. L. Sarmiento, and M. A. Brzezinski (2002), Silicic acid leakage from the Southern Ocean: A possible explanation for glacial atmospheric $p\text{CO}_2$, *Global Biogeochemical Cycles*, 16(3), 1031.
- Matsumoto, K., Z. Chase, and K. Kohfeld (2014), Different mechanisms of silicic acid leakage and their biogeochemical consequences, *Paleoceanography*, 29(3), 238-254.
- McCartney, M. S. (1977), Subantarctic Mode Water in *A voyage of discovery: George Deacon 70th anniversary volume* edited by M. V. Angel, pp. 103-119, Pergamon Press Oxford.
- Mekik, F., R. Francois, and M. Soon (2007), A novel approach to dissolution correction of Mg/Ca-based paleothermometry in the tropical Pacific, *Paleoceanography*, 22(3), PA3217.
- Milanković, M. (1941), Kanon der Erdbestrahlung und seine Anwendung auf das Eiszeitenproblem, *Royal Serbian Academy special publication 132*, 33, 633 pp.
- Mohtadi, M., D. Hebbeln, S. N. Ricardo, and C. B. Lange (2006), El Niño-like pattern in the Pacific during marine isotope stages (MIS) 13 and 11?, *Paleoceanography*, 21(1), PA1015.
- Monterey, G., and S. Levitus (1997), *Seasonal Variability of Mixed Layer Depth for the World Ocean*, NOAA Atlas NESDIS 14, U.S. Government Printing Office, Washington, D.C.
- Moore, J. K., and M. R. Abbott (2000), Phytoplankton chlorophyll distributions and primary production in the Southern Ocean, *Journal of Geophysical Research-Oceans*, 105(C12), 28709-28722.
- Moy, A. D., W. R. Howard, S. G. Bray, and T. W. Trull (2009), Reduced calcification in modern Southern Ocean planktonic foraminifera, *Nature Geoscience*, 2(4), 276-280.
- Müller, P. J., and R. Schneider (1993), An automated leaching method for the determination of opal in sediments and particulate matter, *Deep-Sea Research Part I-Oceanographic Research Papers*, 40(3), 425-444.
- Murray, R. W., M. Leinen, and C. W. Knowlton (2012), Links between iron input and opal deposition in the Pleistocene equatorial Pacific Ocean, *Nature Geoscience*, 5(4), 270-274.
- Murray, R. W., C. Knowlton, M. Leinen, A. C. Mix, and C. H. Polsky (2000), Export production and terrigenous matter in the Central Equatorial Pacific Ocean during interglacial oxygen isotope Stage 11, *Global and Planetary Change*, 24(1), 59-78.
- Naish, T., R. Powell, R. Levy, G. Wilson, R. Scherer, F. Talarico, L. Krissek, F. Niessen, M. Pompilio, T. Wilson, L. Carter, R. DeConto, P. Huybers, R. McKay, D. Pollard, J. Ross, D. Winter, P. Barrett, G. Browne, R. Cody, E. Cowan, J. Crampton, G. Dunbar, N. Dunbar, F. Florindo, C. Gebhardt, I. Graham, M. Hannah, D. Hansraj, D. Harwood, D. Helling, S. Henrys, L. Hinnov, G. Kuhn, P. Kyle, A. Läufer, P. Maffioli, D. Mogens, K. Mandernack, W. McIntosh, C. Millan, R. Morin, Ohneiser, C., Paulsen, T., Persico, D., Raine, I., Reed, J., Riesselman, C., Sagnotti, L., Schmitt, D., C.

- Sjunneskog, P. Strong, M. Taviani, S. Vogel, T. Wilch, and T. Williams (2009), Obliquity-paced Pliocene West Antarctic ice sheet oscillations, *Nature*, 458(7236), 322-384.
- Naveira Garabato, A. C., K. J. Heywood, and D. P. Stevens (2002), Modification and pathways of Southern Ocean Deep Waters in the Scotia Sea, *Deep-Sea Research Part I-Oceanographic Research Papers*, 49(4), 681-705.
- Naveira Garabato, A. C., D. P. Stevens, A. J. Watson, and W. Roether (2007), Short-circuiting of the overturning circulation in the Antarctic Circumpolar Current, *Nature*, 447(7141), 194-197.
- Neil, H. L., L. Carter, and M. Y. Morris (2004), Thermal isolation of Campbell Plateau, New Zealand, by the Antarctic Circumpolar Current over the past 130 kyr, *Paleoceanography*, 19(4), PA4008.
- Ninnemann, U. S., and C. D. Charles (1997), Regional differences in Quaternary subantarctic nutrient cycling: Link to intermediate and deep water ventilation, *Paleoceanography*, 12(4), 560-567.
- Ninnemann, U. S., and C. D. Charles (2002), Changes in the mode of Southern Ocean circulation over the last glacial cycle revealed by foraminiferal stable isotopic variability, *Earth and Planetary Science Letters*, 201(2), 383-396.
- Nürnberg, D. (1995), Magnesium in tests of *Neogloboquadrina pachyderma* sinistral from high northern and southern latitudes, *Journal of Foraminiferal Research*, 25(4), 350-368.
- Nürnberg, D., and J. Groeneveld (2006), Pleistocene variability of the Subtropical Convergence at East Tasman Plateau: Evidence from planktonic foraminiferal Mg/Ca (ODP Site 1172A), *Geochemistry Geophysics Geosystems*, 7, Q04P11.
- Nürnberg, D., J. Bijma, and C. Hemleben (1996), Assessing the reliability of magnesium in foraminiferal calcite as a proxy for water mass temperatures, *Geochimica et Cosmochimica Acta*, 60(5), 803-814.
- Oppo, D. W., and R. G. Fairbanks (1987), Variability in the deep and intermediate water circulation of the Atlantic Ocean during the past 25,000 years: Northern Hemisphere modulation of the Southern Ocean, *Earth and Planetary Science Letters*, 86(1), 1-15.
- Oppo, D. W., R. G. Fairbanks, A. L. Gordon, and N. J. Shackleton (1990), Late Pleistocene Southern Ocean $\delta^{13}\text{C}$ variability, *Paleoceanography*, 5(1), 43-54.
- Orsi, A. H., T. Whitworth, and W. D. Nowlin (1995), On the meridional extent and fronts of the Antarctic Circumpolar Current, *Deep-Sea Research Part I-Oceanographic Research Papers*, 42(5), 641-673.
- Orsi, A. H., G. C. Johnson, and J. L. Bullister (1999), Circulation, mixing, and production of Antarctic Bottom Water, *Progress in Oceanography*, 43(1), 55-109.
- Orsi, A. H., W. M. Smethie, and J. L. Bullister (2002), On the total input of Antarctic waters to the deep ocean: A preliminary estimate from chlorofluorocarbon measurements, *Journal of Geophysical Research-Oceans*, 107(C8), 3122.
- Pahnke, K., R. Zahn, H. Elderfield, and M. Schulz (2003), 340,000 year centennial scale marine record of Southern Hemisphere climatic oscillation, *Science*, 301(5635), 948-952.
- Paillard, D., L. Labeyrie, and P. Yiou (1996), Macintosh program performs time series analysis, *EOS, Transactions American Geophysical Union*, 77(39), 379 p.
- Pardo, P. C., F. F. Pérez, A. Velo, and M. Gilcoto (2012), Water masses distribution in the Southern Ocean: Improvement of an extended OMP (eOMP) analysis, *Progress in Oceanography*, 103, 92-105.

- Parrenin, F., J.M. Barnola, J. Beer, T. Blunier, E. Castellano, J. Chappellaz, G. Dreyfus, H. Fischer, S. Fujita, J. Jouzel, K. Kawamura, B. Lemieux-Dudon, L. Loulergue, V. Masson-Delmotte, B. Narcisi, J. R. Petit, G. Raisbeck, D. Raynaud, U. Ruth, J. Schwander, M. Severi, R. Spahni, J. P. Steffensen, A. Svensson, R. Udisti, C. Waelbroeck, and E. Wolff (2007), The EDC3 chronology for the EPICA Dome C ice core, *Climate of the Past*, 3(3), 485-497.
- Pelejero, C., E. Calvo, T. T. Barrows, G. A. Logan, and P. De Deckker (2006), South Tasman Sea alkenone palaeothermometry over the last four glacial/interglacial cycles, *Marine Geology*, 230(1-2), 73-86.
- Petit, J. R., J. Jouzel, D. Raynaud, N. I. Barkov, J. M. Barnola, I. Basile, M. Bender, J. Chappellaz, M. Davis, G. Delaygue, M. Delmotte, V. M. Kotlyakov, M. Legrand, V. Y. Lipenkov, C. Lorius, L. Pépin, C. Ritz, E. Saltzman, and M. Stievenard (1999), Climate and atmospheric history of the past 420,000 years from the Vostok ice core, Antarctica, *Nature*, 399(6735), 429-436.
- Pichon, J.-J., L. D. Labeyrie, G. Bareille, M. Labracherie, J. Duprat, and J. Jouzel (1992), Surface water temperature changes in the high latitudes of the Southern Hemisphere over the last glacial-interglacial cycle, *Paleoceanography*, 7(3), 289-318.
- Piotrowski, A. M., S. L. Goldstein, S. R. Hemming, and R. G. Fairbanks (2004), Intensification and variability of ocean thermohaline circulation through the last deglaciation, *Earth and Planetary Science Letters*, 225(1-2), 205-220.
- Piotrowski, A. M., S. L. Goldstein, S. R. Hemming, R. G. Fairbanks, and D. R. Zylberberg (2008), Oscillating glacial northern and southern deep water formation from combined neodymium and carbon isotopes, *Earth and Planetary Science Letters*, 272(1-2), 394-405.
- Ravelo, A. C., and C. Hillaire-Marcel (2007), The use of oxygen and carbon isotopes of foraminifera in paleoceanography, *Developments in Marine Geology*, 1, 735-764.
- Reid, J. L. (1986), On the total geostrophic circulation of the South Pacific Ocean: Flow patterns, tracers and transports, *Progress in Oceanography*, 16(1), 1-61.
- Reid, J. L. (1989), On the total geostrophic circulation of the South Atlantic Ocean: Flow patterns, tracers, and transports, *Progress in Oceanography*, 23(3), 149-244.
- Richter, T. O., S. van der Gaast, B. Koster, A. Vaars, R. Gieles, H. C. De Stigter, H. De Haas, and T. C. E. van Weering (2006), The Avaatech XRF Core Scanner: Technical description and applications to NE Atlantic sediments, *Geological Society London Special Publications*, 267, 39-50.
- Rickaby, R. E. M., and H. Elderfield (1999), Planktonic foraminiferal Cd/Ca: Paleonutrients or paleotemperature?, *Paleoceanography*, 14(3), 293-303.
- Rickaby, R. E. M., E. Bard, C. Sonzogni, F. Rostek, L. Beaufort, S. Barker, G. Rees, and D. P. Schrag (2007), Coccolith chemistry reveals secular variations in the global ocean carbon cycle?, *Earth and Planetary Science Letters*, 253(1-2), 83-95.
- Ridgway, K. R., and J. R. Dunn (2003), Mesoscale structure of the mean East Australian Current system and its relationship with topography, *Progress in Oceanography*, 56(2), 189-222.
- Rincón-Martínez, D., F. Lamy, S. Contreras, G. Leduc, E. Bard, C. Saukel, T. Blanz, A. Mackensen, and R. Tiedemann (2010), More humid interglacials in Ecuador during the past 500 kyr linked to latitudinal shifts of the equatorial front and the Intertropical Convergence Zone in the eastern tropical Pacific, *Paleoceanography*, 25, PA2210.

- Rintoul, S., C. Hughes, and D. Olbers (2001), The Antarctic Circumpolar Current system, in *Ocean circulation and climate: Observing and modelling the global ocean*, edited by G. Siedler, J. Church and J. Gould, p. 715, Academic Press, New York
- Robinson, R. S., A. Mix, and P. Martinez (2007), Southern Ocean control on the extent of denitrification in the Southeast Pacific over the last 70 ka, *Quaternary Science Reviews*, 26(1-2), 201-212.
- Robinson, R. S., D. M. Sigman, P. J. DiFiore, M. M. Rohde, T. A. Mashiotta, and D. W. Lea (2005), Diatom-bound $^{15}\text{N}/^{14}\text{N}$: New support for enhanced nutrient consumption in the ice age subantarctic, *Paleoceanography*, 20(3), PA3003.
- Rohling, E. J. (2007), Progress in paleosalinity: Overview and presentation of a new approach, *Paleoceanography*, 22, 9, PA3215.
- Rohling, E. J., and G. R. Bigg (1998), Paleosalinity and $\delta^{18}\text{O}$: A critical assessment, *Journal of Geophysical Research-Oceans*, 103(C1), 1307-1318.
- Ronge, T. A., R. Tiedemann, F. Lamy, P. Köhler, B. V. Alloway, R. De Pol-Holz, K. Pahnke, J. Southon, and L. Wacker (under review), Radiocarbon constraints on the extent and evolution of the South Pacific glacial carbon pool, *Nature*.
- Rosenthal, Y., M. Dahan, and A. Shemesh (2000a), Southern Ocean contributions to glacial-interglacial changes of atmospheric $p\text{CO}_2$: An assessment of carbon isotope records in diatoms, *Paleoceanography*, 15(1), 65-75.
- Rosenthal, Y., G. P. Lohmann, K. C. Lohmann, and R. M. Sherrell (2000b), Incorporation and preservation of Mg in *Globigerinoides sacculifer*: Implications for reconstructing the temperature and $^{18}\text{O}/^{16}\text{O}$ of seawater, *Paleoceanography*, 15(1), 135-145.
- Russon, T., D. Paillard, and M. Elliot (2010), Potential origins of 400–500 kyr periodicities in the ocean carbon cycle: A box model approach, *Global Biogeochemical Cycles*, 24, GB2013.
- Sallée, J. B., K. Speer, and R. Morrow (2008), Response of the Antarctic Circumpolar Current to atmospheric variability, *Journal of Climate*, 21(12), 3020-3039.
- Sallée, J. B., K. G. Speer, and S. R. Rintoul (2010a), Zonally asymmetric response of the Southern Ocean mixed layer depth to the Southern Annular Mode, *Nature Geoscience*, 3(4), 273-279.
- Sallée, J. B., K. Speer, S. Rintoul, and S. Wijffels (2010b), Southern Ocean Thermocline Ventilation, *Journal of Physical Oceanography*, 40(3), 509-529.
- Sarmiento, J. L., N. Gruber, M. A. Brzezinski, and J. P. Dunne (2004), High latitude controls of thermocline nutrients and low latitude biological productivity, *Nature*, 427(6969), 56-60.
- Schaefer, G., J. S. Rodger, B. W. Hayward, J. P. Kennett, A. T. Sabaab, and G. H. Scott (2005), Planktic foraminiferal and sea surface temperature record during the last 1 Myr across the Subtropical Front, Southwest Pacific, *Marine Micropaleontology*, 54(3-4), 191-212.
- Schlitzer, R. (2012), Ocean Data View, <http://odv.awi.de>.
- Shackleton, N. J. (1967), Oxygen isotope analysis and Pleistocene temperature re-assessed, *Nature*, 215, 15-17.
- Shackleton, N. J. (1974), Attainment of isotopic equilibrium between ocean water and the benthonic foraminifer genus *Uvigerina*: Isotopic changes in the ocean during the last glacial, in *Les Methodes*

Quantitative d'Etude des Variations du Climate au Cours du Pleistocene, edited by L. Labeyrie, pp. 203-210, Colloques Internationaux du Centre National de la Recherche Scientifique.

Sigman, D. M., and E. A. Boyle (2000), Glacial/interglacial variations in atmospheric carbon dioxide, *Nature*, 407(6806), 859-869.

Sigman, D. M., M. P. Hain, and G. H. Haug (2010), The polar ocean and glacial cycles in atmospheric CO₂ concentration, *Nature*, 466(7302), 47-55.

Sikes, E. L., W. R. Howard, H. L. Neil, and J. K. Volkman (2002), Glacial-interglacial sea surface temperature changes across the subtropical front east of New Zealand based on alkenone unsaturation ratios and foraminiferal assemblages, *Paleoceanography*, 17(2), 1012.

Skinner, L. C., and N. J. Shackleton (2005), An Atlantic lead over Pacific deep water change across Termination I: implications for the application of the marine isotope stage stratigraphy, *Quaternary Science Reviews*, 24(5-6), 571-580.

Sokolov, S., and S. R. Rintoul (2009a), Circumpolar structure and distribution of the Antarctic Circumpolar Current fronts: 1. Mean circumpolar paths, *Journal of Geophysical Research-Oceans*, 114, C11018.

Sokolov, S., and S. R. Rintoul (2009b), Circumpolar structure and distribution of the Antarctic Circumpolar Current fronts: 2. Variability and relationship to sea surface height, *Journal of Geophysical Research-Oceans*, 114, C11019.

Speer, K., S. R. Rintoul, and B. Sloyan (2000), The diabatic Deacon Cell, *Journal of Physical Oceanography*, 30(12), 3212-3222.

Spero, H. J., J. Bijma, D. W. Lea, and B. E. Bemis (1997), Effect of seawater carbonate concentration on foraminiferal carbon and oxygen isotopes, *Nature*, 390(6659), 497-500.

Srivastava, R., R. Ramesh, S. Prakash, N. Anilkumar, and M. Sudhakar (2007), Oxygen isotope and salinity variations in the Indian sector of the Southern Ocean, *Geophysical Research Letters*, 34(24), L24603.

Stammerjohn, S., T. Maksym, P. Heil, R. A. Massom, M. Vancoppenolle, and K. C. Leonard (2011), The influence of winds, sea surface temperature and precipitation anomalies on Antarctic regional sea ice conditions during IPY 2007, *Deep-Sea Research Part II-Topical Studies in Oceanography*, 58(9-10), 999-1018.

Stephens, B. B., and R. F. Keeling (2000), The influence of Antarctic sea ice on glacial-interglacial CO₂ variations, *Nature*, 404(6774), 171-174.

Stern, J. V., and L. E. Lisiecki (2014), Termination 1 timing in radiocarbon-dated regional benthic $\delta^{18}\text{O}$ stacks, *Paleoceanography*, 29(12), 1127-1142.

Stramma, L., R. G. Peterson, and M. Tomczak (1995), The South Pacific Current, *Journal of Physical Oceanography*, 25(1), 77-91.

Takahashi, T., W. S. Broecker, and A. E. Bainbridge (1981), The alkalinity and total carbon dioxide concentration in the world oceans, in *Carbon cycle modelling*, edited by B. Bolin, pp. 271-286, John Wiley & Sons, New York

Takeda, S. (1998), Influence of iron availability on nutrient consumption ratio of diatoms in oceanic waters, *Nature*, 393(6687), 774-777.

- Tapia, R., D. Nürnberg, T. Ronge, and R. Tiedemann (2015), Disparities in glacial advection of Southern Ocean intermediate water to the South Pacific gyre, *Earth and Planetary Science Letters*, 410, 152-164.
- Thomalla, S. J., N. Fauchereau, S. Swart, and P. M. S. Monteiro (2011), Regional scale characteristics of the seasonal cycle of chlorophyll in the Southern Ocean, *Biogeosciences*, 8(10), 2849-2866.
- Timmermann, A., T. Friedrich, O. E. Timm, M. O. Chikamoto, A. Abe-Ouchi, and A. Ganopolski (2014), Modeling obliquity and CO₂ effects on Southern Hemisphere climate during the past 408 ka, *Journal of Climate*, 27(5), 1863-1875.
- Toggweiler, J. R. (1999), Variation of atmospheric CO₂ by ventilation of the ocean's deepest water, *Paleoceanography*, 14(5), 571-588.
- Toggweiler, J. R., K. Dixon, and W. S. Broecker (1991), The Peru upwelling and the ventilation of the South Pacific thermocline, *Journal of Geophysical Research-Oceans*, 96(C11), 20467-20497.
- Toggweiler, J. R., J. L. Russell, and S. R. Carson (2006), Midlatitude westerlies, atmospheric CO₂, and climate change during the ice ages, *Paleoceanography*, 21(2), PA2005.
- Ullermann, J., F. Lamy, U. Ninnemann, L. Lembke-Jene, R. Gersonde, G. Kuhn, and R. Tiedemann (in preparation a), Pacific-Atlantic Circumpolar Deep Water coupling during the last 500 ka, *Chapter 4 of this thesis*.
- Ullermann, J., R. Tapia, F. Lamy, D. Nürnberg, R. Gersonde, and R. Tiedemann (in preparation b), Evolution of the sea surface temperature and salinity in the central South Pacific during the past 500 ka: Implications on ocean circulation, *Chapter 5 of this thesis*.
- Vázquez Riveiros, N., C. Waelbroeck, L. Skinner, D. M. Roche, J.-C. Duplessy, and E. Michel (2010), Response of South Atlantic deep waters to deglacial warming during Terminations V and I, *Earth and Planetary Science Letters*, 298(3-4), 323-333.
- Volk, T., and M. I. Hoffert (1985), Ocean carbon pumps: Analysis of relative strengths and efficiencies in ocean-driven atmospheric CO₂ changes, in *The carbon cycle and atmospheric CO₂: Natural variations Archean to present*, edited by E. T. Sunquist and W. S. Broecker, pp. 99-110, American Geophysical Union, Washington, D.C.
- Völker, C., and P. Köhler (2013), Responses of ocean circulation and carbon cycle to changes in the position of the Southern Hemisphere westerlies at Last Glacial Maximum, *Paleoceanography*, 28(4), 726-739.
- Waelbroeck, C., L. Labeyrie, E. Michel, J. C. Duplessy, J. F. McManus, K. Lambeck, E. Balbon, and M. Labracherie (2002), Sea level and deep water temperature changes derived from benthic foraminifera isotopic records, *Quaternary Science Reviews*, 21(1-3), 295-305.
- Waelbroeck, C., L. C. Skinner, L. Labeyrie, J. C. Duplessy, E. Michel, N. Vazquez Riveiros, J. M. Gherardi, and F. Dewilde (2011), The timing of deglacial circulation changes in the Atlantic, *Paleoceanography*, 26, PA3213.
- Warnock, J., R. Scherer, and P. Loubere (2007), A quantitative assessment of diatom dissolution and late quaternary primary productivity in the Eastern Equatorial Pacific, *Deep-Sea Research Part II-Topical Studies in Oceanography*, 54(5-7), 772-783.
- Weaver, P. P. E., L. Carter, and H. L. Neil (1998), Response of surface water masses and circulation to Late Quaternary climate change east of New Zealand, *Paleoceanography*, 13(1), 70-83.

Winckler, G., R. F. Anderson, M. Q. Fleisher, D. McGee, and N. Mahowald (2008), Covariant glacial-interglacial dust fluxes in the equatorial Pacific and Antarctica, *Science*, 320(5872), 93-96.

Wolff, E. W., H. Fischer, F. Fundel, U. Ruth, B. Twarloh, G. C. Littot, R. Mulvaney, R. Röthlisberger, M. de Angelis, C. F. Boutron, M. Hansson, U. Jonsell, M. A. Hutterli, F. Lambert, P. Kaufmann, B. Stauffer, T. F. Stocker, J. P. Steffensen, M. Bigler, M. L. Siggaard-Andersen, R. Udisti, S. Becagli, E. Castellano, M. Severi, D. Wagenbach, C. Barbante, P. Gabrielli, and V. Gaspari (2006), Southern Ocean sea ice extent, productivity and iron flux over the past eight glacial cycles, *Nature*, 440(7083), 491-496.

Wunsch, C. (2003), Determining paleoceanographic circulations, with emphasis on the Last Glacial Maximum, *Quaternary Science Reviews*, 22, 371-385.

Yu, J., H. Elderfield, and B. Hoenisch (2007), B/Ca in planktonic foraminifera as a proxy for surface seawater pH, *Paleoceanography*, 22(2), PA2202.

Žarić, S., B. Donner, G. Fischer, S. Mulitza, and G. Wefer (2005), Sensitivity of planktic foraminifera to sea surface temperature and export production as derived from sediment trap data, *Marine Micropaleontology*, 55(1-2), 75-105.

A.1 – Increased dust deposition in the Pacific Southern Ocean during glacial periods

Frank Lamy (1, 2), Rainer Gersonde (1,2), Gisela Winckler (3,4), Oliver Esper (1), Andrea Jaeschke (1,2), G. Kuhn (1), Johannes Ullermann (1), Alfredo Martinez-Garcia (5), Fabrice Lambert (6), Rolf Kilian (7)

Published in Science (2014), vol. 343, 403-407.

Johannes Ullermann contributed benthic $\delta^{18}\text{O}$ (PS75/056-1, PS75/059-2, PS75/076-2, PS75/079-2) and opal (PS75/059-2) data and was further involved in the extraction of organic compounds from core PS75/059-2, used for biomarker analysis.

1. Alfred-Wegener-Institut Helmholtz-Zentrum für Polar- und Meeresforschung, Bremerhaven, Germany
2. MARUM – Center for Marine Environmental Sciences, Bremen, Germany
3. Lamont-Doherty Earth Observatory, Columbia University, Palisades, NY, USA
4. Department of Earth and Environmental Sciences, Columbia University, NY, USA.
5. Geologisches Institut, ETH Zürich, Zürich, Switzerland.
6. Center for Climate and Resilience Research, University of Chile, Santiago, Chile
7. Geologie, Fachbereich Raum- und Umweltwissenschaften, Universität Trier, Trier, Germany

Abstract

Dust deposition in the Southern Ocean constitutes a critical modulator of past global climate variability, but how it has varied temporally and geographically is underdetermined. Here we present data sets of glacial/interglacial dust supply cycles from the largest Southern Ocean sector, the polar South Pacific, indicating 3-fold higher dust deposition during glacial periods than during interglacials for the last million years. Although the most likely dust source for the South Pacific is Australia/New Zealand, the glacial/interglacial pattern and timing of lithogenic sediment deposition is similar to dust records from Antarctica and the South Atlantic dominated by Patagonian sources. These similarities imply large-scale common climate forcings such as latitudinal shifts of the southern westerlies and regionally enhanced glaciogenic dust mobilization in New Zealand and Patagonia.

Main Text

Mineral aerosols (dust) play a crucial role in determining the pattern and magnitude of climate variability. Dust impurities trapped in Antarctic ice point to ~25-fold higher glacial dust fluxes compared to interglacials (1). It has been suggested that an increase in the atmospheric supply of iron (Fe) by dust during glacial periods, may have stimulated marine productivity in the Southern Ocean (SO) contributing to the reduction of atmospheric CO₂ concentrations observed during ice ages (2). Dust-induced Fe fertilization represents one key mechanism potentially affecting past ocean/atmosphere CO₂ exchange (3-5), although the magnitude with respect to other SO processes such as sea-ice extent, overturning strength, and water column stratification is still under debate (5, 6). Antarctic ice cores only allow an indirect qualitative inference of dust deposition over the ocean, and cannot be used to quantitatively estimate dust deposition in the different SO sectors. Marine sediments, however, provide a direct estimate of SO dust deposition and marine export production. To date, marine studies are primarily confined to the Atlantic SO sector located downstream of Patagonia, a strong dust source during glacial periods. In that region, substantially enhanced glacial dust fluxes and Subantarctic productivity have been interpreted to control at most one third to one half of the observed glacial/interglacial atmospheric CO₂ difference (4, 7), consistent with similar results based on the phasing of dust and CO₂ fluctuations in the Epica Dome C (EDC) ice-core (8). This is, however, based on the assumption that dust deposition and Fe fertilization take place equally in the entire Subantarctic Zone. Biogeochemical models with geographically variable dust fields for the SO suggest a somewhat lower CO₂ reduction (9).

Glacial dust recorded in ice-cores from the East Antarctic Plateau originates almost exclusively from South America including Patagonia (10). Model simulations (11) have supported this view and suggested that dust deposition in the Southern Ocean occurs mainly in the Atlantic and western Indian SO sectors. However, a recent simulation indicates that stronger glacial Australian dust sources resulted in a distinct glacial dust deposition field covering most of the Pacific SO sector, but only reaching marginal areas of the Antarctic continent (12) (fig. S1). To date, sediment data on modern and glacial dust deposition in the Pacific SO are restricted to proximal sites around Australia, especially in the Tasman Sea (13) and subordinately east of New Zealand (14). These records show a substantial increase in the deposition of terrigenous material during the last glacial maximum (LGM) compared to the present Holocene, but proximal marine dust records are not necessarily representative of the pelagic Pacific SO. From the open Pacific Ocean a number of short sediment records reveal enhanced lithogenic fluxes during the LGM (15, 16). The contribution of dust remains however inconclusive because most of the coring sites are located in waters potentially affected by the deposition of ice rafted detritus (IRD) (17).

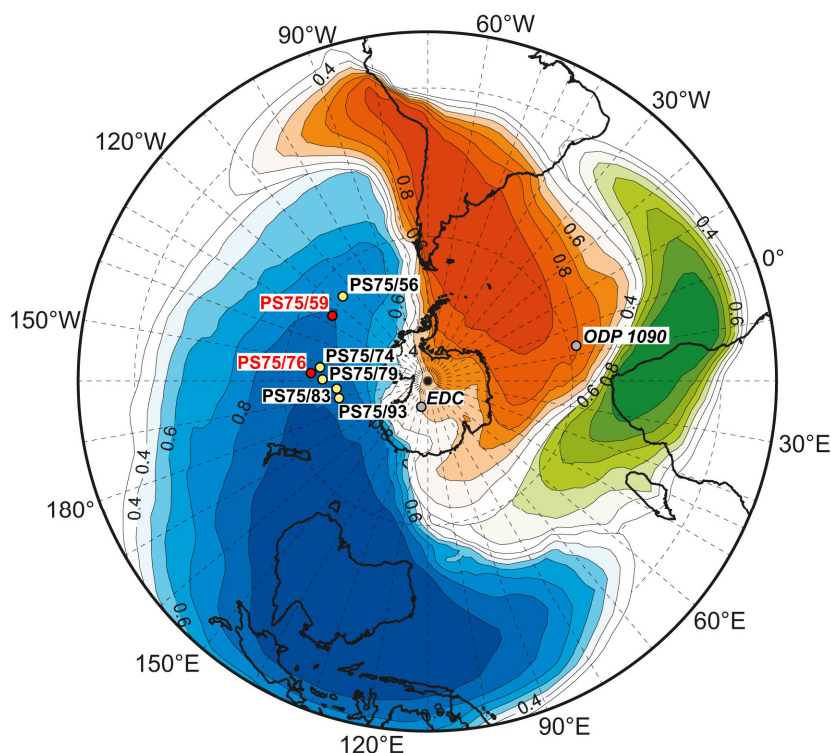


Fig. 1. Map showing the modern relative contributions of the three major dust sources in the Southern Hemisphere (blue: Australia; red: South America; green: South Africa) based on model data (20). Red dots mark primary core locations, yellow dots indicate additional cores.

Here, we report dust flux reconstructions over the last million years based on a suite of sediment cores across the western and central Pacific SO recently collected during the German R/V Polarstern expedition ANT-XXVI/2 (18) (Fig. 1, fig. S2). Based on benthic oxygen isotope stratigraphy and biostratigraphic age control points (19) (fig. S3), Fe-content changes in our sediment records reveal clear similarities to dust content variations documented in Antarctic ice-cores and Atlantic SO sediments (fig. S4). We therefore aligned our high resolution Fe content records to the EDC dust content record (1) back to ca. 800 kyr BP and to the Fe content record of ODP Site 1090 (7) for the interval extending beyond the reach of Antarctic ice-cores (19). The similar pattern in the Fe and dust contents on glacial/interglacial time-scales over the past million years in our Pacific SO sediment records (Fig. 2) extends from the Permanently Open Ocean and Polar Frontal Zone in the southern SW Pacific Basin eastwards to the central Subantarctic Pacific (fig. S2). This geographic pattern largely follows the modeled modern Australian dust plume beneath the maximum westerly winds (20, 21) (Fig. 1) and also simulations of the LGM deposition pattern (12) (fig. S1) and is consistent with a primarily eolian origin of Fe supply to the Pacific SO. Though we cannot exclude minor input of IRD, the strong similarity between Fe content changes and the supply of terrestrial n-alkanes in two cores (fig. S5) strongly supports the predominant eolian origin. Moreover, IRD would not be distributed homogeneously over large distances and thus would not create the consistent variations as shown by our sediment records across the western and central Pacific SO (Fig. 2).

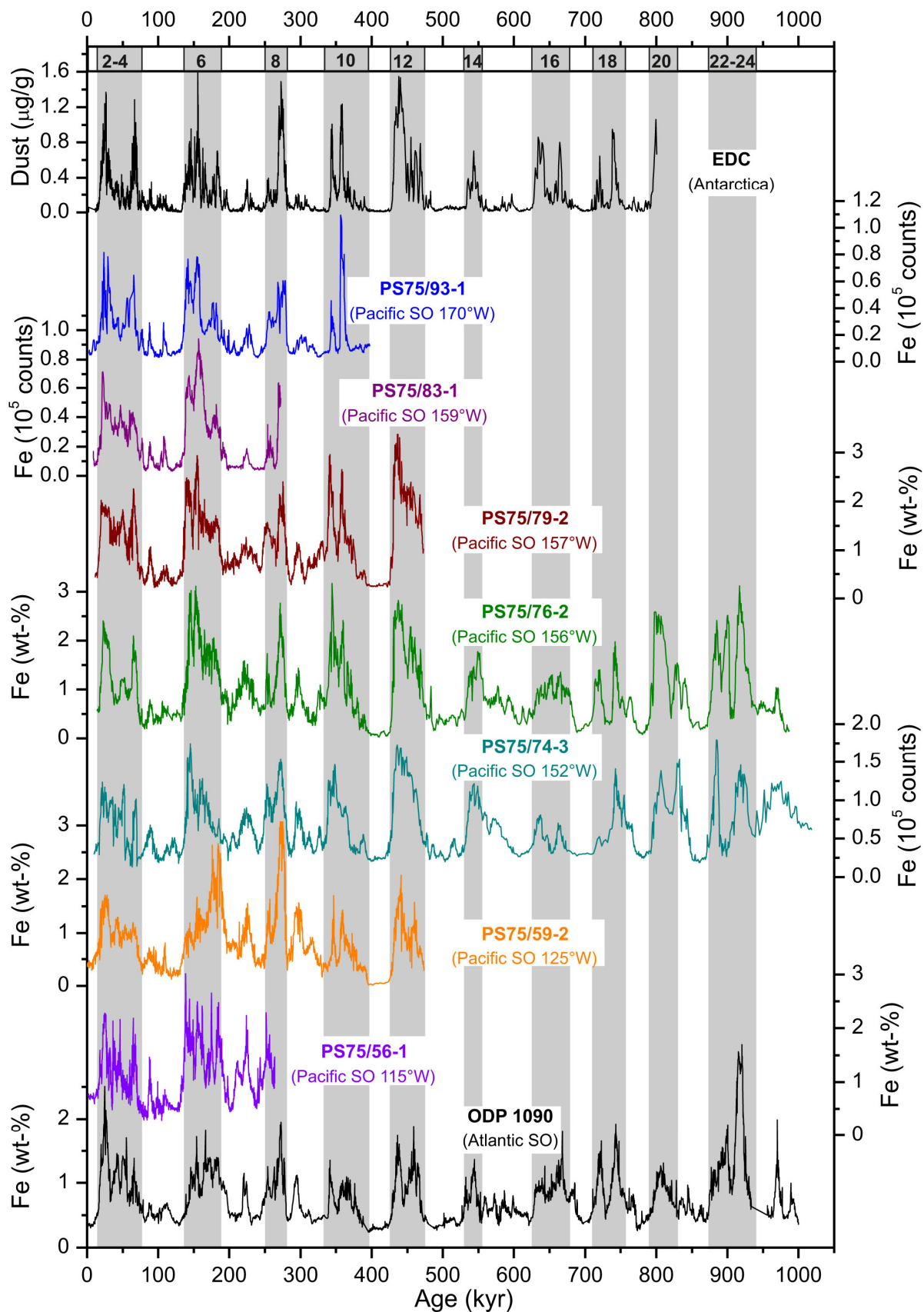


Fig. 2. Iron content fluctuations across the Pacific and Atlantic SO (7) compared to dust content changes in the Epica Dome C (EDC) ice-core (1).

We selected two sediment cores from the suite of ANT-XXVI/2 cores to quantify mass accumulation rates of the lithogenic fraction (MAR_{Litho}) and paleoproductivity estimates (biogenic barium (Ba_{exc}) and opal (19)). Core PS75/76-2 covers the past ~1000 kyr and was recovered close to the Subantarctic Front in the SW Pacific. Core PS75/59-2 reaches back to ~480 kyr BP and is located in the Subantarctic Zone of the central South Pacific (Fig. 1, fig. S2). MAR_{Litho} were obtained by calibrating the high-resolution Fe content records with lithogenic contents calculated from the concentration of ^{232}Th . As with the Fe content records, the shape and glacial/interglacial pattern of the Pacific SO MAR_{Litho} records reveal strong similarities to the EDC ice-core dust MAR and Atlantic SO MAR_{Litho} records from ODP Site 1090 (Fig. 3). Glacial MAR_{Litho} are substantially higher and exceed interglacial values by a factor of ~3-15 (fig. S6).

However, fluxes of both biogenic and lithogenic material in the Southern Ocean may be substantially affected by sediment focusing below the vigorous Antarctic Circumpolar Current (22). In order to correct vertical fluxes for the potential influence of lateral sediment redistribution (focusing), we applied the ^{230}Th normalization method (limited to the past ~300 kyr BP (19)). Glacial $^{230}Th_{norm}$ MAR_{Litho} tend to be considerably lower than the non-normalized values (Fig. 3B and 3C). For each site, the ^{230}Th -normalized MAR_{Litho} show internally consistent variability across the past three glacial/interglacial cycles, indicating ~3-fold increase in lithogenic fluxes during glacials (Fig. 3E; fig. S6), comparable to glacial increases at low latitudes (23). The absolute $^{230}Th_{norm}$ MAR_{Litho} values decrease from west (156°W) to east (125°W) (table S1). The downwind decrease of $^{230}Th_{norm}$ MAR_{Litho} , recorded in our cores, is consistent with a primarily eolian source of the lithogenic material, originating from Australia as also shown in dust simulations (12, 20). However, our interglacial $^{230}Th_{norm}$ MAR_{Litho} are somewhat higher than lithogenic particle fluxes from sediment traps and water samples in the SW Pacific SO (24, 25) and model-based estimates for our core sites (12, 20). In contrast, higher Holocene Australian dust fluxes have been derived from New Zealand peat-bogs (26) (table S1).

Our $^{230}Th_{norm}$ MAR_{Litho} and $^{230}Th_{norm}$ n-alkane MAR records (Fig. 3E-F) document a ~3-fold increase of dust supply to the Pacific SO during glacials (Fig. 3E and fig. S6) consistent with two previous $^{230}Th_{norm}$ MAR_{Litho} records from the central Subantarctic Pacific SO (16) (Fig. 3E) and a compilation of other Pacific dust deposition records (27). Taken together these sediment data suggest a significant enhancement of glacial dust input to the Pacific SO. Though absolute Pacific glacial dust fluxes are ~50% lower than in the Atlantic SO, the relative glacial-interglacial increase is almost as large. Considering the large geographic extension of the Pacific Southern Ocean, this 3-fold increase in Pacific SO dust fluxes requires either a significant enhancement of the Australian dust source, considerable changes in atmospheric circulation, or an additional dust source not active during interglacials.

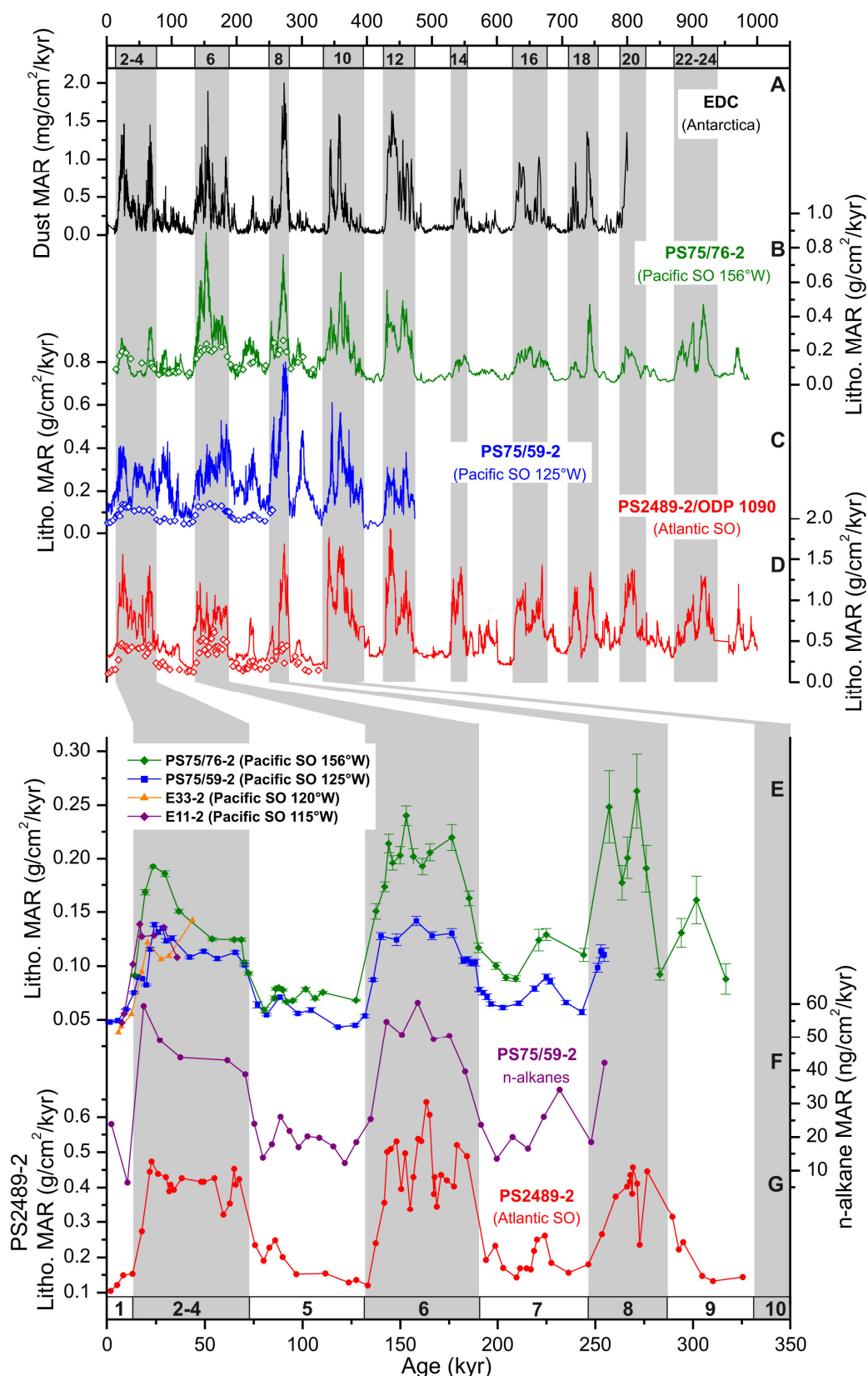


Fig. 3. Changes in lithogenic mass accumulation rates (MAR_{Litho}). (A) Dust MAR in the EDC ice-core (1). (B) MAR_{Litho} core PS75/76-2. (C) MAR_{Litho} core PS75/59-2. (D) MAR_{Litho} ODP Site 1090 (4, 7) (recalculated (19)) Open diamonds in A-C show ²³⁰Th-normalised MAR_{Litho}. (E) ²³⁰Th-normalised MAR_{Litho} values from cores PS75/59-2, PS75/76-2, E11-2, and E33-2 (16). (F) ²³⁰Th-normalised C₂₉ and C₃₁ n-alkane MAR from core PS75/59-2. (G) ²³⁰Th-normalised MAR_{Litho} core PS2489-2 (4, 7).

Modeling of the contribution of the different Southern Hemisphere dust sources to modern dust deposition in the SO shows that more than 80% of modern dust deposition in the western and central Pacific SO originates from Australia (12, 20) (Fig. 1). The large-scale distribution of Southern Hemisphere dust is primarily achieved through transport within the westerly wind belt. The uptake of dust and transport/distribution through the westerly wind belt into the SO primarily occurs in austral winter and spring (21) when the westerlies extend further north. In contrast to Patagonia, Australian dust plumes are transported in the free troposphere and can thus be distributed over very large distances (20). Although there is presently no consensus about glacial changes of the westerlies in climate models (28), most paleodata-based reconstructions imply a strengthening and/or equatorward shift of the wind belt (27). Together with more expanded arid dust source areas in Australia (29) and increases in gustiness in the source regions (30), a northward extent and/or enhancement of the westerlies over SE Australia during glacials would plausibly increase the dust uptake and export into the Pacific SO. Additionally, it is conceivable that New Zealand acted as an additional dust source. The westerlies, enhanced by strong katabatic winds in the lee of the glaciated New Zealand Alps (31), could have transported glacial outwash material out into the Pacific SO, a similar mechanism to that proposed for Patagonian dust sources (32). Distinguishing between an enhanced Australian dust source and the emergence of New Zealand as a glaciogenic dust source, will require additional geochemical information about the provenance of the dust exported to the SO Pacific during glacial times.

$^{230}\text{Th}_{\text{norm}}$ documents substantial sediment focusing at our two sites (fig. S7). Despite this impact of lateral sediment redistribution, the glacial-interglacial pattern and shape of dust fluctuations in the EDC ice-core record are preserved in great detail (both in the MAR and Fe-content records; Fig. 2 and 3). This suggests that the climate-controlled variations in the availability of eolian material are the dominant factor in controlling the shape and pattern of glacial/interglacial lithogenic sediment accumulation even at sites where focusing is significant. A prominent feature of our PS75/76-2 $\text{MAR}_{\text{Litho}}$ beyond the range of $^{230}\text{Th}_{\text{norm}}$ is a decrease in glacial $\text{MAR}_{\text{Litho}}$ before MIS 12 (~480 kyr BP) (Fig. 3B, fig. S6). A very similar decrease is likewise seen in the Fe content record from core PS75/74-3 excluding a local origin of this feature (Fig. 2). This change coincides with a less pronounced Mid-Brunhes shift in glacial/interglacial amplitudes in the EDC and ODP Site 1090 records (Figs. 3A, 3D and S6). Assuming that the shift in our $\text{MAR}_{\text{Litho}}$ is not entirely controlled by a systematic change in sediment focusing through bottom currents during the Mid-Brunhes interval, our data document reduced glacial dust input for the pre-MIS 11 interval. One explanation could be a different sensitivity of the Australian dust sources to glacial severity. In contrast to Patagonia, which lies at higher latitudes, Australian dust sources may require colder global temperature to achieve a similar increase to their Patagonian counterparts. Pre-MIS12 glacials were generally shorter than younger ones (1). Therefore, the time of high dust productivity may have been much shorter for

Australian/New Zealand dust sources compared to Patagonia, explaining the more substantial decrease in pre-MIS 12 glacial Pacific dust fluxes.

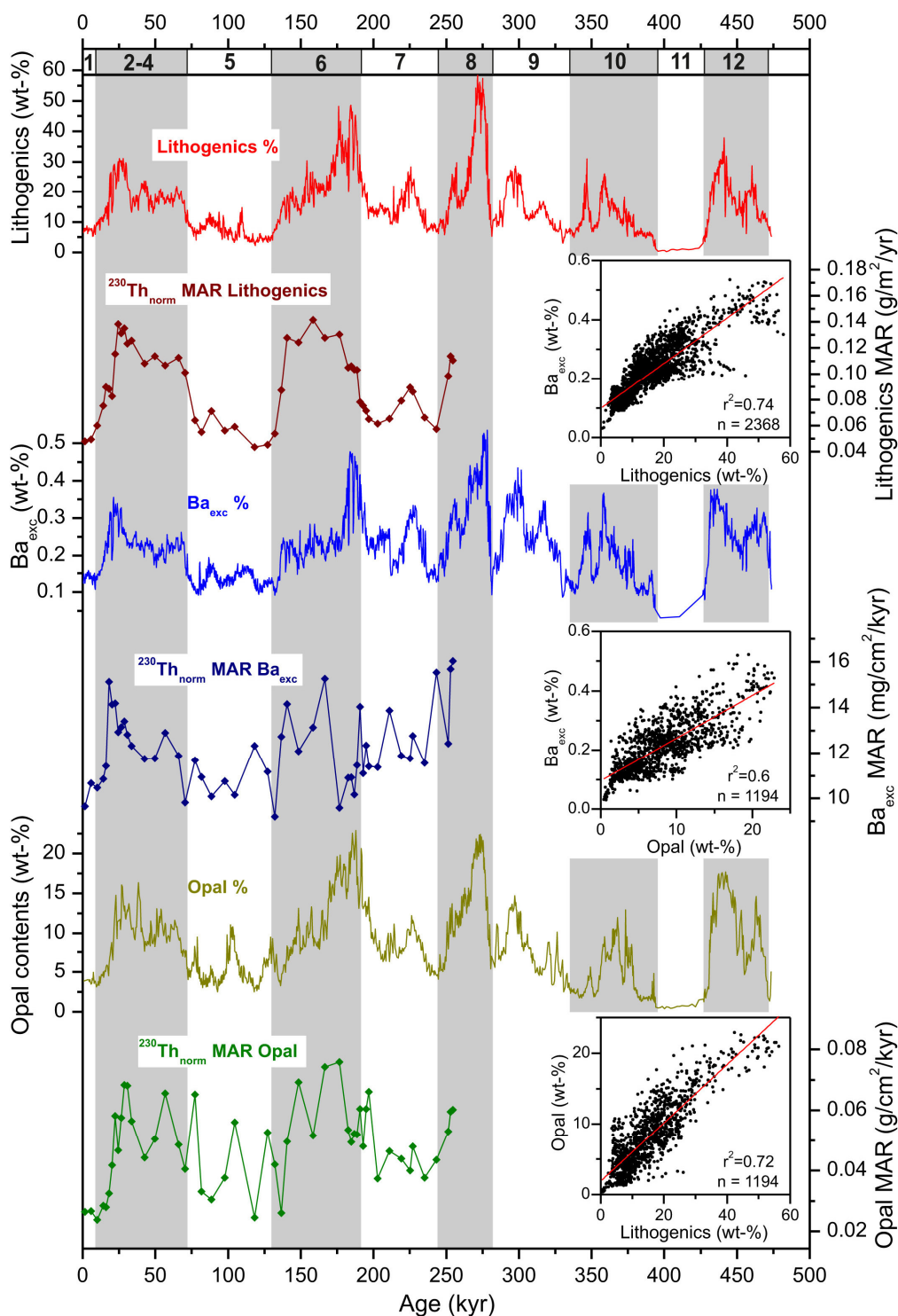


Fig. 4. Proxy records for paleoproductivity from Subantarctic core PS75/59-2. Shown are ^{230}Th -normalised MAR records of Ba_{exc} , biogenic opal and lithogenics together with their contents. Scatter diagrams show positive correlation between lithogenics, Ba_{exc} , and biogenic opal suggesting that the paleoproductivity and lithogenic supply records largely covary.

Taken together our sediment records document a substantial glacial dust supply from Australian or New Zealand sources to the Pacific SO sector eastward to at least 125°W. The ~3-fold increase in glacial dust accumulation in the Pacific SO confirms the enhanced LGM/Holocene dust flux ratios from simulations (12) (fig. S1). Our Pacific SO data revise the current picture of Patagonia representing the almost exclusive source region for glacial dust deposited in the glacial SO. The previously unmeasured dust input to the largest SO sector during several glacial periods may have substantial implications for biological productivity on a global scale. Preliminary paleoproductivity estimates based on Ba_{exc} and biogenic opal records from our Subantarctic core PS75/59-2 suggest ~2-3 times higher glacial values, i.e. the same order of magnitude as the dust increase (Fig. 4). This is consistent with other available sediment records from the Pacific SO (15, 16) that reveal generally higher opal MAR north of the modern Antarctic Polar Front during glacials. However, these data also indicate that this increase is compensated by decreasing productivity southward, a pattern that has been suggested to extend across multiple glacial/interglacial cycles in the Atlantic SO (33). Furthermore, opal MAR do not necessarily reflect productivity of the surface ocean and enhanced organic carbon export particularly in the seasonal ice-zone (3).

Acknowledgments

We thank the captain, crew, and scientific party of R/V Polarstern for their support during cruise ANT-XXVI-2. J. Collins and R. Tiedemann, and three anonymous reviewers provided comments and suggestions that substantially improved the paper. We acknowledge data contributions by P. Köhler and S. Steph and thank S. Albani and N. Mahowald for making their model output available. U. Bock, J. Hefter, R. Fröhlking and S. Wiebe provided technical support at AWI. G.W. thanks R. Schwarz and M. Q. Fleisher for excellent laboratory support. We acknowledge financial support for this work through the Alfred-Wegener-Institut Helmholtz-Zentrum für Polar- und Meeresforschung, the MARUM – Center for Marine Environmental Sciences, University of Bremen, and the EU project Past4future.

References and Notes:

1. F. Lambert *et al.*, Dust-climate couplings over the past 800,000 years from the EPICA Dome C ice core. *Nature* 452, 616-619 (2008).
2. J. H. Martin, Glacial-Interglacial CO₂ change: The Iron Hypothesis. *Paleoceanography* 5, 1-13 (1990).
3. A. Abelmann, R. Gersonde, G. Cortese, G. Kuhn, V. Smetacek, Extensive phytoplankton blooms in the Atlantic sector of the glacial Southern Ocean. *Paleoceanography* 21, PA1013 (2006).
4. A. Martinez-Garcia *et al.*, Links between iron supply, marine productivity, sea surface temperature, and CO₂ over the last 1.1 Ma. *Paleoceanography* 24, PA1207 (2009).

5. D. M. Sigman, M. P. Hain, G. H. Haug, The polar ocean and glacial cycles in atmospheric CO₂ concentration. *Nature* 466, 47-55 (2010).
6. H. Fischer *et al.*, The role of Southern Ocean processes in orbital and millennial CO₂ variations - A synthesis. *Quat. Sci. Rev* 29, 193-205 (2010).
7. A. Martinez-Garcia *et al.*, Southern Ocean dust-climate coupling over the past four million years. *Nature* 476, 312-315 (2011).
8. F. Lambert, M. Bigler, J. P. Steffensen, M. Hutterli, H. Fischer, Centennial mineral dust variability in high-resolution ice core data from Dome C, Antarctica. *Clim Past* 8, 609-623 (2012).
9. L. Bopp, K. E. Kohfeld, C. Le Quere, O. Aumont, Dust impact on marine biota and atmospheric CO₂ during glacial periods. *Paleoceanography* 18, PA1046 (2003).
10. D. M. Gaiero, Dust provenance in Antarctic ice during glacial periods: From where in southern South America? *Geophys Res Lett* 34, L17707 (2007).
11. N. M. Mahowald *et al.*, Change in atmospheric mineral aerosols in response to climate: Last glacial period, preindustrial, modern, and doubled carbon dioxide climates. *J. Geophys. Res. Atmos.* 111, D10202 (2006).
12. S. Albani, N. M. Mahowald, B. Delmonte, V. Maggi, G. Winckler, Comparing modeled and observed changes in mineral dust transport and deposition to Antarctica between the Last Glacial Maximum and current climates. *Clim. Dyn.* 38, 1731-1755 (2012).
13. P. P. Hesse, G. H. McTainsh, Last glacial maximum to early Holocene wind strength in the mid-latitudes of the Southern Hemisphere from aeolian dust in the Tasman Sea. *Quat. Res.* 52, 343-349 (1999).
14. J. Thiede, Wind Regimes over the Late Quaternary Southwest Pacific Ocean. *Geology* 7, 259-262 (1979).
15. L. I. Bradtmiller, R. F. Anderson, M. Q. Fleisher, L. H. Burckle, Comparing glacial and Holocene opal fluxes in the Pacific sector of the Southern Ocean. *Paleoceanography* 24, PA2214 (2009).
16. Z. Chase, R. F. Anderson, M. Q. Fleisher, P. W. Kubik, Accumulation of biogenic and lithogenic material in the Pacific sector of the Southern Ocean during the past 40,000 years. *Deep-Sea Res. Part II* 50, 799-832 (2003).
17. J. Tournadre, F. Girard-Arduin, B. Legresy, Antarctic icebergs distributions, 2002-2010. *J. Geophys. Res. Oceans* 117, C05004 (2012).
18. R. Gersonde, "The expedition of the research vessel "Polarstern" to the polar South Pacific in 2009/2010 (ANT-XXVI/2 - BIPOMAC)" (Alfred Wegener Institute for Polar and Marine Research, Bremerhaven, 2011).
19. Materials and methods are available as supplementary material on *Science Online*.
20. F. Li, P. Ginoux, V. Ramaswamy, Distribution, transport, and deposition of mineral dust in the Southern Ocean and Antarctica: Contribution of major sources. *J. Geophys. Res. Atmos.* 113, D10207 (2008).
21. H. McGowan, A. Clark, Identification of dust transport pathways from Lake Eyre, Australia using Hysplit. *Atmos. Environ.* 42, 6915-6925 (2008).

22. T. L. Noble *et al.*, Greater supply of Patagonian-sourced detritus and transport by the ACC to the Atlantic sector of the Southern Ocean during the last glacial period. *Earth Planet. Sci. Lett.* 317, 374-385 (2012).
23. G. Winckler, R. F. Anderson, M. Q. Fleisher, D. Mcgee, N. Mahowald, Covariant glacial-interglacial dust fluxes in the equatorial Pacific and Antarctica. *Science* 320, 93-96 (2008).
24. C. I. Measures, S. Vink, On the use of dissolved aluminum in surface waters to estimate dust deposition to the ocean. *Global Biogeochem. Cycles* 14, 317-327 (2000).
25. F. L. Sayles, W. R. Martin, Z. Chase, R. F. Anderson, Benthic remineralization and burial of biogenic SiO₂, CaCO₃, organic carbon, and detrital material in the Southern Ocean along a transect at 170 degrees West. *Deep-Sea Res. Part II* 48, 4323-4383 (2001).
26. S. K. Marx, B. S. Kamber, H. A. McGowan, J. Denholm, Detailed history of Holocene climate variability in Australia from dust records in peat cores. *Geochim. Cosmochim. Acta* 73, A843 (2009).
27. K. E. Kohfeld *et al.*, Southern Hemisphere westerly wind changes during the Last Glacial Maximum: Paleo-data synthesis. *Quat. Sci Rev* 68, 76-95 (2013).
28. L. C. Sime *et al.*, Southern Hemisphere westerly wind changes during the Last Glacial Maximum: Model-data comparison. *Quat. Sci Rev* 64, 104-120 (2013).
29. P. P. Hesse, G. H. McTainsh, Australian dust deposits: modern processes and the Quaternary record. *Quat. Sci Rev* 22, 2007-2035 (2003).
30. D. Mcgee, W. S. Broecker, G. Winckler, Gustiness: The driver of glacial dustiness? *Quat. Sci Rev* 29, 2340-2350 (2010).
31. B. V. Alloway *et al.*, Towards a climate event stratigraphy for New Zealand over the past 30 000 years (NZ-INTIMATE project). *J. Quaternary Sci.* 22, 9-35 (2007).
32. D. E. Sugden, R. D. McCulloch, A. J. M. Bory, A. S. Hein, Influence of Patagonian glaciers on Antarctic dust deposition during the last glacial period. *Nat. Geosci.* 2, 281-285 (2009).
33. S. L. Jaccard *et al.*, Two Modes of Change in Southern Ocean Productivity Over the Past Million Years. *Science* 339, 1419-1423 (2013).

A.2 – Supplement: Increased dust deposition in the Pacific Southern Ocean during glacial periods

Frank Lamy, Rainer Gersonde, Gisela Winckler, Oliver Esper, Andrea Jaeschke, G. Kuhn, Johannes Ullermann, Alfredo Martinez-Garcia, Fabrice Lambert, Rolf Kilian

Johannes Ullermann contributed benthic $\delta^{18}\text{O}$ (PS75/056-1, PS75/059-2, PS75/076-2, PS75/079-2) and opal (PS75/059-2) data and was further involved in the extraction of organic compounds from core PS75/059-2, used for biomarker analysis.

Materials and Methods

Sediment cores

The sediment cores were recovered during RV Polarstern cruise ANT-XXVI/2 (18) from the Pacific Southern Ocean (fig. S2). Except gravity core PS75/56-1, all cores are piston cores. We investigated 5 cores in the western South Pacific. Core PS75/93-1 (60°52.33'S; 169°32.89'W; 3762 m water depth; length 12.84 m) was retrieved from the Permanently Open Ocean Zone (POOZ) close to the Polar Front to the north of the Pacific Antarctic Ridge (PAR). Sediments are predominantly siliceous oozes with variable mud content. Biogenic carbonate is absent except for short intervals corresponding to peak interglacials. Similar lithologies characterize core PS75/83-1 (60°16.13'S; 159°03.59'W; 3599 m water depth, length 13.13 m) recovered in the central POOZ ~370 nm to the east PS75/93-1 and core PS75/79-2 (57°30.16'S; 157°14.25'W; 3770 m water depth; length 18.51 m) located close to the modern Polar Front. Further to the northeast, cores PS75/74-3 (56°14.65'S, 152°39.30'W, 3295 m water depth, length 20.95 m) and PS75/076-2 (55°31.71'S; 156°08.39'W; 3742 m water depth; core length 20.59 m) are situated in the Polar Frontal Zone. Sediments in these cores are characterized by a cyclic succession of primarily calcareous oozes during interglacials and muddy siliceous oozes during glacials. In the central Pacific Southern Ocean, core PS75/59-2 (54°12.90'S; 125°25.53'W, 3613 m water depth; core length 13.98 m) was retrieved from the Subantarctic Zone slightly west of the East Pacific Rise. Here, sediments are more carbonate-rich with CaCO_3 contents of >90 wt-% during interglacials that decrease to 30-60 wt-% during glacials when opal and lithogenic contents reach 10-20 wt-% and 30-50 wt-%, respectively. Similar sediments have been recovered west of the East Pacific Rise (core PS75/56-1: 55°09.74'S; 114°47.31'W; 3581 m water depth; length 10.21 m).

Age Models

Preliminary age models were constructed from biostratigraphic time markers (based on siliceous and calcareous microfossils (18)) from all cores (fig. S4) and benthic oxygen isotope records (measured on the benthic foraminifera *Cibicidoides wuellerstorfi* and *Cibicidoides kullenbergi*) from cores PS75/56-1, PS75/59-2, PS75/76-2, and PS75/79-2 (fig. S3). In cores PS75/76-2 and PS75/79-2, benthic

foraminifera are only preserved during interglacials and parts of glacial terminations (fig. S3) and thus no continuous records could be constructed at these sites. Benthic oxygen isotope stratigraphies in the deep Pacific may substantially deviate from the global LR04 reference (34) and ice-core age models (35). Therefore, we decided to primarily rely on tuning to the EDC ice-core record. Such tuning to Antarctic ice core dust records has been previously performed for magnetic susceptibility records from different SO sectors (36). We thus used the initial age models as the base for the alignment of the iron content records to the high resolution dust content record from the EDC ice-core (1) back to ca. 800 kyr BP, and to the iron content record from ODP Site 1090 (7) for the interval extending beyond the reach of Antarctic ice-cores (Fig. 2). For the EDC ice-core, we used the most recent age model AICC12 (37, 38). The benthic oxygen isotope records were also used for improving the cross-correlation of our cores. The resulting excellent correlations suggest very similar dust/iron content pattern on glacial/interglacial time-scales of the past million years. Comparing the benthic oxygen isotope records on our dust tuned age-scale to the global isotope LR04 stack (34), suggests that the our deep Pacific SO records are partly offset at glacial terminations consistent with Lisieki et al.'s (35) findings and modeling results (39). All correlations were performed with the AnalySeries software (40) using a minimum number of tie points preferentially at glacial terminations.

Geochemistry

The high-resolution elemental analysis of Fe and Ba was performed at 0.5-1cm downcore resolution using an AVAATECH profiling X-ray Fluorescence (XRF) core scanner at the Alfred Wegener Institute. The reproducibility of the XRF core scanner for the heavy elements Fe and Ba was calculated as the mean relative standard deviation (%RSD) from all adjoining measurement triplets (n= 9903, each measurement 0.5 cm apart) as 6.8% and 5.5% respectively. This deviation takes into account XRF sediment matrix effects, variations in X-ray tube emission, XRF counting statistics and background correction, as well as inhomogeneities in nearby analyzed sediment volumes. This is consistent with earlier studies (41).

For cores PS75/56-1, PS75/59-2, PS75/76-2, and PS75/79-2, we converted the high-resolution estimates of Fe measured with the XRF core-scanner into quantitative concentrations. The same has been done for Ba for our two key cores PS75/59-2 and PS75/76-2. For this purpose, we used a series of 30 to 40 discrete atomic absorption spectrophotometry (AAS) measurements for each core. Measurements were performed with a VARIAN SeptrAA220 at the University of Trier. Samples of 100 mg of sediment were dried (105°C) and fused completely in Pt skillets with 400 mg of flux material (mixture of Lithiumtetraborate, Lithium carbonate and Lanthanium oxide). The produced glass beads were dissolved in 40 ml HCl (0.5N). Liquids of samples and international standards (MRG-1, SY-2 and JG-2) were measured by the AAS. Determined major elements plus loss of ignition (1050°C) and independently detected contents of CO₂ and SO₂ resulted in sums of 99 to 101 wt.%. Fig. S8 shows the regression lines between XRF core scanner and AAS discrete measurements

used to calculate element concentrations. The high resolution XRF data have been smoothed with a 3-point moving average and resampled for the depths of the AAS data.

The biogenic fraction of Ba (Ba_{excess}) was estimated through normalization by Fe: $Ba_{\text{excess}} = Ba - (Fe * 0.0157)$ using the 5-point smoothed Fe and Ba records. The resulting values are very similar to those obtained through normalization by Ti and Al. Th-normalized Ba_{excess} MAR were calculated from interpolated Ba_{excess} contents to the lower resolution ^{230}Th -normalized mass accumulation rates (Fig. 4).

Bulk sediment parameter

Total (organic) carbon (TOC, TC) were quantified using the LECO CS-200 system. Calcium carbonate content (CaCO_3) was calculated employing the standard equation $\text{CaCO}_3 [\text{wt.}\%] = (\text{TC} [\text{wt.}\%] - \text{TOC} [\text{wt.}\%]) * 8.333$. For the determination of Opal contents, we applied the Automated Leaching Method with a relative analytical precision of 4-10% (42). A high resolution opal content record from core PS75/59-2 was obtained from polynomial regression between GRA-density and the discrete biogenic opal measurements (fig. S9). Th-normalized Opal MAR were from interpolated opal contents to the lower resolution ^{230}Th -normalized mass accumulation rates after applying a 3-point smoothing to the high resolution opal content record (Fig. 4).

Lithogenic content

In order to obtain high resolution lithogenic content records for cores PS75/59-2 and PS75/76-2, we calibrated the 3-point moving average XRF core scanner-based Fe contents with discrete ^{232}Th concentrations assuming an upper continental crust average concentration of 10.7 ppm (43) (fig. S9). We followed a similar approach in the case of the Atlantic core ODP Site 1090. We calibrated ICP-MS Fe concentrations with ^{232}Th (fig. S10), and use this relationship to estimate lithogenic contents from the previously published high resolution XRF core scanner based Fe concentrations (7). The resulting lithogenic contents correspond well to those calculated from bulk sediment parameters for core PS75/59-2 but reveal more scatter in core PS75/76-2 related to the partly high biogenic opal contents and resulting uncertainties in opal measurements (fig. S10). Therefore, we prefer the ^{232}Th -based quantifications of lithogenic contents.

Biomarker

Sediment samples for n-alkane analysis (3-6 g) were freeze-dried, homogenized, and extracted using an automated solvent extractor (ASE 350, Dionex) with dichloromethane/methanol (9:1, v:v). The n-alkanes were separated from the ketone and polar fractions by column chromatography (SiO_2) using n-hexane as eluent. The hydrocarbon fraction was analyzed by gas chromatography (GC/FID; HP-6891; splitless injection mode, carrier gas He (flow rate 1.5 ml/min); DB-5 column, 30 m length, 0.25 mm diameter, 0.25 μm film thickness; oven temperature was programmed to be held at 60°C for 2 min, then increased at 15°C/min to 150°C, at 3°C/min until 320°C, and held for 20 min). Compounds were

identified by comparison with an n-alkane standard mixture. For quantification, squalane was added as an internal standard prior to extraction. For core PS75/59-2, total lipid extracts were analyzed by GC/TOF-MS according to Hefter (44).

Mass accumulation rate (MAR) calculation

MAR of individual components were calculated by multiplying linear sedimentation rates with values of dry bulk density (DBD) and the concentrations of the respective sediment components. DBD has been estimated for each XRF measurement interval from the gamma ray attenuation (GRA) density measurements measured at 1cm resolution onboard R/V Polarstern (18). Samples for DBD discrete measurements were taken immediately after splitting the sediment cores onboard. Discrete DBD measurements were performed on a total of 138 and 203 samples for cores PS75/59-2 and PS75/76-2, respectively. The high resolution GRA bulk density record has been converted into DBD values using the regression lines shown in Figure S9.

U/Th isotope analysis

Uranium and thorium isotope abundances from cores PS75/59-2 and PS75/76-2 were determined by isotope dilution using an Axiom single-collector ICP-MS at LDEO following the methods of Fleisher and Anderson (45). Process blanks and replicate samples were processed with each batch of 18 samples. All blank values were < 0.5% of sample isotope abundances. Uncertainties reported for $^{230}\text{Th}_{\text{xs}}$ activities reflect uncertainties associated with mass spectrometric measurements and the detrital U/Th ratio.

Calculation of ^{230}Th -normalized mass accumulation rates

$^{230}\text{Th}_{\text{xs}}$ -normalized mass accumulation rates (MARs) were calculated using the following equation:

$$(1) \text{MAR} = \beta_{230} * z / x_s^{230}\text{Th}_0$$

where β_{230} is the water column production rate of ^{230}Th ($0.0256 \text{ dpm m}^{-3} \text{ yr}^{-1}$), z is the water depth, and $x_s^{230}\text{Th}_0$ is the excess sedimentary ^{230}Th concentration in dpm g^{-1} corrected for (i) radioactive decay, (ii) the fraction supported by uranium within lithogenic material (assuming a mean regional detrital $^{238}\text{U}/^{232}\text{Th}$ activity ratio of 0.4 ± 0.1 ; (46)), and (iii) the fraction of the in-situ produced ^{230}Th by decay of authigenic ^{238}U (47). The ^{230}Th profiling method is described in Francois et al.(47). Briefly, ^{230}Th is produced in the water column by α -decay of ^{234}U and shows low concentrations in seawater as a result of efficient particle scavenging (e.g., (47-50)). Therefore, its scavenged flux to the seafloor can be assumed to be approximately equal to its production rate in the overlying water column ($\beta_{230} = 2.56 \times 10^{-5} \text{ dpm cm}^{-3} \text{ kyr}^{-1}$). The ^{230}Th profiling method offers advantages over the conventional stratigraphic MARs in that the ^{230}Th -normalized fluxes are insensitive to lateral sediment redistribution and age model uncertainties, and do not rely on the determination of dry bulk density (e.g., (23, 46, 47)). Systematic errors in ^{230}Th -derived MARs may exist due to inaccuracy in the assumption that $^{230}\text{Th}_{\text{xs}}$ fluxes to the sediments are equal to ^{230}Th production in the water column. The model of Henderson et al. (50) suggests that the magnitude of this offset should be smaller than 30%. This systematic error

would affect the accuracy of estimated fluxes but should have a smaller impact on the relative changes downcore. Furthermore, ^{230}Th normalization may slightly underestimate vertical fluxes in opal-rich sediments(51).

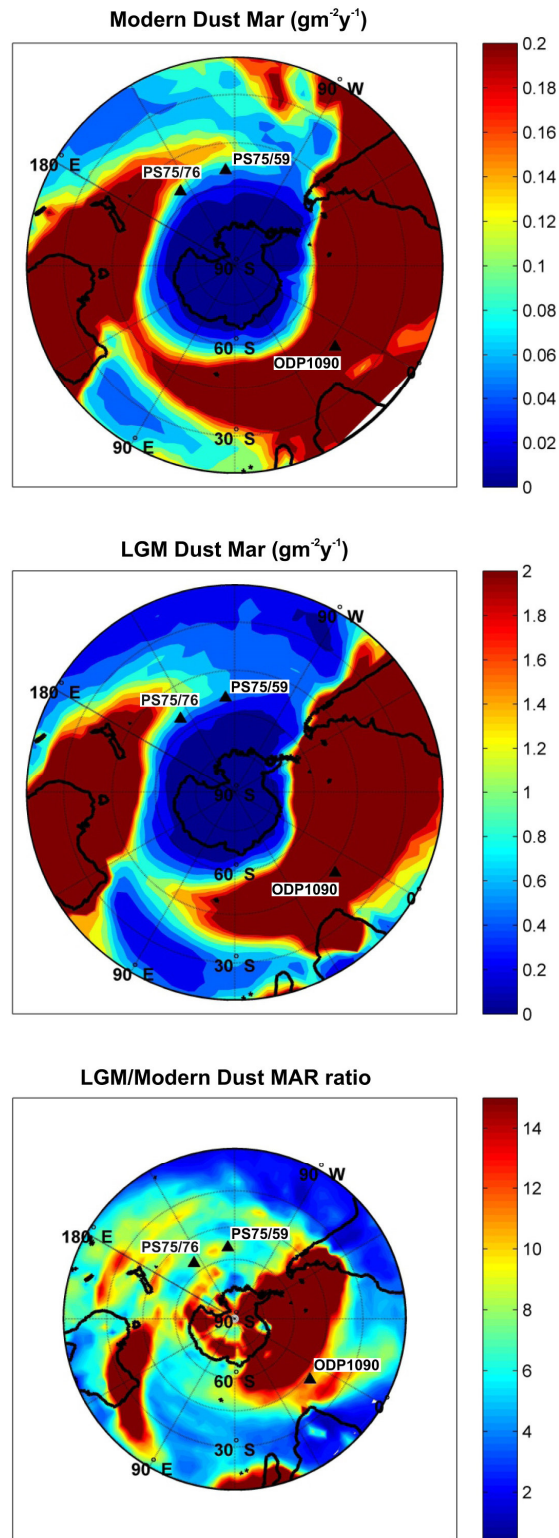


Fig. S1. Modern and glacial dust flux from the most recent model simulation by Albani et al. (12). Lowermost panel shows dust flux ratio between LGM and modern conditions. Triangles indicate core locations in the Pacific and Atlantic SO.

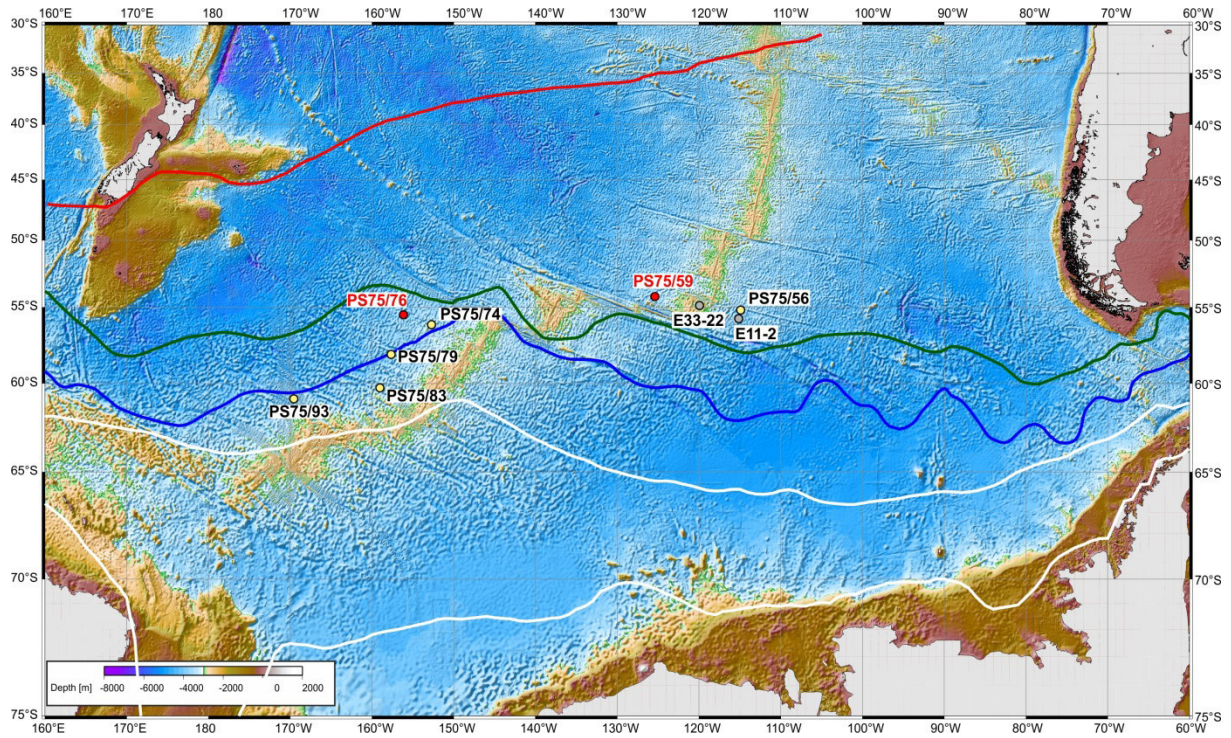


Fig. S2. Bathymetric map of the Pacific SO with core locations (Red dots mark primary core locations, yellow dots indicate additional cores, and grey dots are published sediment records discussed in the text (16). Lines indicate major fronts (52) (red: Subtropical front; green: Subantarctic front ; blue: Polar front white: winter and summer sea ice edge).

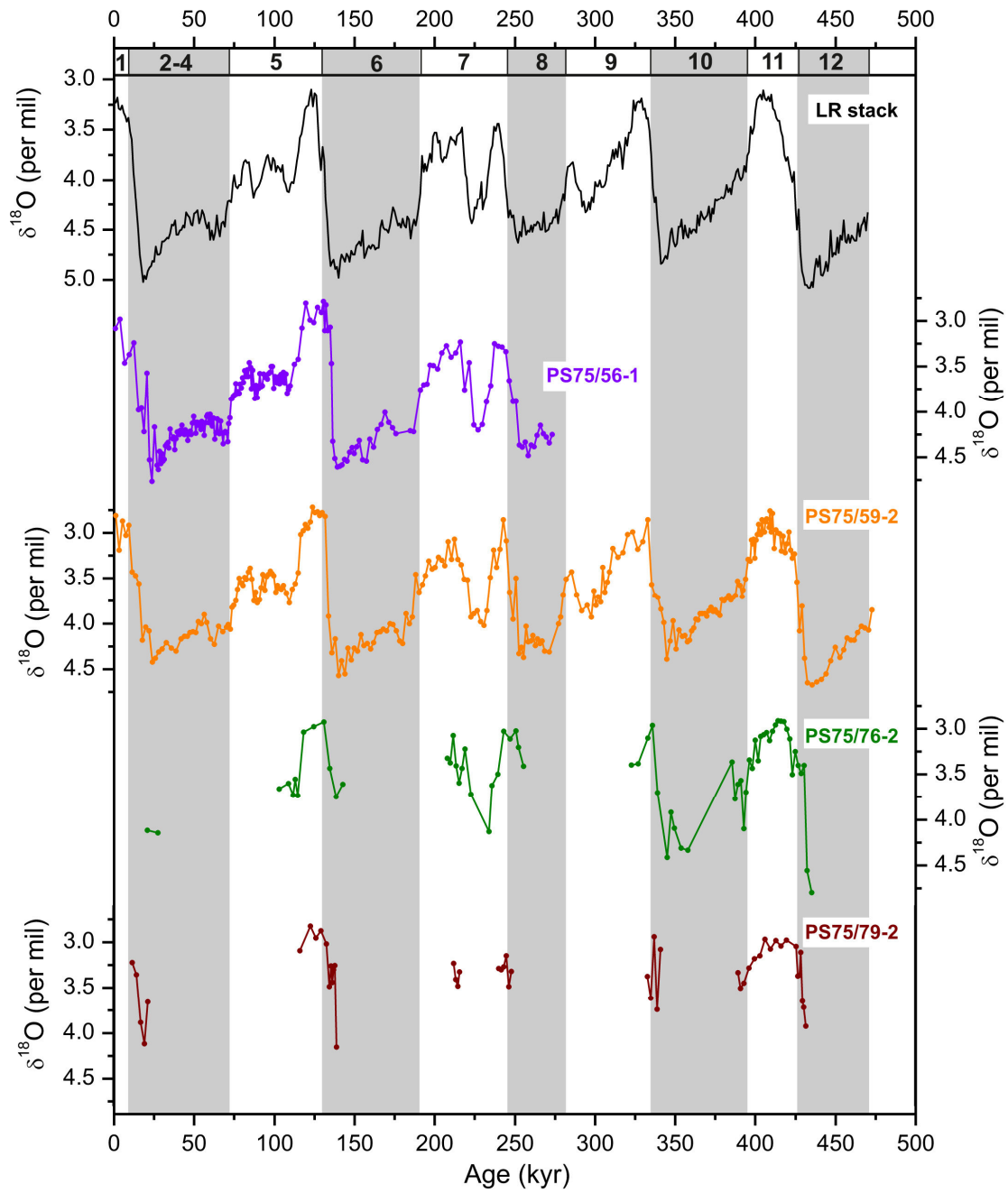


Fig. S3. Benthic oxygen isotope records from cores PS75/56-1, PS75/59-2, PS75/76-2, and PS75/79-2 compared to the LR stack (34).

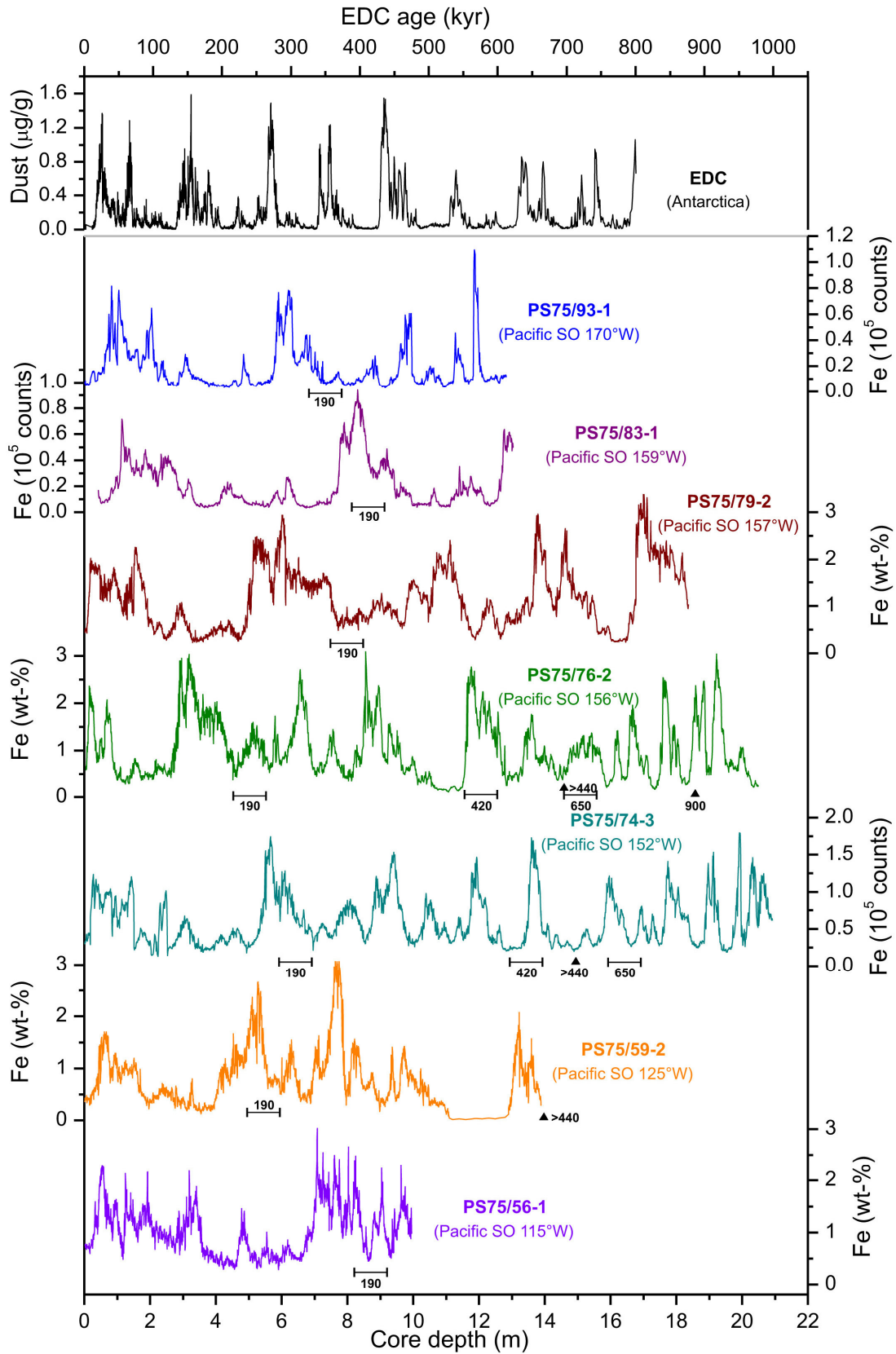


Fig. S4. Unaligned iron content records from Fig. 2 plotted versus core depth with biostratigraphic age control points. Numbers give approximate biostratigraphic age in kyr.

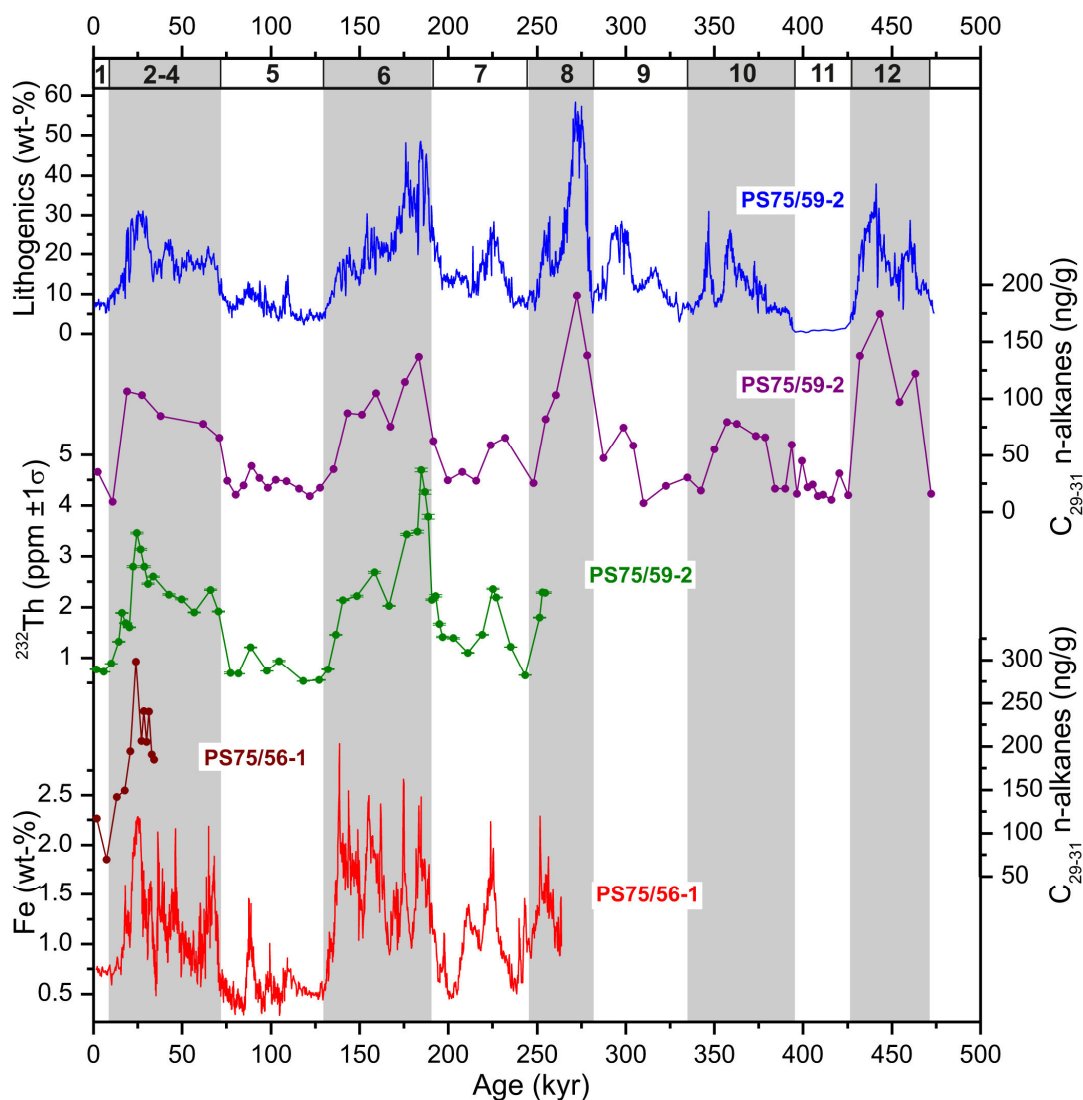


Fig. S5. Terrestrial biomarker records from core PS75/59-2 compared to the lithogenic content record (calculated from high resolution Fe record) and the ^{232}Th contents. The n-alkane distribution in both cores exhibits a clear odd carbon number predominance of long-chain n-alkanes (CPI values are typically 3 to 10), the major homologues being C_{29} and C_{31} . This is characteristic of leaf waxes from terrestrial plants (53) that are commonly found in the organic fraction of dust (54, 55). Other potential contributions from reworked organic material transported by icebergs via ice rafted debris (IRD) or ocean currents are considered to be minor as the geochemical signature would correspond to mature organic matter without odd C-numbered preference (56). Though we can not strictly exclude subsequent hemipelagic transport of eolian supplied n-alkanes in the SW Pacific, we regard this process of minor importance for explaining the first order glacial-interglacial pattern in our records. There is presently no consistent evidence of substantial glacial/interglacial changes in hemipelagic sediment redistribution from the SW Pacific SO eastward that would be necessary to explain the 3-fold increase in lithogenic fluxes across a major part of the Pacific SO. Therefore, the close correlation of the n-alkanes as a measure of continental vegetation and inorganic dust proxies strongly suggests an eolian source of lithogenic material to the Pacific SO.

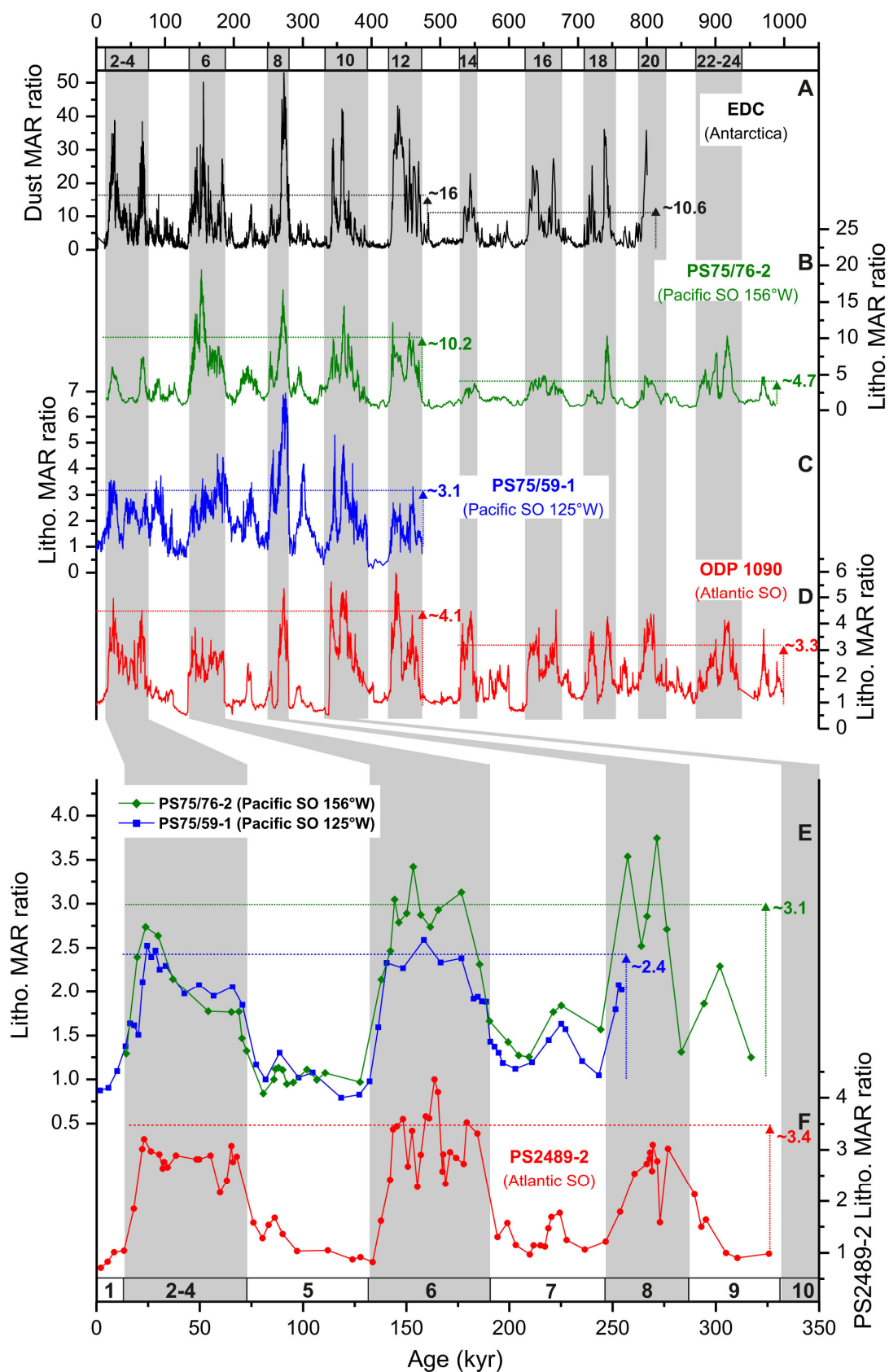


Fig. S6. Lithogenic MAR records shown in Fig. 3 plotted as ratios to the 10th percentile of each data-set (representing average interglacial values). Arrows with numbers indicate average glacial/interglacial MAR_{Litho} ratios defined here as the 90th percentile/10th percentile.

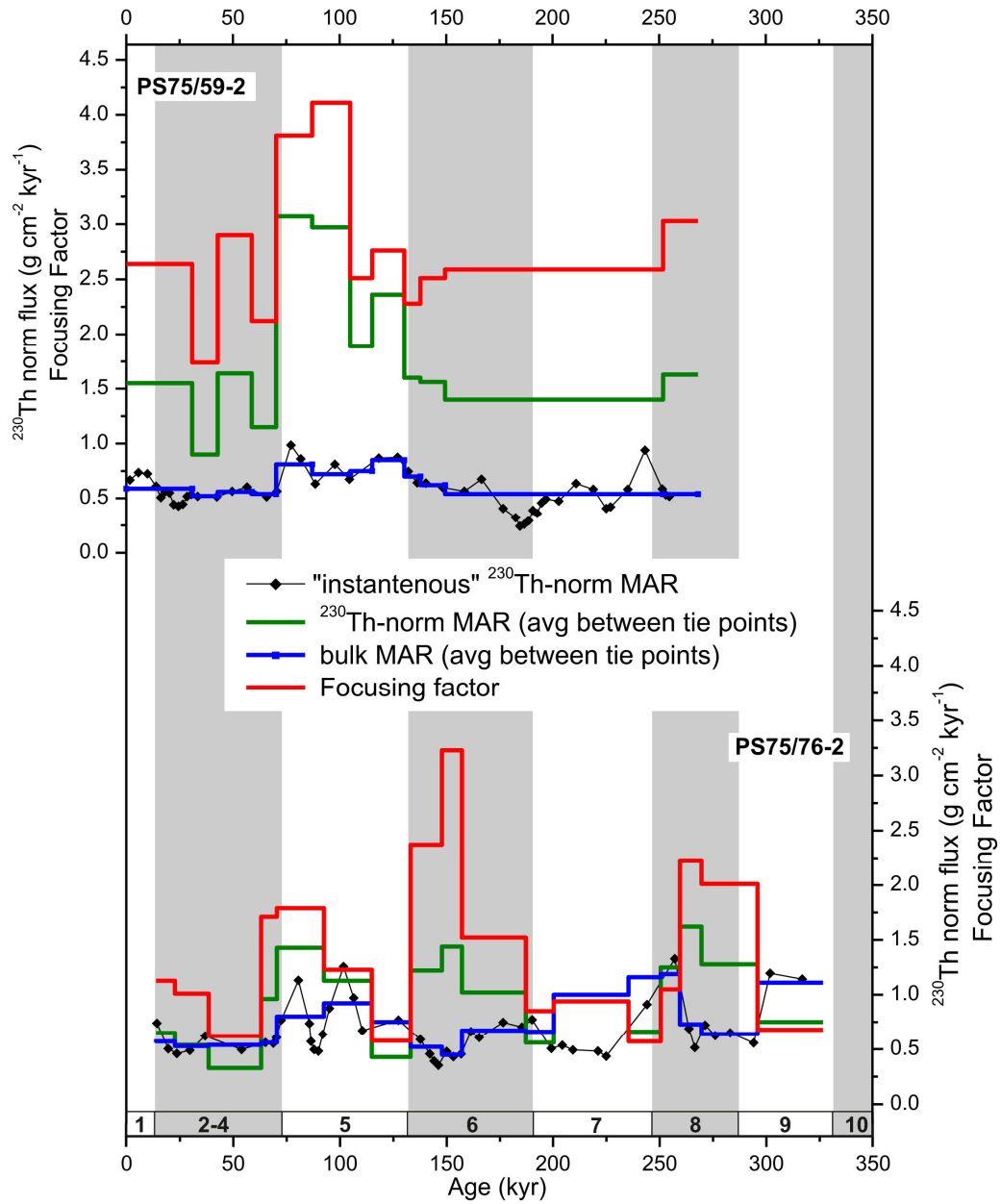


Fig. S7. Comparison of conventional and ^{230}Th -normalized MAR for cores PS75/59-2 and PS75/76-2 and resulting focusing factors (47).

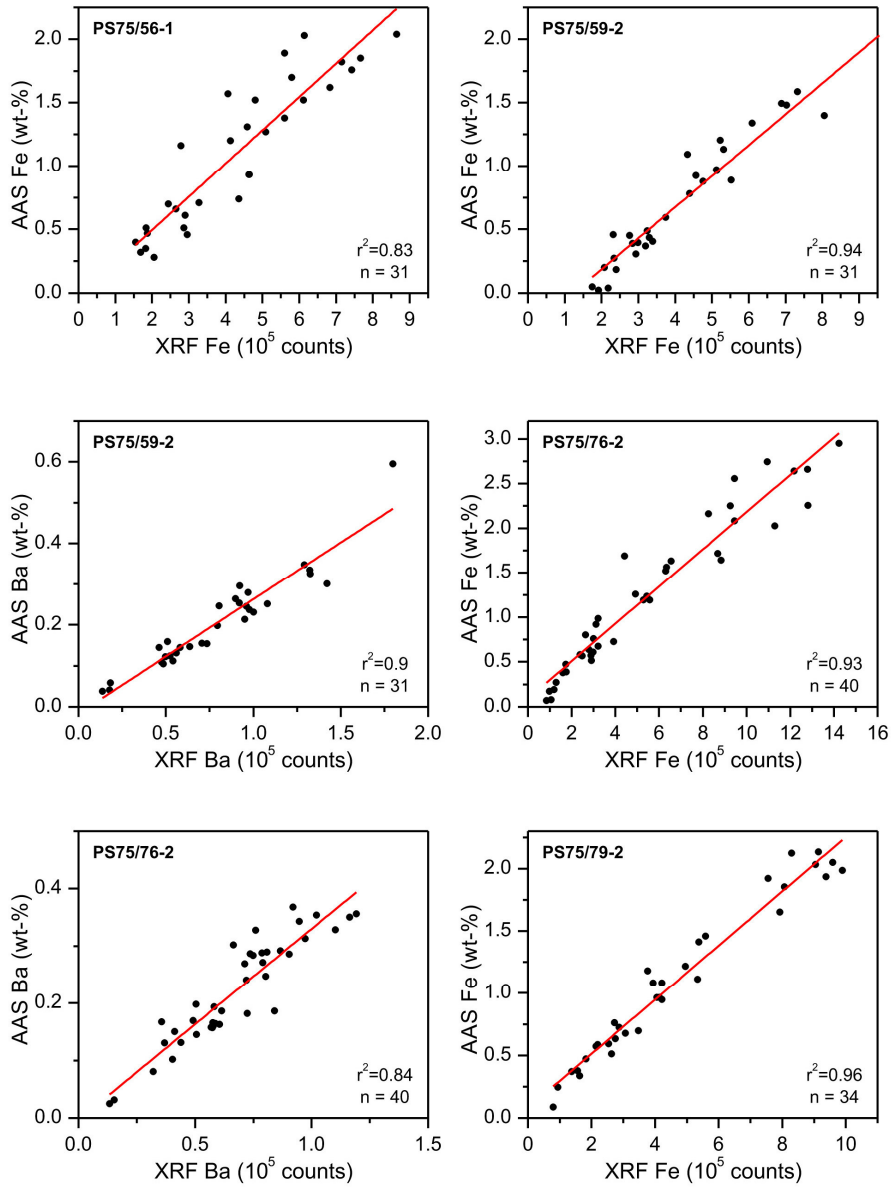


Fig. S8. Linear regressions between XRF and AAS-based Fe and Ba concentrations used to obtain high resolution element content records.

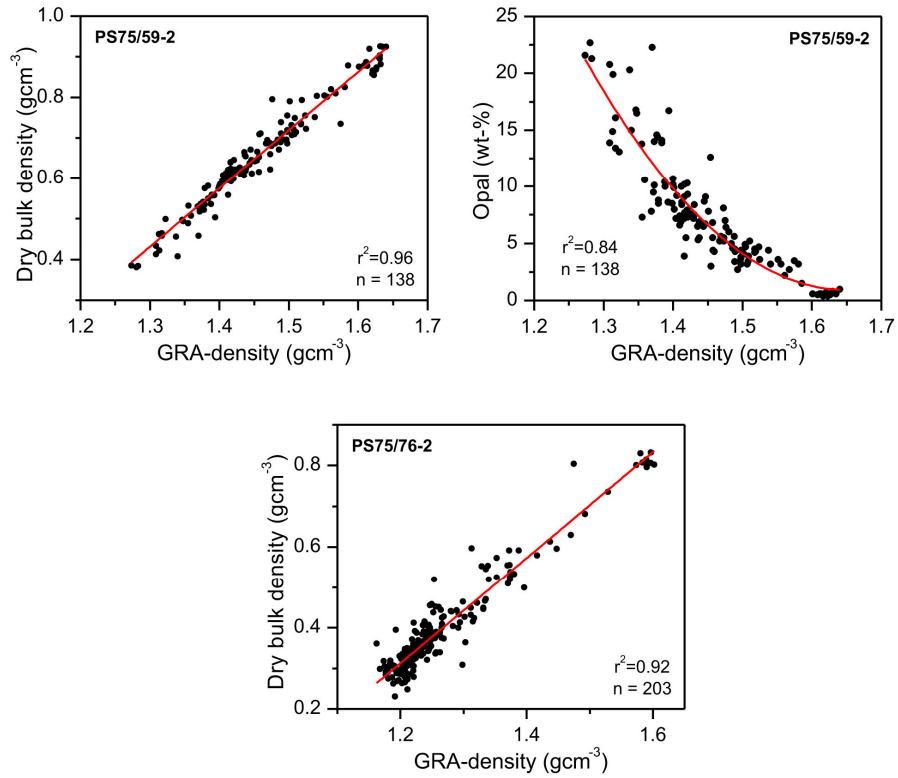


Fig. S9. Linear regressions between gamma-ray attenuation (GRA) density and dry bulk density for both cores. Opal contents in core PS75/59-2 were obtained from a polynomial regression between GRA-density and biogenic opal discrete measurements.

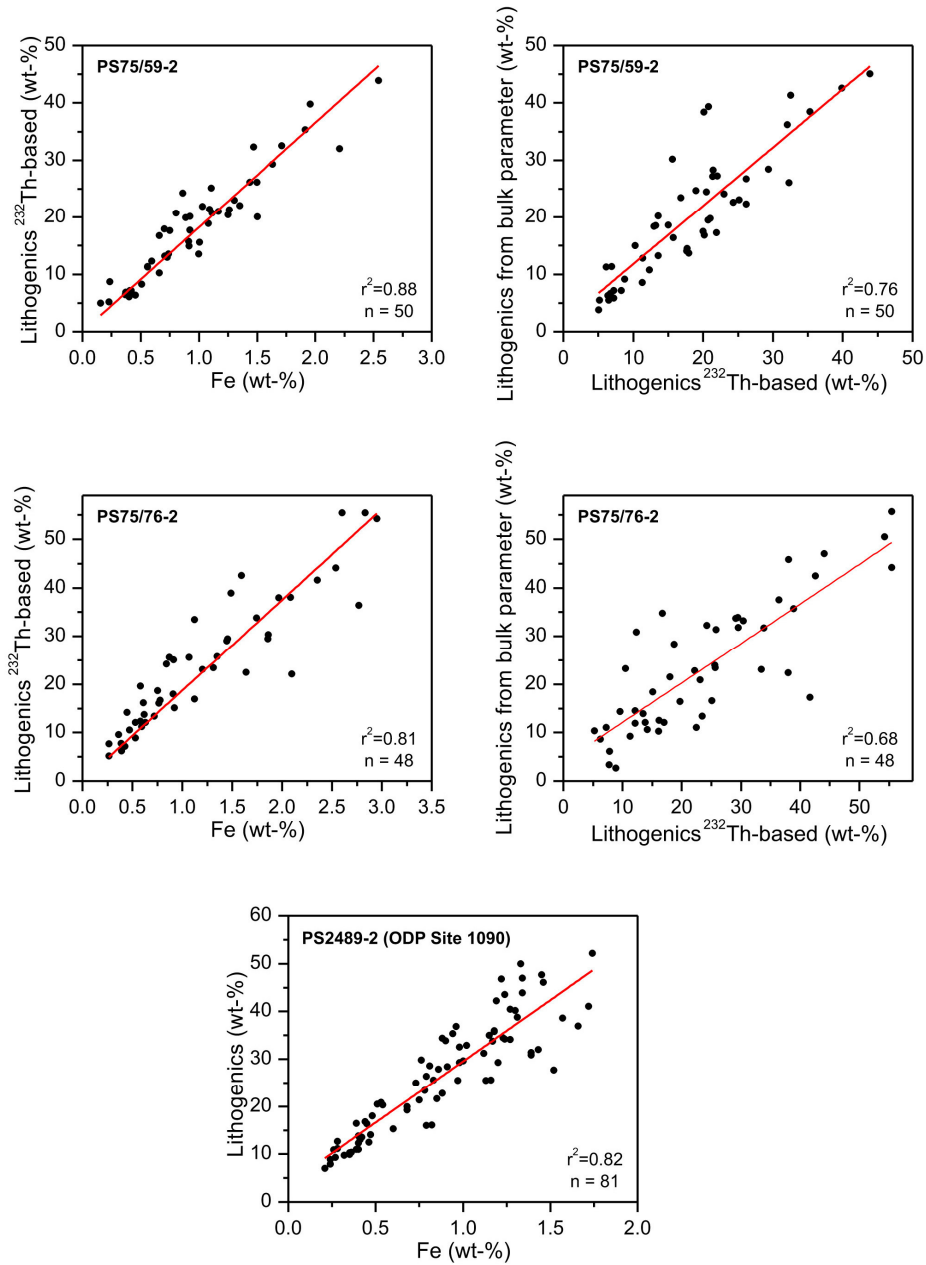


Fig. S10. Linear regressions between iron contents and total lithogenics. Total lithogenic content was derived from the concentrations of ^{232}Th assuming an average concentration of 10.7 ppm for the upper continental crust. Also shown is the comparison of ^{232}Th -based quantifications of lithogenic contents to lithogenic contents calculated from bulk sediment parameters.

Table S1. Estimates of South Pacific lithogenic fluxes from sediment cores, peat bogs, sediment traps, water samples, and dust models. Note that the sediment trap data are from the AESOPS transect in the SW Pacific which is located at the western end of our core transect (at the longitude of core PS75/93-1). This area is more susceptible to a potential hemipelagic contributions from the New Zealand realm including the Campbell Plateau (25). There might be a principal bias between sediment data and sediment trap values as well as dust estimates from water samples. This offset may be related to the fact that sediment data integrate over longer time-periods and may thereby smooth-out substantial interannual and decadal-scale variability that is often recorded in sediment traps. This is consistent with the large seasonal and interannual variability of dust transport to New Zealand's South Island based on a 12 year time-series (57). Compared to dust flux estimates from water samples close to New Zealand (24), estimates of Holocene Australian dust deposition from the peat bog record in New Zealand are substantially higher.

	Modern/interglacial (g/cm ² /kyr)	LGM/glacial (g/cm ² /kyr)	Reference
Sediment cores			
PS 75/76 ~56°S; 156°W	0.07*	0.22*	this study
PS75/59 ~54°S; 125°W	0.05*	0.14*	this study
E11-22 ~56°S; 115°W	0.05	0.13	(58)
E33-2 ~55°S; 120°W	0.04	0.12	(58)
NZ peat bog			
~45°S; 169°W	0.04-0.14		(26)
Sediment traps			
M2-4 (~57-63°S; 170°W)	0.012		(25)
M1 (~53°S; 174°W)	0.073		(25)
Water samples			
~46-47°S; 176-177°W)	0.01		(24)
Dust models			
~56°S; 156°W (at PS75/76)	0.019		(20)
~54°S; 125°W (at PS75/59)	0.013		(20)
~56°S; 156°W (at PS75/76)	0.010	0.079	(12)
~54°S; 125°W (at PS75/59)	0.007	0.050	(12)

*10th/90th percentile of ²³⁰Th-normalized MAR_{Litho} representing average interglacial/glacial dust fluxes (fig. S6).

References and notes

34. L. E. Lisiecki, M. E. Raymo, A Pliocene-Pleistocene stack of 57 globally distributed benthic $\delta^{18}\text{O}$ records 20, PA1003 (2005). *Paleoceanography* 20, PA1071 (2005).
35. L. E. Lisiecki, M. E. Raymo, Diachronous benthic $\delta^{18}\text{O}$ responses during late Pleistocene terminations. *Paleoceanography* 24, PA3210 (2009).
36. R. S. Pugh, I. N. McCave, C. D. Hillenbrand, G. Kuhn, Circum-Antarctic age modelling of Quaternary marine cores under the Antarctic Circumpolar Current: Ice-core dust-magnetic correlation. *Earth Planet. Sci. Lett.* 284, 113 (2009).
37. L. Bazin *et al.*, An optimized multi-proxy, multi-site Antarctic ice and gas orbital chronology (AICC2012): 120-800 ka. *Clim Past* 9, 1715-1731 (2013).
38. D. Veres *et al.*, The Antarctic ice core chronology (AICC2012): an optimized multi-parameter and multi-site dating approach for the last 120 thousand years. *Clim Past* 9, 1733-1748 (2013).
39. T. Friedrich, A. Timmermann, Millennial-scale glacial meltwater pulses and their effect on the spatiotemporal benthic $\delta^{18}\text{O}$ variability. *Paleoceanography* 27, PA3215 (2012).
40. D. Paillard, L. Labeyrie, P. Yiou, Macintosh program performs time-series analysis. *Eos Trans. AGU* 77, 379 (1996).
41. R. Tjallingii, U. Rohl, M. Kolling, T. Bickert, Influence of the water content on X-ray fluorescence core-scanning measurements in soft marine sediments. *Geochem. Geophys. Geosy.* 8, Q02004 (2007).
42. P. J. Müller, R. Schneider, An automated leaching method for the determination of opal in sediments and particulate matter. *Deep-Sea Res. Part I* 40, 425-444 (1993).
43. S. R. Taylor, S. M. McLennan, The geochemical evolution of the continental crust. *Rev. Geophys* 33, 241-265 (1995).
44. J. Hefter, Analysis of alkenone unsaturation indices with fast gas chromatography/time-of-flight mass spectrometry. *Anal. Chem.* 80, 2161-2170 (2008).
45. M. Q. Fleisher, R. F. Anderson, Assessing the collection efficiency of Ross Sea sediment traps using ^{230}Th and ^{231}Pa . *Deep-Sea Res. Part II* 50, 693-712 (2003).
46. G. M. Henderson, R. F. Anderson, The U-series toolbox for paleoceanography. *Uranium-Ser. Geochem.* 52, 493 (2003).
47. R. Francois, M. Frank, M. M. R. van der Loeff, M. P. Bacon, ^{230}Th normalization: An essential tool for interpreting sedimentary fluxes during the late Quaternary. *Paleoceanography* 19, PA1018 (2004).
48. R. F. Anderson, M. P. Bacon, P. G. Brewer, Removal of ^{230}Th and ^{231}Pa from the open ocean. *Earth Planet. Sci. Lett.* 62, 7-23 (1983).
49. M. P. Bacon, R. F. Anderson, Distribution of thorium isotopes between dissolved and particulate forms in the deep-sea. *J. Geophys. Res. Oceans* 87, 2045-2056 (1982).
50. G. M. Henderson, C. Heinze, R. F. Anderson, A. M. E. Winguth, Global distribution of the Th-230 flux to ocean sediments constrained by GCM modelling. *Deep-Sea Research Part I-Oceanographic Research Papers* 46, 1861-1893 (1999).

51. S. Kretschmer, W. Geibert, M. M. R. van der Loeff, G. Mollenhauer, Grain size effects on ^{230}Th xs inventories in opal-rich and carbonate-rich marine sediments. *Earth Planet. Sci. Lett.* 294, 131-142 (2010).
52. A. H. Orsi, T. Whitworth, W. D. Nowlin, On the meridional extent and fronts of the Antarctic Circumpolar Current. *Deep-Sea Res. Part I* 42, 641-673 (1995).
53. G. Eglinton, R. J. Hamilton, Leaf epicuticular waxes. *Science* 156, 1322-1335 (1967).
54. S. Fietz, F. G. Prahl, N. Moraleda, A. Rosell-Mele, Eolian transport of glycerol dialkyl glycerol tetraethers (GDGTs) off northwest Africa. *Org. Geochem.* 64, 112-118 (2013).
55. R. B. Gagosian, E. T. Peltzer, J. T. Merrill, Long-range transport of terrestrially derived lipids in aerosols from the South-Pacific. *Nature* 325, 800-803 (1987).
56. J. Villanueva, J. O. Grimalt, E. Cortijo, L. Vidal, L. Labeyrie, A biomarker approach to the organic matter deposited in the North Atlantic during the last climatic cycle. *Geochim Cosmochim Acta* 61, 4633-4646 (1997).
57. S. K. Marx, B. S. Kamber, H. A. McGowan, Estimates of Australian dust flux into New Zealand: Quantifying the eastern Australian dust plume pathway using trace element calibrated Pb-210 as a monitor. *Earth Planet. Si. Lett.* 239, 336-351 (2005).
58. Z. Chase, R. F. Anderson, M. Q. Fleisher, P. W. Kubik, Scavenging of ^{230}Th , ^{231}Pa and ^{10}Be in the Southern Ocean (SW Pacific sector): The importance of particle flux, particle composition and advection. *Deep-Sea Res. Part II* 50, 739-768 (2003).